

Contents

1	Vertical Dynamics (Suspension)	4
1.1	Suspension - Demands and Possibilities of Implementation	4
1.2	The Road as the Source of Excitation.....	6
1.2.1	Spectral Density of Road Unevenness	9
1.2.2	Data Acquisition of Road Unevenness	12
1.3	Components of the Suspension System	16
1.3.1	Tires.....	16

1 Vertical Dynamics (Suspension)

1.1 Suspension - Demands and Possibilities of Implementation

Roads commonly used by motor vehicles are uneven. This unevenness induces vertical displacements of the vehicle and the passengers in the process of driving.

The vehicle comes into contact with the road over the tire. Road unevenness which is negligible compared to the size of the tire contact patch can be compensated by tire elasticity, whereas larger unevenness entails a vertical acceleration or deflection of the wheels. In order not to transfer these accelerations to the vehicle body, a displacement compensating element has to be placed between the wheel and the vehicle body.

Steel springs are technically the simplest displacement compensating elements. As a result, they are also the most commonly used displacement compensating element, where the spring force is a function of displacement. It is commonly used in the suspensions of motor vehicles. An oscillatory system results when various elements are connected together over springs. Hence an additional energy absorbing element, the damper, has to be included.

The objective of the suspension in the motor vehicle is to reduce these vertical movements. The essential criteria defining the quality of a suspension can be listed as follows:

- Suspension comfort for the passengers (Effective acceleration affecting the passengers)
- Forces affecting the load (Effective value of structure acceleration)
- Wheel load fluctuations (Effective value of the dynamic wheel load), which influence the grip between tires and road (driving safety) and the transferable load on the road surface.

A number of further demands which are partially contradictory, are made on the suspension of a motor vehicle (Fig. 1.1-1)

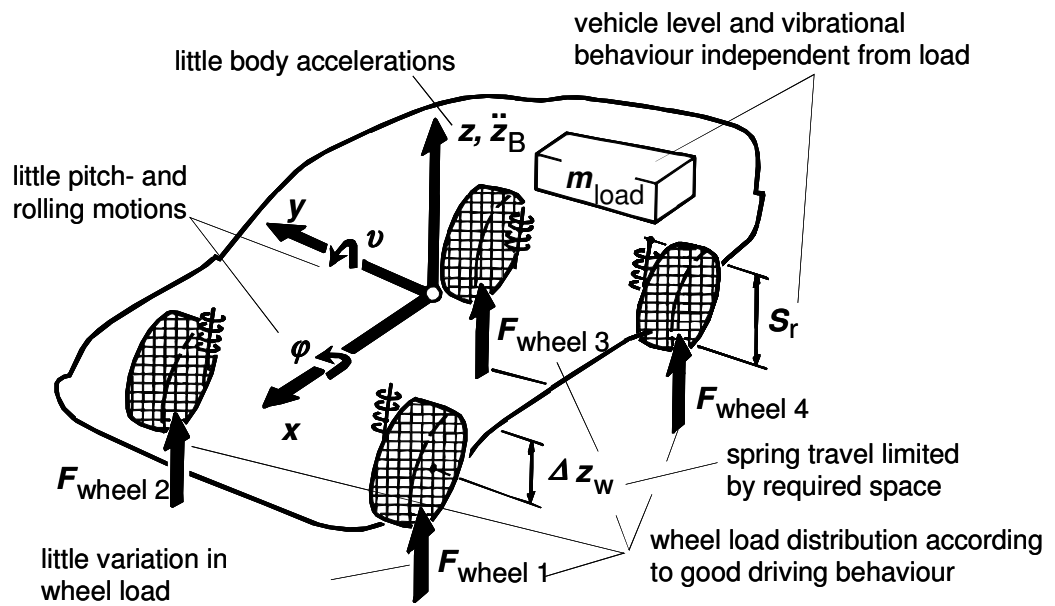


Fig 1.1-1: Demands on a vehicle suspension

Before dealing with the technical details of the spring and damper elements, the road and the mathematical description of its unevenness is firstly presented.

1.2 The Road as the Source of Excitation

The unevenness of the road represents the most intensive source of excitation for the vibratory system of the motor vehicle in the frequency range up to approximately 30 Hz. The unevenness of the road induces vertical displacements of the vehicle body, and as a consequence, the road is in turn affected by the wheel load fluctuations.

Excitation as a result of road unevenness is generally characterized by differing amplitudes and wavelengths at irregular periods of time. This is called the stochastic excitation of the vehicle. In order to be able to examine the effects of road unevenness on the vibratory motor vehicle system (see chapter 1.4), this unevenness has to be firstly described mathematically.

When a simple harmonic (sinusoidal) wave is considered, where the road unevenness excites an amplitude 'h' at equal distances L, an unevenness characteristic as shown in Fig. 1.2-1 results.

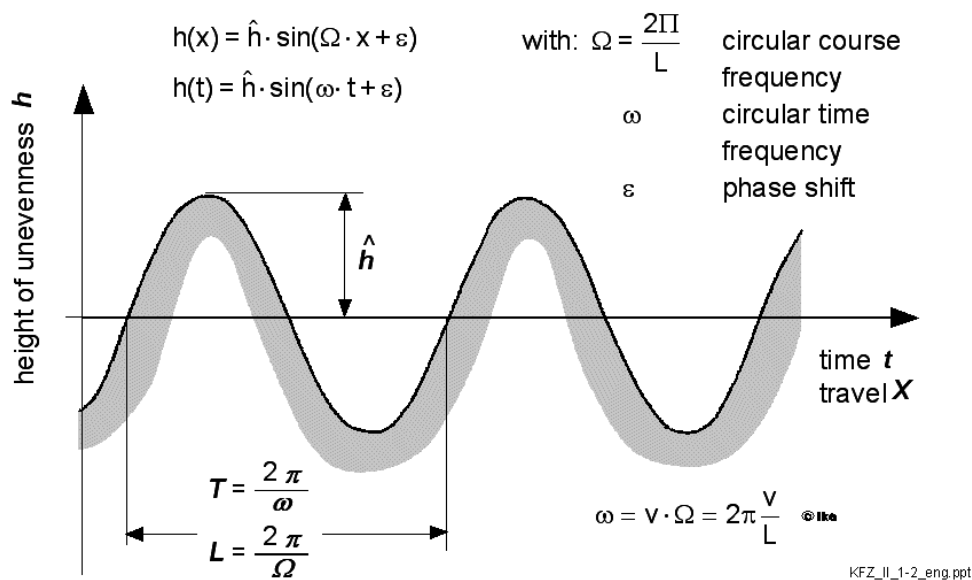


Fig. 1.2-1: Sinusoidal pattern of unevenness

The amplitude of unevenness can be described as follows:

$$h(x) = \hat{h} \cdot \sin(\Omega \cdot x + \varepsilon) \quad (1.2-1)$$

including: $\Omega = \frac{2\Pi}{L}$ as the distance-dependent angular frequency and ε as phase shift.

When driving on such a road at a constant velocity v , the distance-dependent unevenness can be converted into a time-dependent relation:

$$h(t) = \hat{h} \cdot \sin(\omega \cdot t + \varepsilon) \quad (1.2-2)$$

with: ω as time-dependent angular frequency.

The equality of $h(x)$ and $h(t)$ entails $\omega \cdot t = \Omega \cdot x$, and with the relationship $x = v \cdot t$ the time-dependent angular frequency follows:

$$\omega = v \cdot \Omega = 2\pi \cdot \frac{v}{L} \quad (1.2-3)$$

The next step in the description of the road unevenness is the transition to a non-sinusoidal, but periodic, unevenness (Fig. 1.2-2).

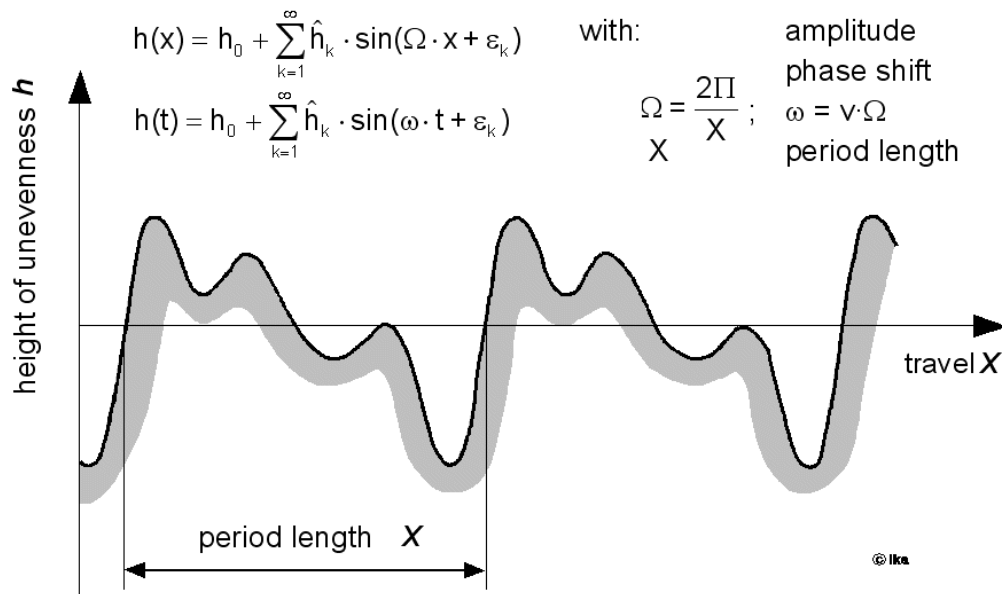


Fig. 1.2-2: Periodic pattern of unevenness

This unevenness can be represented as Fourier series as follows:

$$h(x) = h_0 + \sum_{k=1}^{\infty} \hat{h}_k \cdot \sin(\Omega \cdot x + \varepsilon_k) \quad (1.2-4)$$

or:

$$h(t) = h_0 + \sum_{k=1}^{\infty} \hat{h}_k \cdot \sin(\omega \cdot t + \varepsilon_k) \quad (1.2-5)$$

with: \hat{h}_k Amplitude

ε_k phase shift;

$$\Omega = \frac{2\pi}{X}, \quad \omega = v \cdot \Omega$$

X period length

When the individual amplitudes \hat{h}_k of the Fourier series are plotted versus the frequency, a discrete amplitude spectrum (line spectrum), belonging to the periodic unevenness, results (Fig. 1.2-3).

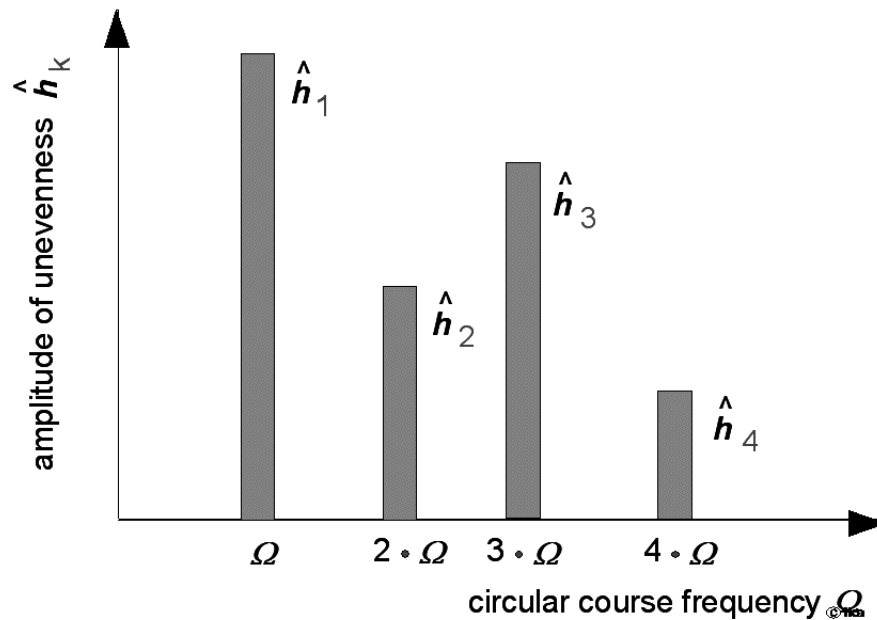


Fig. 1.2-3: Line spectrum of a periodic pattern of unevenness

For the description of real roads a further step has to be taken, since the excitation shows no periodic unevenness, but instead a varying (stochastic) one. The representation of the Fourier series in a complex equation, results as following:

$$h(x) = \sum_{k=1}^{\infty} \hat{h}_k \cdot e^{jk\Omega x} \quad (1.2-6)$$

$$h(t) = \sum_{k=1}^{\infty} \hat{h}_k \cdot e^{jk\omega t} \quad (1.2-7)$$

$$\text{with: } \hat{h}_k = \frac{\Omega}{2\pi} \cdot \int_{-\frac{x}{2}}^{\frac{x}{2}} h(x) \cdot e^{-ik\Omega x} dx \quad (1.2-8)$$

Assuming that the considered time interval is very large, the distance between the frequencies in the amplitude spectrum $\Delta\omega$ becomes very small.

At the boundary condition ' $X \rightarrow \infty$ implies $\Delta\Omega \rightarrow 0$ ' which means that the Fourier transformation changes into a Fourier integral as follows:

$$h(x) = \frac{1}{2\pi} \int_{-\infty}^{\infty} \hat{h}(\Omega) \cdot e^{j\Omega x} d\Omega \quad (1.2-9)$$

with the continuous amplitude spectrum

$$\hat{h}(\Omega) = \int_{-\infty}^{\infty} h(x) \cdot e^{-j\Omega x} dx \quad (1.2-10)$$

$$h(t) = \frac{1}{2\pi} \int_{-\infty}^{\infty} \hat{h}(\omega) \cdot e^{j\omega t} d\omega \quad (1.2-11)$$

$$\hat{h}(\omega) = \int_{-\infty}^{\infty} h(t) \cdot e^{-j\omega t} dt = \frac{1}{v} \cdot \hat{h}(\Omega) \quad (1.2-12)$$

1.2.1 Spectral Density of Road Unevenness

For theoretical investigation of vehicle oscillations induced by road unevenness, the representation of unevenness as a function of time or the distance is usually not of significance. The statistical mean excitations induced by a road of characteristic unevenness is of higher significance. This implies the determination of the amplitudes and frequencies of excitation induced by the road at certain fixed distances.

The resulting mean square value is defined as follows:

$$\bar{x}^2(t) = \frac{1}{T} \int_0^T x^2(t) dt \quad (1.2-13)$$

The characteristic profile of unevenness results as follows:

$$\bar{h}^2(x) = \frac{1}{x} \int_0^x h^2(x) dx = \int_0^\infty \lim_{x \rightarrow \infty} \frac{|\hat{h}(\Omega)|^2}{x} d\Omega \quad (1.2-14)$$

or:

$$\bar{h}^2(t) = \frac{1}{T} \int_0^T h^2(t) dt = \int_0^\infty \lim_{T \rightarrow \infty} \frac{|\hat{h}(\omega)|^2}{T} d\omega \quad (1.2-15)$$

The limit values occurring here indicate that these simple expressions give a result only for very large time intervals T or distances X . The expressions

$$\Phi_h(\Omega) := \lim_{X \rightarrow \infty} \frac{|\hat{h}(\Omega)|^2}{X} \quad \text{and} \quad (1.2-16)$$

$$\Phi_h(\omega) := \lim_{T \rightarrow \infty} \frac{|\hat{h}(\omega)|^2}{T} \quad (1.2-17)$$

are called Angular Path Frequency or Periodical Spectral Power Density (power density spectrum).

With $X = v \cdot T$ (see above) similarly the following relationship results for the unevenness spectra:

$$\Phi_h(\omega) = \frac{1}{v} \cdot \Phi_h(\Omega) \quad (1.2-18)$$

If one measures the power density spectra $\Phi_h(\Omega)$ of different roads and represents them on a double-logarithmic scale, then similar characteristic curves result for all types of roads (Fig. 1.2-4).

Here the power density spectra can be approximated by straight lines, which then can be described by the following equation:

$$\Phi_h(\Omega) = \Phi_h(\Omega_0) \cdot \left(\frac{\Omega}{\Omega_0} \right)^{-w} \quad (1.2-19)$$

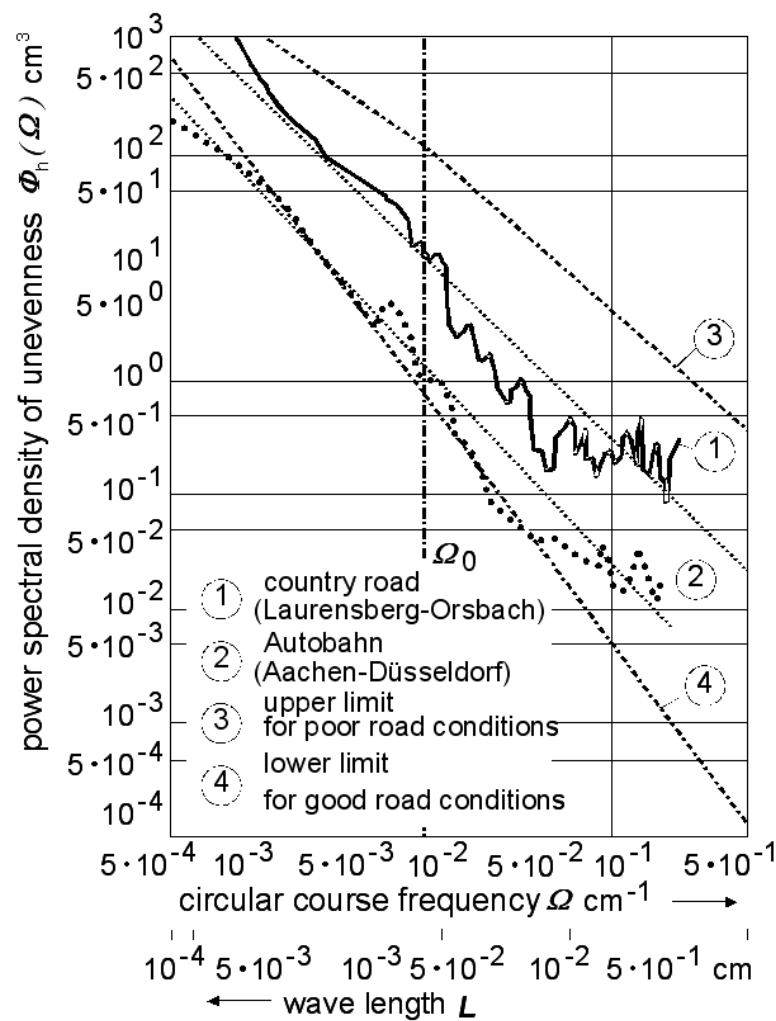


Fig. 1.2-4: Power spectral density of unevenness dependent on circular course frequency.

Here $\Phi_h(\Omega_0)$ represents the power spectral density dependent on Ω_0 (reference angular path frequency), which is usually selected as $\Omega_0 = 10^{-2} \text{ cm}^{-1} = 1 \text{ m}^{-1}$. This corresponds to a reference wavelength of $L_0 = 2\pi/\Omega_0 = 6.28 \text{ m}$. $\Phi_h(\Omega_0)$ is also called the degree of unevenness of the road.

W defines the gradient of the straight line and is also called the Index of Unevenness (undulation) (in German: "Welligkeit"). The index of unevenness (undulation) of the road varies depending on road design between 1.7 and 3.3 (standardized road: $w = 2$) /7/.

The degree of unevenness (and undulation) are considered as assessment criteria for the condition of a road. An increase of $\Phi_h(\Omega_0)$ corresponds to a larger unevenness of the road, while an increasing value of ' W ' implies a higher proportion of long waves in the spectrum.

The relationship between the curve of the spectral density and an increase of the degree of unevenness $\Phi_h(\Omega_0)$ or undulations w is shown in Fig 1.2-5.

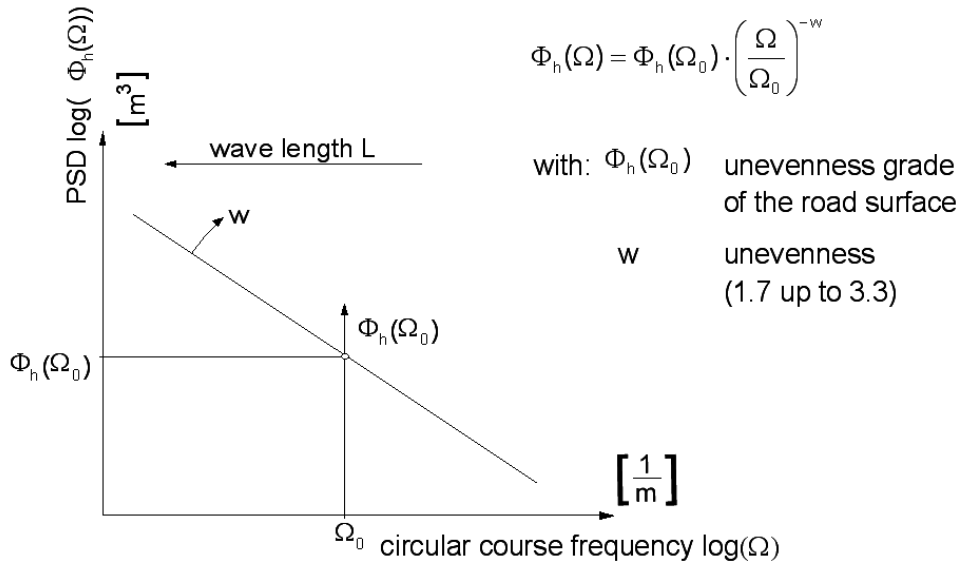


Fig. 1.2-5: Power spectral density dependent on the circular path frequency

Road unevenness of wavelengths L between 0.15 m to 80 m lead to excitation frequencies Ω from 0.06 Hz up to 267 Hz (see eq. 1.2-3) for driving speeds v between 5 m/s (≈ 20 km/h) and 40 m/s (≈ 160 km/h).

1.2.2 Data Acquisition of Road Unevenness

For the determination of the spectral power density of road unevenness, the longitudinal section of the road is taken into consideration. For the measurement of road unevenness different measuring procedures were developed, which are partially adapted to both road construction as well as for automotive applications. About 70 different unevenness measuring procedures are available.

An accurate measurement of the road surface is possible only with subgrade level and levelling instrument. Since the measurement of long distances is time intensive and disturbs the free flow of traffic etc. these approaches are not widely used in technical application. The so-called geometrical unevenness measuring instruments were developed mainly for application in road construction.

The measuring procedures used in automotive technology, function according to the principle of the dynamic unevenness measurement. During these measuring procedures the reference level is not fixed, but derived continuously from an average value of the road unevenness, formed over a sufficiently long period of time. Fig 1.2-6 shows a test vehicle equipped with devices for the measurement of road unevenness.



Fig. 1.2-6: Instrumentation for unevenness measurements (ika)

The measuring task is divided into two sub-tasks:

- 1) Measurement of the change in distance Δz between road surface and reference point on the vehicle body
- 2) Measurement of the vertical body movement z_A at the points of reference

The vertical displacement Δz is recorded continuously for each track with the help of a contactless laser measuring system. The measuring system is based on the triangulation principle, Fig. 1.2-7.

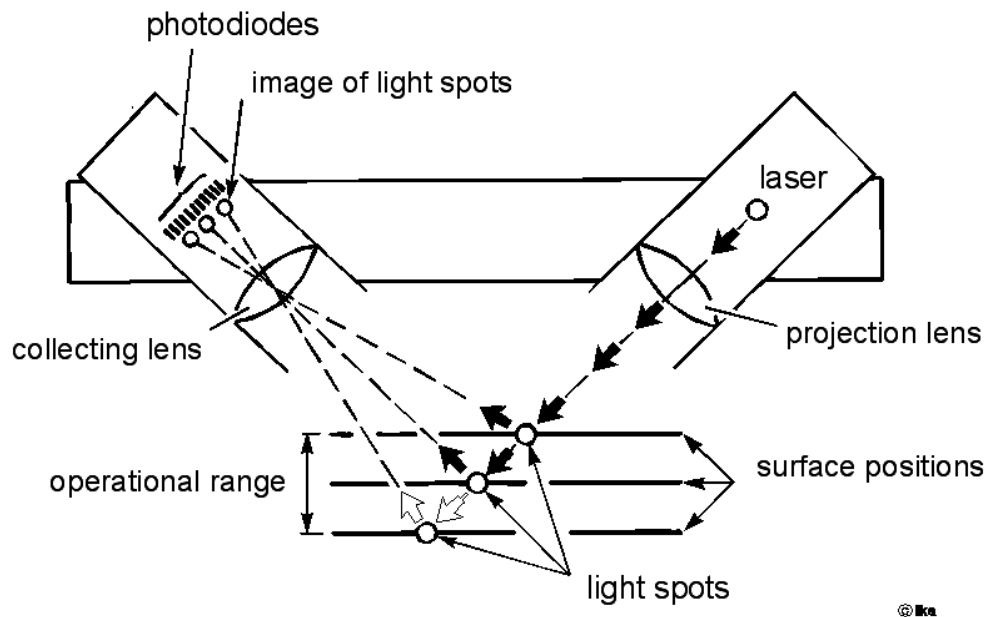


Fig. 1.2-7: Operational principle of the contactless distance measurement

With the help of a laser beam incident at a certain angle on the road surface, a spot of light is produced, which is received through a lens on the surface of a light-sensitive photodiode. Depending on the angle of incidence of the laser beam, the spot of light on the surface of the photodiode shifts as illustrated. This movement is proportional to the vertical distance between the point of reference and the road surface. It can hence be converted into a measuring signal.

The measurement of the displacement of the vehicle body z_B is managed by accelerometers fastened to the vehicle bodywork perpendicularly over the points of reference for distance measurement.

The low-pass effect of the vehicle suspension system results in accelerations \ddot{z}_B of max. 1 to 2 g, and so sensitive acceleration sensors can be selected accordingly, which record low-frequency body accelerations with sufficient accuracy.

The displacement of the vehicle body z_B is determined continuously by the double integration of the vehicle body acceleration \ddot{z}_B . The characteristic of unevenness $h(t)$ or $h(x)$ results from the addition of the displacement of the vehicle body z_A and the change in distance Δz .

The procedure to define the determination of the unevenness spectrum $\Phi_h(\Omega)$ metrologically from a recorded measuring signal $h(t)$ is schematically represented in Fig 1.2-8 /38/.

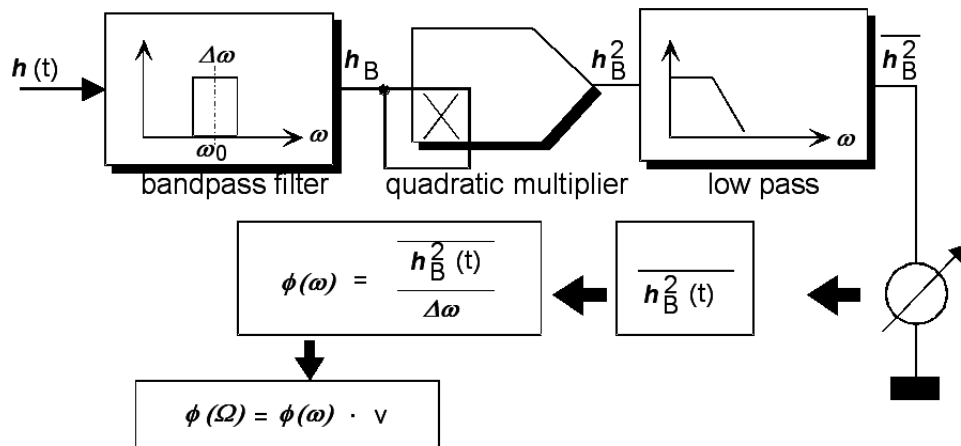


Fig. 1.2-8: Metrological determination of an unevenness spectrum

From the measured signal which can be analyzed using a bandpass filter of mean frequency ω_0 , a frequency range $\Delta\omega$ is filtered. The band-pass filter signal generated is then squared and the average value is calculated over a certain period of time. From this average value, defined in Fig 1.2-8 as $\overline{h_B^2}$, the value of the power density spectrum for ω_0 is determined by division with the filter bandwidth $\Delta\omega$.

By shifting the center frequency of the bandpass filter, the power density spectrum for the entire frequency range of interest can be determined.

From the time-frequency-dependent power density spectrum, the spectral density of unevenness can be calculated as a function of the angular path frequency Ω by simple multiplication with the driving speed v (see Eq. 1.2-18). In this case it is assumed that the measurement of the characteristic of unevenness $h(t)$ was determined at constant driving speed v .

1.3 Components of the Suspension System

1.3.1 Tires

In the following section, the vehicle tire is considered only from the technical point of view of the suspension and damping. Further representation of the characteristics of vehicle tires can be found in chapter 2.2, where the transverse characteristics of the tire are described, e.g. the generation and transfer of side forces.

- Tire as a Spring

The wheel load is transferred to the tire by the rim and pressure is applied to this contact area. The reaction force, which opposes the load on the tire, consists of different components. Fig. 1.3-1 shows the proportions of the load carrying components of a tire as a function of compression.

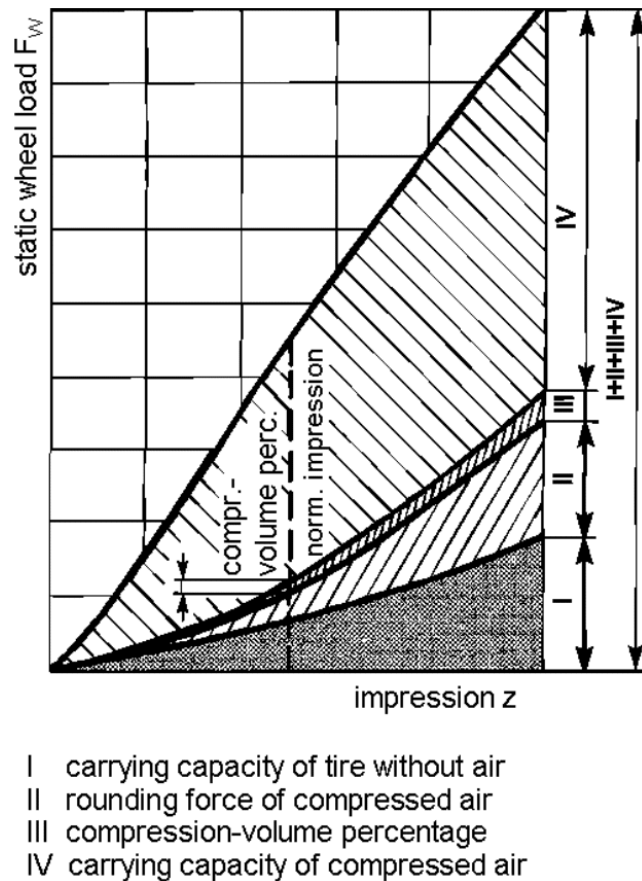


Fig. 1.3-1: Structure of the spring characteristic of a pneumatic tire/41/

The component I corresponds to the proportion of the load carrying capacity of the solid rubber fabric body, due to elastic deformation. The component II represents the so-called

circular retaining force of the compressed air, which reinforces the tire in its walls (balloon effect). The component III represents the very small proportion of the air compression.

The component IV represents the principal part, which is based on the adaption of the road contact area A to the vertical load G_w :

$$G_w \approx p_i \cdot A$$

(with p_i representing the inflation pressure, which implies that the pressure in the tire contact area A corresponds to the inflation pressure.)

Due to the tire compression, an oscillatory subsystem develops in the wheel or in the unsprung masses. In this way, the spring characteristic of a tire influences natural frequency of the wheel or axle.

The inflation pressure also has a decisive influence on the tire spring beside the structure of the tire. Fig. 1.3-2 shows as an example, the spring characteristics of a commercial vehicle tire for differing air pressures.

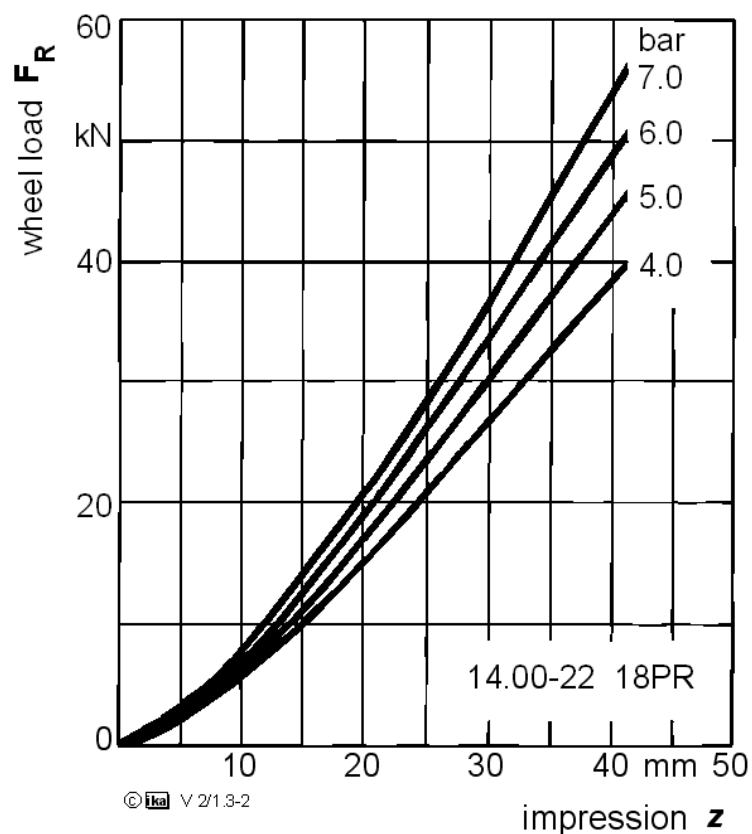


Fig. 1.3-2: Spring characteristic of a Truck tire with four different air pressures

The spring characteristics indicate a linear behaviour in the operating range. By the modification of the vertical load F_W as function of the compression z_W (lowering of the wheel axle) the spring rate c_W can be determined.

$$c_W = \frac{dF_W}{dz_W} \quad (1.3-1)$$

Since the force characteristic is not a constant function of compression, the spring rate is variable. Therefore a constant spring rate can be considered only as an approximation for a certain range of the curve, where the static wheel load $F_{W,Stat}$ and the compression $z_{W,Stat}$ according to Fig. 1.3-3.

spring rate of tire:

$$c_W = \frac{dF_W}{dz_W}$$

within operating range:

$$c_W = \frac{F_{W,stat}}{z'_{W,stat}} ; z'_{W,stat} = 1,7 \dots 2,9 \text{ cm}$$

$$\Rightarrow F_{dyn} = c_W \cdot z_{dyn}$$

eigenfrequency of wheel:

$$\omega_{eW} = \sqrt{\frac{c_W}{m_W}} ; f_{eW} = 8 - 14 \text{ Hz}$$

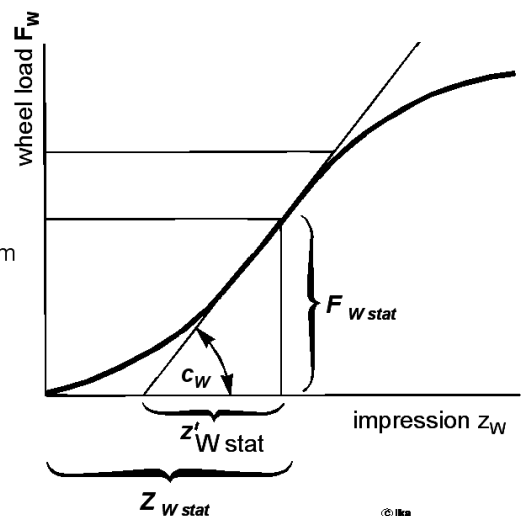


Fig. 1.3-3: Linearisation of the tire spring rates.

In the operation range, the spring rate is given by

$$c_W = \frac{F_{W,stat}}{z'_{W,stat}} \quad (1.3-2)$$

If the tire compression is increased or reduced over z_{dyn} , the force approximation changes to

$$F_{dyn} = c_W \cdot z_{dyn} \quad (1.3-3)$$

As a measure for driving safety and protection of the road, the ratio of total load to the static load is indicated as:

$$\frac{F}{F_{W,stat}} = \frac{F_{W,stat} + F_{dyn}}{F_{W,stat}} \quad (1.3-4)$$

With the equation (1.3-2)

$$\frac{F}{F_{Wstat}} = 1 + \frac{c_W}{F_{Wstat}} \cdot z_{dyn} \quad (1.3-5)$$

The quotient $\frac{F_{Wstat}}{c_W}$ is according to Fig. 1.3-3 equal to the sub-tangent with the length z'_{Wstat}

$$z'_{Rstat} = F_{Wstat} / c_W \quad (1.3-6)$$

This parameter is a measure for the additional load relative to the static load with a compression z_{dyn} , e.g. as a result of unevenness. In general, for all tires (passenger cars and trucks):

$$z'_{Wstat} = 1.7 \dots 2.9 \text{ cm}$$

The lower value refers to diagonal tires and the upper value to radial tires, that means the latter are softer and with a certain tire compression z_{dyn} , induce smaller additional loads F_{dyn} . With this reference value, the approximate wheel natural frequency can be determined:

$$\omega_{eW} = \sqrt{\frac{c_W}{m_W}} \approx \sqrt{\frac{F_{Wstat}}{z'_{Wstat} \cdot m_W}} \quad (1.3-7)$$

The wheel natural frequency is usually approximately $f_{eW} = 8-14 \text{ Hz}$. This estimation proceeds from a static spring characteristic of the tire. In actual driving conditions, the radial spring rigidity of the tire is further influenced by a multiplicity of parameters. Due to the viscoelastic behavior of rubber, the spring stiffness increases e.g. when excited by road unevenness of increasing excitation frequency (chapter 1.4).

Besides, the respective operating point of the tire also influences the spring rate. While e.g. with increasing driving speed the influence of the centrifugal force at the tire circumference causes an increase of the spring rigidity, the side forces generated at the tire due to the side slip angles (Chapter 2.2.4), lead to a lateral displacement of the tire-road contact area. This results in an uneven load on the tire shoulders and hence to a reduction of the spring rate.

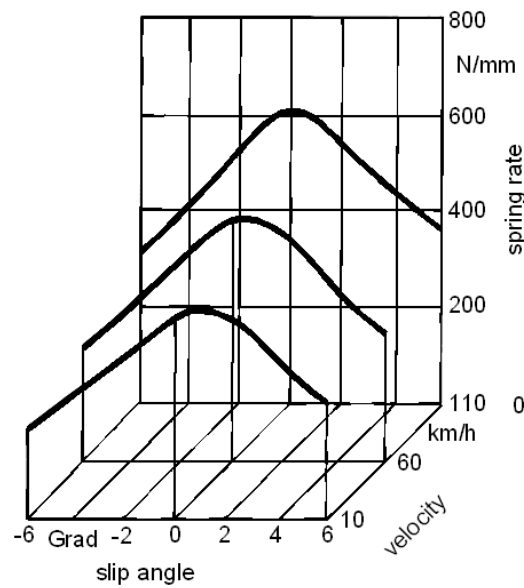


Fig. 1.3-4: Radial spring stiffness of a truck tire as a function of vehicle velocity and side slip angles/17/

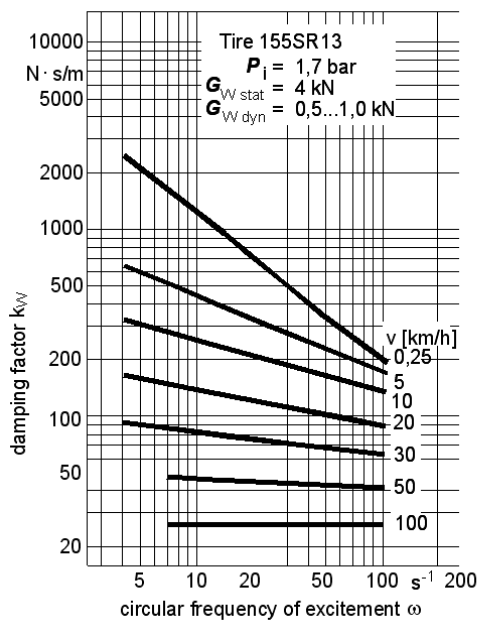
- Absorption Capacity of the Tire

Apart from the springing capacity of the tyre, its absorption capacity also assumes special meaning, since it is in direct relation to the tire comfort.

The term absorption capacity hence characterizes the property of the tire to absorb unevenness, which are short in relation to the tire contact length, without vertical movement of the axle /9/. In relation to such unevenness, the tire behaves along a relatively softer characteristic when compared to an equivalent high compression of the entire tire contact patch. The absorption capacity is influenced mainly by the rigidity of the sidewall.

- Tire Damping

Tire damping is a form of material damping, which leads to a rise in the temperature of the tire and increases with the number of plies and the material mass in the tire. The damping factor k_w is thereby not constant and depends on several influencing parameters, such as the radial spring stiffness of the tire, Fig. 1.3-5.



experimentally determined damping rule:

$$k_W = \frac{\lambda}{\omega^e}$$

with: λ constant } tire specific and
 e exponent } dependent on velocity
 ω circular frequency of excitement

approximation formula for
damping factor:

$$k_W \approx \frac{0,1 \cdot c_W}{\omega}$$

tire damping within resonance range:

$$D_{Wres} = \frac{k_W}{2 \cdot m_W \cdot \omega_{eW}} = \frac{0,1 \cdot c_W}{2 \cdot m_W \cdot \omega_{eW} \cdot \omega_{eW}} = \frac{0,1 \cdot \omega_{eW}^2}{2 \cdot \omega_{eW}^2} = 0,05$$

© Ifka

KFZ_II_1-3_eng.ppt

Fig. 1.3-5: Damping factor k_W of a tire as a function of rolling speed and excitation frequency

The influence of the excitation frequency of unevenness can be described based on experimental tests, using the following damping law /20.

$$k_w = \frac{\lambda}{\omega^e} \quad (1.3-8)$$

ω angular frequency of excitation

The constant λ and the exponent e not only depend on the tire design, but also on the rolling speed v .

With high rolling speeds, $e \approx 0$, i.e: k_w depends only on λ or v and is hence independent of ω (see Fig. 1.3-5).

For the estimation of the order of magnitude of the tire damping rate D_W , the following approximation formula for the damping factor is applicable.

$$k_w \approx \frac{0,1 \cdot c_R}{\omega} \quad (1.3-9)$$

The tire damping is important particularly in the resonance area ($\omega = \omega_{eW}$). With the approximation formula (Gl.1.3-8):

$$D_{W\text{res}} = \frac{k_W}{2 \cdot m_W \cdot \omega_{eW}} = \frac{0,1 \cdot c_W}{2 \cdot m_W \cdot \omega_{eW} \cdot \omega_{eW}} = \frac{0,1 \cdot \omega_{eW}^2}{2 \cdot \omega_{eW}^2} = 0,05 \quad (1.3-10)$$

A damping rate of $D_{W\text{res}}$ of 0.05 is not sufficient for the damping of the wheel masses. For a satisfactory absorption of the wheel oscillations, a damping rate of D_W of approximately 0.4 is required which means that the hydraulic vibration damper for the body (see chapter 1.3.3) must also simultaneously function as the wheel damper.

Contents

1.3	Components of the Suspension System	23
1.3.1	Body Springs	23
1.3.1.1	Leaf Springs.....	23
1.3.1.2	Torsion Bars	29
1.3.1.3	Coil Springs	31
1.3.1.4	Gas Springs.....	35
1.3.2	Shock Absorbers.....	46
1.3.3	Seats	58
1.3.4	Evaluation of Oscillations by Humans	59
1.4	Single Wheel Suspension Model	65
1.4.1	Single Mass Model.....	67
1.4.2	Dual-Mass Equivalent System	69
1.4.2.1	Parametric Study - Automobile Suspension	74
1.4.2.2	Parametric Study of a Truck Suspension	87
1.4.3	Extension of the Model by the Seat Suspension	89
1.5	Single-Track Suspension Model	91
1.5.1	Double-axle Vehicle with bending resistant Structure.....	91
1.5.1.1	Excitation by Real Road Unevenness	93
1.5.1.2	Mass and Spring Coupling	95
1.5.2	Two-Axle Vehicle with additional Degrees of Freedom.....	99
1.6	Two-Track Suspension Model	103
1.6.1	Roll Suspension	103
1.6.1.1	Stabilizer and Compensating Spring	105
1.6.1.2	Vehicle Design and Suspension Characteristics	106
1.6.2	Distortion of the Body (twisting).....	108
1.6.3	Rigid Axle Tramp	110
1.7	Methods for Suspension Investigation	112

1.3 Components of the Suspension System

1.3.1 Body Springs

Those elements of wheel suspension systems, which produce a restoring force under elastic deformation, are described as body springs in this chapter. Besides conventional coil, leaf and torsion bar springs, gas springs can also be mentioned.

1.3.1.1 Leaf Springs

Leaf springs represent the classical design of springs, which were used in carriages.

The substantial advantage of leaf springs in relation to other spring design concepts consists of the fact that they can not only be used as spring elements, but also as constructional elements for the coupling of body and axle (particularly for axle guidance) as well. Multilayer leaf springs inherently possess damping characteristics due to frictional forces between the leaves.

Conventional leaf springs are used nowadays in combination with rigid axles only in few car designs (station wagons and off-road vehicles). Front and rear suspension systems of trucks are also commonly designed likewise. Fig. 1.3-1.

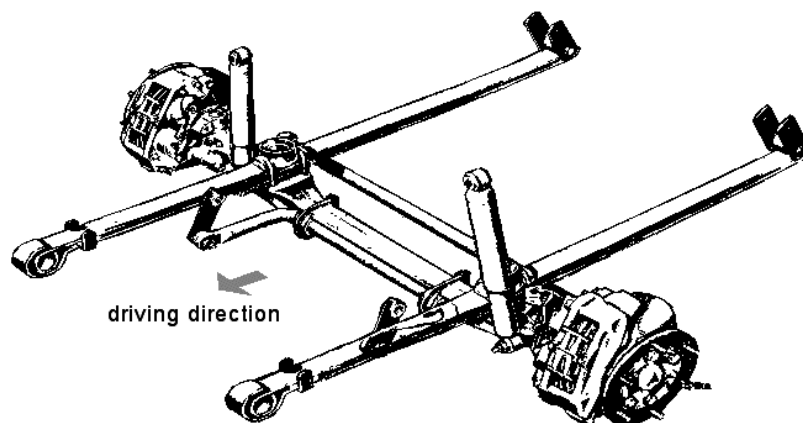


Fig. 1.3-1: Leaf spring guided front axle of a truck (Daimler-Benz)

In the absence of special measures, the spring characteristic of the leaf spring is linear. The relationship between the deflection f and the load L at the end of a cantilever beam is known from strength of materials and is given by:

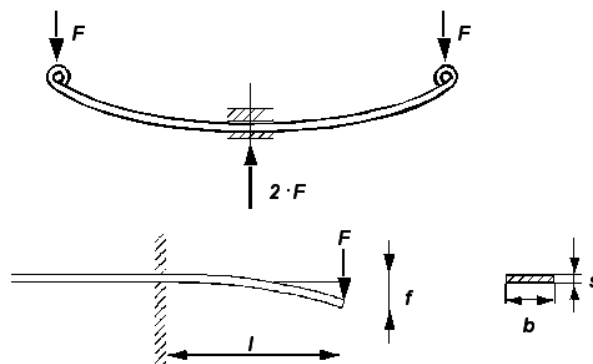
$$f = \frac{F \cdot l^3}{3 \cdot E \cdot J} \quad (1.3-11)$$

With l : length of the bending beam,

E : modulus of elasticity

J : moment of inertia

$$J = \frac{b \cdot s^3}{12} \quad (1.3-12)$$



$$f = \frac{F \cdot l^3}{3 \cdot E \cdot J} \quad E = E \text{ modulus}$$

$$J = \frac{b \cdot s^3}{12} \quad J = \text{planar moment of inertia}$$

$$\frac{F}{f} = c = \frac{1}{4} \cdot \frac{b \cdot s^3}{l^3} \cdot E = \text{const}$$

leaf spring has a linear characteristic curve

Fig. 1.3-2: Deflection of a leaf spring

Hence, the following spring rate results for one half of a leaf spring system corresponding to Fig 1.3-7:

$$c = \frac{F}{f} = \frac{1}{4} \cdot \frac{b \cdot s^3}{l^3} \cdot E \approx \text{const} \quad (1.3-13)$$

In order to ensure the effective guidance of the axle leaf spring, the width b and the thickness s can be varied for the definition of the leaf spring rigidity c only within certain limits. Usually relatively large spring lengths are necessary in practice. Truck leaf springs are up to 1800 mm long.

Since the bending force correspondingly decreases from the spring center to the ends, spring leaves of varying length are arranged in layers such that a high and uniform degree of material utilization is achieved.

The bending stress corresponds to a single-leaf in the form of a trapezoid as in Fig. 1.3-3. This kind of leaf spring is hence called the trapezoidal spring.

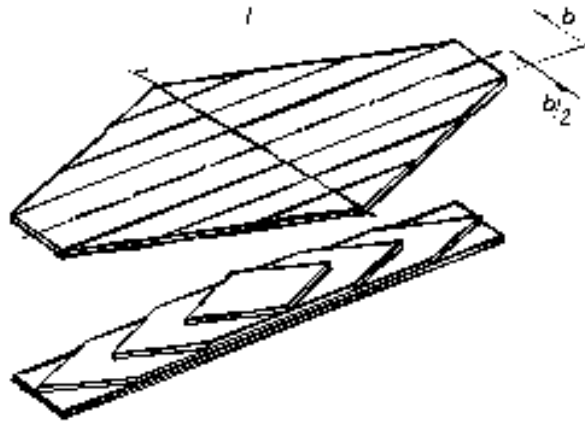


Fig. 1.3-3 Trapezoidal spring

As a result of the linear spring characteristic, two main disadvantages result:

- Spring travel

When a load is applied on the spring, the available spring travel $\Delta z_{\text{Reserve}}$ can often reduce to insufficient values (recommended values for passenger car: $\Delta z_{\text{Reserve}}$ 50mm, truck: $\Delta z_{\text{Reserve}}$ 70mm)

- Natural frequency \neq const.

Since the spring stiffness does not change with load, the body natural frequency in the unloaded condition is larger than the natural frequency in the loaded condition because of $m_{\text{B,loaded}} > m_{\text{B,unloaded}}$. The acceleration of the body mass is described in chapter 1.4.

These disadvantages of multi layer leaf springs can be reduced through a progressive design of the spring characteristic. This can be achieved by the application of varying pre-loads on individual leaves and/or by the parallel addition of auxiliary springs, which come into operation only when the load exceeds a certain limit, Fig. 1.3-4.

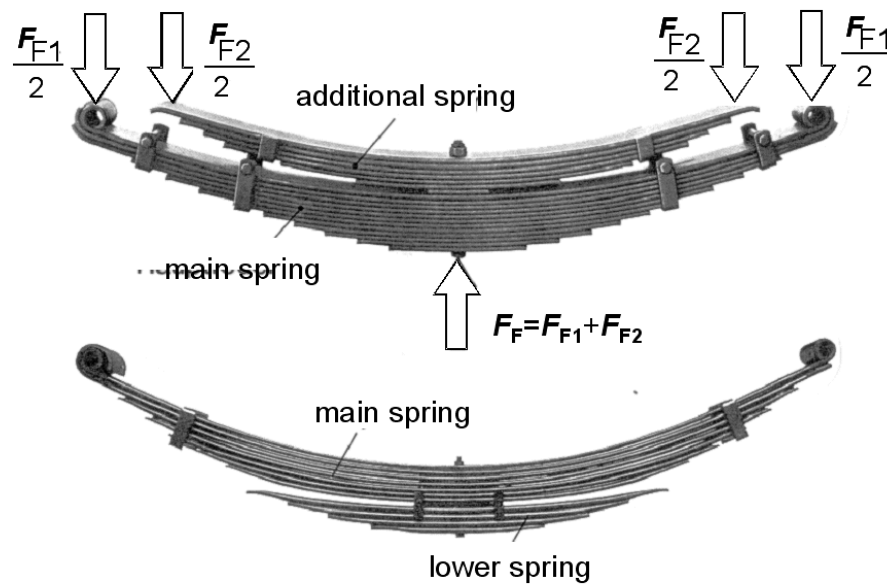


Fig. 1.3-4 Leaf springs with auxiliary springs

The natural frequency remains constant, if the gradient of the spring characteristic changes proportional to the load:

$$\frac{c_{\text{loaded}}}{c_{\text{empty}}} = \frac{m_{B_{\text{loaded}}}}{m_{B_{\text{empty}}}} \quad (1.3-14)$$

As a result of a progressive characteristic, the difference in spring travel between unloaded and loaded condition decreases. This implies a reduction of the entire spring travel, which is important from the point of view of space requirement in wheel housings or the entrance height of buses etc., Fig. 1.3-5.

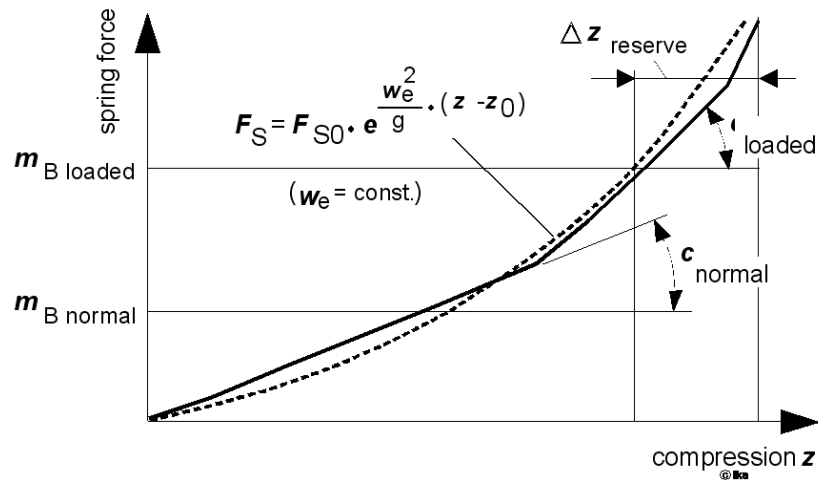


Fig. 1.3-5: Spring rate of a leaf spring with additional springs

Another disadvantage of the leaf spring involves dry friction which occurs both in the suspension as well as between the leaves of the multi layer leaf spring (Fig. 1.3-6). This dry friction has an unfavorable influence on the suspension characteristics.

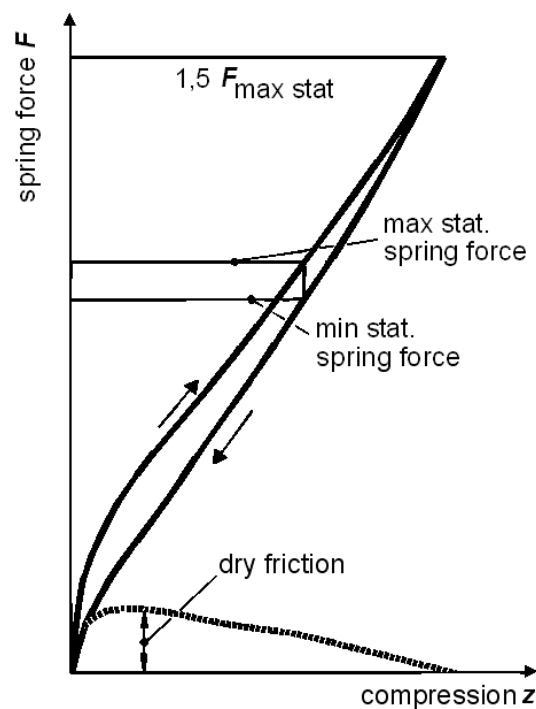


Fig. 1.3-6: Spring characteristics of a leaf spring with dry friction (rear axle of a commercial van)

The disadvantages can be compensated to a certain extent by the use of shackles instead of sliding shoes in the suspension or by the introduction of plastic layers between the spring leaves.

The use of a small number of leaves in the spring particularly influences the reduction of frictional forces positively. This is possible, not by the use of additional spring leaves but by the use of stronger leaves capable of withstanding higher bending forces at the spring centre. This leads to a higher degree of utilisation of material.

The bending stress along the length of the leaf is constant, if the spring halves indicate a parabolic profile in the longitudinal section. Leaf springs with such leaves are called parabolic springs.

The development of the conventional laminated leaf spring to the parabolic spring is illustrated in Fig. 1.3-7:

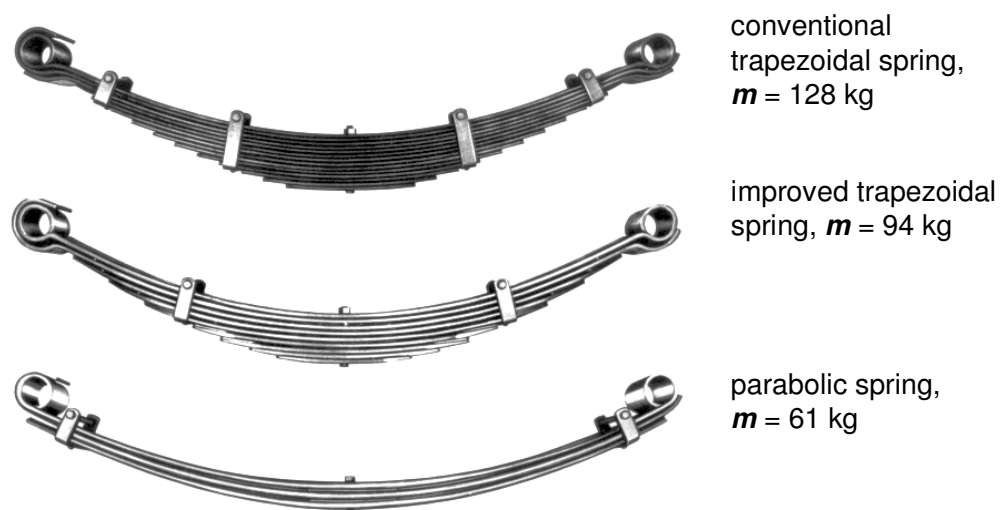


Fig. 1.3-7: Parabolic spring

The three springs considered here have the same length, spring rate and nominal load. The advantage of the parabolic spring, apart from the decrease of friction, is the decrease of the spring weight by around 50% (minimization of unsprung masses). The main advantage of the leaf spring is the combination of suspension and axle location, which is partially lost with the transition to parabolic springs with few leaves. During braking, the parabolic springs tend to be affected by the S-impact, which must be prevented by an additional torque support. Otherwise, relative velocities between the road and tire can result in brake-hopping (Fig. 1.3-8).

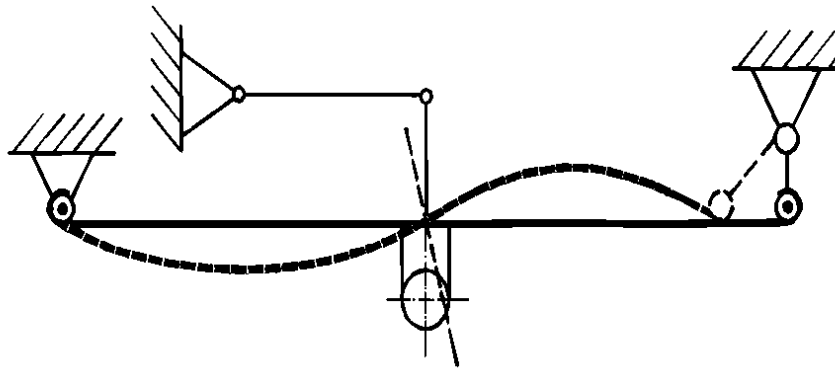


Fig. 1.3-8: Leaf spring with torque support

1.3.1.2 Torsion Bars

Torsion bars are mainly used in the suspensions of passenger cars and light commercial vehicles.

Torsion bars are rods made of spring steel, that are predominantly stressed by torsion. These shafts are clamped at one end and free to twist at the other, so that the shaft can be twisted flexibly along its axis by a moment.

In order to use torsion bars as vehicle suspension elements, the elastic twist of the bar is converted into a reciprocating motion with the help of a crank which is located at the swivel-free end and which applies the twisting moment, Fig. 1.3-9.

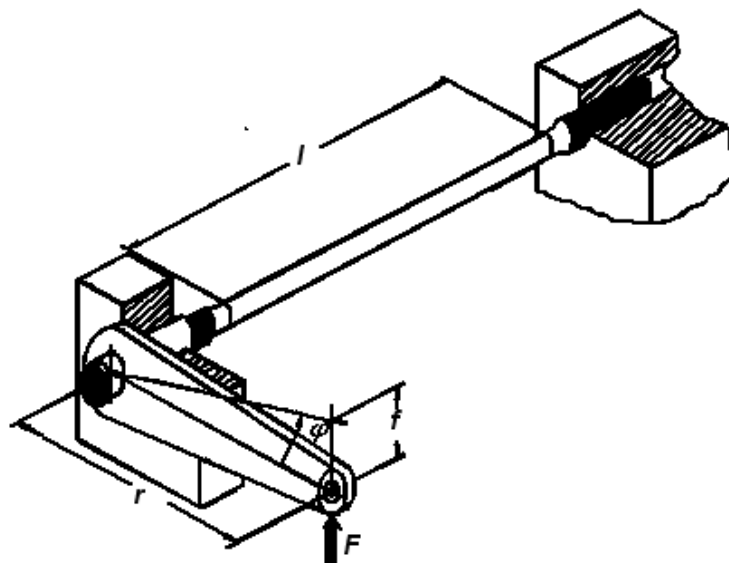


Fig. 1.3-9: Crank mechanism of a torsion bar

The strut of the axle or the suspension forms the crank. Torsion bars are normally arranged along the body-side bearing axis of the strut, at the opposite end of which the vertical wheel force acts as an external load.

Between the twisting angle φ and the torsional moment M_t of a torsion bar with circular cross-section, the following relationship exists:

$$\varphi = \frac{M_t \cdot l}{G \cdot J_p} \quad (1.3-15)$$

with G : shear modulus

J_p : polar surface moment of inertia

L : length of torsion bar

The polar moment of inertia of a full bar with a circular cross-section is given by:

$$J_p = \frac{\pi \cdot d^4}{32} \quad (d : \text{shaft diameter}) \quad (1.3-16)$$

So the torsional stiffness c_{tor} of such a bar is given by :

$$c_{\text{tor}} = \frac{G}{l} \cdot \frac{\pi \cdot d^4}{32} \quad (1.3-17)$$

Related to the crank end the spring stiffness approximately follows:

$$\Delta z \approx r \cdot \Delta \varphi$$

$$\Delta F \approx \frac{1}{r} \cdot \Delta M_t$$

$$c = \frac{\Delta F}{\Delta z} = \frac{1}{r^2} \cdot c_{\text{tor}} \quad (1.3-18)$$

While the spring characteristic of a torsion bar is linear, the effective spring stiffness at the crank end depends on the kinematics of the strut arrangement. In the equation 1.3-18 corresponding trigonometric relations have to be used for exact calculations.

At the surface of a torsion bar with circular cross section the shear stress amounts to:

$$\tau_t = \frac{16 \cdot M_t}{\pi \cdot d^3} \quad (1.3-19)$$

The torsion bar diameter d cannot be selected freely in order to achieve a suitable torsional rigidity c_{tor} . A minimum diameter which is a function of the expected maximum twisting moment and the admissible shear stress, has to be specified.

In practice, to achieve a suitable spring stiffness, relatively large torsion bar lengths are necessary.

Torsion bar springs are combined both with transverse and longitudinal struts and in some cases even with semi-trailing links. They are arranged predominantly parallel to the vehicle floor.

For front wheel suspensions torsionbars are used predominantly in combination with wishbones and arranged in the vehicle's longitudinal direction, Fig. 1.3-10. With the axle shown in the picture a vertical adjustment is intended at the end of the bars.

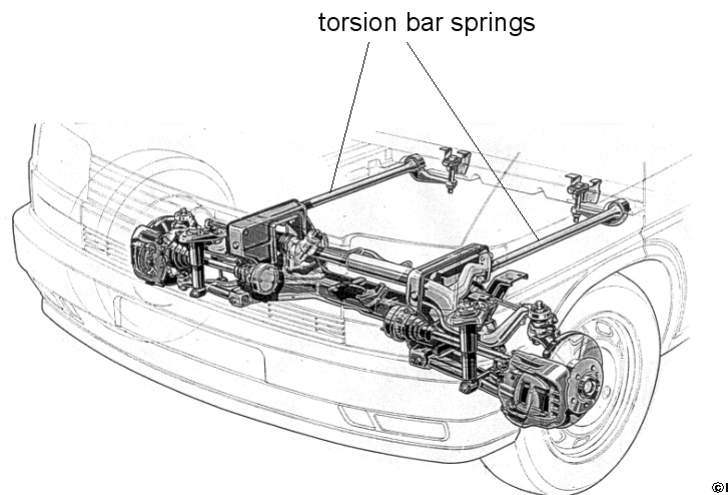


Fig. 1.3-10: Torsion bar suspension (VW T4)

1.3.1.3 Coil Springs

The most common spring used in passenger cars is the coil spring. The coil spring is the equivalent of a wound torsion bar. The spring material is loaded predominantly by torsion.

If r is considered as the lever arm at which the spring force F acts and $D/2$ as half the diameter of the coil spring, the spring stiffness is determined by the equation 1.3-18:

$$c \approx \frac{4}{D^2} \cdot c_{\text{tor}} \quad (1.3-20)$$

$$\text{with } c_{\text{tor}} = \frac{G}{l} \cdot \frac{\pi \cdot d^4}{32}$$

The total length l of the wound torsion bar follows approximately as:

$$l \approx i \cdot \pi \cdot D \quad (1.3-21)$$

with: i number of turns

Hence, the spring stiffness of a cylindrical coil spring with circular wire cross-section can be

$$\text{determined from Eq.1.3-20 and Eq.1.3-21: } c \approx \frac{G \cdot d^4}{i \cdot 8 \cdot D^3} \quad (1.3-22)$$

The normally linear characteristic of the coil spring can be changed into a progressive characteristic by the variation of the overall diameter, the wire thickness and the gradient, see Fig. 1.3-11:

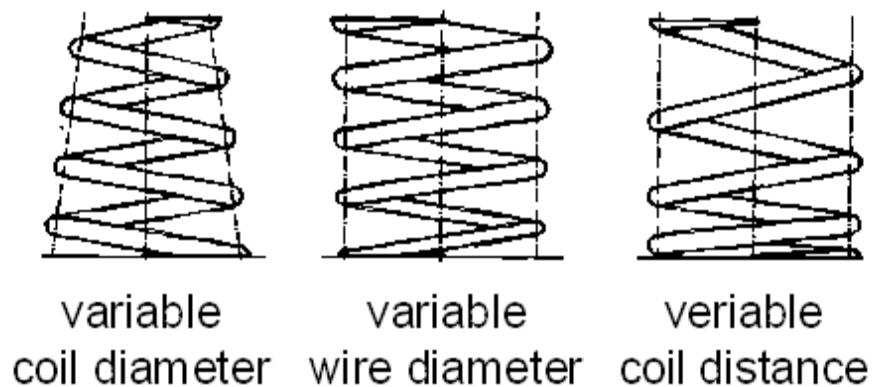


Fig. 1.3-11 Coil springs

This effect is based on the fact that an increasing spring load leads to some of the windings coming into contact each other, whereby the effective length l of the wound torsion bar shortens, see equation 1.3-22.

The combination of all three measures results in the so-called mini block spring, shown in Fig. 1.3-17. Apart from its progressive behavior, the low overall height of the mini-block spring is also an advantage, since the coils partially move into one another under a load.

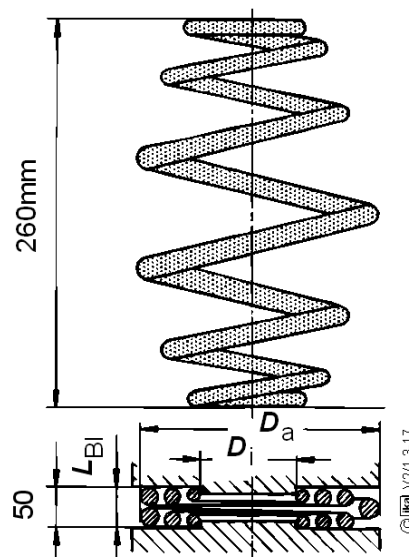


Fig. 1.3-17: Miniblock spring

Since coil springs can essentially withstand higher forces along their longitudinal axis in comparison with their transverse axis, they are used similar to torsion bars in combination with the struts of the wheel suspension, which support those components of forces which cannot be withstood by the springs, Fig. 1.3-18.

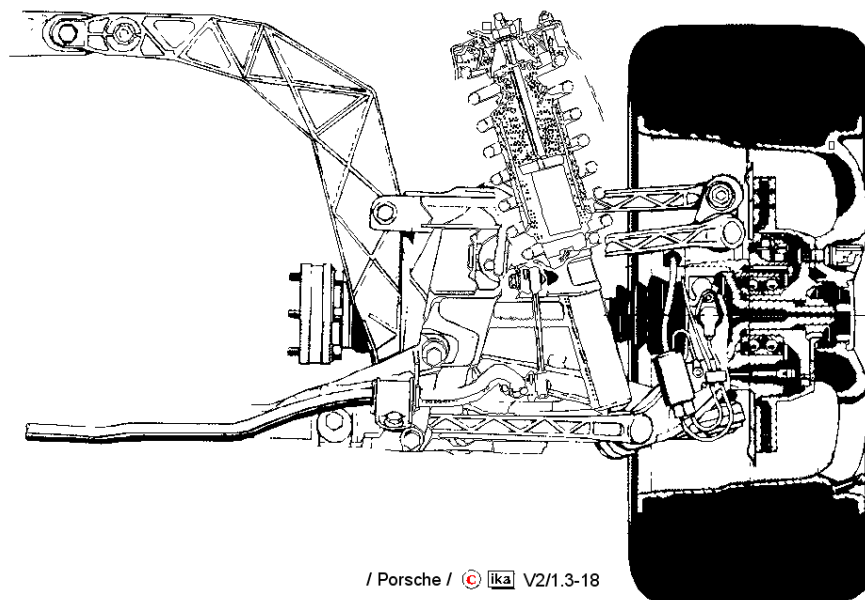


Fig. 1.3-18: LSA rear wheel suspension (Porsche 911 Carrera)

The spring is connected on the one hand with the body and on the other hand with the strut, on whose axle-side the wheel load acts as an external force.

Depending on the kinematics of the wheel suspension and the arrangement of the springs, the ratio i represents the relationship between the displacement of the body spring Δf and the displacement of the tire contact patch Δz_w in independent suspensions:

$$i = \frac{\Delta f}{\Delta z_w} \quad (1.3-23)$$

The spring ratio i is usually smaller than 1 and not constant, but changes depending on the instantaneous position of the transmission components of the wheel suspension, hence dependent on the instantaneous compressed condition.

The following state of equilibrium exists between the wheel load F_w and the spring load F_s for a leverage i

$$F_s = \frac{F_w}{i} \quad (1.3-24).$$

This way, the so-called wheel specific spring stiffness of an independent suspension for a specific state of compression can be determined.

$$\begin{aligned} c_{\text{radbezogen}} &= \frac{dF_w}{dz_w} = \frac{d(F_F \cdot i)}{dz_w} \\ &= \frac{dF_F}{dz_w} \cdot i + \frac{di}{dz_w} \cdot F_F \\ &= \frac{dF_F}{df} \cdot \frac{df}{dz_w} \cdot i + \frac{di}{dz_w} \cdot F_F \\ &= c \cdot i^2 + \frac{di}{dz_w} \cdot F_F \end{aligned} \quad (1.3-25)$$

A progressive characteristic of the suspension can also be obtained possibly by an appropriate configuration of the wheel suspension kinematics.

1.3.1.4 Gas Springs

In the springs considered so far, the working medium was solid and the spring absorbed energy as a result of deformation. In the springs considered in this paragraph however, the operating medium is gaseous and the spring absorbs energy through variation of volume. Fig. 1.3-19 shows the principle structure of an air spring.

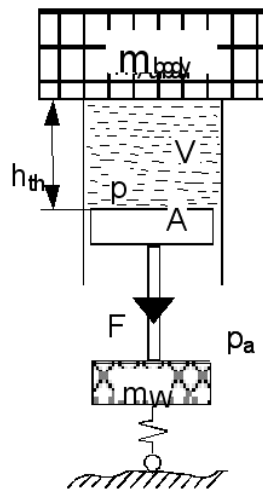


Fig. 1.3-19: Piston cylinder gas spring

The theoretical spring length h_{th} is a characteristic dimension which results from the quotient of the active volume V (inclusive of additional volume) and the effective surface area A affected by the gas pressure:

$$h_{th} = \frac{V}{A} \quad (1.3-26)$$

The spring force F is given by

$$F = (p - p_a) \cdot A \quad (1.3-27)$$

With: p : gas pressure

p_a : external pressure

Considering the gas equation $p \cdot v^n = \text{const.}$ with n as the polytropic exponent, the spring rigidity of an air spring can be calculated from the relation:

$$c(f) = \left. \frac{dF_F}{df} \right| \quad (1.3-28)$$

$$c(f) = A \cdot n \cdot p(f) \cdot \frac{1}{h_{th}} \quad ; \quad h_{th} = \frac{V(f)}{A} \quad (1.3-29)$$

The polytropic exponent is situated between $n=1$ (isothermal, slow spring movement) and $n=1.4$ (adiabatic, quick spring movement). Fig. 1.3-20 shows, that with finite h_{th} the spring action changes for both quasi-static (F_{stat}) and dynamic (F_{dyn}) movements.

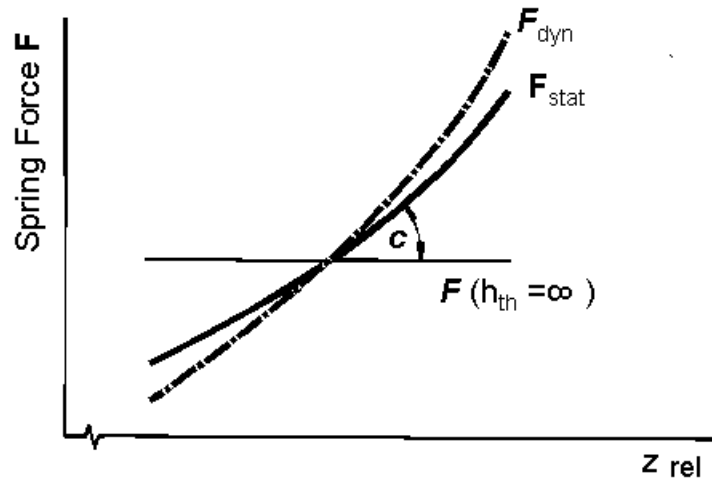


Fig. 1.3-20: Spring force in relation to the compression of a gas spring

The relation between variation of the spring force and the variation of the spring travel is defined by the spring stiffness c . As a reference value, a line for $h_{th} = \infty$, $c = 0$ is added. A low spring stiffness (low natural frequency) requires a large h_{th} , implying a large spring volume.

The oscillation of a mass m on an air spring results in the following natural frequency:

$$\omega_e = \sqrt{\frac{c}{m}} = \sqrt{\frac{c \cdot g}{(p - p_a) \cdot A}}$$

with equation 1.3-29 follows:

$$\omega_e = \sqrt{\frac{g \cdot n \cdot p}{h_{th} \cdot (p - p_a)}} \quad (1.3-30)$$

Considering a spring ratio i (simplified here as $di / dz_W = 0$), the equations 1.3-24 and 1.3-25 result in:

$$\omega_e = \sqrt{\frac{c_{wheel\ rel.}}{G_W / g}} = \sqrt{\frac{g \cdot n \cdot p}{h_{th} \cdot (p - p_a)}} \quad (1.3-31)$$

Assuming relatively small spring diameters: $p \gg p_a$. The equations for spring stiffness and natural frequency are simplified to:

$$c \approx \frac{g \cdot n \cdot m}{h_{th}} \quad ; \quad m \cdot g \approx p \cdot A$$

$$\omega_e = \sqrt{\frac{g \cdot n}{h_{th}}} \quad (1.3-32)$$

The theoretical piston-cylinder gas spring is used in motor vehicles only in a modified form. In practice, gas springs are differentiated into Hydropneumatic springs and Gas Bellows or U-Bellows.

- Hydropneumatic Spring

Hydropneumatic springs are used by Citroen in different cars, Fig. 1.3-21.

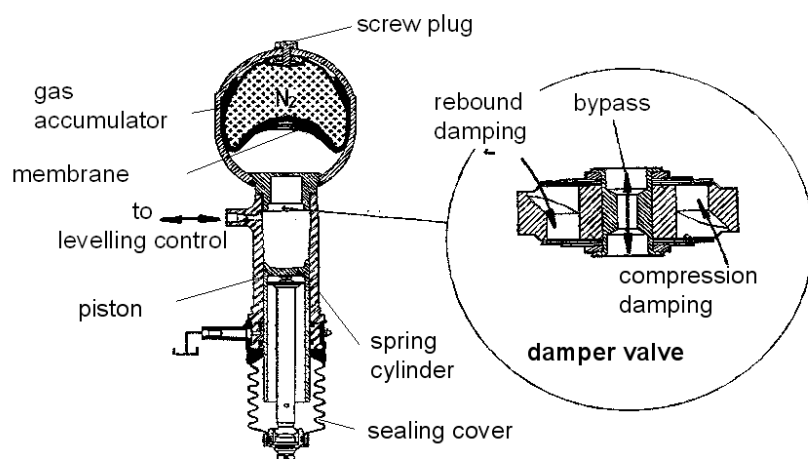


Fig. 1.3-21: Hydropneumatic spring (Citroen)

The spring action is transferred by a piston, first to a fluid and then to a gas. Fluid and gas are separated by an impermeable rubber membrane.

The presence of the fluid to a large extent permits a wear-free and low-friction sealing between piston and cylinder. Additionally, there is a possibility of providing the spring elements with an integrated hydraulic damper and a hydraulic level regulator. The hydropneumatic air spring with level control has the following characteristic:

Gas weight = const.

In hydro-pneumatic springs, the compression Δz as a result of an increased load can be balanced only by pumping fluid. The theoretical spring length is given by ($A \approx \text{const.}$):

$$h_{th} \approx h_{th1} - \Delta f \quad (1.3-33)$$

A change of the operating point of an air spring implies $n=1$. The Gas equation then simplifies to

$$p_1 \cdot V_1 = p \cdot V \quad \text{with} \quad A = \text{const.}$$

$$p_1 \cdot h_{th} = p \cdot (h_{th1} - \Delta f) \quad (1.3-34)$$

The spring stiffness of a hydropneumatic suspension follows from equation (1.3-29):

$$c(f) \approx A \cdot n \cdot p^2(f) \cdot \frac{1}{h_{th1} \cdot p_1} \quad (1.3-35)$$

As a result, the spring stiffness in this case increases with the square of the spring load (the body mass which has to be sprung):

$$\frac{c_{load}}{c_{empty}} > \frac{F_{load}}{F_{empty}} = \frac{m_{load}}{m_{empty}} \quad (1.3-36)$$

As a result of the compression-dependent decrease of h_{th} , the natural frequency of body oscillations increases with the increasing load.

Hydropneumatic spring elements are used predominantly on the rear axles of vans, station wagons and heavy limousines, since they enable effective level control. Also partially loaded systems are used in combination with steel springs (parallel connection), Fig. 1.3-22. The advantage of this combination consists in the fact that the natural frequencies of the two spring types can be tuned against each other leading to a suspension with an almost constant natural frequency.

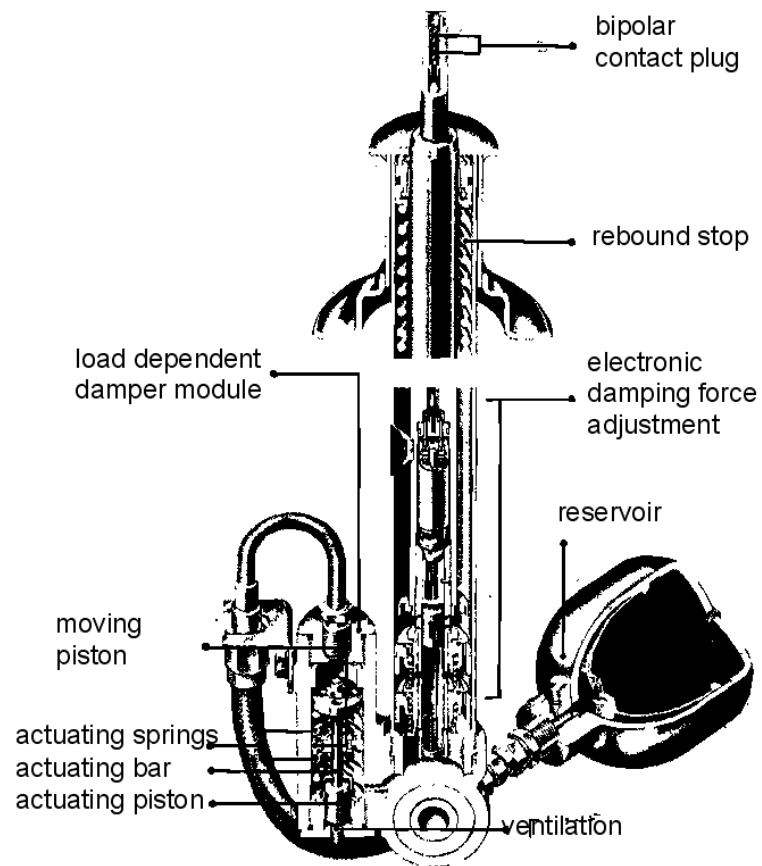


Fig. 1.3-22: Partially carrying spring cylinder with hydraulic level regulation and adjustable damping (Sachs)

- Gas Spring Bellows

Fig. 1.3-23 shows the two designs of bellows, the Convuluted Tube Gas Spring Bellow and the Rolling Lobe Gas Spring Bellow or U Bellows. Similar to a tire, the gas spring bellow is composed of rubber material reinforced by textile fabric.

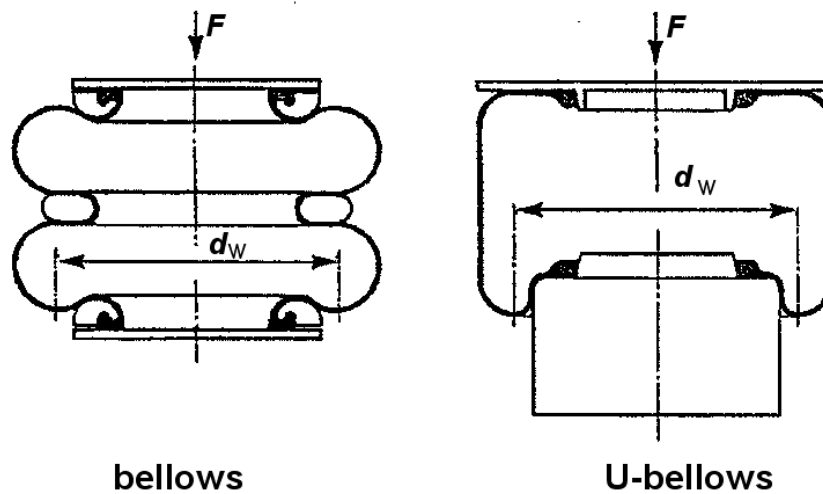


Fig. 1.3-23: Gas spring bellows

The cross-sectional area of the pneumatic spring exposed to the positive pressure, which produces a force on the vehicle structure, is called effective area of cross-section A_w . In contrast to the above mentioned hydropneumatic gas spring, the effective area of cross-section A_w of the gas spring bellows changes proportional to its travel. In Fig.1.3-23, the effective area of cross-section is represented by the effective diameter d_w for both designs.

The load carrying capacity of the spring is determined by the product of positive pressure and effective surface area. Particularly in the case of rolling lobe bellows, a possibility of direct influence is available since the effective cross-sectional area is determined by the external contour of the piston, Fig. 1.3-24 and Fig. 1.3-25.

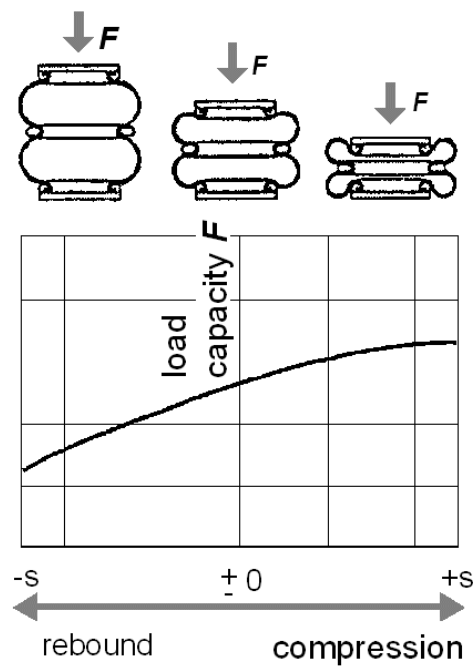


Fig. 1.3-24: Characteristics of the load capacity of an air spring bellow

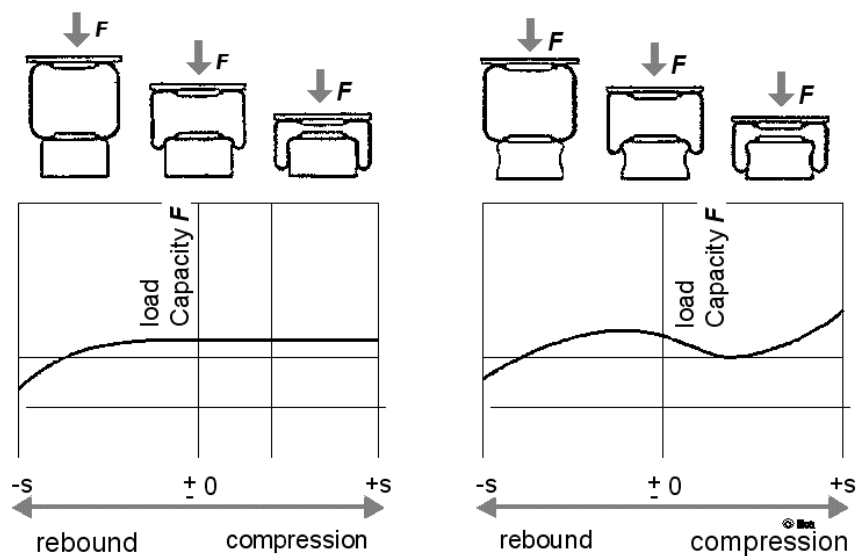


Fig. 1.3-25: Characteristics of air springs with u bellows

Further, it is possible to include an additional volume in the form of an air chamber (increase of h_{th}) in order to realise a less progressive spring rate.

Gas spring bellows also enable a level control of the vehicle body with increasing load. The static spring compression is balanced by the additional pumping of gas. Hence the

theoretical spring length h_{th} remains constant. The feature of a gas spring bellow with pneumatic regulation is hence given by:

Gas volume = const.

As a result, for the spring stiffness of a gas spring bellow is given by:

$$c(f) = A \cdot n \cdot p(f) \cdot \frac{1}{h_{th}} \quad (1.3-37)$$

In this case, the spring stiffness is directly proportional to the spring load:

$$\frac{c_{bel}}{c_{leer}} = \frac{F_{bel}}{F_{leer}} = \frac{m_{bel}}{m_{leer}} \quad (1.3-38)$$

As a consequence, the natural frequency of the body oscillation does not change here with load ($h_{th} = \text{const.} \Rightarrow \omega_e = \text{const.}$).

Gas springs (in most cases U-bellows) are mainly used in buses (fixed entrance height) and trucks (high pay-load in comparsion to unladen weight). A spring element with fully supported pneumatic U-type bellow for a passenger car is shown in Fig. 1.3-26.

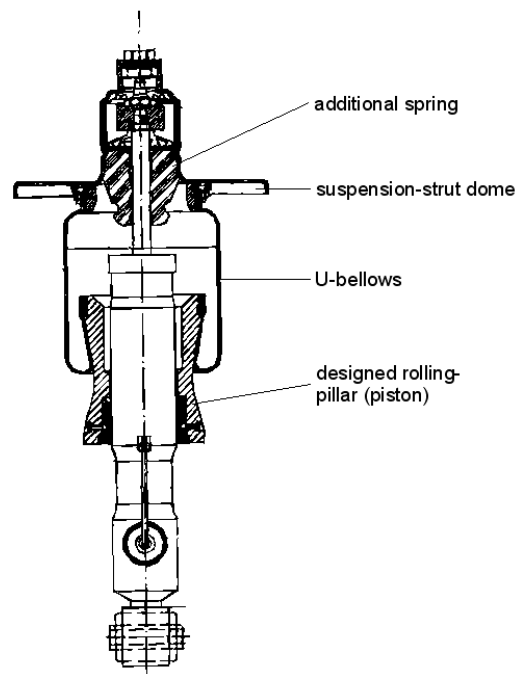


Fig. 1.3-26: Gas spring and damper unit with U-type bellow

Apart from level control, a stepless pneumatic damping adjustment is realised in this case (soft characteristic favourable for driving comfort, stiffer characteristic favourable for driving stability).

A defined contour of the rolling piston influences the spring characteristic by a variation of the effective surface area A_W . Additionally, the auxiliary spring (bumper) leads to a steep progressive behavior of the spring characteristic in compression.

The response of a pneumatic spring is influenced particularly by the orientation of the cord angle in the spring bellow. Clear improvements are noticed, when the load carrier is arranged axial to spring direction. However this cord orientation requires an external guidance of the pneumatic spring bellow realised in the form of a supporting tube, in order to be able to compensate tangential forces. A final overview of the most significant features of steel and pneumatic springs is given in figs. 1.3-27 and 28.

Steel Spring

1.) Driving Comfort (Fig. 1.3-27)

The driving comfort changes depending on load. The natural frequency is a measure of the driving comfort and is proportional to c/F and hence changes with const. spring stiffness c and variable load F .

2.) Total Spring Travel (Fig. 1.3-28)

The total spring travel results from the addition of the static and the dynamic compression:

$$s = s_{\text{stat}} + s_{\text{dyn}}$$

A steel spring cannot be dimensioned along a soft characteristic, since the total spring travel would be then be too large. The necessary space is not available in the wheel housing. The driving comfort however is directly proportional to the softness of the spring.

3.) Level Control

Due to static compression, a vehicle suspended on steel springs indicates different body level positions depending on load.

4.) Space Requirement

Modern designs of coil springs allow for an ever decreasing space requirement. The overall height is minimized to a small number of coil diameters by the use of spiral coil springs.

Air Spring

The driving comfort remains almost constant, independent of the load. With constant effective surface area, the natural frequency is proportional to p/p_0

The total spring travel is given by:

$$s_{\text{tat}} = s_{\text{dyn}}$$

The static spring travel is completely absent, since the load levelling system varies the air pressure in the springs depending upon the load condition, maintaining a constant body height. As a result, the pneumatic suspension can be dimensioned along a softer characteristic when compared to a steel spring suspension.

An air-sprung vehicle maintains a constant level due to the absence of static compression.

U-bellows always require additional components (covers and rolling pistons). In this case, the length of the rolling piston is proportional to half of the pneumatic spring's travel. The block dimension of the pneumatic spring corresponds to the height of its components.

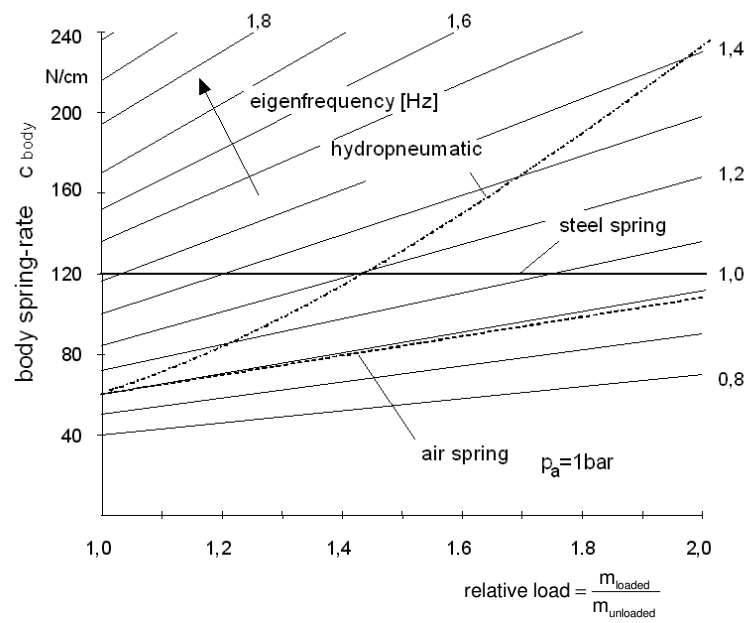


Fig 1.3-27: Natural frequencies of different suspension systems dependent on the additional load

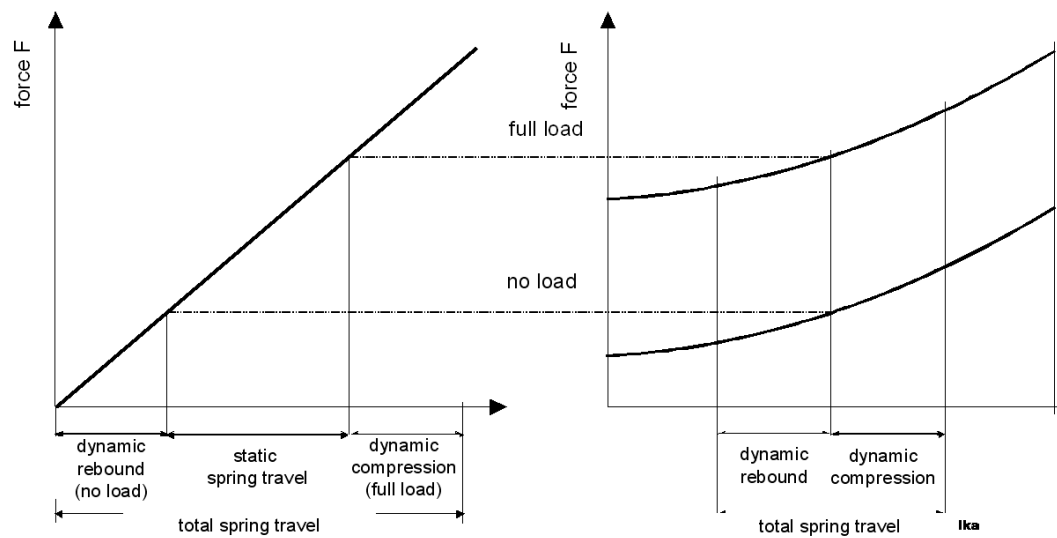


Fig 1.3-28: Differences between steel and air springs

1.3.2 Shock Absorbers

Shock absorbers serve both to guarantee driving safety of a vehicle as well as to optimise driving comfort (Fig. 1.3-29).

Driving safety is highly influenced by the road grip of the wheels. Oscillations of the wheel masses, which are also called unsprung masses together with the proportionate masses of the wheel suspension components, have to be minimised by damping, since they are suspended only on the tire spring but not on the vehicle body suspension ($c_R \gg c_A$).

A satisfactory driving comfort requires on the one hand, that the amplitudes of the body oscillations are small, and on the other hand, that the body accelerations which are induced by the damping forces are as small as possible. This implies the need for a rather weak damping.

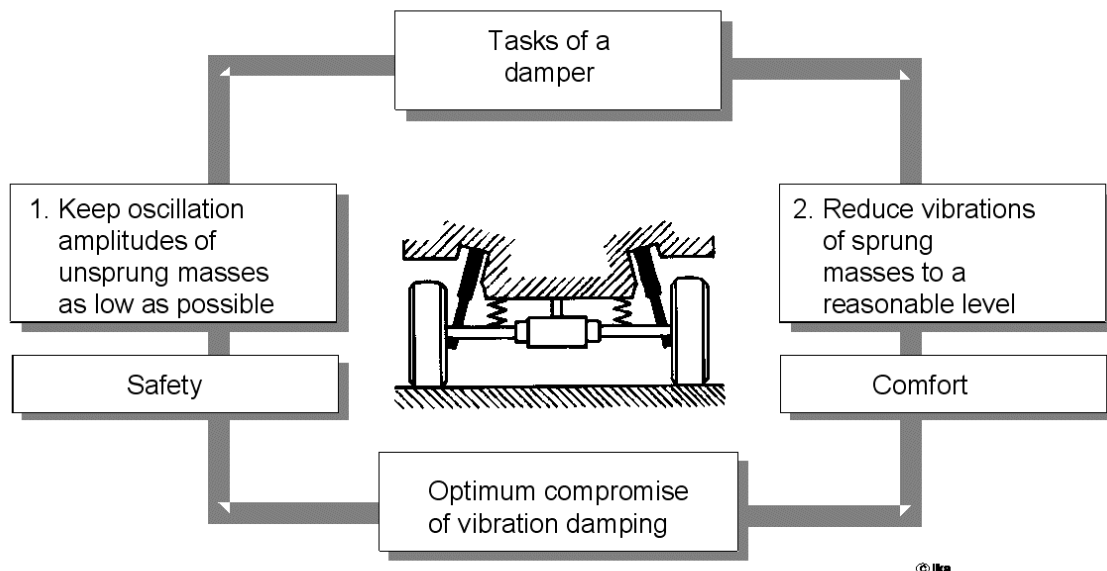


Fig. 1.3-29: Functions of the shock absorber

During the selection of a damper therefore a compromise between hard damping for safety and a soft damping for comfort has to be implemented.

Vibration dampers or shock absorbers differ basically in the type of friction, which causes the transformation of oscillation energy into heat, Fig. 1.3-30.

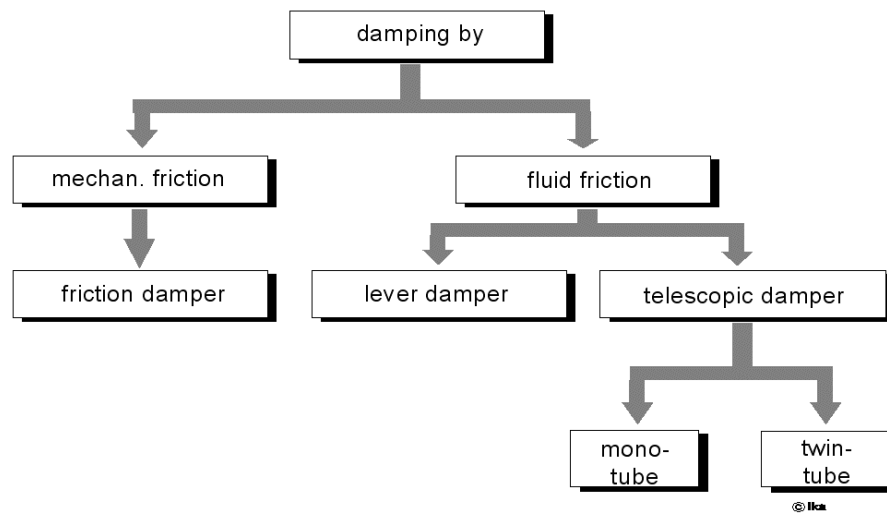


Fig. 1.3-30: Different damper designs

While shock absorbers of vehicles in the 20s and the 30s operated on mechanical friction, liquid dampers became generally accepted in the course of development, since the resulting exponential relationship between damping force and the spring rate allows for a better adaptation of the absorption characteristics to the vibratory vehicle system. It enables an asymmetrical configuration for rebound and compression with relatively ease. These dampers also predominantly show a better response (damper force application at very low compression velocities).

The first shock absorbers based on liquid friction were called the lever dampers. In these dampers, oil is forced through a valve by a piston which is displaced by a lever. The lever is often realised in the form of a transverse arm. This type of damper is rarely used nowadays. Telescopic shock absorbers are used almost exclusively today.

Apart from the absence of wearing parts such as levers, bearings and operating cams, these dampers are advantageous from the point of view of the possibility of more precise adjustments in damping in comparison to lever-type dampers. This is due to the fact that the spring travel and plunger lift mostly correspond. Due to the large plunger lift, the liquid recirculation is larger. The direct damper can hence operate with a much lower pressure (compared with the lever damper), which facilitates the design of the damper valves and has a favourable effect on its life span.

Telescopic dampers can be differentiated into mono tube and twin-tube dampers. Fig. 1.3-31 shows the configuration and principle of the two damper systems.

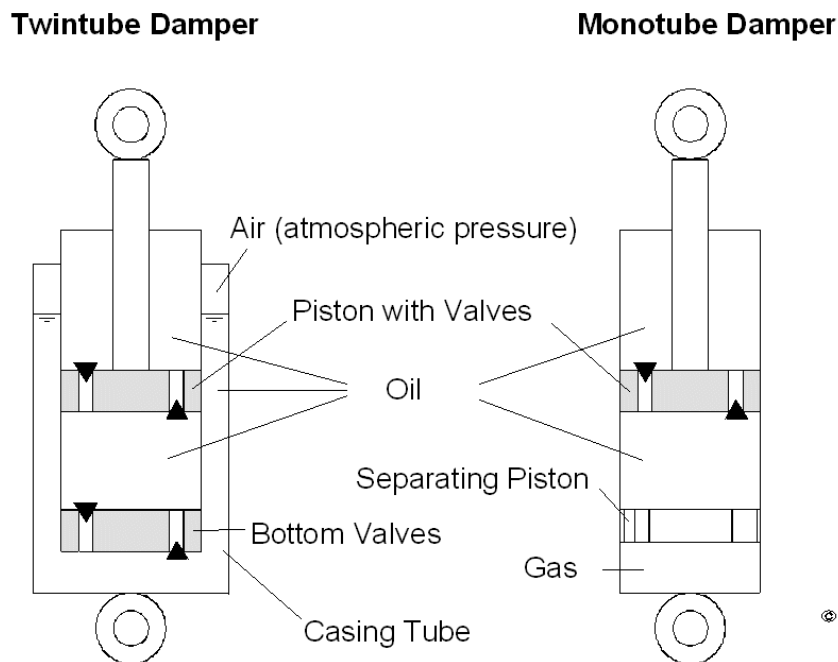


Fig. 1.3-31: General assembly of different damper designs

Both damper types include a piston consisting of throttle elements which travel in a cylinder filled with liquid by overcoming the flow resistance. The mechanical work absorbed is converted into heat and transferred to the environment over the external tube of the damper. If the damper surface is not large enough for heat dissipation, the surface must be enlarged. Otherwise the absorber would overheat, which could cause damage to the rubber parts.

In the conventional Twin Tube Damper, the liquid volume displaced by the immersing piston rod is transferred over the bottom valve into the casing tube which serves as the compensational volume and returns when the piston rod is withdrawn. At rest, the liquid pressure is equal to the ambient pressure.

In order to reduce cavitation at the valves, considerable damping work can be achieved by those oil flows, which are not drawn into an enlarging part of the working chamber.

During the compression of the twin-tube absorber, most of the damping work is done by the oil flow through the bottom valve into the casing tube as result of the intrusion of the piston rod. A second part of the oil flows into the upper part of the working chamber without any resistance.

On the other hand, during the rebound phase of the conventional twin-tube damper, the damping work is done by oil flow, which takes place through the piston valve from the upper part of the working chamber to the lower part. Accordingly, a resistance-free return of oil takes place from the compensating volume as a result of the returning piston rod.

In the Mono Tube Damper, the liquid volume displaced by the piston rod is compensated by the compression of a gas volume included in the damper. This gas volume when located above the surface of the oil, is separated from it by an impact plate, or by a dividing piston when the gas is placed below the oil surface in the damper.

The force exerted on the piston surface of the damper by gas pressure must be larger than the maximum damping force, since otherwise, the gas volume would be compressed by the sudden movement of the piston, while in the part of the damper working chamber facing the gas volume, the pressure would drop to 0 bar. The sudden reversal of the direction of the piston rod movement, would cause a brief breakdown of the damper and cavitation in the area around the piston valves. The gas pressure usually amounts to 30-40 bar. The gas pressure acting on the cross section of the piston rod results in a force which drives the piston rod outwards. This must be taken into consideration in the design of the body suspension.

The advantage of the twin tube damper is its cost and life span. The disadvantages include its tendency towards cavitation, unfavourable heat dissipation, its relatively large diameter and the fact that it can generally be installed only in the vertical position or at low inclinations.

The main disadvantage of the mono tube damper in comparison to the twin tube damper is the fact that the precision required in production makes it more expensive and its life span may be shorter because of the critical piston rod sealing.

- Design Examples

The constructional design of telescopic dampers are not only different from one manufacturer to another, but in addition also vary based on the targeted field of application.

Fig. 1.3-32 shows a telescopic damper designed according to the principle developed by De Carbon in the 40s where a dividing piston separates the gas volume from the oil in order to prevent the foaming of oil.

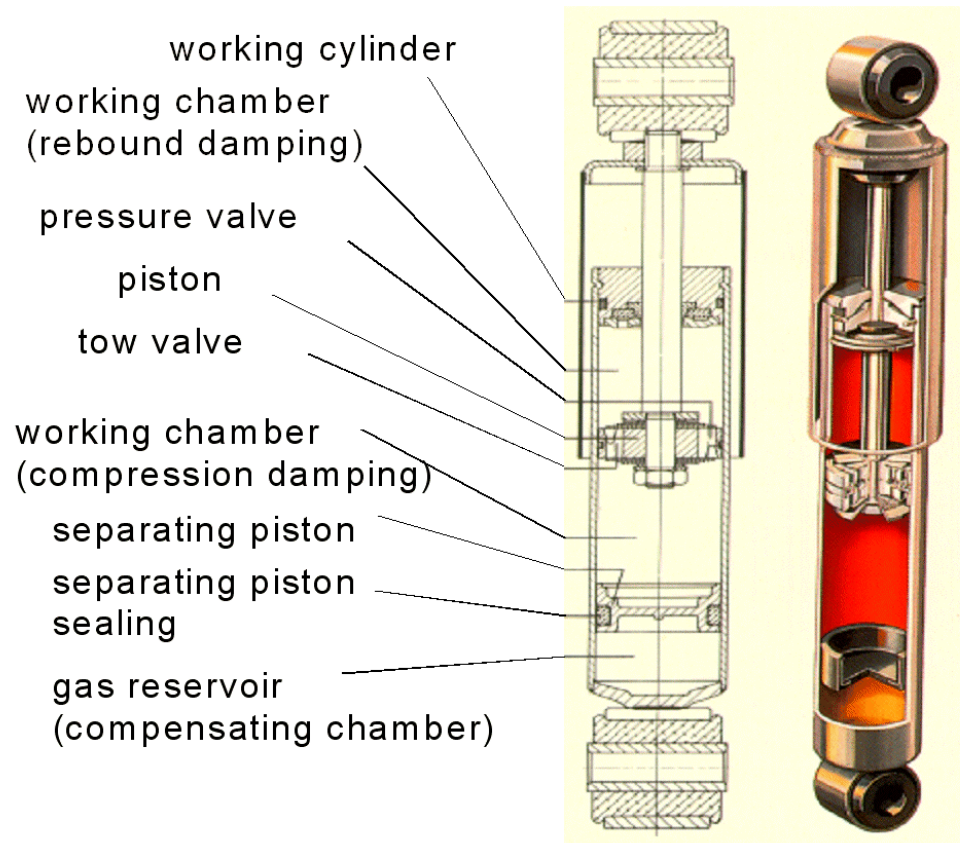


Fig. 1.3-32: Example of a mono tube absorber

This dividing piston allows for any arbitrary constructional length, but does not influence the function of the damper. The foaming of oil and gas can also be prevented by other measures. An impact disk for example, reduces the foaming of oil and gas, by deviating and decelerating the high speed oil jets escaping from the piston valves and rushing towards the cylinder wall.

A sectional view of the twin tube damper is shown in Fig. 1.3-33. The working volume, in which the piston moves, is completely filled with oil while the reserve volume between the working cylinder and the container pipe is filled with up to $2/3^{\text{rd}}$ its level by oil. This tube space serves as a compensating volume for the oil displaced by the immersing piston rod. The damping valves - valves at the base and piston valves - consist of a system of spring washers and valve bodies with throttle bores. The valves are held in position against the valve seat by a weak coil spring and also simultaneously function as non return valves.

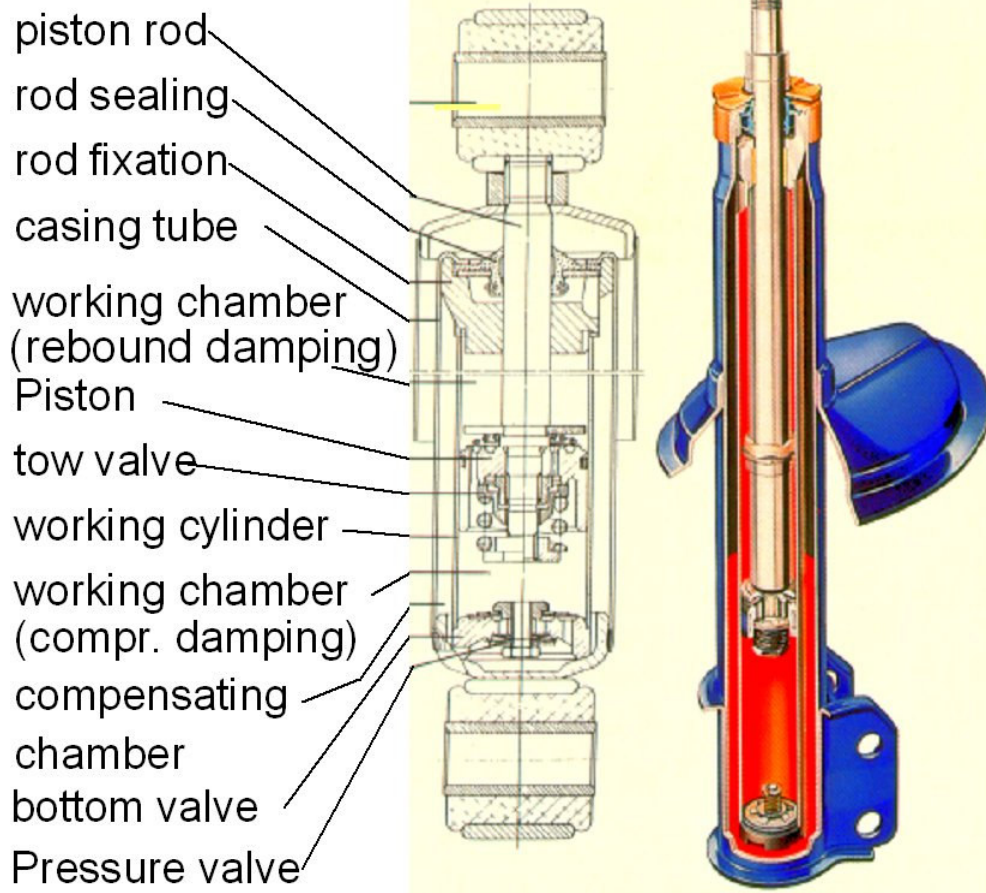


Fig. 1.3-33: Design of a twin tube absorber

The Gas Pressure Twin Tube Damper was developed specially for its application in suspension struts. With spring suspension and shock absorber strut wheel suspensions, the piston rod of the damper is not only used for the transfer of the damper forces, but also simultaneously for wheel guidance. In order to keep a deflection of the piston rod caused by the transverse forces within limits, large piston rod diameters (~ 25 mm) are necessary in comparison to dampers or spring carriers exclusively stressed by expansion and compression (~ 12 mm).

As a result of the larger rod diameters, during the inward and outward stroke of the piston rod, the oil volumes flowing from the working chamber into the compensating volume and vice versa are also correspondingly larger. This results in a larger risk of cavitation at the non return valves in the piston and base of the damper, which can lead to a brief failure of the damper. A significant improvement of the operational behavior of these dampers can be obtained if the oil reservoir is exposed to a relatively small gas pressure (usually 6-8 bar).

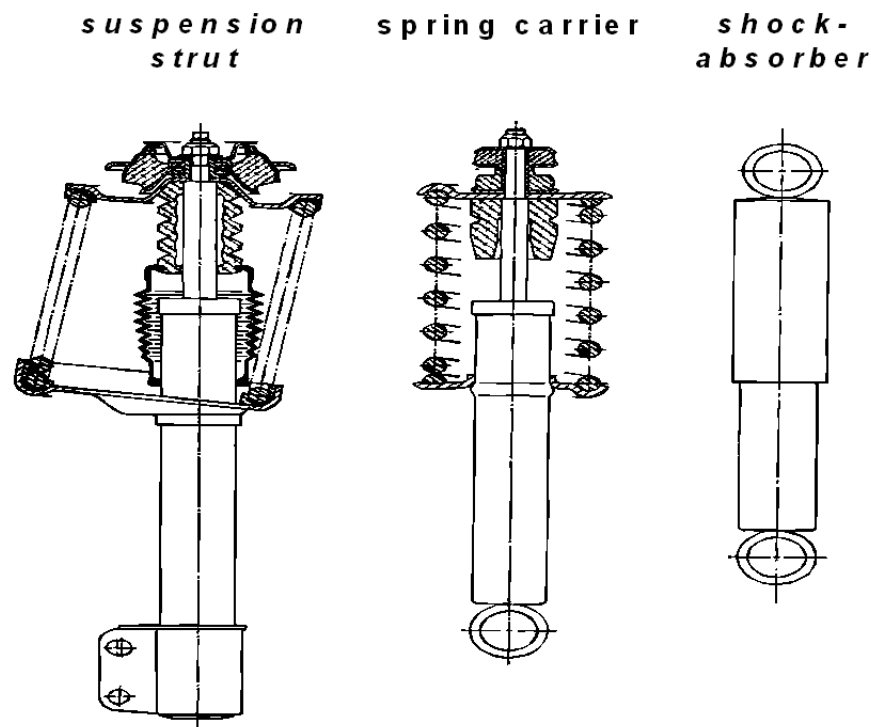


Fig. 1.3-34: Typical designs of absorbers

This way, a more precise operation of the damper can be achieved without having to accept the disadvantage of a mono tube damper, where the response of the damper is impaired by the clamping friction due to the piston rod seal which has to be dimensioned with high surface pressure resulting from the high internal pressure.

- Operating Behavior and Damper Characteristics

As previously mentioned, dampers today operate without exception based on hydraulics. The damping force F_D is a function of the compression velocity, and hence follows the relation:

$$F_D = -\text{sign}(\dot{z}_{\text{rel}}) \cdot k \cdot |\dot{z}_{\text{rel}}|^n \quad (1.3-39)$$

with :

n damping exponent

k damping factor

“sign (\dot{z}_{rel})” indicates the direction of the damper force. The damper characteristics describe the functional relation between the damping force and compression velocity. In order to determine the damping characteristics of a damper in application, the damping forces can be measured on a testing machine consisting of a thrust-crank mechanism of constant stroke

and varying test speeds, which produce different max. piston speeds in each case, Fig. 1.3-35.

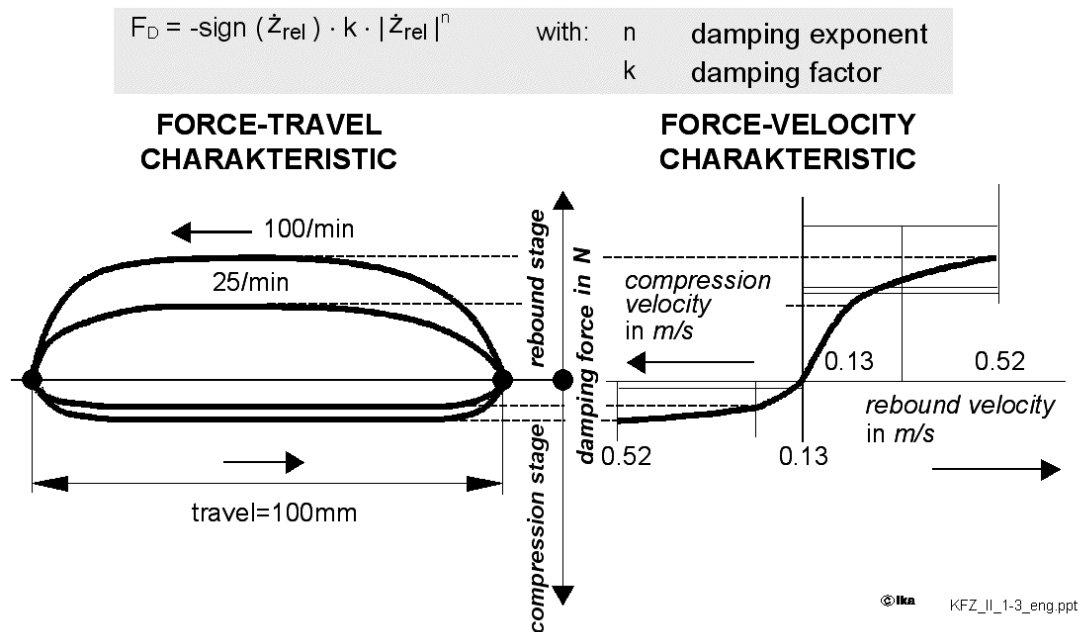


Fig. 1.3-35: Operational chart for damper operation in the determination of damper characteristics

In order to adjust the damper characteristics, the max. compressive and rebound forces are measured as functions of the max. piston speed.

The operating diagram and characteristic are closely associated. Fig. 1.3-36 shows the possible designs.

The degressive characteristic “3” has to be assigned to the operating diagram with the largest surface area, and hence the design indicates the highest mean damping. When compared to designs “1” and “2”, the gradient at the zero point is higher, implying a relatively large damping force at low piston speeds. This has an unfavourable effect on the damping capacity of the suspension for small road unevenness, which however brings certain advantages from the point of view of roll and pitch damping.

The progressive damping in “1” is advantageous since the forces around the zero point are small and hence favour smooth rolling comfort, even for hard tires. The piston forces, which significantly rise at higher piston speeds, cause an increase of wheel and body damping, which positively affects the contact to the ground on bad road surfaces.

The mean damping is lower than in the case of the degressive dimensioning “3”, as shown in the operating diagram.

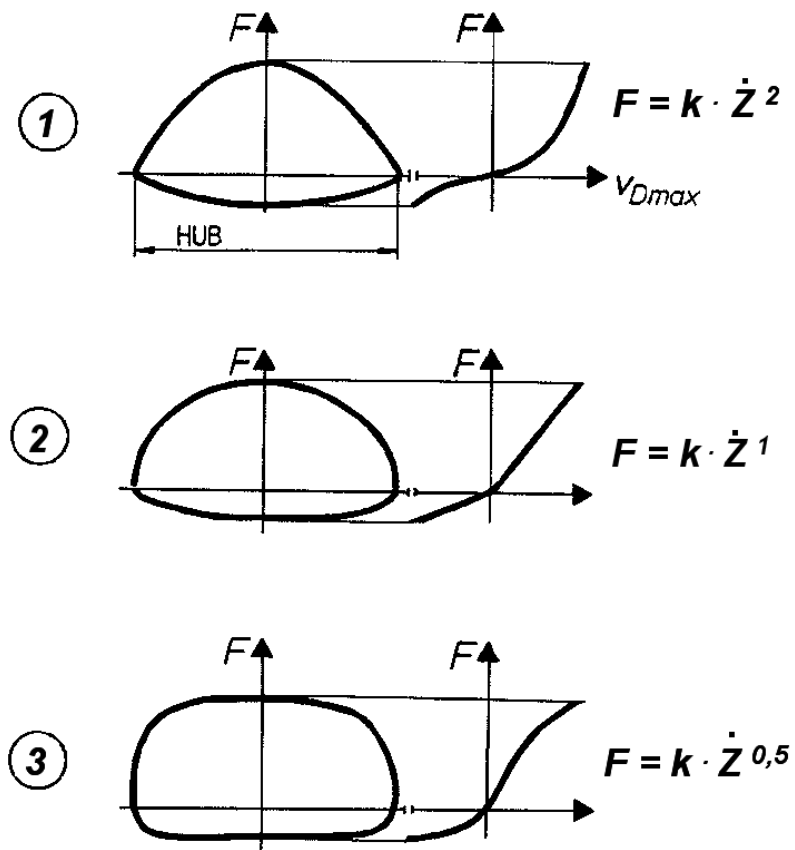


Fig. 1.3-36: Damper force depending on relative velocity at different damping coefficients

The relation between the expansion and compression stage is different depending on the manufacturer and the targeted application of the vehicle. Fig. 1.3-37 shows the influence of the damper layout on the wheel load fluctuations.

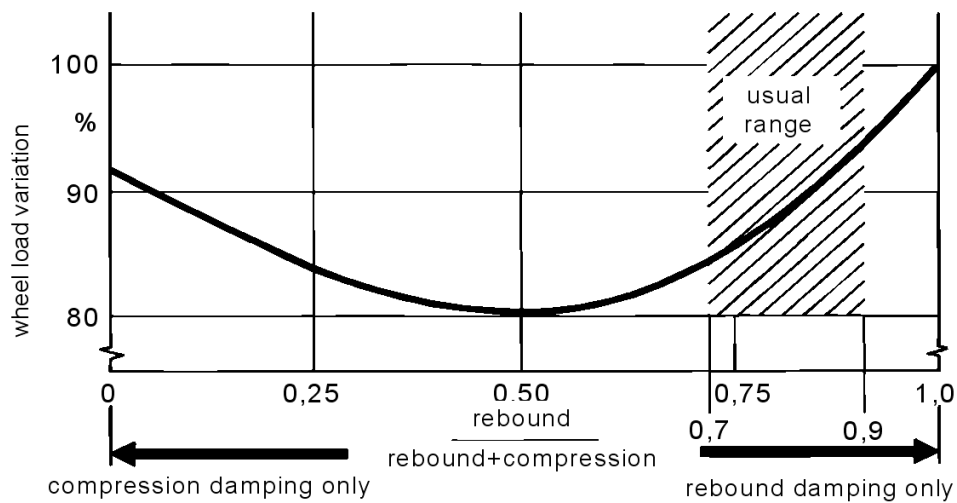


Fig. 1.3-37: Influence of damper layout on wheel load variation

A relation of 1 between rebound and compression stages ensures the quick fading away of axle oscillations. The wheel load fluctuations achieve a minimum at this setting, which implies a better road grip of the wheels. This layout is however not favourable from the point of view of suspension comfort.

Both the relation between rebound and compression stage as well as the absolute magnitude of the damping constant “k” are usually investigated based on tests. This way, an optimum damper design is determined for the spectrum of the possible load conditions of a vehicle over all possible road surfaces.

In order to reduce the conflicting aims between a high driving safety and max. attainable comfort as far as possible, some vehicles are provided with an adjustable chassis damping.

Fig. 1.3-38 shows a so-called double piston damper where the damping characteristics can be varied stepwise.

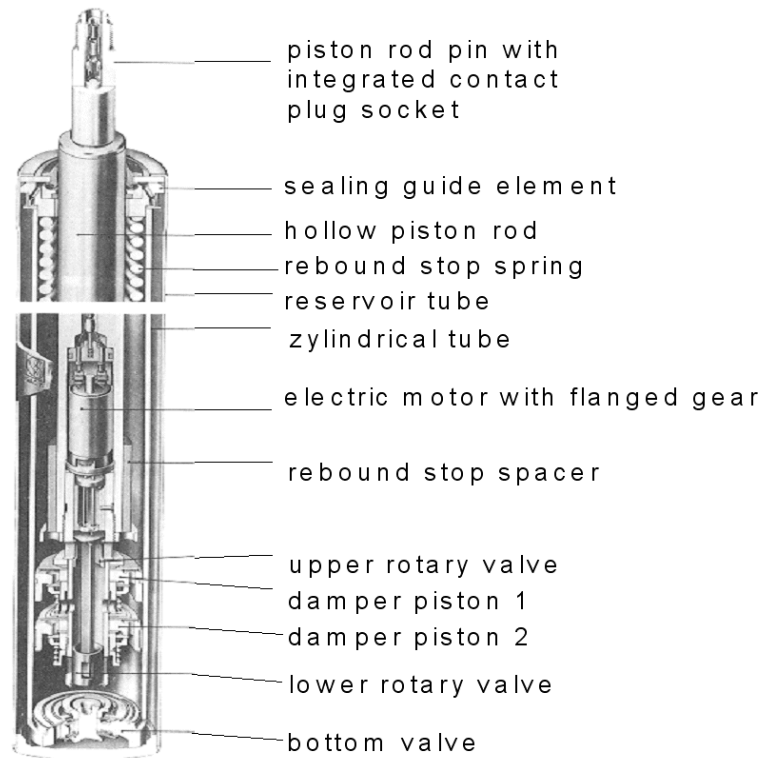


Fig. 1.3-38: Double piston damper with stepwise variable damper characteristics

The primary components include a coupled piston and a direct current motor located in the hollow piston rod. This motor actuates two rotary disks situated in the piston rod, which are both equipped with individual piston valves. This way, two independent characteristics can be realized as in Fig. 1.3-39. In order to make the adjustment effective both in the rebound and compression directions, a spring loaded check valve is assigned to each rotary valve for the rebound stage and a soft one for the compression stage.

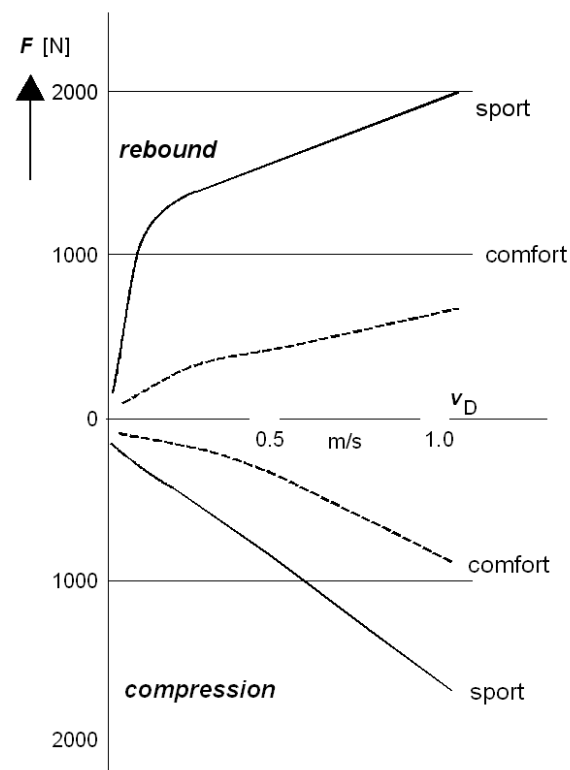


Fig. 1.3-39: Damper characteristics with the 'Sport' and 'Comfort' settings

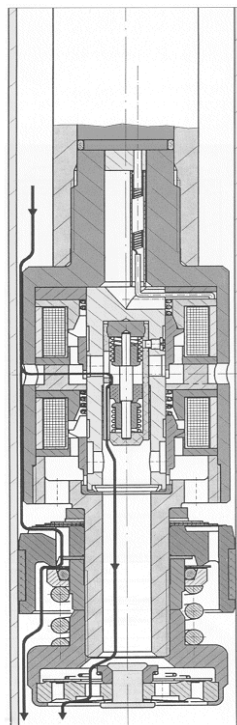


Fig. 1.3-40: Adjustable damper with internally operated valves

The adjustment times for the ADC-1 system are in a time range of 30-200 ms, which does not allow the system to react to single obstacles. Adjustable dampers with internally operated valves on the other hand, enable significantly shorter switching times (20-100 ms) and also a reaction to individual obstacles to a limited extent. Fig. 1.3-40 shows an adjustment system fully integrated into the damper. The control of the piston valves is performed by electromagnets (solenoid valves).

Steplessly adjustable absorbers without fixed characteristics which could be implemented by proportional valves, for example, are presently in the developmental stage.

1.3.3 Seats

Seats with spring cores originally serve only one function, 'cushioning'. The seat with a human occupant forms an oscillatory system, whose natural frequency is in the range of 2.5 – 5 Hz, depending on the spring rigidity of the upholstery, Fig. 1.3-41.

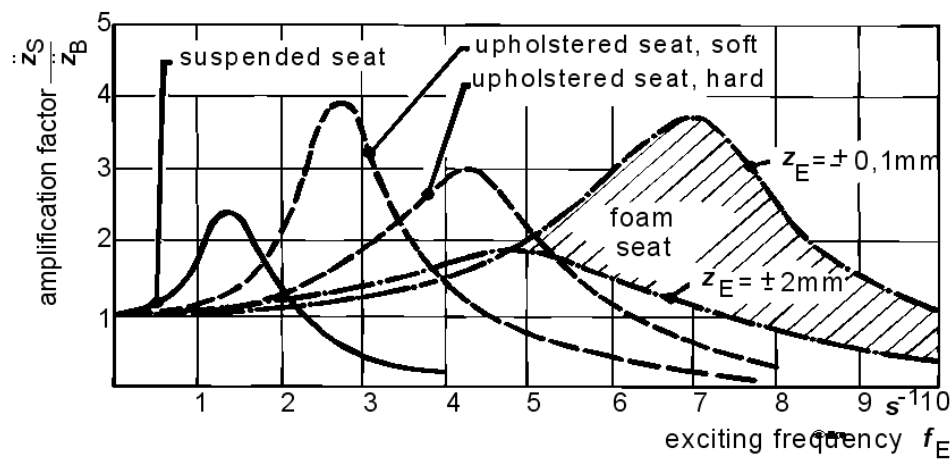


Fig. 1.3-41: Amplification functions of different vehicle seats

The location of the resonance peak between seat (\ddot{z}_S) and body acceleration (\ddot{z}_A) of $\frac{\ddot{z}_S}{\ddot{z}_A} > 3$ reduces the suspension comfort significantly, particularly, if the body natural frequency is high. This is the case in construction machines, agricultural tractors and to some extent in trucks, since body and seat resonances are close to each other. This problem can be overcome by the application of suspended seats, Fig. 1.3-42.



Fig. 1.3-42: Suspended seat

1.3.4 Evaluation of Oscillations by Humans

The quantitative evaluation of the oscillation comfort predetermines the effects of oscillations (and a reference test track). Serial investigations in this context have led to the guidelines VDI 2057 and ISO 2631. In these guidelines, a difference between the perception intensity and the duration of exposure exists.

- Intensity of Perception of a Seated Human

The human body represents an oscillatory system, which can be approximated by an equivalent system for humans seated in the vehicle according to Fig.1.3-43.

Humans are oscillatory systems themselves. Hence it is humanly impossible to evaluate the effects of oscillation based only by their intensity, rather one tends to perceive oscillations of the same intensity but of different frequencies differently. As a consequence, a frequency-dependent evaluation exists between the physically measured values and subjective perception, which is different for individual parts of the body and different directions of action.

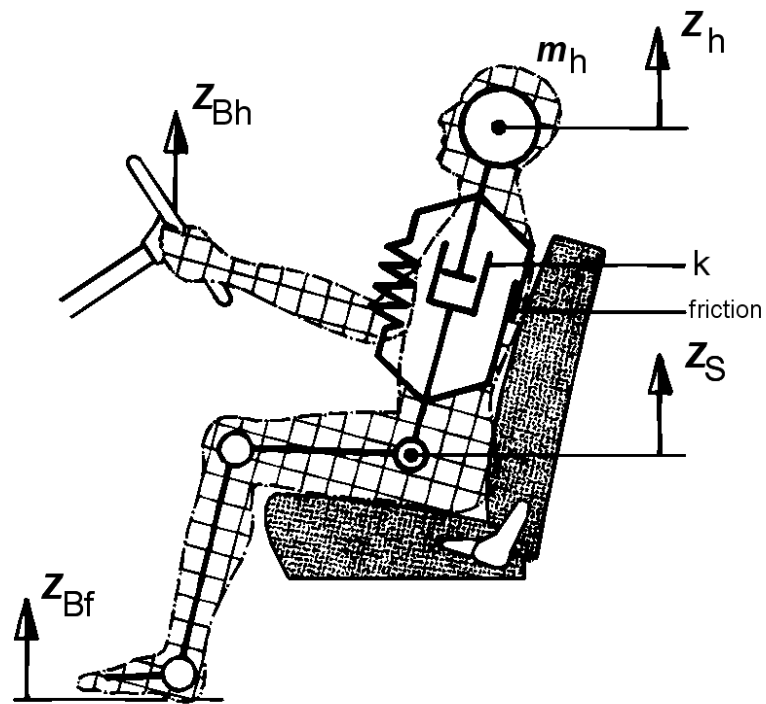


Fig. 1.3-43: Backup system of a seated person

If one considers at first only the excitation of the body by the seat and if the average friction R occurring in the cushion between back and backrest is added to the velocity-dependent damping, then the following results are given for this simple damped oscillator due to appropriate tests with different test persons:

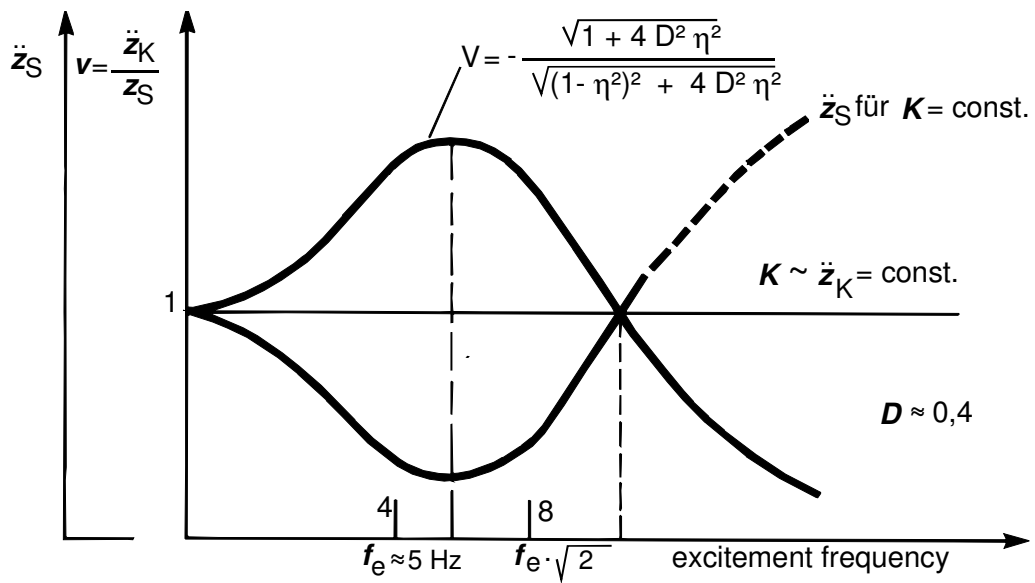
$$f_e \approx 5s - 1, D \approx 0,45$$

and the appropriate amplification function, see Fig. 1.3-44.

$$V = z_k(f)/z_s(f) \quad (1.3-40)$$

or, for sinusoidal vibration simulation:

$$V = \ddot{z}_k(f)/\ddot{z}_s(f) \quad (1.3-41)$$



© Ika KFZ_II_1-3_eng

Fig. 1.3-44: Amplification function of head acceleration during vertical excitation of seat

If the vertical acceleration of the head \ddot{z}_K is considered as a measure for the perception intensity, then the perception intensity:

$$K \approx \ddot{z}_K(f) = V(f) \cdot \ddot{z}_S(f) \quad (1.3-42)$$

considering the amplification function V for a simple oscillator:

$$K \approx \ddot{z}_S \cdot \frac{\sqrt{1 + 4 D^2 \eta^2}}{\sqrt{(1 - \eta^2)^2 + 4 D^2 \eta^2}} \quad (1.3-43)$$

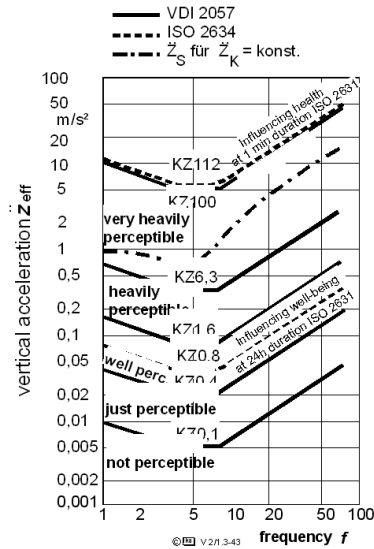
with: $\eta = \frac{f}{f_e}$

This entails the excitation $\ddot{z}_S(f)$, which leads to a constant perception intensity K^* :

$$\ddot{z}_S(f) \approx \frac{1}{V(f)} \quad (\text{for } K^* = \text{const.}) \quad (1.3-44)$$

Fig. 1.3-45 shows the curves of equal perception intensity determined for sitting and standing humans in the VDI specification 2057. For comparison, the reciprocal amplification function (eq. 1.3-44) is included.

The curves are divided into three areas, which were linearised for the simplification of the analysis.



Devision in three ranges:

$$1 < f < 4 \text{ Hz} : KZ = 10 \cdot \frac{\ddot{z}}{\text{m/s}^2} \cdot \sqrt{f/\text{Hz}}$$

$$4 < f < 8 \text{ Hz} : KZ = 20 \cdot \frac{\ddot{z}}{\text{m/s}^2}$$

$$8 < f < 80 \text{ Hz} : KZ = 160 \cdot \frac{\ddot{z}}{\text{m/s}^2} \cdot \frac{1}{f/\text{Hz}}$$

© Ika

KFZ_III_1-3_eng.ppt

Fig. 1.3-45: Curves of equal perception intensity KZ of sitting and standing humans according to VDI 2057 and ISO 2631.

Since all investigations done up to now show a correspondence to the fact that the perception of humans begins at approx. 0.8 to 1 Hz and ends at approx. 70 to 100 Hz, the curves are applied in a frequency range between 1 and 80 Hz. The first segment of the curve is from 1 to 4 Hz. Within this segment the KZ values are calculated as follows:

$$KZ = 10 \cdot \frac{\ddot{z}}{\text{m/s}^2} \cdot \sqrt{f/\text{Hz}} \quad (1.3-45)$$

With \ddot{z} as the effective value in a narrow frequency band Δf around the frequency f .

In the range between 4 and 8 Hz humans have the highest sensitivity to oscillation:

$$KZ = 20 \cdot \frac{\ddot{z}}{\text{m/s}^2} \quad (1.3-46)$$

Within the range between 8 and 80 Hz the KZ value is calculated as follows:

$$KZ = 160 \cdot \frac{\ddot{z}}{\text{m/s}^2} \cdot \frac{1}{f/\text{Hz}} \quad (1.3-47)$$

While the appearance of oscillation can be perceived immediately, the stress resulting from it depends not only on the intensity of the oscillation, but also on the duration of exposure. Fig. 1.3-46 shows the evaluated vibration intensities of equal intensities (effective value of vertical accelerations evaluated according to the equations 1.3-45 to 1.3-47) as a function of the duration of exposure based on the criteria 'well-being', 'performance' and 'health'.

As a consequence, durations of exposure between 1 and 10 minutes lead to the same stress. If the exposure continues for a longer time, the stress remains the same, if the square of the evaluated vibration intensity K decreases with respect to the exposure time t (Fig. 1.3-45 with double logarithmic scale)

A K -value of 20 is considered as a limiting value, which impairs the well-being of humans even when the exposure is limited to short durations. When exposed to the same stress for more than 1.5 hours, impairments of performance increase, and a daily duration of exposure of more than 4 hours can lead to a negative impact on health.

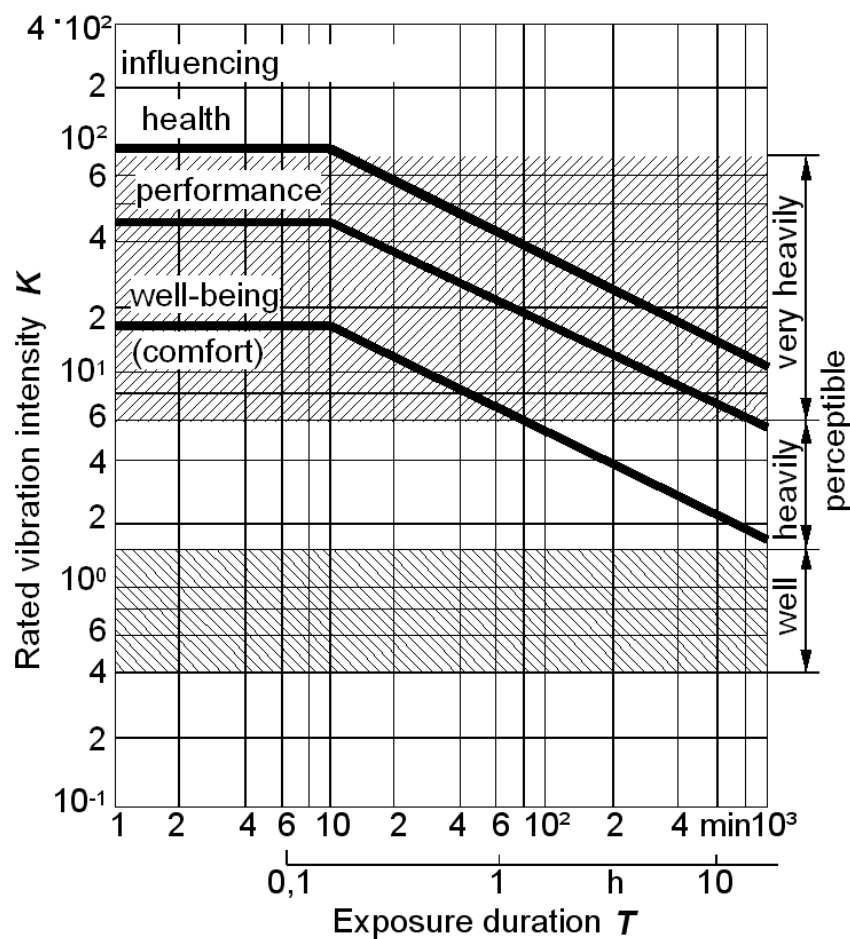


Fig. 1.3-46: Evaluated vibration of equal intensity as a function of the duration of exposure based on the criteria 'well-being', 'performance' and 'health'.

- Perception Intensity of Lying Humans

The effects of oscillation on lying humans is of special interest in long distance trucks with sleeping cabins or in ambulances and rescue cars. A huge number of test results already available point to the fact that, since oscillations have a direct effect on the head, the emerging accelerations here can be applied as a measure for the stress related to oscillation

of lying humans without weightage. The curves of equal perception intensity for lying humans prescribed in the VDI specification 2057 are given in Fig. 1.3-47.

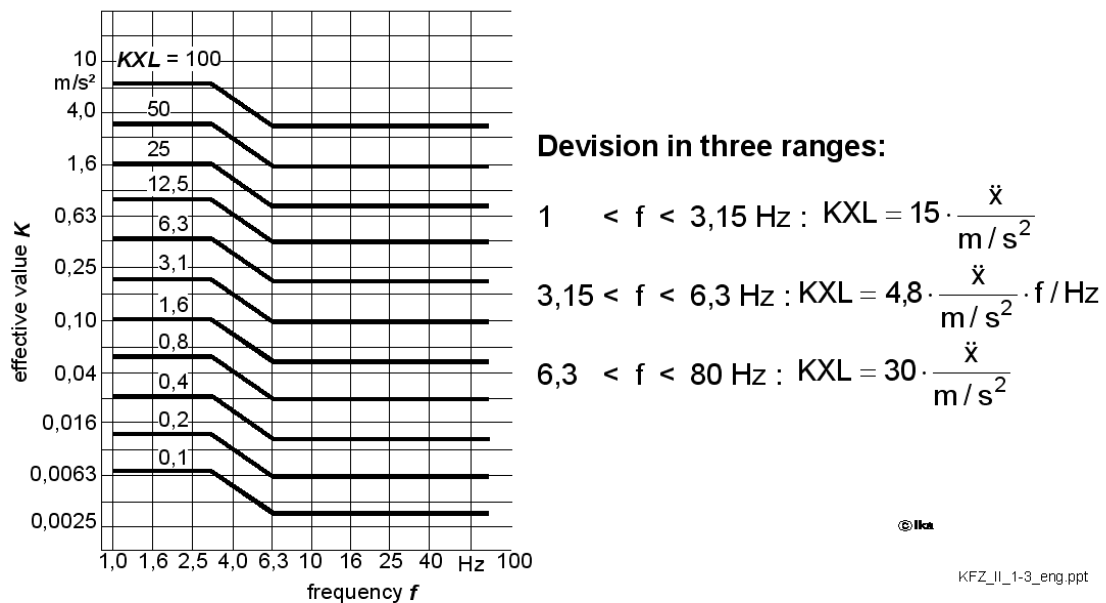


Fig. 1.3-47: Curves of equal perception intensity for lying humans based on VDI 2057

The frequency range is also divided into three ranges for exposure perpendicular to the direction of the spinal column:

$$1 \leq f \leq 3,15 \text{ Hz} \quad KXL = 15 \cdot \frac{\ddot{x}}{\text{m/s}^2} \quad (1.3-48)$$

$$3,15 \leq f \leq 6,3 \text{ Hz} \quad KXL = 4,8 \cdot \frac{\ddot{x}}{\text{m/s}^2} \cdot f / \text{Hz} \quad (1.3-49)$$

$$6,3 \leq f \leq 80 \text{ Hz} \quad KXL = 30 \cdot \frac{\ddot{x}}{\text{m/s}^2} \quad (1.3-50)$$

1.4 Single Wheel Suspension Model

To describe the vertical dynamics of motor vehicles, different mechanical models can be used. They vary from the simple single-mass system up to spatial vehicle oscillation models. In the following section, a few models are presented.

Of central importance to all model approaches is the model of the vertical tire characteristics, Fig.1.4-1.

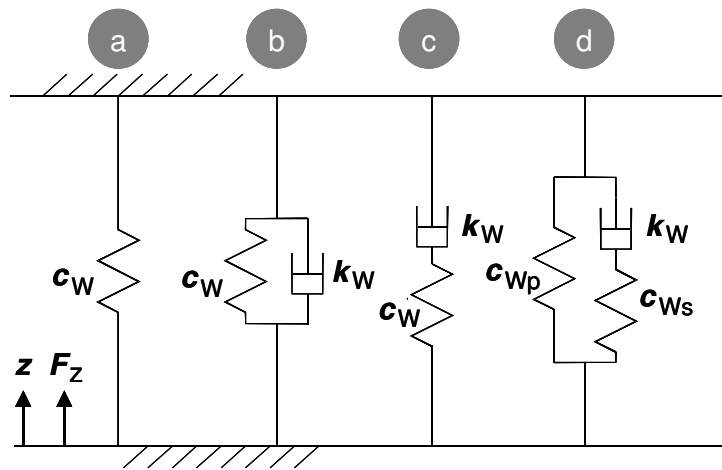


Fig.1.4-1: Tire models (vertical dynamics)

In the simplest case the tire can be modelled as a linear spring (a). The tire damping mentioned in chapter 1.3.1 is considered in the models after Voigt-Kelvin (b), Maxwell (c) and Gehmann (d).

Below, the four modeling approaches will be compared with regards to their dynamic behavior. For this purpose, the Laplace transformations

$$\text{Model a} \quad \frac{F_z(s)}{z(s)} = c_W \quad (1.4-1a)$$

$$\text{Model b} \quad \frac{F_z(s)}{z(s)} = c_W + k_W \cdot s \quad (1.4-1b)$$

$$\text{Model c} \quad \frac{F_z(s)}{z(s)} = \frac{k_W \cdot s}{1 + \frac{k_W}{c_W} \cdot s} \quad (1.4-1c)$$

Model d

$$\frac{F_z(s)}{z(s)} = \frac{c_{wp} + k_w \cdot \left(1 + \frac{c_{wp}}{c_{ws}}\right) \cdot s}{1 + \frac{k_w}{c_{ws}} \cdot s} \quad (1.4-1d)$$

of the four models are presented in the frequency domain.

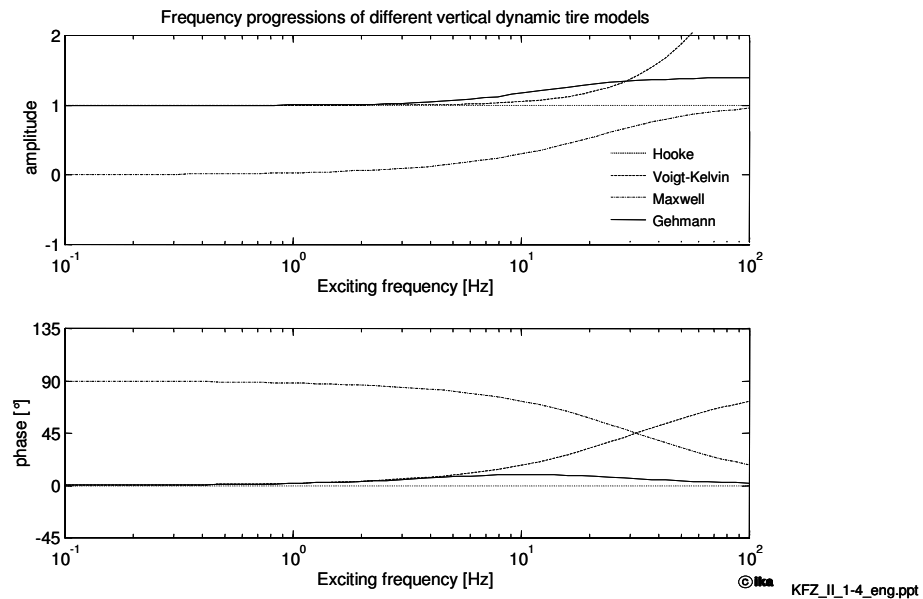


Fig.1.4-2: Frequency responses of the tire models according to Fig.1.4-1 (the amplitude response shows the normalised response z)

The behavior of Hooke's approach (a) expresses itself in a constant amplitude response without phase. In comparison, the tire models with damping elements (b)-(d), show frequency dependent responses, whereby it becomes evident that the Maxwell model is inapplicable as a tire model. The static spring rate disappears, while over the entire frequency range the standardised absolute value of the amplitude is smaller than unity.

The increase in dynamic spring stiffness, which takes place in rubber tires as the excitation frequency increases, can be simulated using the Voigt Kelvin (b) and Gehmann (d) models, as their respective amplitude responses show. As this stiffening transitions into saturation, the Gehmann model describes the tire behavior in a more realistic manner.

In chapter 1.3.1 (Fig. 1.3-5) it was shown that, when tires are at standstill (slow rolling), the tire damping decreases with increasing excitation frequency. This effect is also reproduced by model (d), as the phase response of the Gehmann model shows. At high frequencies the phase response of model (d) reduces to zero.

Overall, the Gehmann model provides the best approximation for the vertical-dynamic tire behavior. For fundamental investigations, as carried out in the following, the Voigt Kelvin model can also be used.

1.4.1 Single Mass Model

The simplest vehicle model is the single mass model as shown in Fig.1.4-3. The mass corresponds to the proportion of body mass, which acts on the wheel. The axle mass is connected as unsprung mass to the body. The task of the suspension - e.g. in construction machines or dumper trucks - is entirely taken over by the tire. Only the tire damping acts as a shock absorber.

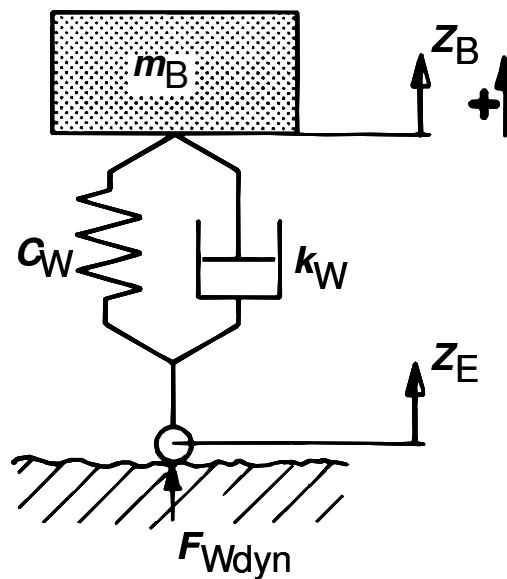


Fig.1.4-3: Single mass suspension model

The system is described by the following equation of motion:

$$m_B \cdot \ddot{z}_B = -k_W \cdot (\dot{z}_B - \dot{z}_E) - c_W \cdot (z_B - z_E) \quad (1.4-2)$$

$$\ddot{z}_B = -\frac{k_W}{m_B} \cdot (\dot{z}_B - \dot{z}_E) - \frac{c_W}{m_B} \cdot (z_B - z_E) \quad (1.4-3)$$

The natural frequency ω_e as well as Lehr's damping coefficient D can be derived by neglecting the base excitation z_E , i.e. by solving the homogeneous portion of this differential equation by means of the approach $z = z_0 \cdot e^{\omega t}$:

$$\omega_e = \sqrt{\frac{c_w}{m_B}} \quad \text{and} \quad D = \frac{k_w}{k_{krit}} = \frac{k_w}{2 \cdot m_B \cdot \omega_e} \quad (1.4-4)$$

Thereby the following correlation exists between undamped natural frequency ω_e , damped natural frequency $\omega_{e.m.D}$ and damping D :

$$\omega_{e.m.D.} = \omega_e \sqrt{1 - D^2} \quad (1.4-5)$$

To determine the motion of the body as well as the spring and damper forces during arbitrary excitation (e.g. a measured road surface profile) computers are most suitable, particularly when non-linear characteristics (e.g. tire lift off, deflected shock-absorber and spring characteristics) are to be considered.

If a sinusoidal wave is used (sinusoidal signal of constant amplitude and varied frequency) as an excitation signal, the amplification function can be determined from the peak values of body amplitude and excitation amplitude:

$$V(f) = \frac{z_B}{z_E} \quad (1.4-6)$$

Note: The amplification function z_B/z_E for the body amplitudes normalised to the excitation amplitudes is identical to the amplification function \ddot{z}_B/\ddot{z}_E for body acceleration normalised to the excitation accelerations, as follows from the double differentiation of a sinusoidal oscillation with the frequency $f = 2 \cdot \pi \cdot \omega$:

$$\ddot{z}_E(t) = -\omega^2 \cdot z_E(t)$$

$$\ddot{z}_B(t) = -\omega^2 \cdot z_B(t)$$

with

$$\frac{z_B(t)}{z_E(t)} = \frac{\ddot{z}_B(t)}{\ddot{z}_E(t)}$$

The amplification function of the single mass suspension model is shown in Fig.1.4-4 for tire data in as per paragraph 1.2.1.

Due to the negligible self damping behavior of the tires, a pronounced resonance peak occurs. The natural frequency – resulting from proportionate body and axle mass and the tire spring rate – which is approximately 3 - 4 Hz, is situated in a frequency range of high human sensitivity to vibration.

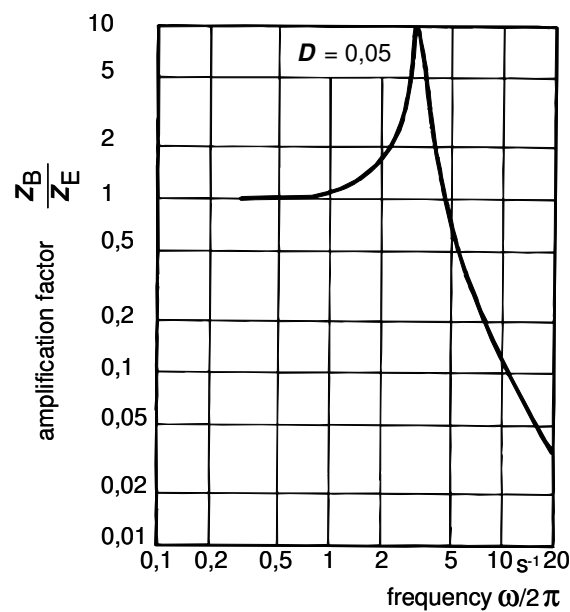


Fig.1.4-4: Amplification function of the single-mass suspension system

1.4.2 Dual-Mass Equivalent System

Conventional motor vehicles are not only suspended on tire springs (wheel) but also on body suspension. The simplest equivalent system, which nevertheless possesses essential features of a real vehicle suspension, is represented by the dual-mass equivalent system described below. It is derived by the reduction of a four-wheel vehicle, where the considered body mass is substituted by the proportion of the entire vehicle mass acting on the considered wheel. Among other things, the influence of mass coupling is neglected.

Fig. 1.4-5 shows the structure of a dual-mass equivalent system. The system consists of the proportional body mass, a wheel or axle mass, the body springs and dampers as well as the tire (wheel) suspension and damping.

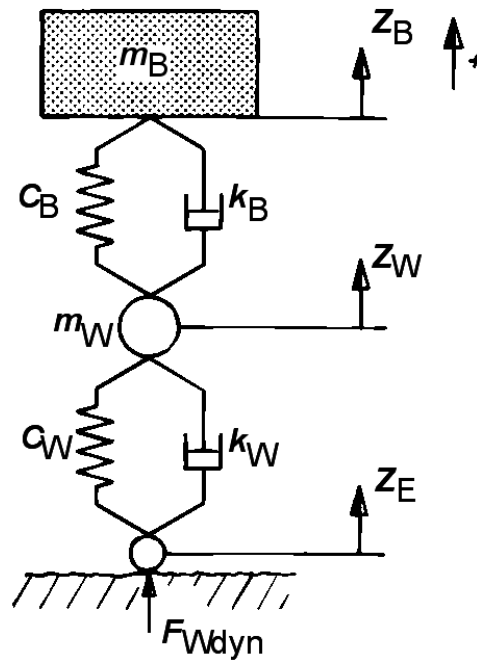


Fig. 1.4-5: Dual-mass suspension model

The differential equations describing the system result from the formulation of the force balance on body mass (equation 1.4-7) and wheel mass (equation 1.4-8):

$$m_B \cdot \ddot{z}_B = -k_B \cdot (\dot{z}_B - \dot{z}_W) - c_B \cdot (z_B - z_W) \quad (1.4-7)$$

$$m_W \cdot \ddot{z}_W = -k_B \cdot (\dot{z}_W - \dot{z}_B) - c_B \cdot (z_W - z_B) - k_W \cdot (\dot{z}_W - \dot{z}_E) - c_W \cdot (z_W - z_E) \quad (1.4-8)$$

These differential equations are coupled via body suspension or body damping. For *approximate* determination of the two natural angular frequencies ω_e and the damping values D , coupling of the two differential equations is to be neglected, so that only the homogenous parts of the differential equations are considered.

Hence, for a body mass m_A :

$$m_B \cdot \ddot{z}_B + k_B \cdot \dot{z}_B + c_B \cdot z_B = 0 \quad (1.4-9)$$

follows:

$$\omega_{eB} = \sqrt{\frac{c_B}{m_B}} \quad (1.4-10)$$

$$D_B = \frac{k_B}{2m_B \omega_{eB}} \quad (1.4-11)$$

for natural angular frequency ω_{eA} and damping D_A .

For the wheel mass m_W from :

$$m_W \cdot \ddot{z}_W + (k_W + k_B) \cdot \dot{z}_W + (c_W + c_B) \cdot z_W = 0 \quad (1.4-12)$$

follow natural angular frequency ω_{eR} and damping D at:

$$\omega_{eW} = \sqrt{\frac{c_W + c_B}{m_W}} \quad (1.4-13)$$

$$D_W = \frac{k_B + k_W}{2 m_W \omega_{eW}} = \frac{k_B + k_W}{2 \sqrt{m_W (c_W + c_B)}}$$

Furthermore, by setting up a force balance at the tire contact center and with using equations 1.4-6 and 1.4-7, an expression can be determined for the tire forces acting on the road, i.e. an equation for the dynamic wheel load $F_{W_{dyn}}$:

$$F_{W_{dyn}} = -k_W \cdot (\dot{z}_W - \dot{z}_E) - c_W \cdot (z_W - z_E) = m_B \cdot \ddot{z}_B + m_W \cdot \ddot{z}_W \quad (1.4-14)$$

Using this equation, a method of indirect measurement of dynamic wheel load can be derived through the measurement of body and wheel mass acceleration and known masses.

In the single-mass equivalent system, the amplification function was determined by means of a smooth sinusoidal excitation signal z_E acting on the system and calculation of the peak values of the body amplitude z_A . It is also possible to excite the system with the aid of a artificially generated road signal, so as to determine the magnification function. This method is demonstrated for the dual-mass equivalent system.

This method uses simulation to determine the spectral power density of body acceleration $\phi_{\ddot{z}_A}(\omega)$. The spectral density of the excitation amplitude $\phi_{z_E}(\omega)$ is determined by the road. It must be converted to the spectral density of the excitation acceleration $\phi_{\ddot{z}_E}(\omega)$. By the combination of power density and the quadratic mean value of the amplitude in the time domain

$$\bar{z}_E^2(t) = \int_0^\infty \Phi_{z_E}(\omega) d\omega \quad (1.4-15)$$

and the analogous relation for the exciting acceleration

$$\ddot{z}_E^2(t) = \int_0^\infty \Phi_{\ddot{z}_E}(\omega) d\omega \quad (1.4-16)$$

as well as from the interrelationship between exciting acceleration and exciting amplitude

$$\ddot{z}_E(t) = -\omega^2 \cdot z_E(t) \quad (1.4-17)$$

a relation between the power density spectrum of the

exciting amplitude and the exciting acceleration can be determined as follows:

$$\Phi_{\ddot{z}_E}(\omega) = \omega^4 \cdot \Phi_{z_E}(\omega) \quad (1.4-18)$$

The amplifying function V can then be determined on the basis of the following relationship:

$$V^2 = \frac{\left(\frac{\ddot{z}_B}{\ddot{z}_E} \right)^2}{\frac{\Phi_{\ddot{z}_B}(\omega)}{\Phi_{\ddot{z}_E}(\omega)}} \quad (1.4-19)$$

Fig. 1.4-6 illustrates above relationships.

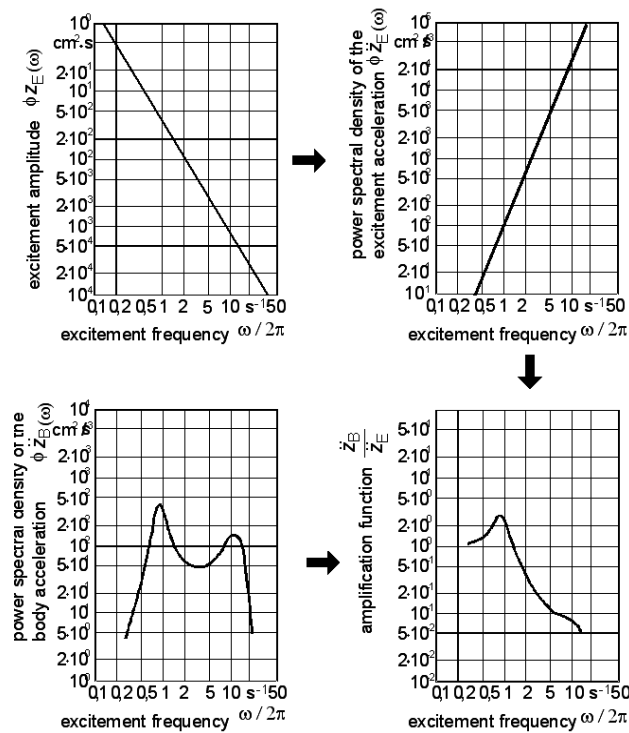


Fig. 1.4-6: Determination of the magnification function \ddot{z}_B / \ddot{z}_E on the basis of the spectral density of the body acceleration $\phi_{\ddot{z}_B}(\omega)$ and the spectral density of the excitation amplitude $\phi_{z_E}(\omega)$

With the help of the relationships explained above, the influence of various roads (degree of unevenness $\phi_h(\Omega_0)$ and undulations w) on the spectral density of body acceleration $\phi_{z_A}(\omega)$ can be discussed.

For example, a road with a very high proportion of short-wave excitations (low undulations w) would, on the basis of equation 1.4-17, result in a high density of the excitation acceleration in the range of high frequencies. This again would on the one hand accentuate the resonance peak in the range of the wheel natural frequency ($f_{nW} \approx 12 \text{ Hz}$) and on the other attenuate the resonance peak in the range of the body natural frequency ($f_{nB} \approx 1 \text{ Hz}$).

Analogous to the amplification function for body amplitudes, a magnification function for the dynamic wheel load fluctuations relating to the exciting amplitudes $F_{W,dyn} / z_E$ can be determined. This magnification function is given here as a standard value for the static wheel load $F_{W,stat}$ (Fig. 1.4-7). It follows directly from the spectral density of the exciting amplitude $\phi_{z_E}(\omega)$:

$$V^2 = \left(\frac{F_{W,dyn}}{F_{W,stat} \cdot z_E} \right)^2 = \frac{\phi_{F_{R,dyn}/F_{R,stat}}(\omega)}{\phi_{z_E}(\omega)} \quad (1.4-20)$$

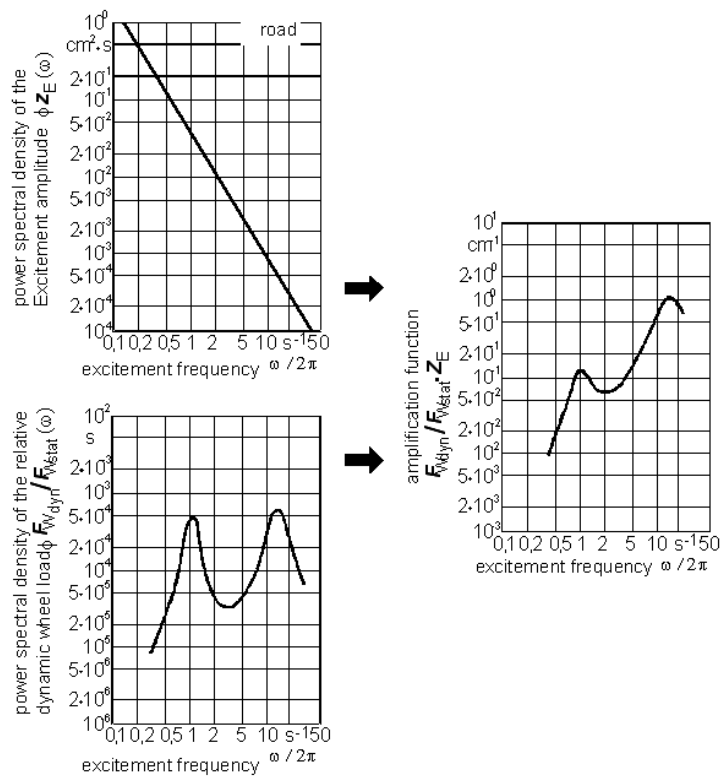


Fig. 1.4-7: Determination of the magnification function $F_{R_{dyn}} / (F_{R_{stat}} \cdot Z_E)$ from the spectral density of excitation amplitude $\phi_{Z_E}(\omega)$ and dynamic wheel load $\phi_{F_{R_{dyn}}/F_{R_{stat}}}(\omega)$

1.4.2.1 Parametric Study - Automobile Suspension

In the following section, the effects of modifying the essential parameters of the dual-mass model on the body acceleration are investigated. Even without a human evaluation of the seat suspension and vibration, this investigation can be considered as a rough assessment criterion for the suspension comfort and relative (specific) dynamic wheel load, i. e. road grip of the wheels (driving safety).

The equations of vibrations for the dual-mass model, equation 1.4-7 and equation 1.4-8, are constructed in MATLAB and excited by an artificially generated road signal. On the basis of the simulation results, the spectral power densities of body acceleration and dynamic wheel load are determined. The road signal used for simulation is shown in Fig. 1.4-8 as displacement-time function as well as time-frequency-dependent power density.

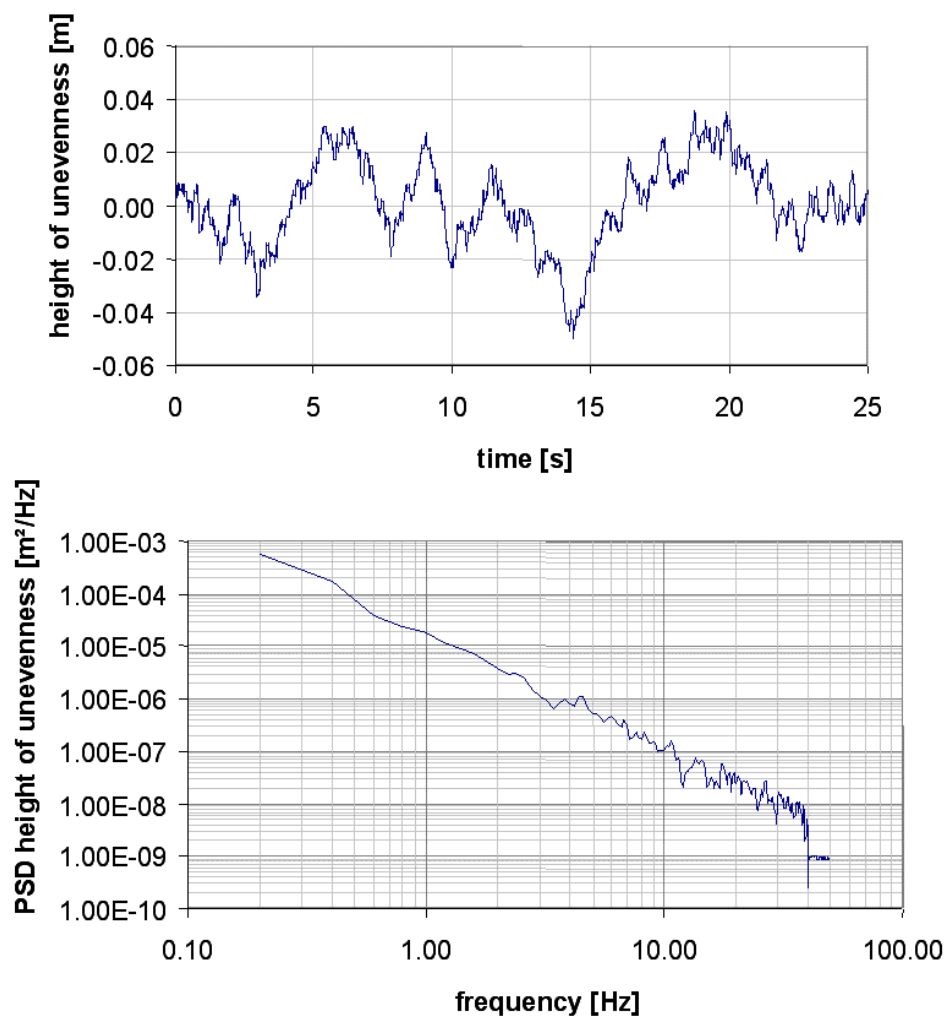


Fig. 1.4-8: Synthetically generated road signal with $w = 2.14$ and $\phi_h(\Omega_0) = 3.7 \cdot 10^{-6} \text{ m}^3$

The initial model consists of a quarter vehicle with the following parameters:

$$c_W = 150,000 \text{ N/m}; \quad c_B = 21,000 \text{ N/m}; \quad k_W = 100 \text{ Ns/m}; \quad k_B = 1500 \text{ Ns/m}; \quad m_W = 40 \text{ kg}; \\ m_B = 400 \text{ kg}$$

Fig. 1.4-9 shows the effects of the road signal in Fig. 1.4-8 on the vertical displacements, velocities and accelerations of the wheel and body. Damping and reduction of the motion parameters between road and body can be clearly seen. For better understanding, the curves for body and wheel have been vertically displaced.

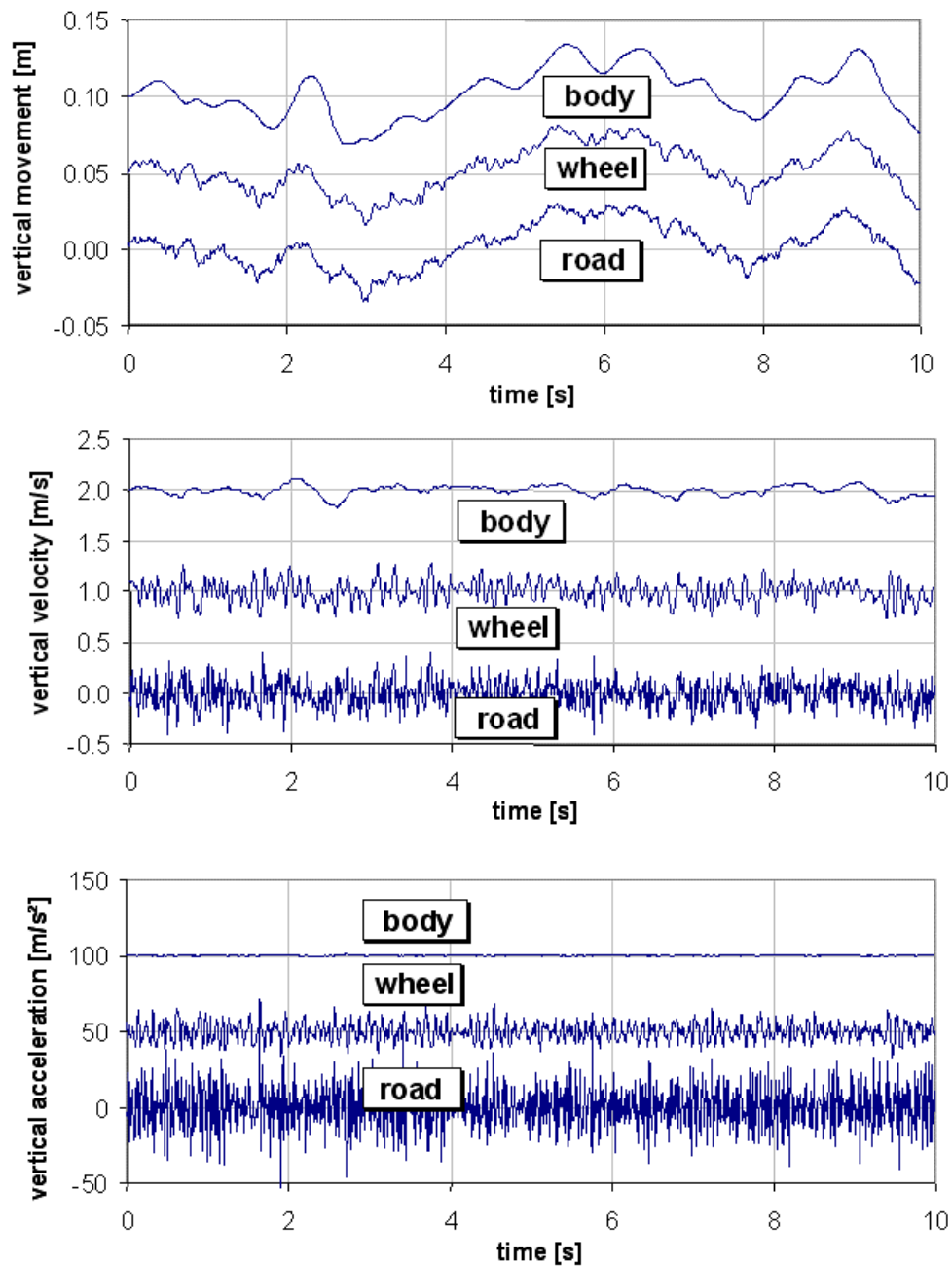


Fig. 1.4-9: Vertical motion, speed and acceleration of road, wheel and body

- Variation of the Wheel Mass m_w

In Fig. 1.4-10 the wheel mass is varied first. In reference to the body resonance, this has neither an effect on the position of the body natural frequency nor on its intensity.

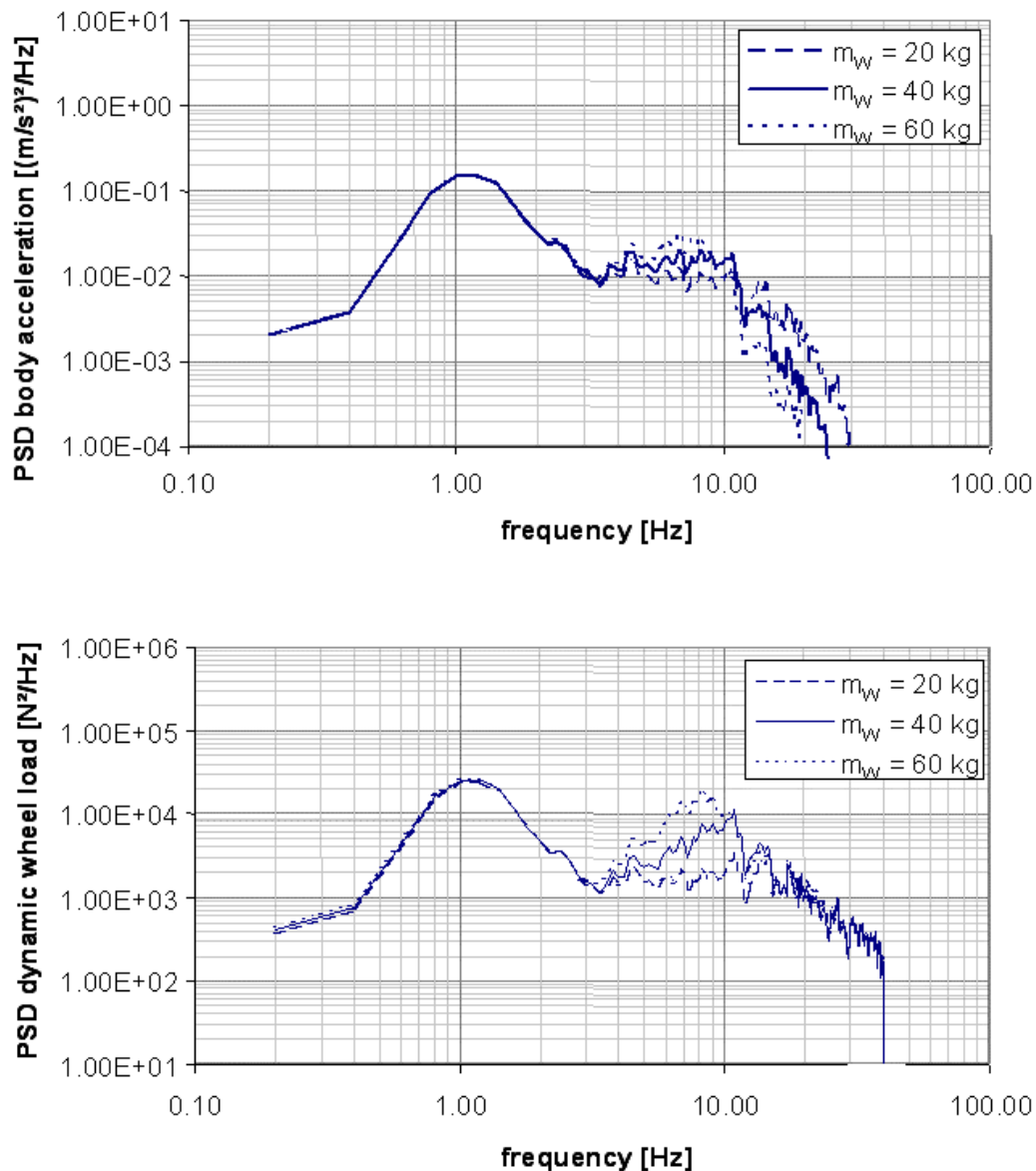


Fig. 1.4-10: Parameter variation with varying wheel mass

In reference to wheel resonance however, a clear increase in the (specific) dynamic wheel load fluctuations is noticeable as a result of the increased wheel mass. This is due to the fact that a larger mass has to be stabilized by unchanged dampers. Consequently, as small a wheel mass as possible is to be aimed at with respect to the dynamic wheel load fluctuations, and hence with regard to driving safety.

- Variation of the Spring Stiffness of the Tire (tire spring rate) c_w

In Fig. 1.4-11 the spring rate of the tire is varied. A softer tire rate tends to reduce wheel natural frequency and the dynamic wheel loads, i.e. road grip is improved. Softer tires would

thus clearly improve driving safety. Realization of such tires is however, only possible within narrow limits due to the associated increase in rolling resistance and flexing energy.

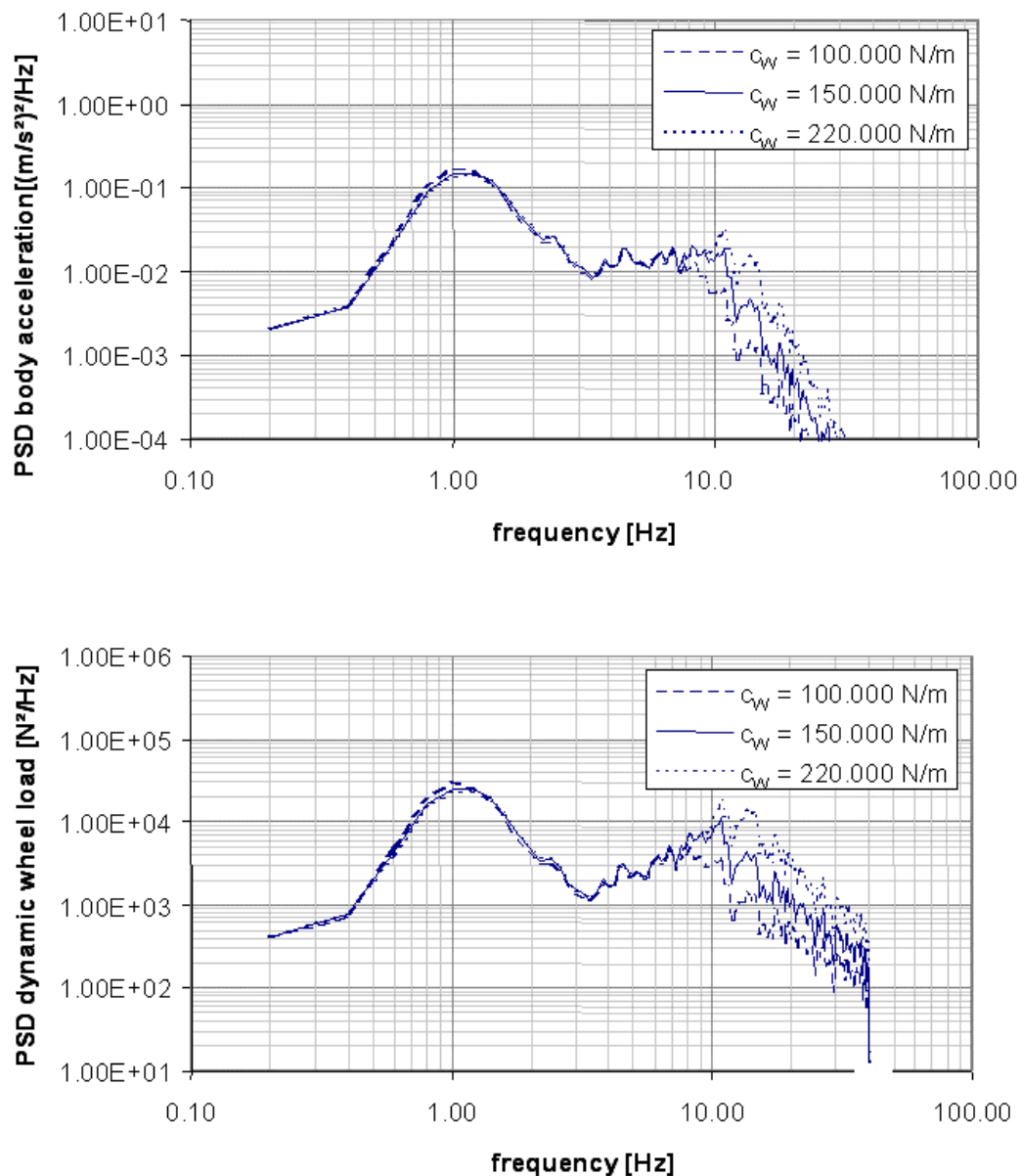


Fig. 1.4-11: Parameter variation with varying stiffness/spring rate of the tire

- Variation of the Spring Stiffness of Body Suspension c_B

In Fig. 1.4-12 the spring rate of the body suspension is varied. A softer body suspension rate reduces body natural frequency while the relative damping increases as a result. Body acceleration and dynamic wheel load fluctuations are reduced.

A softer body suspension rate would thus have a positive effect on driving safety and ride comfort. This can only be realized to a limited extent due to the negative effects of soft springs on body roll during cornering and brake dive. Softer springs would also mean considerable changes in ride height depending on load and the need for considerable spring travels.

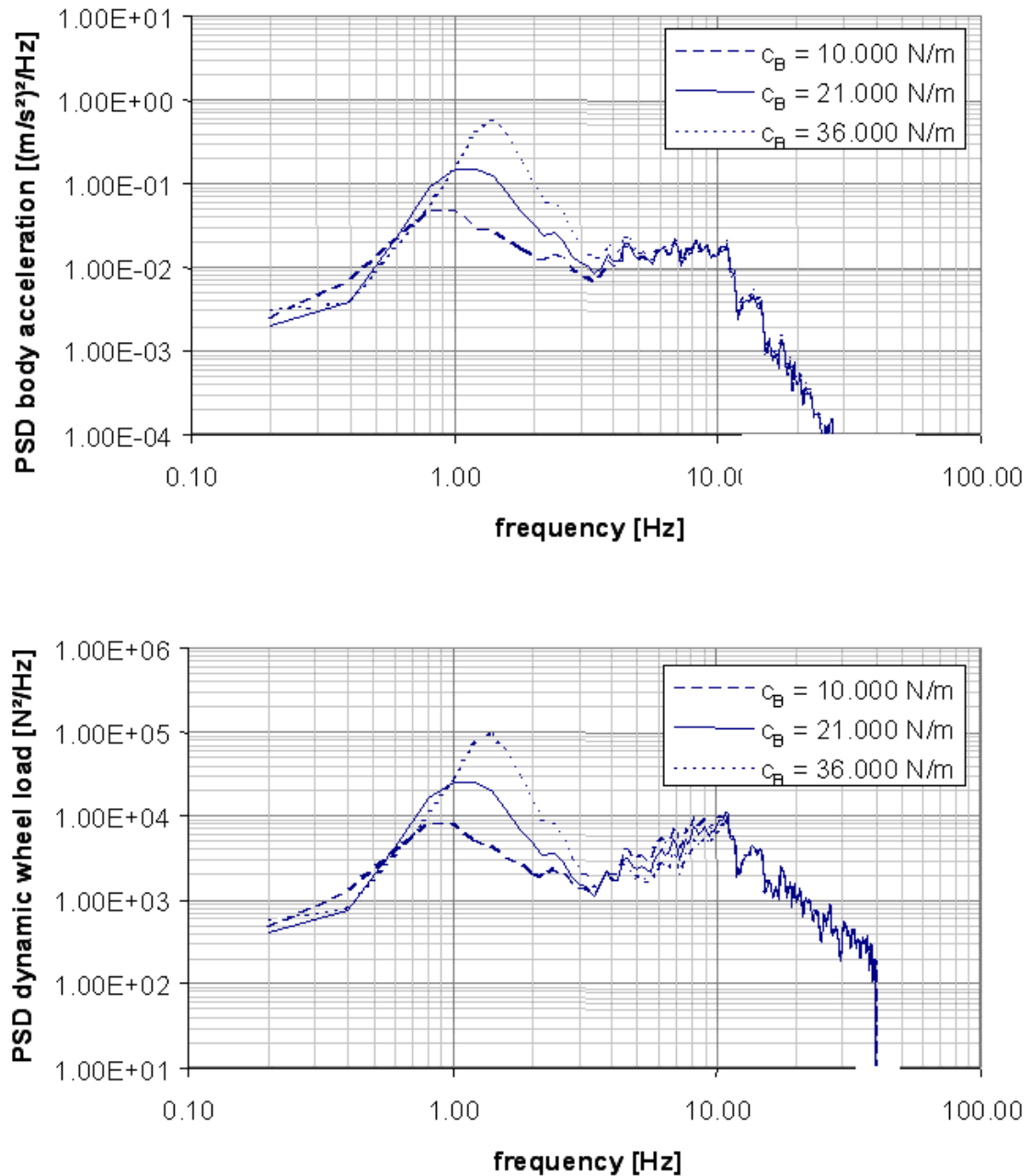


Fig. 1.4-12: Parameter variation with varying stiffness/spring rate of body suspension

• Variation of Body Damping k_B

In Fig. 1.4-13, the body damping is varied. Stiffer body damping has a positive effect around the range of natural frequencies of both body acceleration (suspension comfort) and the dynamic wheel load fluctuation (road grip of the wheels, active safety). In the ranges outside the points of resonance however, the body acceleration is positively influenced by a soft damper.

Tuning of body damping consequently always requires a compromise to be made between the requirements of the various frequency ranges.

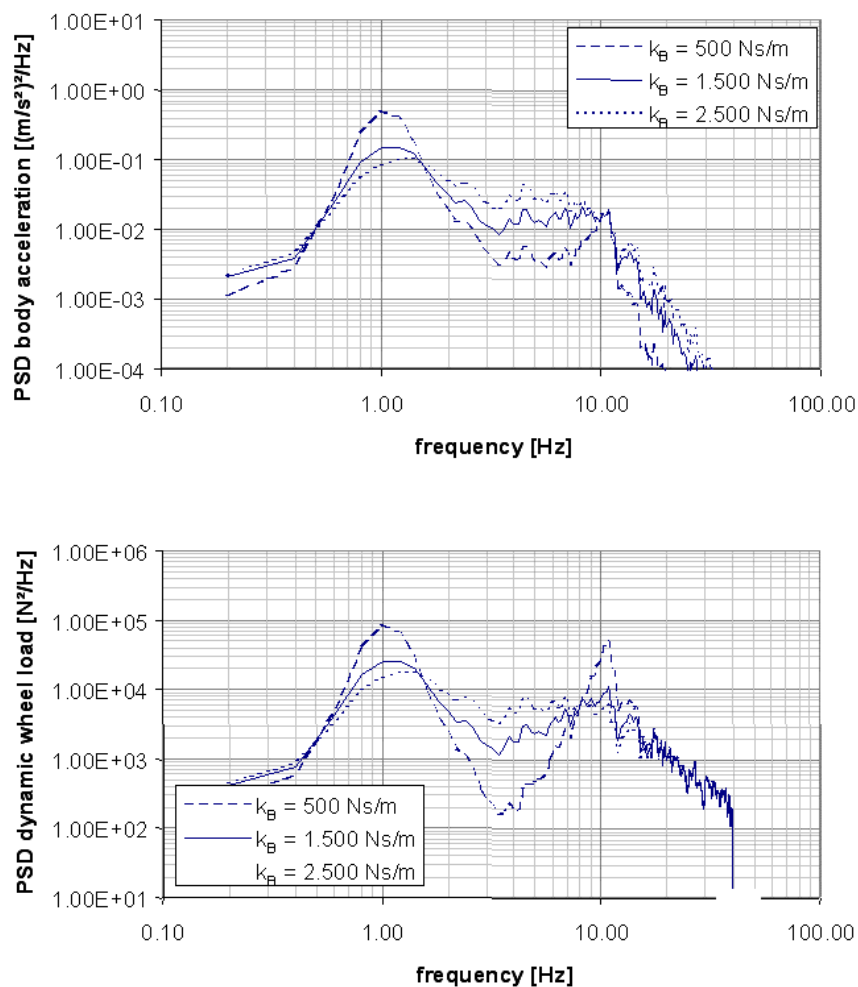


Fig. 1.4-13: Parameter variation with varying body damping

In Fig. 1.4-14 the results gained on the basis of Figs. 1.4-10 - 1.4-13 with regard to driving safety and riding comfort are summarized in a table. Analogous to body and wheel natural frequencies, a difference is made between the effects of long and short-waves.

	driving safety		ride comfort	
	long wave	short wave	long wave	short wave
excitement:				
action:				
soft support spring :	↑	↑	↑	↑
soft shock absorber:	↓	↓	↓	↑
softer tires:		↑	↑	↑
lighter axle:		↑		↑
advice:				
support spring:	soft		soft	
shock absorber:	strong	strong	strong	weak
tires:		soft		soft
axle:		light		light

Fig. 1.4-14: Effects of design changes on the suspension system with respect to driving safety (dynamic wheel loads) and riding comfort (body acceleration);

↑ = positive, ↓ = negative

In addition to the "conventional" methods of influencing suspension behavior dealt with so far, "unconventional" solutions are being presented below. In contrast to passive systems, the force F acting here on the body does not depend on a single characteristic of the compression travel z and the compression rate \dot{z} of the suspension elements. Fig. 1.4-15 presents a summary of regulated suspension systems.

Adaptive systems, unlike the passive system, can switch between various component characteristics. However, here as in passive systems, the direction of the force remains determined by the signs of compression travel and compression rate.

In the *semiactive* state, the switching frequencies are larger than the characteristic vibration periods of wheel and body. This allows the possibility to switch from one characteristic to another at such speeds that every intermediate operating point can be reached dynamically.

Adaptive and semiactive systems only need energy for the control of actuators and the electronics.

Only in the case of *active* suspension can the force F between body and wheel become independent of the compression movement of the wheel. The actuating force however, requires external energy supply.

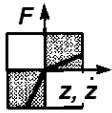

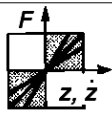

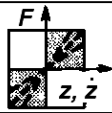
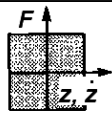

	forces	switching frequency	power demand	
passive		-	-	
adaptive		smaller than characteristic oscillating frequencies	little	
semiactive		larger than characteristic oscillating frequencies	little	
active		larger than characteristic oscillating frequencies	large	

Fig. 1.4-15: Classification of controlled suspension systems

• Adaptive Damper Control

The results of parameter variation on damper stiffness (Fig. 1.4-13) suggested that body acceleration as well as wheel load variations can be minimized for a wide frequency range, if a relatively high level of damping is available in the areas of body and wheel resonance while a softer damping is available in the range outside the points of resonance.

A clear improvement of conventional suspension systems can hence theoretically also be achieved by a damping system which depends on the excitation frequency of the system, Fig. 1.4-16.

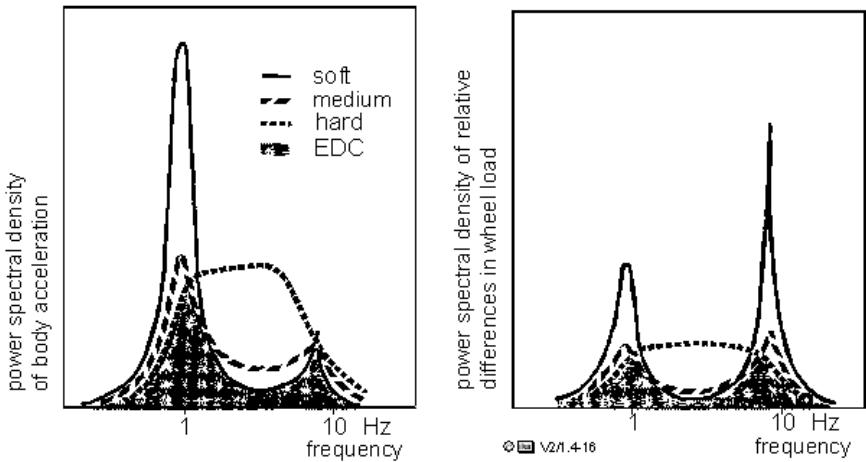


Fig. 1.4-16: Simulation results with a single-wheel suspension model for ideal frequency-dependent damper force adjustment /21/

The potential for improvement which can be achieved by damper control is limited by the fact that the selection of a definite frequency is not possible as a result of the randomness of road irregularities. Apart from that, the improvement potential also depends on the achievable range of variation of damper characteristics and to what extent the system life can be reduced.

The EDC system (Electronic Damper Control) of BMW was developed in cooperation with Boge and VDO. Here, the damper characteristics are adjusted in three steps using control electronics. The EDC system identifies the road excitation over an acceleration sensor mounted on the body.

The sensor signals are processed by the ECU in a manner allowing the determination of separate characteristics for excitations with respect to body and axle natural frequencies. Depending on vehicle load and the intensity of instantaneous vibration excitation, different threshold values will result in a stepped damper adjustment.

The effectiveness of the system is illustrated with the help of a conflict diagram between comfort and driving safety, Fig. 1.4-17.

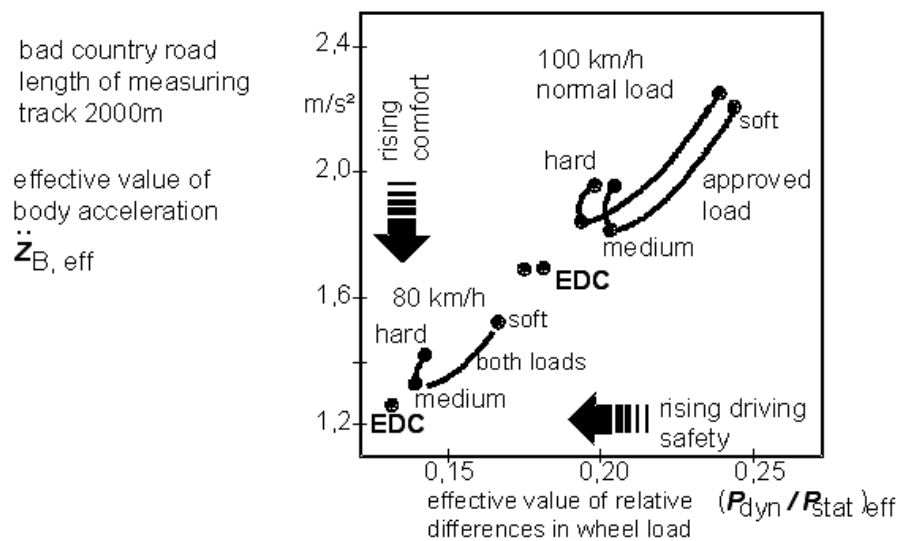


Fig. 1.4-17: Comparison of suspension behavior of a test vehicle with different damper settings of the EDC system illustrated by the conflict diagram comfort/driving safety /21/

In the adaptive damping system (ADS) of Mercedes-Benz, whose system functions are comparable to those of the EDC system, the damping adjustment which is dependent on the road irregularities takes place in 4 steps according to a characteristic map which considers comparative values both for the spectral power density of the irregularities $\Phi(\Omega_0)$ and the undulations w of the road being driven on, Fig. 1.4-18.

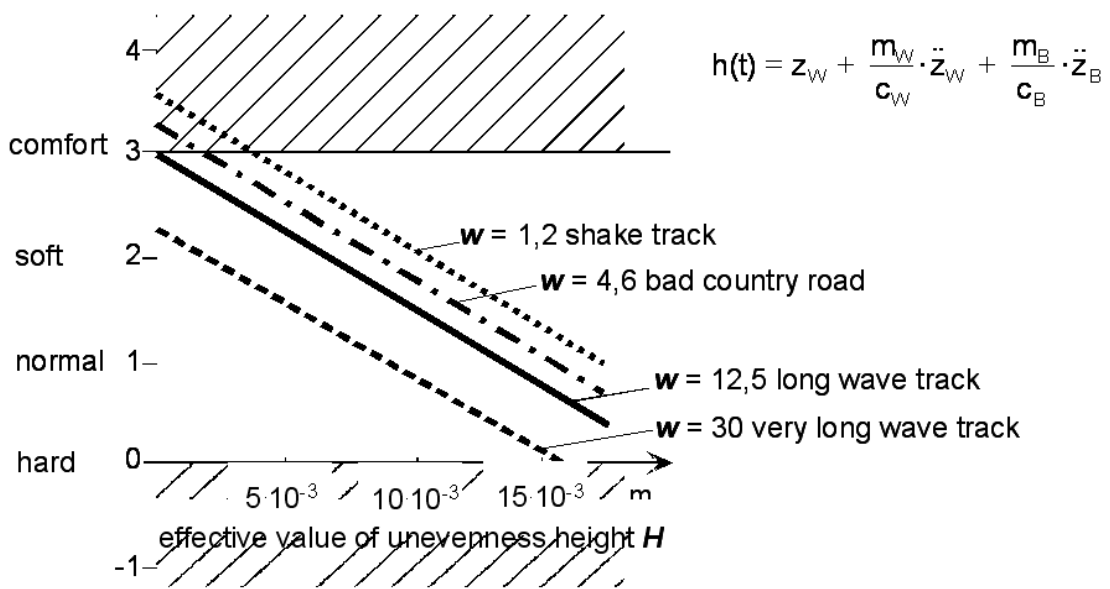


Fig. 1.4-18: Map for damper force adjustment of the adaptive damping system ADS of Mercedes-Benz /25/

An effective value H of the course of irregularity $h(t)$ in the frequency range 0.5 - 20 Hz, ($\Phi' = H(0.5 - 20 \text{ Hz})$) determined by exponential smoothing is used as a comparative value for the spectral power density $\Phi(\Omega_0)$.

The comparative value for undulations is formed as a quotient resulting from the respective effective values for the ranges of body and axle resonance.

$$(w' = H(0.5 - 2 \text{ Hz}) / H(8 - 20 \text{ Hz}))$$

The characteristic of the road irregularity $h(t)$ is indirectly determined by the measurement of wheel acceleration \ddot{z}_w and body acceleration \ddot{z}_B . The algorithm used can be derived from equations 1.4-7 and 1.4-8.

$$z_E = h(t) :$$

$$h(t) = z_w + \frac{m_w}{c_w} \cdot \ddot{z}_w + \frac{m_B}{c_B} \cdot \ddot{z}_B \quad (1.4-21)$$

• Active Suspension

Due to its low power/weight ratio and its high power density, a hydraulic cylinder is suited as a displacing element for the active control of the ride-level (Fig. 1.4-19).

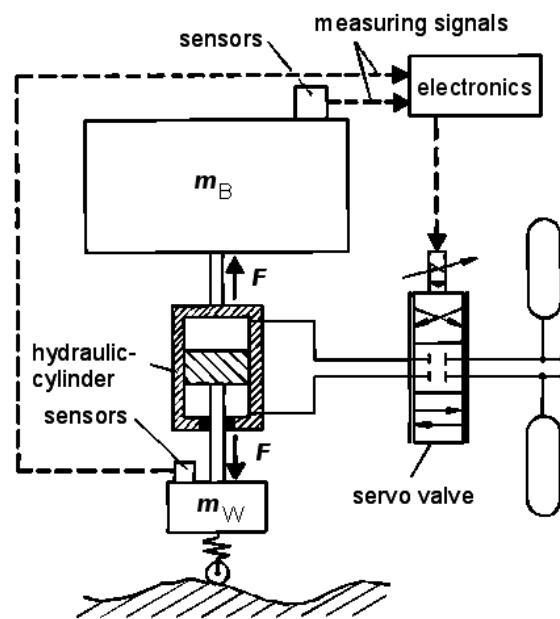


Fig. 1.4-19: Single-wheel suspension model with active suspension

Cylinder pressure is controlled by means of a quick-acting servo valve, which receives the control signals from an electronic control unit. Various information about the driving condition picked up by sensors on the vehicle can be fed to the control logic. The active adjusting force can be controlled in relation to the wheel or body acceleration or by the pre-determination of the road irregularities.

Unlike a fully active suspension, the active version of the hydropneumatic suspension also provides a spring action without inflow and outflow of hydraulic oil. The control valves supply or withdraw oil only if the system recognizes that it can improve the vehicle handling by an active intervention. The advantage here is that even under extreme driving conditions, the energy input required is significantly lower.

In Fig. 1.4-20 the spectral power densities of active hydropneumatic and fully active suspension are compared with those of passive systems. Suspension comfort as well as road grip of the wheels are clearly improved over a wide range of frequencies.

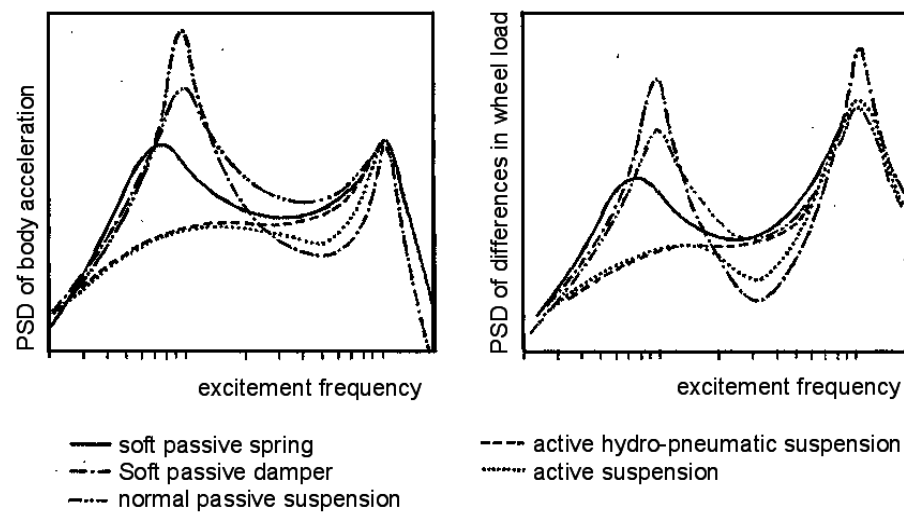


Fig. 1.4-20: Theoretical riding comfort and safety potential of various suspension systems

Realization of motor vehicles with significantly improved suspension comfort is technically possible. Drawbacks are seen in the higher design expenditure and the energy requirements, which for a standard-size car amounts to between 7 kW (active hydropneumatic suspension) and 20 kW (fully active suspension).

1.4.2.2 Parametric Study of a Truck Suspension

The suspension characteristics of trucks differ substantially from those of a passenger car.

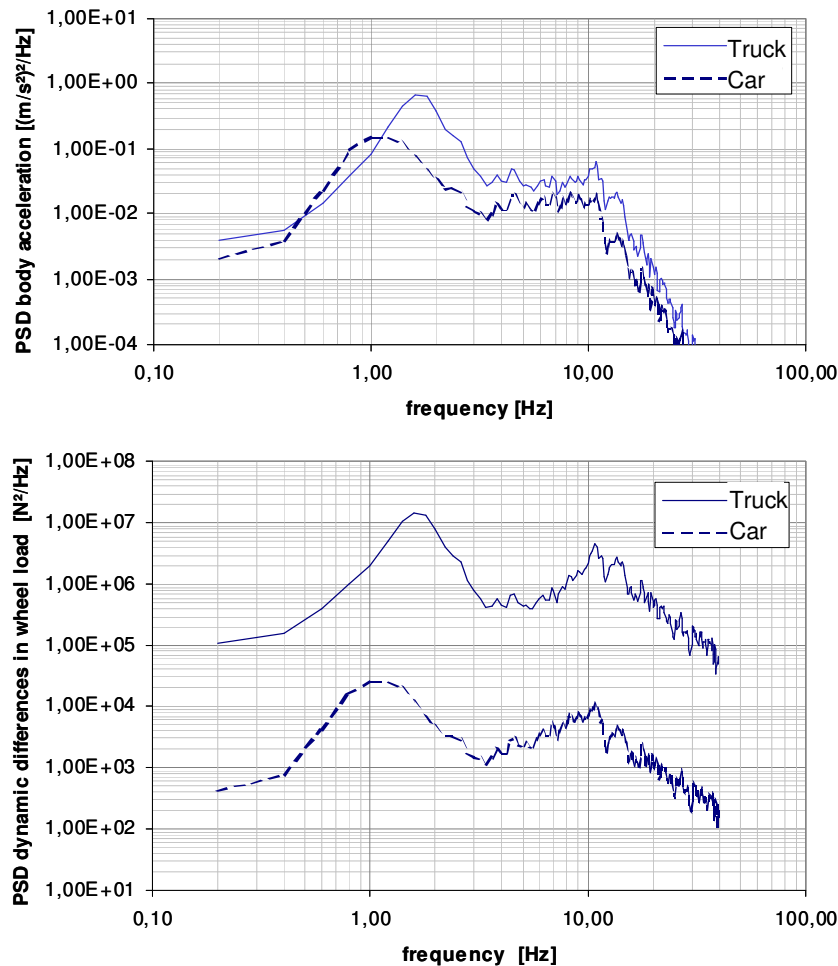


Fig.1.4-21: Comparison of body acceleration and dynamic wheel load between trucks and passenger cars

Fig. 1.4-21 shows the spectral power densities of body acceleration and dynamic wheel load of a truck in comparison to a passenger car.

The simulation of the truck is based on the following data:

$c_W = 3,000,000 \text{ N/m}$; $c_A = 570,000 \text{ N/m}$; $k_W = 100 \text{ Ns/m}$; $k_B = 21,000 \text{ Ns/m}$; $m_W = 650 \text{ kg}$;
 $m_B = 4500 \text{ kg}$

The body natural frequency of 1.4 Hz is significantly higher than the passenger car used in the earlier example. Also, the magnitudes of body acceleration and the dynamic wheel load

are larger. The suspension behavior of trucks is therefore less favourable than that of passenger cars.

- Influence of Frictional Forces in Springs

The body springs of trucks usually consist of stacked leaf springs. The characteristics of these springs show hysteresis (see paragraph 1.2.1.1), resulting from the friction between the spring leaves. This leads to a temporary blockage of the body spring during the course of an oscillation, thereby turning the two-mass system into a single mass system as shown in Fig.1.4-3. The body and wheel mass then oscillate in conjunction on the stiff and poorly damped tire spring.

Fig.1.4-22 shows the velocity difference between body and wheel with and without friction. In the model which takes friction into account, the phases where the leaf springs block, as indicated by the velocity difference reaching zero, are clearly visible.

Fig.1.4-23 shows the effect of the frictional force on the body acceleration of the exemplary truck. Particularly in the range of the highest vibration sensitivity of humans, i.e., between 4-8 Hz, friction leads to a considerable degradation of the suspension behavior.

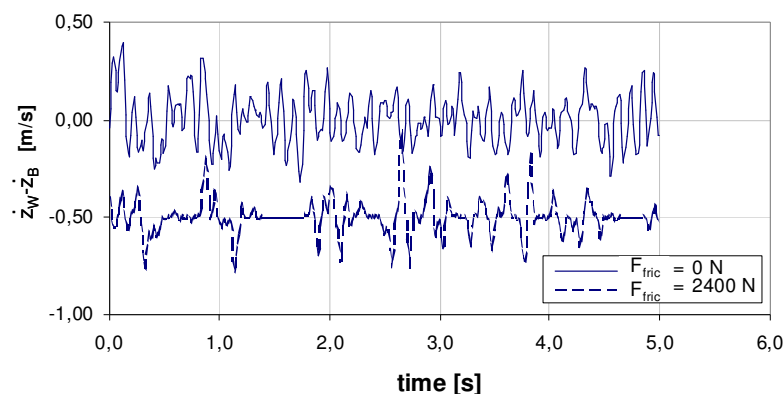


Fig.1.4-22: Velocity difference between body and wheel

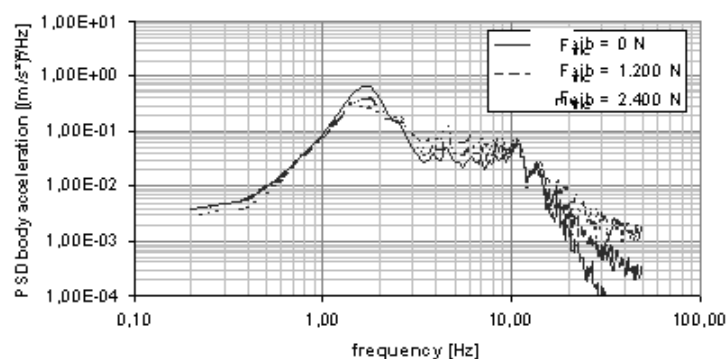


Fig.1.4-23: Parametric variation with different amounts of friction within the leaf spring

1.4.3 Extension of the Model by the Seat Suspension

The extension of the two-mass suspension model, which has been discussed so far, by the seat suspension, results in a three-mass suspension model (Fig.1.4-24).

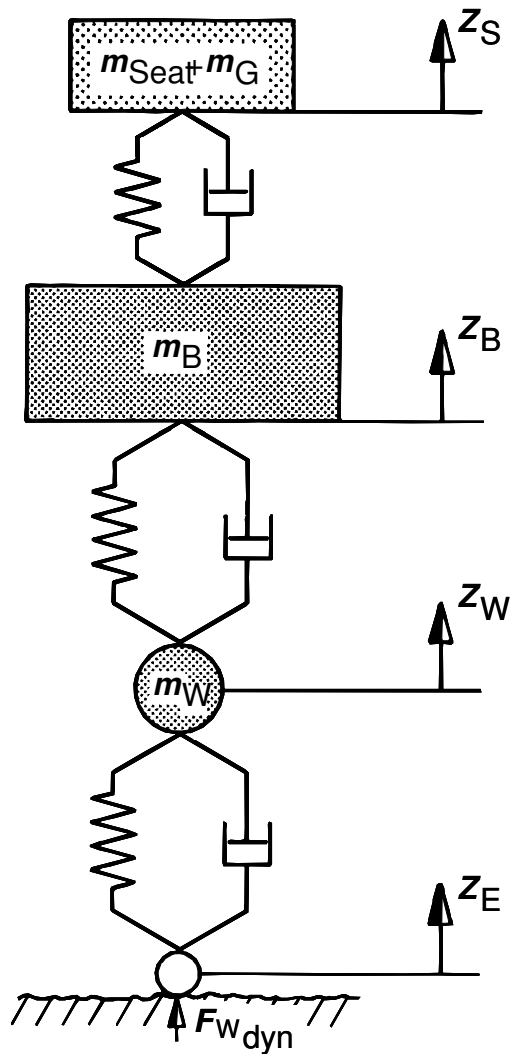


Fig.1.4-24: Structure of a three-mass suspension model

The added mass represents the mass of the sprung parts of the seat and the person sitting on it. Due to the negligible mass added with respect to the mass of the body, the resulting feedback to the body can be neglected. One can therefore begin with a two-mass system and add a simple oscillator.

In the following figures, this extension is achieved by superimposing two different seat masses on the reference car from paragraph 1.4.2.1. Fig.1.4-5 shows the amplification function, while Fig.1.4-6 shows the spectral power density of seat acceleration resulting from the seat's filtering effect.

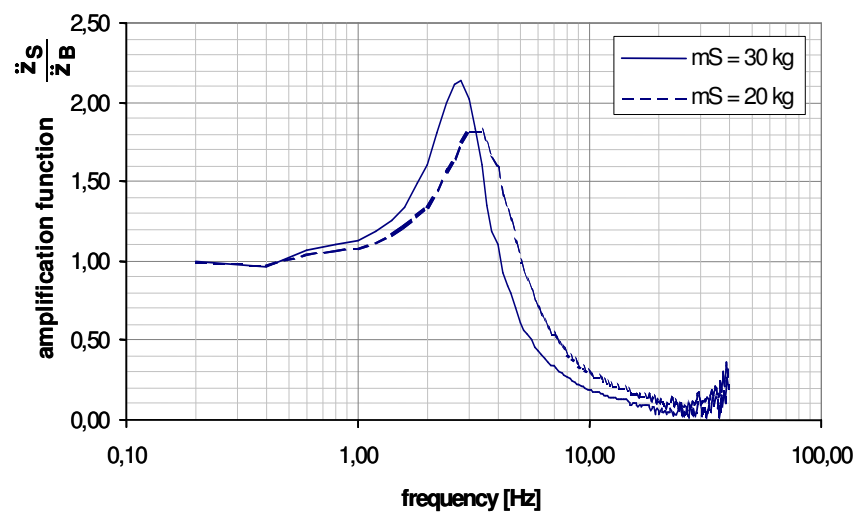


Fig.1.4-5: Amplification function of a three-mass suspension model

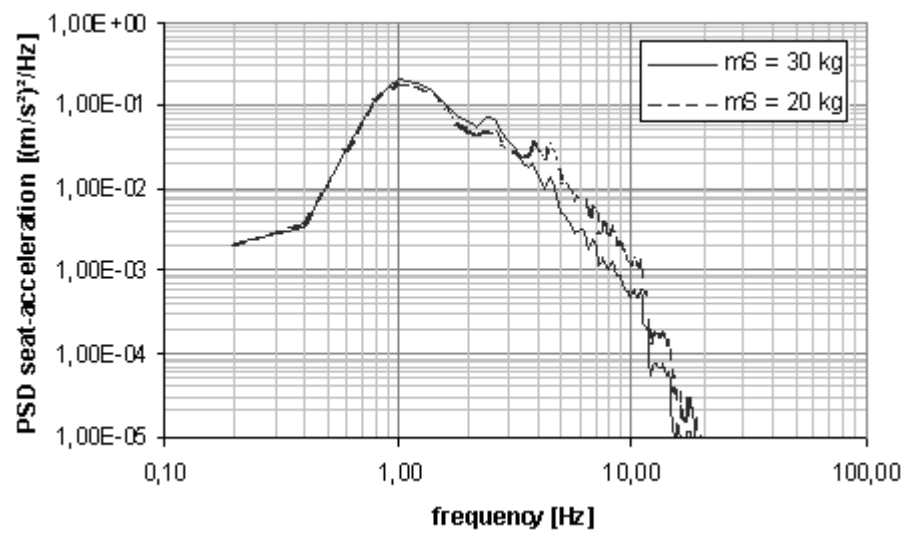


Fig.1.4-6: Seat acceleration of a three-mass suspension model

1.5 Single-Track Suspension Model

1.5.1 Double-axle Vehicle with bending resistant Structure

In single-track suspension models, the body is not considered as a point mass but as a mass inflicted beam. In its simplest form, the single track vehicle consists of the model of a two-axle vehicle with a rigid body, i.e. a flexurally stiff beam (Fig. 1.5-1).

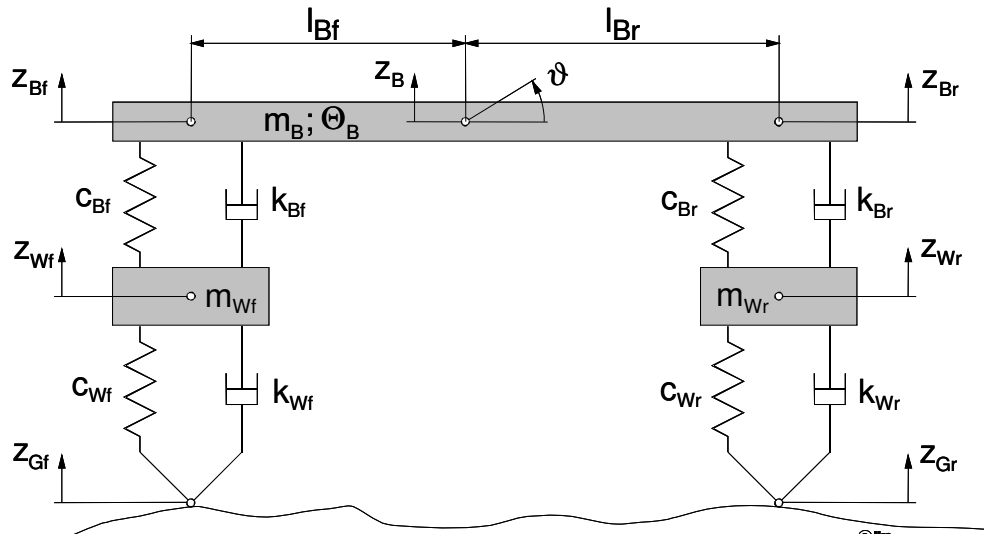


Fig.1.5-1: Single track suspension model

First we need to formulate the differential equations. The single-track suspension model for a two-axle vehicle according to Fig. 1.5-1 has four degrees of freedom:

- lift and pitch of the body,
- lift of front and rear axles.

The equations applicable for the center of gravity of the body are:

$$m_B \ddot{z}_B = -k_{Bf} (\dot{z}_{Bf} - \dot{z}_{Wf}) - c_{Bf} (z_{Bf} - z_{Wf}) - k_{Br} (\dot{z}_{Br} - \dot{z}_{Wr}) - c_{Br} (z_{Br} - z_{Wr}) \quad (1.5-1)$$

$$I_B \ddot{\theta}_B = l_f k_{Bf} (\dot{z}_{Bf} - \dot{z}_{Wf}) + l_f c_{Bf} (z_{Bf} - z_{Wf}) - l_r k_{Br} (\dot{z}_{Br} - \dot{z}_{Wr}) - l_r c_{Br} (z_{Br} - z_{Wr}) \quad (1.5-2)$$

Front and rear axles follow the equations:

$$m_{Wf} \ddot{z}_{Wf} = k_{Bf} (\dot{z}_{Bf} - \dot{z}_{Wf}) + c_{Bf} (z_{Bf} - z_{Wf}) - k_{Wf} (\dot{z}_{Wf} - \dot{z}_{Gr}) - c_{Wf} (z_{Wf} - z_{Gr}) \quad (1.5-3)$$

$$\begin{aligned}
m_{Wr} \ddot{z}_{Wr} &= k_{Br} (\dot{z}_{Br} - \dot{z}_{Wr}) - c_{Br} (z_{Br} - z_{Wr}) \\
&- k_{Wr} (\dot{z}_{Wr} - \dot{z}_{Gr}) - c_{Wr} (z_{Wr} - z_{Gr})
\end{aligned} \tag{1.5-4}$$

Between the displacements of the body above the axles z_{Av} and z_{Ah} , the motion of the center of gravity of the body z_A and the pitch angle ϑ the following relationships are applicable:

$$z_{Bf} = z_B - l_f \vartheta \tag{1.5-5}$$

$$z_{Br} = z_B + l_r \vartheta \tag{1.5-6}$$

As for the single-wheel suspension model, natural angular frequencies and damping values can also be derived from the differential equations for the single-track suspension model, if the coupling of the differential equations is neglected. Starting from the notion that all degrees of freedom – except for the one under consideration – are blocked, the following results:

	natural circular frequency	damping factor	
travel	$\sqrt{\frac{c_{Bf} + c_{Br}}{m_B}}$	$\frac{k_{Bf} + k_{Br}}{2\sqrt{m_B(c_{Bf} + c_{Br})}}$	
body front	$\sqrt{\frac{c_{Bf}}{m_{Bf}}}$	$\frac{k_{Bf}}{2\sqrt{m_{Bf}c_{Bf}}}$	
body rear	$\sqrt{\frac{c_{Br}}{m_{Br}}}$	$\frac{k_{Br}}{2\sqrt{m_{Br}c_{Br}}}$	
pitch	$\sqrt{\frac{l_{Bf}^2 c_{Bf} + l_{Br}^2 c_{Br}}{\Theta_B}}$	$\frac{l_{Bf}^2 k_{Bf} + l_{Br}^2 k_{Br}}{2\sqrt{\Theta_B(l_{Bf}^2 c_{Bf} + l_{Br}^2 c_{Br})}}$	
front axle	$\sqrt{\frac{c_{Bf} + c_{Wf}}{m_{Wf}}}$	$\frac{k_{Bf} + k_{Wf}}{2\sqrt{m_{Wf}(c_{Bf} + c_{Wf})}}$	
rear axle	$\sqrt{\frac{c_{Br} + c_{Wr}}{m_{Wr}}}$	$\frac{k_{Br} + k_{Wr}}{2\sqrt{m_{Wr}(c_{Br} + c_{Wr})}}$	(1.5-7)

The axle-proportionate body masses result from the position of the centre of gravity:

$$m_{Bf} = m_B \frac{l_{Br}}{l_{Bf} + l_{Br}} \quad (1.5-8)$$

$$m_{Br} = m_B \frac{l_{Bf}}{l_{Bf} + l_{Br}} \quad (1.5-9)$$

From the point of view of suspension comfort, the pitch natural frequency should be low. For a predetermined spring stiffness of the vertical dynamic springs however, a target-specific adjustment is difficult, since the other influencing parameters are usually determined by differing factors (location of the center-of-gravity, wheelbase) or more or less resulting from the vehicle concept (moment of inertia).

1.5.1.1 Excitation by Real Road Unevenness

Unlike the single-wheel suspension model, the single-track suspension model is excited by every road irregularity twice: that is, first on the front axle and then once more on the rear axle. As a result, the body acceleration of the two-axle model not only depends on the excitation frequency but also on parameters such as the driving speed, the body natural frequency and the location of the measuring point in the vehicle.

In the following section, the irregularity profile of the road excites the vehicular vibratory system respectively on the front and rear axles over a time delay of $\Delta t = l / v$ (l wheelbase, v driving speed). The equations of motion are solved with the aid of the MATLAB simulation tool.

- Influence of Driving Speed

While the power spectral density of body acceleration and dynamic wheel load fluctuations permit a differentiated assessment of a vehicle suspension, it is possible to assess a trend also on the basis of the respective effective values.

This approach makes sense, for example, if those parameters which affect the entire power spectral density are used in the trend assessment, since then a value for suspension comfort or road grip can be stated as a function of the varied parameter.

The effective value of body acceleration can be determined on the basis of the time dependent curve of acceleration:

$$\ddot{z}_{\text{Beff}} = \sqrt{\frac{1}{T} \cdot \int_0^T \ddot{z}_B^2 dt}$$

The effective value of body acceleration above the rear axle for an average load was determined this way in relation to the driving speed of a model vehicle, Fig. 1.5-2.

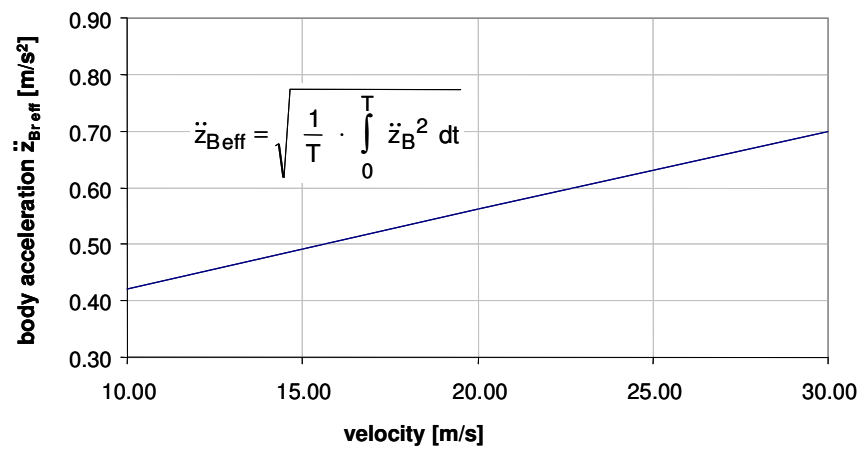


Fig.1.5-2: Body acceleration \ddot{z}_{Ah} in relation to the driving speed

- Influence of Body Natural Frequency

For determining the influence of the spring rates of the body springs – and hence the body natural frequency – on the body acceleration, the spring rates are gradually reduced. For the model vehicle with average load and a driving speed of 22 m/s, a curve as shown in Fig. 1.5-3 is obtained.

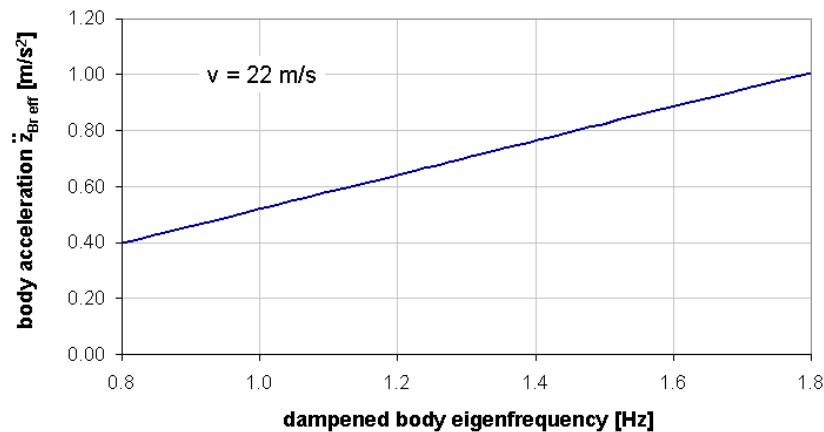


Fig.1.5-3: Body acceleration \ddot{z}_{Ah} in relation to the body natural frequency

In order to achieve a low body acceleration and good suspension comfort, it is of crucial importance to realize soft body springs, i.e. a low body natural frequency. This however, requires a suitable vehicle concept, such as a low center of gravity and wide spring tracks. These boundary conditions were neglected in the considerations according to Fig. 1.5-3.

- Location of Measuring Point

In Fig. 1.5-2 and Fig. 1.5-3, a point on the body directly above the rear axle was defined as the "measuring point" for body acceleration. With otherwise identical conditions, the value of body acceleration also depends on the location of the measuring point on the body in the longitudinal direction of the vehicle. This influence is shown in Fig. 1.5-4 for the original state.

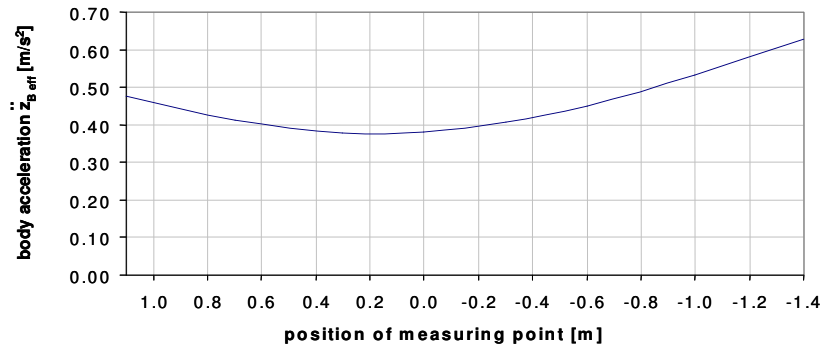


Fig.1.5-4: Body acceleration in relation to the location of the measuring point in the vehicle
(The 0-value marks the center of gravity)

A minimum amount of body acceleration is found in the area of the center of gravity of the vehicle. With increasing distance from the center of gravity, the effect of the overlap of lift and pitch oscillations of the body on the resulting acceleration increases.

1.5.1.2 Mass and Spring Coupling

For further considerations, it seems practical to split the mass of the beam-shaped body into three individual point masses (Fig. 1.5-5).

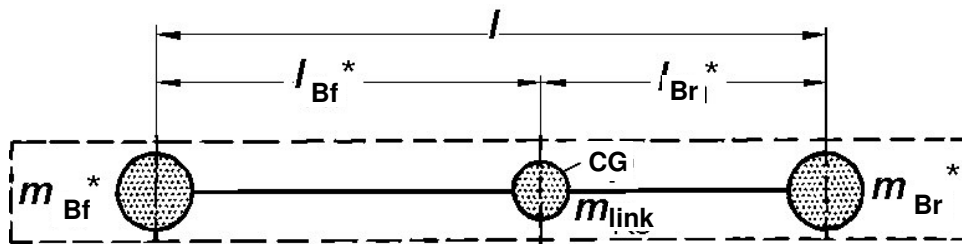


Fig.1.5-5: Configuration of the single-track suspension model with coupled mass m_{Link}

Since total mass m_B center-of-gravity location l_{Av}^* , l_{Ah}^* and moment of inertia Θ_B must remain the same, the following three conditional equations follow:

$$m_{Bf}^* + m_{Br}^* + m_{link} = m_B \quad (1.5-10)$$

$$m_{Bf}^* \cdot l_{Bf}^* = m_{Br}^* \cdot l_{Br}^* \quad (1.5-11)$$

$$m_{Bf}^* \cdot l_{Bf}^{*2} + m_{Br}^* \cdot l_{Br}^{*2} = \Theta_B \quad (1.5-12)$$

Out of this the so-called coupling mass m_{link} results too:

$$m_{link} = m_B - \frac{\Theta_B}{l_{Bf}^* \cdot l_{Br}^*} \quad (1.5-13)$$

- Mass Coupling

When a vehicle's front axle passes over a bump, the shock/impact force acting on the body will result in its motion composed of a combination of a displacement of the body center of gravity S_B and a rotary motion about the transverse axis of the vehicle (pitching motion) through the center of gravity.

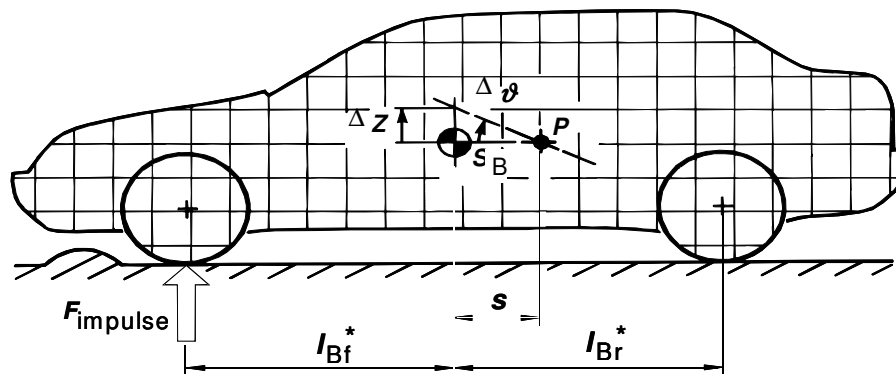


Fig.1.5-6: Shock excitation in the single-track suspension model

Associated with this body movement, there exists a point in the longitudinal central plane of the vehicle which remains at rest, called the center of impact /1/. The location of this point can be determined with the aid of the principles of linear and angular momentum:

$$\int_{t_1}^{t_2} F_{impulse} dt = m_B \cdot \dot{z}_2 - m_B \cdot \dot{z}_1 \quad (1.5-14)$$

$$\int_{t_1}^{t_2} F_{impulse} \cdot l_{Bf}^* dt = \Theta_B \cdot \dot{\varphi}_2 - \Theta_B \cdot \dot{\varphi}_1 \quad (1.5-15)$$

In consideration of the geometric relationship

$$s \cdot \Delta \vartheta \approx \Delta z$$

$$s(\dot{\vartheta}_2 - \dot{\vartheta}_1) = \dot{z}_2 - \dot{z}_1 \quad (1.5-16)$$

follows:

$$s = \frac{\Theta_B}{l_{Bf}^* \cdot m_B} \quad (1.5-17)$$

With the help of this relation, the three possible cases for the magnitude of the coupled mass, which is a purely theoretical parameter (can also assume negative values), can be illustrated:

1. Coupling Mass equal to Zero ($m_{link} = 0$):

For the special case where the coupled mass equals zero,

$$\Theta_B = m_B \cdot l_{Bf}^* \cdot l_{Br}^*$$

applies and thus for an impact on the front axle

$$s = l_{Br}^*$$

In this case, the body above the rear axle remains at rest (unexcited), which means impacts are decoupled.

2. Coupling Mass greater than Zero ($m_{link} > 0$):

If the coupled mass is greater than zero, the following equation applies for the impact on the front axle:

$$s < l_{Br}^*$$

The center of impact in this case is located between body center of gravity and rear axle. This means that with identical total mass and identical wheelbase, the pitching motion of the body is intensified, which is disadvantageous from the point of view of the ride comfort.

3. Coupling Mass less than Zero ($m_{link} < 0$):

If the relation between body mass, mass moment of inertia and center-of-gravity distances is such that the coupled mass is less than zero, then the following equation applies for the impact on the front axle:

$$s > l_{Br}^*$$

The center of impact in this case is no longer found between the axles. This implies that a body movement resulting from the shock force on the front axle, would include a larger proportion of vertical displacement than that of a pitching motion. This is considered favorable with respect to ride comfort.

These considerations can be made in a similar way for the rear axle travelling over a bump.

- Spring Coupling :

Spring coupling as realized, for example, by the BLMC hydrolastic springing system, functions similar to a mass coupling, $m_{ko} < 0$. By means of a hydraulic connection, the compression of the front axle (due to a bump) results in a rebound of the rear axle, a response which counter-balances the pitching motion of the body.

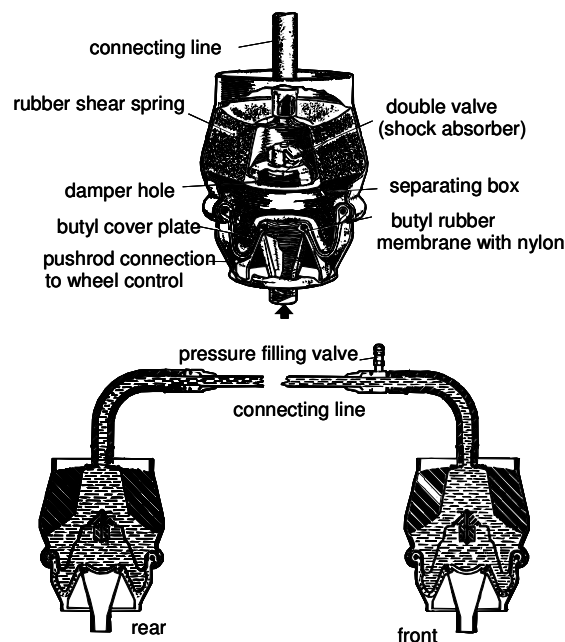


Fig.1.5-7: "Hydrolastic" compound suspension system in the Morris 1100, 1962

Spring coupling acc. to Fig. 1.5-8 is an alternative way of reducing pitching natural frequency without changing the natural frequency for vertical displacement. While all springs are involved in vertical motion, only the outer springs are involved in the pitching motion.

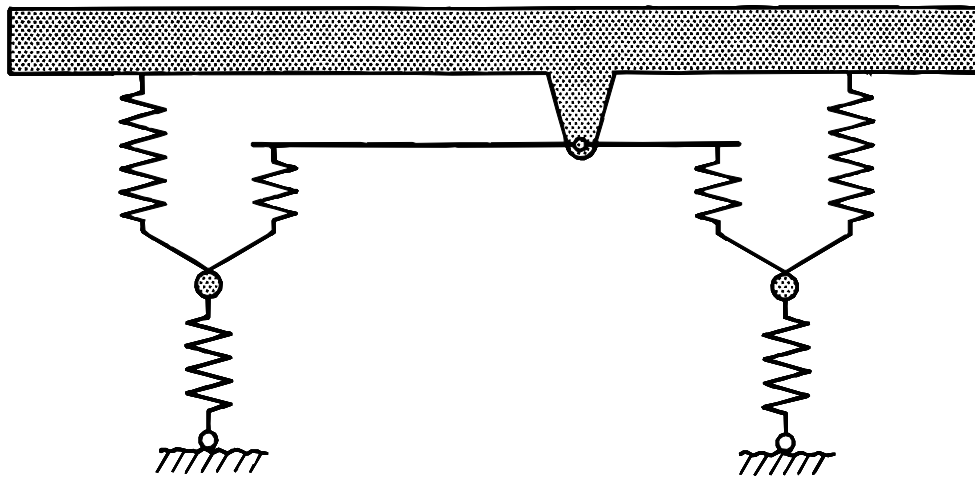


Fig.1.5-8: Two-axle vehicle with spring coupling

The potential for the improvement of suspension behavior by means of coupled masses or springs is very limited, since the necessary measures are often hard to realize or the latitude of design with respect to the influencing parameters is low.

1.5.2 Two-Axle Vehicle with additional Degrees of Freedom

In the two-axle vehicle according to Fig. 1.5-1, the body was assumed to be rigid. As opposed to cars and vans, the bending elasticity of the chassis frame as well as the elasticity of engine and cab suspension (heavy commercial vehicles usually feature elastic cab suspension for better isolation against vibration and torsion of the frame) in trucks cannot be neglected, since these factors significantly influence the behaviour of their suspension. Fig. 1.5-9 shows the equivalent system of a truck with 15 degrees of freedom.

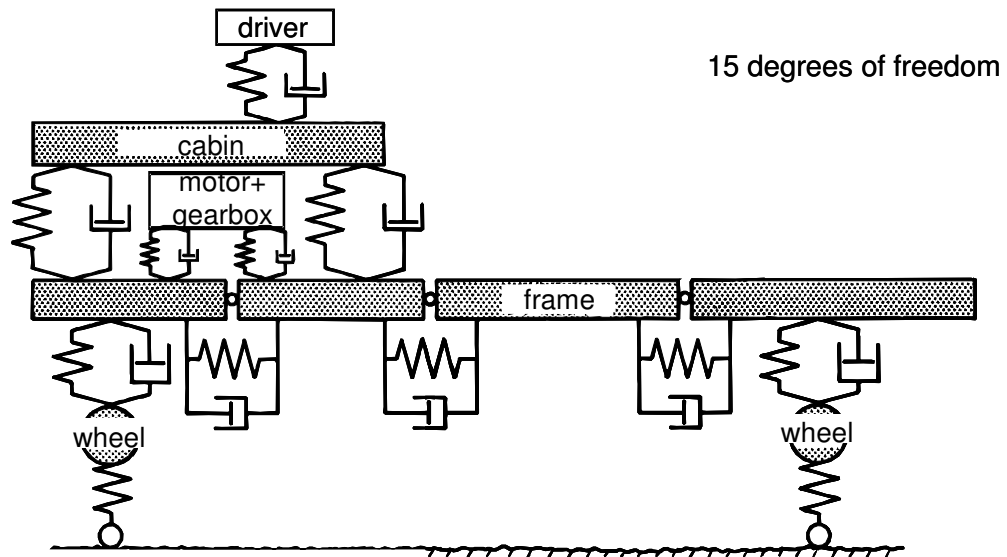


Fig.1.5-9: Structural model of a platform truck

Semi Trailer Truck

The semi-trailer truck is a type of vehicle which experiences particular problems in reference to its suspension and driving stability. In this case, the semitrailer and tractor are linked via a joint in the vertical and transverse axes, Fig. 1.5-10.

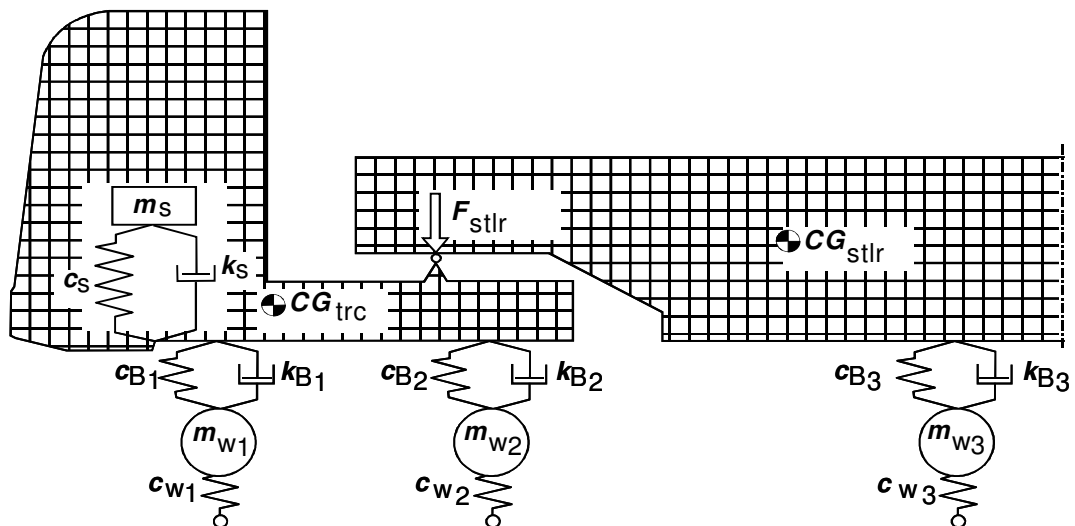


Fig.1.5-10: Structural model of a semitrailer unit

Since the semitrailer transfers a vertical load (fifth wheel load) F_{Sattel} onto the tractor, an appropriate suspension, i.e., a stiff suspension, which is capable of carrying this load is necessary. The moment of inertia resulting out of the pitching motion of the tractor is however, relatively small. The high moment of inertia of the semitrailer has no effect due to the trailer coupling. The consequence of this is a correspondingly high pitch natural

frequency resulting in high K-values. Some improvement can be achieved by means of soft front springs on the tractor.

A drawback as a result of this measure includes an amplification of squatting during acceleration and diving during braking. In extreme cases even dynamic pitch angle and acceleration of the center-of-gravity are increased.

By means of a number of additional measures and target-specific tuning, the suspension behavior of trailer trucks have in the meantime been significantly improved and adapted to that of other commercial vehicles.

- Tandem Axles of Commercial Vehicles

In heavy-duty trucks, tandem axles are commonly used in the form of:

- driven rear axles of trucks and tractor trailers,
- non-driven rear axles of trailers and semitrailers

The following example shows a driven tandem axle of a 22-t semitrailer truck, Fig. 1.5-11, whose design is described by the equivalent system according to Fig. 1.5-12.

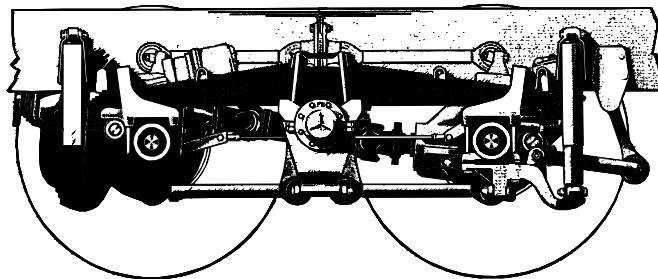


Fig.1.5-11: Swinging tandem axle with hydraulic damping (MB)

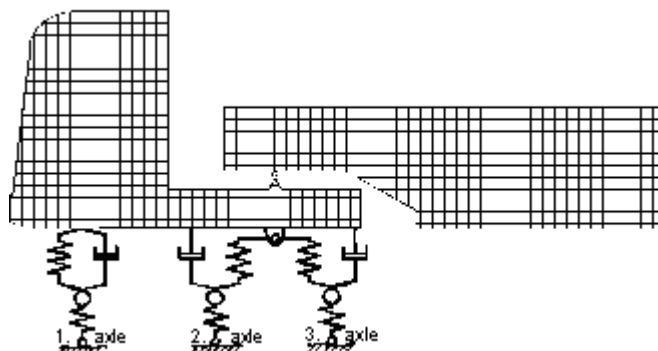


Fig.1.5-12: Equivalent system of a semitrailer truck with hydraulically damped tandem axle

Such tandem axles possess two degrees of freedom: identical and opposed vertical motion of the two axles. Vibration at natural frequency is characterized in particular by high dynamic axle loads, i.e. road load.

1.6 Two-Track Suspension Model

Using a two-track suspension model as shown in Fig. 1.6-1, the following degrees of freedom are dealt with:

- Roll Suspension
- Twisting of the body
- Trample of rigid axles

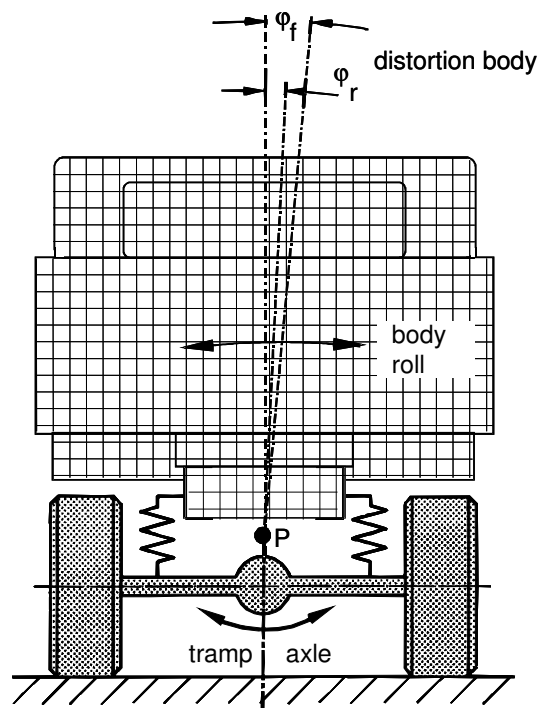


Fig.1.6-1: Two-track suspension model (truck)

1.6.1 Roll Suspension

The roll suspension is first considered for a vehicle with rigid front and rear axles (e.g. truck, jeep), since this case is kinematically simple.

While cornering, the body is laterally displaced due to the centrifugal force. This deflection takes place around an axis of rotation, which passes through the roll poles at the front and rear axles and is called the Roll Axis.

The positions of the roll poles, which depend on the kinematics of the wheel control or the axle coupling to the body, will be dealt with in the chapter on "wheel suspensions".

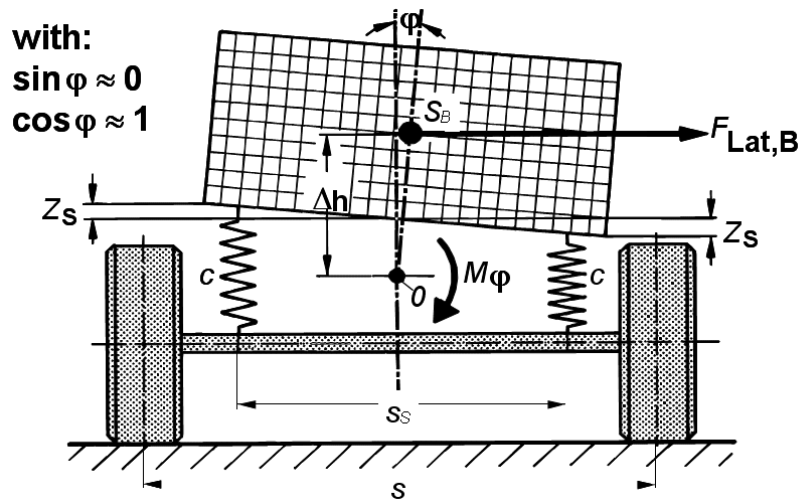


Fig.1.6-2: Equivalent system model for the suspension

The centrifugal force $F_{Lat,B}$, acting at the centre of gravity of the body, gives rise to a torque M_φ around the roll axis according to fig. 1.6-2:

$$M_\varphi = F_{Lat,B} \cdot \Delta h \cdot \cos \varphi + m_B \cdot g \cdot \Delta h \cdot \sin \varphi \quad (1.6-1)$$

with Δh : vertical distance between the centre of gravity of the body S_B and the roll axis

The inclination of the roll axis in the vehicle longitudinal plane is thus neglected. The torque generated by the body weight is also usually neglected in passenger cars, i.e. $\sin \varphi \ll \cos \varphi$ is applicable here.

With these simplifications, the aligning torques applied by the body springs around the roll axis are given by:

$$F_{Lat,B} \cdot \Delta h = 2 \cdot \frac{s_{Sf}}{2} \cdot c_{Bf} \cdot f_{Sf} + 2 \cdot \frac{s_{Sr}}{2} \cdot c_{Br} \cdot f_{Sr} \quad (1.6-2)$$

with:

- $s_{Sf,r}$: Spring track width in front, rear
- $f_{Sf,r}$: Spring compression in front, rear
- $c_{Bf,r}$: Body spring rigidity in front, rear

With $f_F \approx \varphi \cdot \frac{s_S}{2}$ one finally receives for the roll angle φ :

$$\varphi = \frac{2 \cdot \Delta h}{c_{B,f} \cdot s_{S,f}^2 + c_{B,r} \cdot s_{S,r}^2} \cdot F_{Lat,B} \quad (1.6-3)$$

The roll angle ' φ ' is thus inversely proportional to the square of the spring track width. For a small body inclination, the spring track width should therefore be as high as possible while driving along curves.

1.6.1.1 Stabilizer and Compensating Spring

Anti-roll suspension (roll damping) can be stiffened without changing vertical suspension by the installation of a stabilizer spring, Fig. 1.6-3.

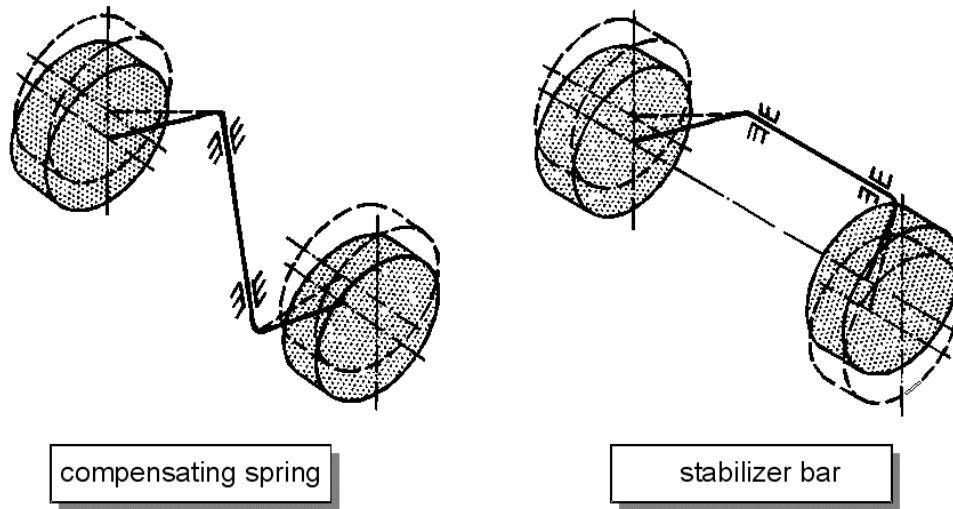


Fig. 1.6-3: Functional principle of stabilizer and compensating spring

During the rolling motion of the body, i.e. an oppositely phased motion of the wheels, the stabilizer is subjected to a torsion and thus provides a self-aligning torque around the roll axis, which reduces body roll. Vertical displacements in the same direction have no effect on the stabilizer. A stabilizer track width s_{Stab} , to which the stabilizer stiffness c_{Stab} relates, is defined analogous to the spring track width s_F .

Stabilizer stiffness c_{Stab} then corresponds to the stabilizer force at the ends of the stabilizer spring referred to half the difference of the compression at these ends.

For the roll angle φ thus applies:

$$\varphi = \frac{2 \cdot \Delta h \cdot F_{\text{Lat,B}}}{c_{B,f} \cdot s_{F,f}^2 + c_{\text{Stab},f} \cdot s_{\text{Stab},f}^2 + c_{B,r} \cdot s_{F,r}^2 + c_{\text{Stab},r} \cdot s_{\text{Stab},r}^2} \quad (1.6-4)$$

Should the ratio of the shares of the rolling moment M_φ supported by the stabilizers on front and rear axles differ from the ratio of the shares supported by the body suspension, or if only one axle has a stabilizer spring installed, then not only the roll angle will be reduced, but the

distribution of the wheel load differentials, which occur during cornering between the wheels of the right and left vehicle sides, among front and rear axle will be influenced.

The influences on vehicle handling caused by this are dealt with in the chapter on "Lateral Dynamics".

The compensation spring has an opposite effect counteracting that of the stabilizer spring. As a purely vertical suspension element it has not effect on the rolling motion of the body.

In the past, the compensating spring was used for axle designs whose wheel suspension kinematics required wheel load differentials to be as low as possible in order to suppress the so-called bottoming-out effect (cf. chapter on wheel suspensions). The stiffness of body suspension and thus the share of the rolling moment supported on the axle considered could then be reduced accordingly. The compensating spring is no longer found in modern wheel suspension systems.

Fig. 1.6-4 shows an automobile front axle (Opel Senator) as an example for the installation of a stabilizer

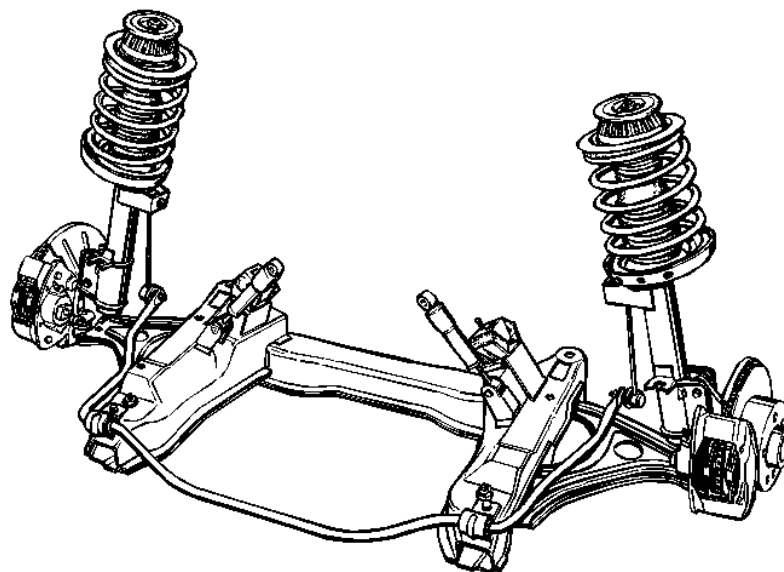


Fig. 1.6-4: Stabilizer spring on an automobile front axle

1.6.1.2 Vehicle Design and Suspension Characteristics

The parameter studies in the paragraph 1.4.2.1 (passenger car) and 1.4.2.2 (truck) show that a necessary prerequisite for the achievement of good suspension characteristics is a low body-eigenfrequency or sufficiently soft body springs.

On the other hand, the lower limit of body eigenfrequency or spring rates is determined in particular by static and quasi-static effects such as changes in level as a result of load and body roll while driving along curves. While static level modifications can be eliminated by load-sensitive regulating springs, roll can only be reduced to a small extent using stabilizers. The relationship between body roll, body natural frequency and body acceleration is therefore considered in the following.

According to paragraph 1.6.1.1, a roll angle is generated when driving along curves (steady-state cornering):

$$\varphi = \frac{2 \cdot \Delta h \cdot F_{\text{Lat,B}}}{(c_B + c_{\text{Stab}}) \cdot s_S^2} \quad (1.6-5)$$

The centrifugal force

$$F_{\text{Lat,B}} = \frac{m_B \cdot v^2}{r} \quad (1.6-6)$$

leads to

$$\varphi = \frac{2 \cdot \Delta h \cdot m_B \cdot v^2}{(c_B + c_{\text{Stab}}) \cdot s_S^2 \cdot r} \quad (1.6-7)$$

With the equation

$$f_{eB} = \frac{1}{2\pi} \cdot \sqrt{\frac{2 \cdot c_B}{m_B}} \quad (1.6-8)$$

With the body eigenfrequency for vertical oscillation, resolved to m_B

$$m_B = \frac{2 \cdot c_B}{4\pi^2 \cdot f_{eB}^2} \quad (1.6-9)$$

The roll angle is given by

$$\varphi = \frac{2 \cdot \Delta h \cdot v^2 \cdot 2 \cdot c_B}{(c_B + c_{\text{Stab}}) \cdot s_S^2 \cdot r \cdot 4 \cdot \pi^2 \cdot f_{eB}} \quad (1.6-10)$$

and by solution f_{eB} is given by

$$f_{eB} = \frac{v}{\pi} \cdot \sqrt{\frac{1}{r}} \cdot \sqrt{\frac{1}{\varphi}} \cdot \sqrt{\frac{\Delta h}{s_S^2}} \cdot \sqrt{\frac{1}{1 + \frac{c_{\text{Stab}}}{c_B}}} \quad (1.6-11)$$

Note $c_B = c_{Bf} + c_{Br}$, where c_{Bf} or c_{Br} is the spring rate of one spring on the front or rear axle.

The first three factors of this product depend on the respective driving conditions. If a standard case is assumed, which is characterized by a curve radius $r = r_0 = 50$ m and a driving speed $v = v_0 = 16$ m/s, then a computation carried out on numerous cars shows - in agreement with subjective feeling - that for this case, a roll angle of $\varphi = \varphi_0 = 3^\circ$ is acceptable. With this standardisation the body eigenfrequency of a vehicle still depends on various factors related to the design of the vehicle, i.e. on the dimensions Δh and s_S as well as the relation of the spring constants c_{Stab} and c_B .

This relationship is represented in the lower section of Fig.1.6-5.

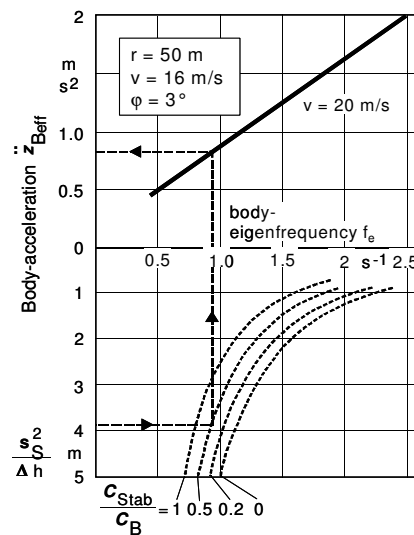


Fig.1.6-5: Influence of the height of the centre of gravity and spring track width on body natural frequency and effective value of body acceleration

In the upper part of Fig.1.6-5, the relationship between body eigenfrequency and body acceleration is represented for a vehicle with two axles at $v=20$ m/s. The characteristic curve is well-known from fig. 1.5-3 for the single track model of the exemplary passenger car.

1.6.2 Distortion of the Body (twisting)

The closed bodies of vehicles such as sedans, transporters and buses can be assumed to be rigid in terms of the handling of the vehicle suspension system, since the bending or torsional rigidity of the body is much higher here than the rigidity in the suspension system.

In contrast, the torsional rigidity of the chassis in commercial vehicles with ladder-type frames, Fig.1.6-6, cannot be neglected. The frame in this case, is designed to be torsionally elastic, in order to reduce the stress on the material in the interconnecting points between

transverse and longitudinal members, i.e. riveting is used instead of welding at the joints and open profiles are used instead of closed profiles for longitudinal and transverse beams.

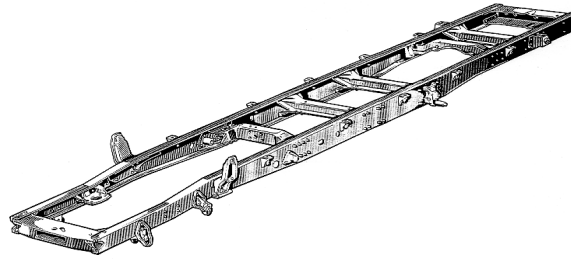


Fig.1.6-6: Torsionally elastic framework of a light truck

For commercial vehicles used on construction-sites or off-road purposes, a torsionally elastic framework offers the advantage that larger surface irregularities can be absorbed without loss of traction (wheels lifting off the surface of the road) than with the sole use of the spring travel offered by the body springs.

A computational handling of the twisting of the framework is relatively simple, if one divides the body into two subsystems with individual centres of gravity, Fig.1.6-7.

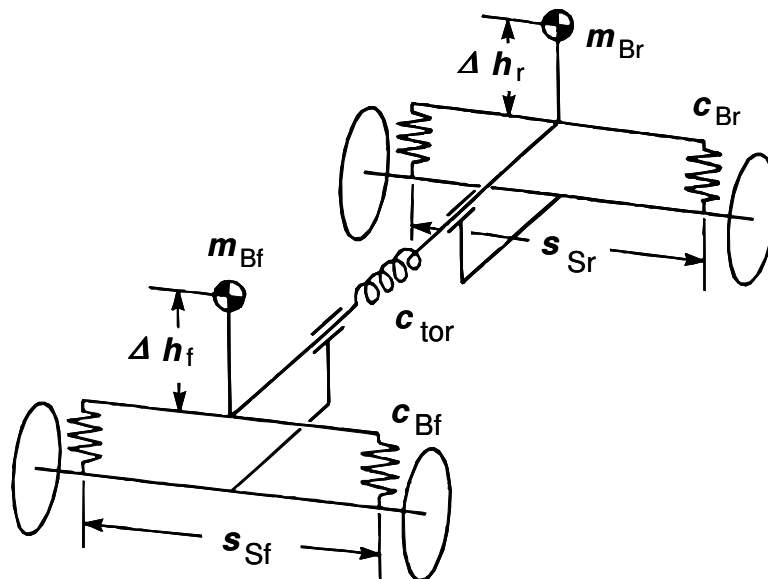


Fig.1.6-7: Replacement system of a vehicle with a torsionally elastic framework

For steady-state cornering, the equilibriums of torques set up around the roll axis for front and rear ends separately result in two equations for the two unknown roll angles ϕ_f and ϕ_r :

$$m_{Bf} \cdot a_y \cdot \Delta h_f = \varphi_f \cdot \frac{s_{Sf}^2}{2} \cdot c_{Bf} + (\varphi_f - \varphi_r) \cdot c_{tor} \quad (1.6-12)$$

$$m_{Br} \cdot a_y \cdot \Delta h_r = \varphi_r \cdot \frac{s_{Sr}^2}{2} \cdot c_{Br} + (\varphi_r - \varphi_f) \cdot c_{tor} \quad (1.6-13)$$

Since the difference between spring forces on an axle depends on the roll angle of the appropriate body sub-system, the proportion of the total roll torque supported at the considered axle in vehicles with torsionally elastic chassis is influenced not only by the distribution of the body spring stiffness and stabilizer stiffness on the front and rear axles, but also by the torsional rigidity of the frame. Accordingly, the wheel load differences during cornering at the front and the rear axle depend additionally on the torsional rigidity of the framework.

The influence of these wheel load differences on the steering behavior during cornering is treated in the section 'Lateral Dynamics' in connection with the effects of stabilizer springs.

1.6.3 Rigid Axle Tramp

Fig. 1.6-8 shows an equivalent model for the investigation of the vibrational behavior of rigid axles.

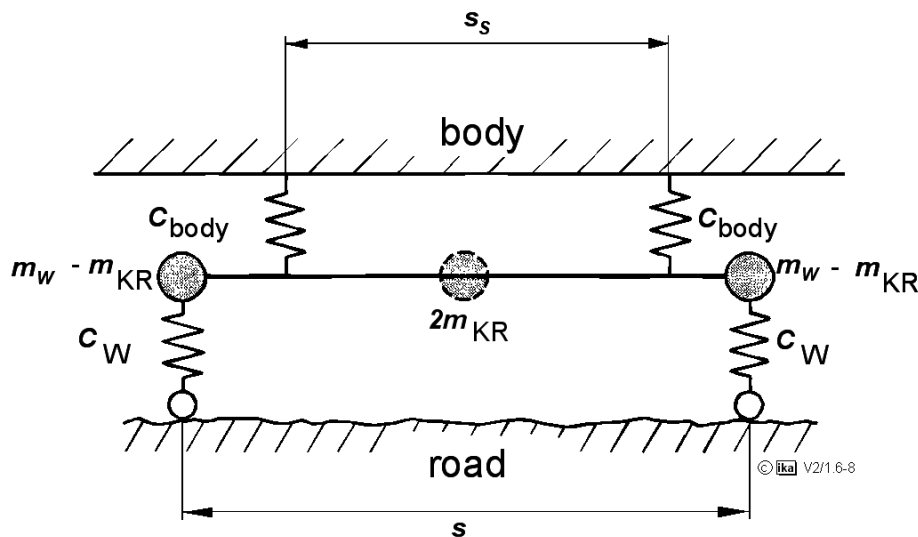


Fig. 1.6-8: Axle equivalent system

The excitation of rigid axles as a result of road irregularities not only result in vertical oscillations (bounce) as discussed so far, but also in axle tramp. The two forms of motion are usually (with left/right axle symmetry) decoupled. The natural frequencies for vertical motion can be approximately obtained as follows:

$$\omega_{e\text{rec}} = \sqrt{\frac{c_{\text{Body}} + c_W}{m_W}} \approx \sqrt{\frac{c_W}{m_W}} \quad (1.6-14)$$

Only in the theoretical case that $2 m_{\text{KR}} = 0$, i.e. the mass of the entire axle is concentrated on the two wheels, the axle tramp will be given by:

$$\omega_{e\text{Tr}} \approx \sqrt{\frac{2(s/2)^2 \cdot c_W}{\Theta}} \approx \sqrt{\frac{2(s/2)^2 \cdot c_W}{2(s/2)^2 \cdot m_W}}$$

$$\omega_{e\text{Tr}} \approx \sqrt{\frac{c_W}{m_W}} \quad (1.6-15)$$

In reality, the natural frequency for tramp exceeds that for the vertical motion, with the latter being in the range of $f_e = 9 - 14 \text{ s}^{-1}$ (lower in the case of tandem axles and front axle driven trucks).

A similar investigation of the damping coefficient D , reveals that it is lower for tramp as compared to vertical motion. Rigid axle tramp would therefore result in higher dynamic wheel load fluctuations than vertical motion, provided the excitation of both forms of motion by the road is approximately of the same magnitude. Usually however, vertical excitation (symmetrical) is found to be dominant in normal roads.

The resulting dynamic wheel loads of the rigid axle are higher than for independent wheel suspension. Moreover, the rigid axle is heavier.

1.7 Methods for Suspension Investigation

The term ride comfort usually characterizes the vibrational comfort of a motor vehicle. The low-frequency comfort perception in an automobile is not only influenced by the vibration excitation of the automotive body as a result of road roughness, but also due to non-uniformities (wheel, tire) and the gas and mass forces of the engine, Fig. 1.7-1.

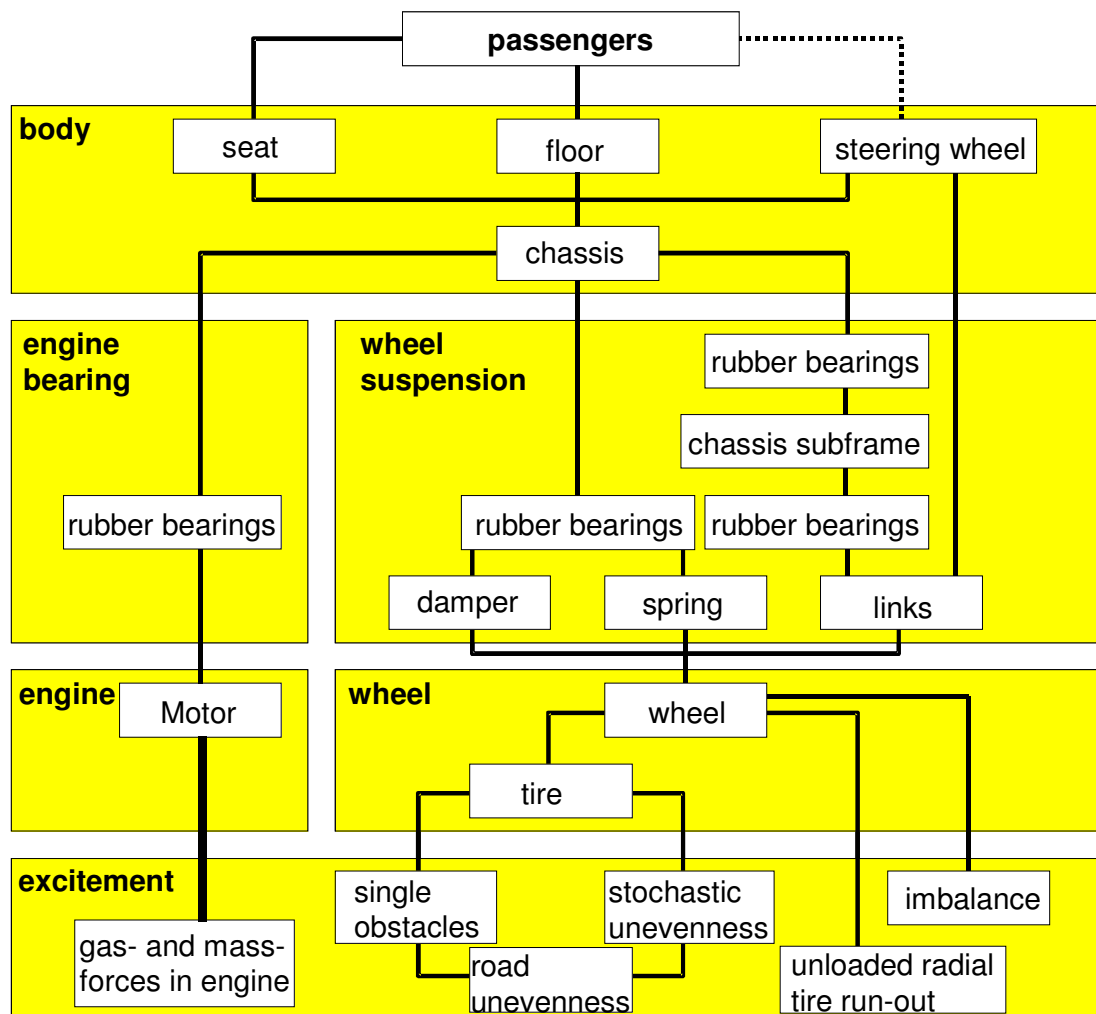


Fig.1.7-1: Paths of transmission of vibration excitation to the vehicle occupant

The forms of excitation listed, result in a multitude of vibration phenomena perceived by the vehicle occupant via the floor, seat and steering wheel (driver) in the form of body, chassis and engine mount vibration, shaking, jerking, or in the form of shocks.

Fig. 1.7-2 provides a more detailed overview of vibration phenomena which determine the ride comfort. Apart from information about the frequency ranges involved, the responsible excitations can be identified as well as the influences of individual assemblies of the vehicle

on the vibration phenomena.

		<u>excitement</u>	influence of parameters											
		road unevennesses unloaded radial tire run-out (wheel, brake) gas- and mass-forces within engine												
vibration/ noise phenomenon	frequency range		body	cabin	front axle	rear axle	suspension/ damping	steering assembly	engine	drive train	engine bearings	exhaust		
			● great influence											
			○ small influence											
body vibrations	1 - 2	●			○	○	●		○					
lateral jerking	4 - 10					○		○		●	●	●		○
abrupt load alteration	8 - 20									●	○	○	●	○
engine shake	10 - 13	●	○		●	○	●		●		○	○	○	○
axle vibrations	10 - 15	●	○		●	●	●		●		○	○	○	
wheel/rattle	10 - 20			●		●	●	○	○	○	○	○	○	
brake judder	15 - 25			●		●	●	○	○	○				
idle shake/ drone	20 - 30			●		●	○		○	○	○	○	○	○
steering wheel shake	20 - 35	○		○	●	○	○		○	○	○	○	○	
body shake	20 - 35	○		○	●	○	○	○						
body drone	25 - 75	●	○		○	○	○	○		○		○		
axle roughness	30 - 80	●			○	○	○	○						
drive roughness	50 - 100			●	○	○				●	●	●		○
exhaust vibrations	50 - 200			●	○					○				●
driving noise	50 - 250	●			●	○	●	○						
engine resonances	100 - 250			●	●	○				●	●	●		○

Fig.1.7-2: Vibrational phenomena / 27 /

A high level of riding comfort implies a low level of disturbing vibrations, shaking, jerking or bumping (shocks).

Various methods of measurement and analysis are employed for the design and tuning of vehicle suspensions. In the following section, the most important methods will be described followed by a discussion on their advantages and disadvantages.

- Computational Model

Simple computational models, such as the single-wheel suspension model or the single-track suspension model, were comprehensively dealt with in the preceding chapters. With the assistance of modern computers, significantly more complex models which produce more accurate results can be generated. Fig. 1.7-3 , for example, shows the FE simulation model of a complete vehicle. This model not only considers the dynamic properties of chassis and drivetrain but also the deformation behavior of the body.

FE-simulation model of a complete vehicle
(Audi A8)

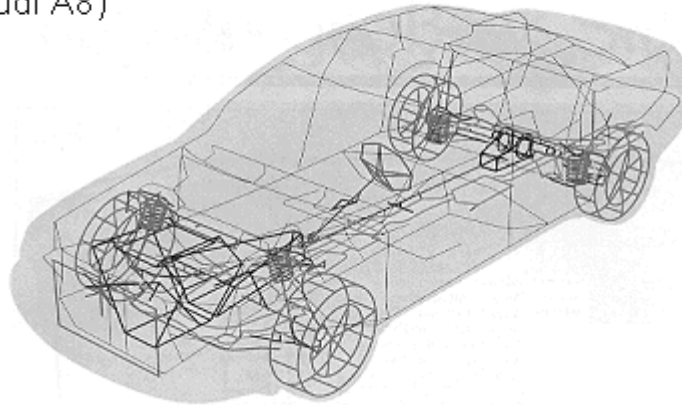


Fig.1.7-3: FE complete-vehicle simulation model of the Audi A8

In addition to complete vehicles, also individual vehicle assemblies are subjected to simulation studies. Fig. 1.7-4 shows an example of FE modeling of a front end with steering, wheel suspension, axle carriers and wheels.

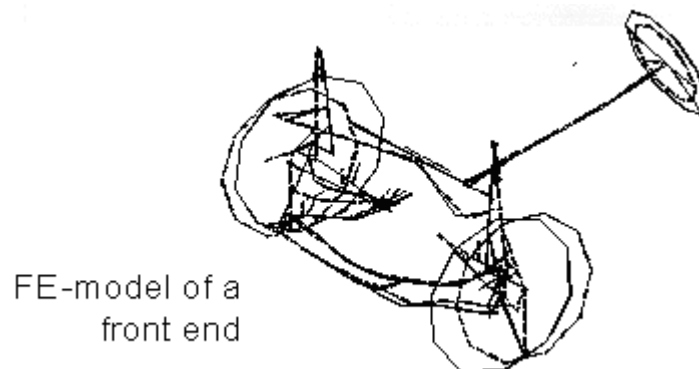


Fig.1.7-4: FE modeling of an automobile front end

Such a model can be used to determine preventive measures against vibration from the steering (niggle) (cf. Fig. 1.7-2), which can be excited by tire non-uniformities or wheel imbalance.

Nevertheless, complex models also involve a multitude of simplifications which significantly affect the precision of computational models and under certain circumstances may even result in erroneous interpretation of trends. The major benefits of computational models are represented by the fact that they can be employed at a very early stage of development and that their transparency facilitates analysis and the implementation of target-oriented improvement measures.

- Excitation on the Servo-Hydraulic Test Bench

While computer models can be applied at any point in time during vehicle development, a vibrational analysis based on the servo-hydraulic test bench usually requires a complete vehicle. The excitation here can be realised in the form of a 'real' or simulated road unevenness profile, or a sinusoidal signal. Fig.1.7-5 shows the testing of an ambulance on the hydraulic 4-cylinder test bench at the ika.



Fig.1.7-5: 4-cylinder servo-hydraulic test bench

The lab environment of a hydropulse measurement particularly offers a number of advantages:

- good overview of the entire suspension system (analysis and diagnosis),
- reproducibility of measuring results,
- acceleration of endurance tests by amplitude magnification,
- short mounting and dismounting times,
- the vehicle need not be roadworthy.

A vibrational analysis on the servo-hydraulic test bench leads to problems when the influence of the rolling wheel and the longitudinal dynamics in the chassis play a role, Fig. 1.7-6.

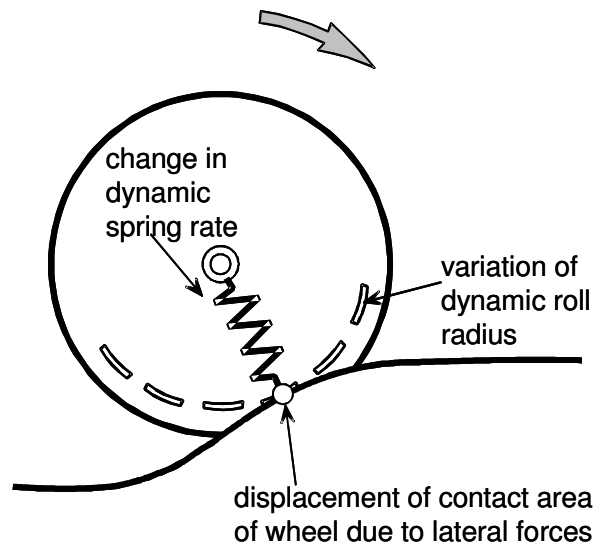


Fig.1.7-6: Effects of the rolling wheel that cannot be simulated on the hydropulser

- The stiffness and damping of the rolling wheel differ greatly from that of the stationary wheel.
- The variation of the dynamic rolling radius as a result of vertical deformation of the wheel causes rotational acceleration of the wheels and hence longitudinal forces in the tire-contact point.
- Road unevenness results in local gradients and hence in displacements of the tire-contact point. This effect also induces additional longitudinal forces in the chassis.

The considerable amount of equipment required and the fact that at least one prototype has to be available also serve as disadvantages of servo-hydraulic vibration measurement.

- Driving Tests

The subjective assessment of the suspension behavior of a vehicle by driving tests is most obvious and still remains the most important method, since the driver is able to obtain an immediate impression of the behavior of the vehicle.

The drawback of this method is the fact that assessment is only possible after design and construction of at least one prototype, i.e. at an advanced stage of development that usually allows only minor details to be changed. Moreover, since the suspension is composed of many individual effects, its analysis is very difficult and constitutes a poor basis for specific improvement measures. Driving tests are usually employed today for fine-tuning at a late stage of development.

Fig. 1.7-7 summarizes the methods discussed

technique	mathematical model	hydropulser	driving test
statement of subjective assessments		certain effects are neglected, problems can be clearly approached	identical with reality, use of appropriate roads necessary
relevance of measuring results	only as good as the models used	can be complicated under certain circumstances	good
reproducibility		good	medium
representative for analysis	good within the limits of the model	good	can be complicated due to superposition of both axles

Fig.1.7-7: Summary of methods discussed

Contents

2	Lateral Dynamics (Driving Stability)	4
2.1	Demands on Vehicle Behavior	4
2.2	Tires	7
2.2.1	Demands on Tires.....	7
2.2.2	Tire Design	8
2.2.2.1	Bias Ply Tires.....	11
2.2.2.2	Radial Tires.....	12
2.2.3	Transfer of Forces in Circumferential Direction	14
2.2.4	Force Transmission in Lateral Direction	19
2.2.4.1	Lateral Forces and Aligning Torque by Tire Slip.....	19
2.2.4.2	Lateral Forces and Aligning Torques generated by Wheel Camber	23
2.2.5	Superposition of Lateral and Circumferential Forces.....	25
2.2.6	Transient Tire Behavior.....	27

2 Lateral Dynamics (Driving Stability)

2.1 Demands on Vehicle Behavior

As is the case in all vehicles which are not track-bound, the driver of a motor vehicle has to manage not only the control or regulation of driving speed, but also the driving direction.

The control activity of the driver in the determination of the driving direction consists of three cybernetic tasks, Fig. 2.1- 1:

1. Based on all the available routes, a specific route has to be selected based on criteria such as the necessary time or distance.
2. From the selected route, the desired course has to be defined, whereby the information monitored continuously during driving (traffic both in the same direction as well as in the opposite direction, signals, route navigation) is evaluated.
3. The vehicle has to be navigated along the previously mentioned desired course over its control elements.

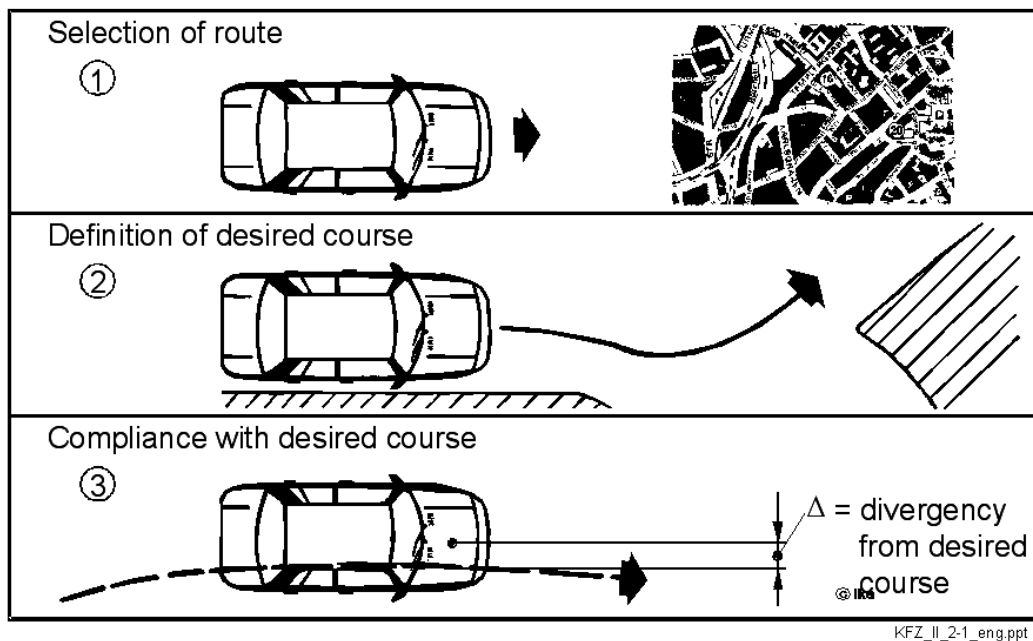
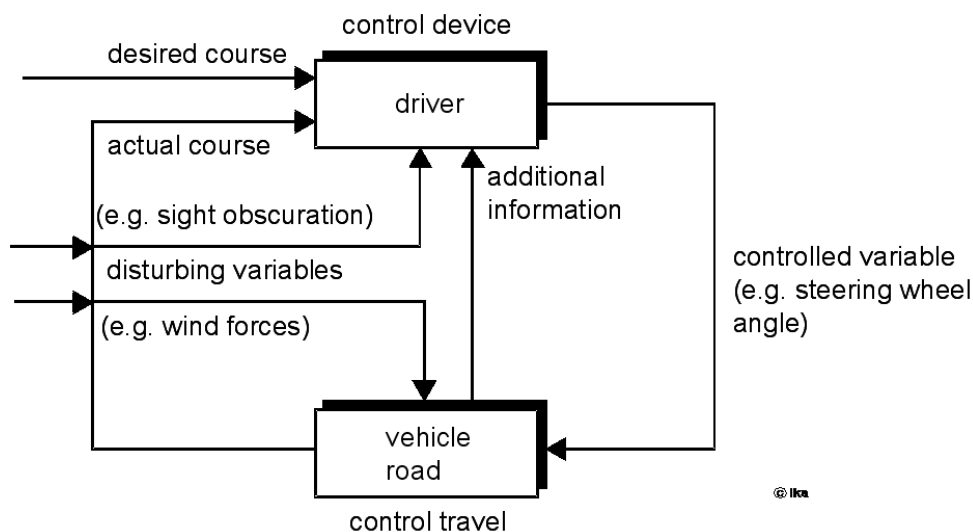


Fig. 2.1- 1: Cybernetic tasks of the driver in the guidance of a motor vehicle

In the last of the three functions, the human being undertakes the function of a control device from the point of view of driving stability. The vehicle represents the control loop, such that the interactions between driver intervention and vehicle response can be understood as processes in a closed control circuit, Fig. 2.1- 2.



KFZ_II_2-1_eng.ppt

Fig. 2.1- 2 : Control loop driver - vehicle

In this control loop, disturbing variables act on the driver (e.g. relative motion driver - vehicle, sight obscuration) and on the vehicle (e.g. crosswind, road irregularity). The steering wheel angle particularly represents the controlled variable with respect to the vehicle's transverse dynamics. A deviation in control is noticed by the driver as a difference between the desired course and the actual course.

The closed control loop is a dynamic operating system. Due to the limited possibility for the adaptation of the control device "driver", the system substantially depends on laws of vehicle behavior, if the overall driver - vehicle system remains stable from the point of view of course holding when large deviations have to be compensated quickly and under the influence of disturbances.

The characteristics of the control loop or "vehicle" has to match the abilities of the control device or "driver". The quality of this adjustment is characterized by the term "handling". From the point of view of achieving "good handling", the following demands are made on the vehicle characteristics:

- The driver should be able to recognise a reasonable and clear relationship between a change in the steering angle and the resulting change of course (transfer behavior of the control loop "vehicle", driving stability)
- The driver should be able to receive reasonable feedback about the state of motion of the vehicle (e.g. modification of characteristics of the steering-wheel torque, increasing sideslip angle and tire noise before reaching the physical limits of driving stability).
- External disturbances acting on the vehicle (e.g. wind forces) should cause little or no course deviation (inherent stability of the control loop "vehicle").

- The achievable cornering speeds and lateral acceleration of the vehicle should be high from the point of view of driving safety and driving performance (stability margin of the vehicle control loop).

Legal regulations in relation to vehicle handling are not presently available.

In view of these demands, the following chapter on Lateral Dynamics describes the laws and mechanics of lateral dynamics of vehicles by investigating the control loop or "vehicle" after separating it from the control device or "driver".

The tire characteristics are firstly considered as the basis for the study of vehicle dynamics. A presentation of the basic physical relationships of vehicle motion in a plane follows on the basis of a simplified vehicle model with linearized characteristics (Single-track vehicle model).

The most important aspects of driving stability during stationary and transient vehicle movement can already be pointed out here. This is followed by the discussion of the effects of nonlinear tire characteristics on the lateral dynamic response of vehicles in connection with the design features of the vehicle (wheel control, suspension) using simulation results. These simulation results are based on calculations using a three-dimensional nonlinear vehicle model and measurement results from driving tests.

The implementation of design features and hence certain vehicle characteristics related to lateral dynamics will be explained in more detail in the sections on "Steering" and "Wheel Suspensions".

2.2 Tires

2.2.1 Demands on Tires

The tire being the essential constructional element, transfers and influences the forces between the vehicle and road.

The type and area of application of the vehicle (road vehicle, off-road vehicle, passenger car, truck, tractor, earthmover) determine the demands according to which an appropriate tire must be selected.

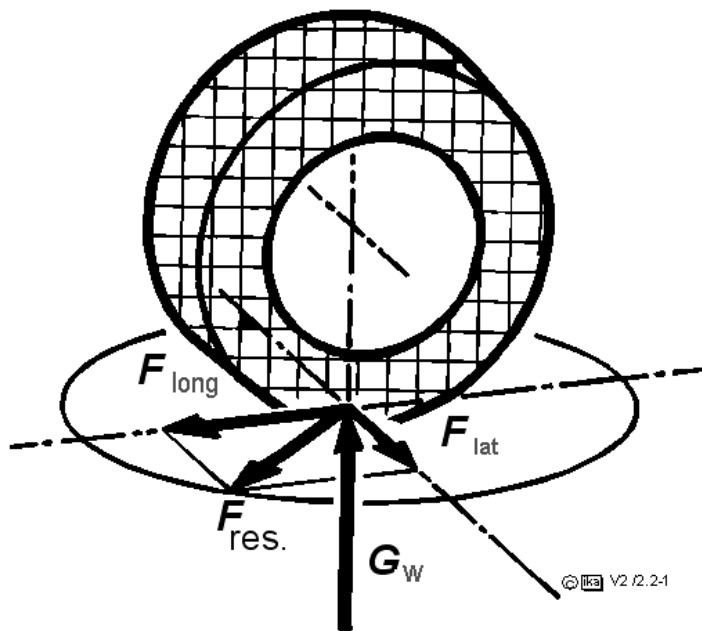


Fig 2.2-1: Forces in the tire contact patch

The following demands are made on a tire for road vehicles:

1. Safety

- high friction coefficients for all operating conditions
- adequate (long-term) top speed
- negligible wheel-load variation
- guarantee against breakdown
- flat-running properties

2. Comfort

- low rolling hardness, matched suspension characteristics
- smoothness

3. Economy

- high durability
- low rolling resistance
- low dynamic wheel loads (road load)
- low construction volume (space requirements of wheel houses, spare-wheel recess)
- high load carrying capacity

These demands are to be fulfilled individually during selection of suitable tire construction parameters. Ideally, a tire should meet as many of the demands as possible. Since the possibilities of implementation are however partly contradictory, a compromise which is appropriate to the tire specification and the vehicle's field of application must be found.

2.2.2 Tire Design

The following constructional elements can be differentiated in today's vehicle tires (fig.2.2-2):

-Tire bead

-Carcass

-Sidewall

-Tread

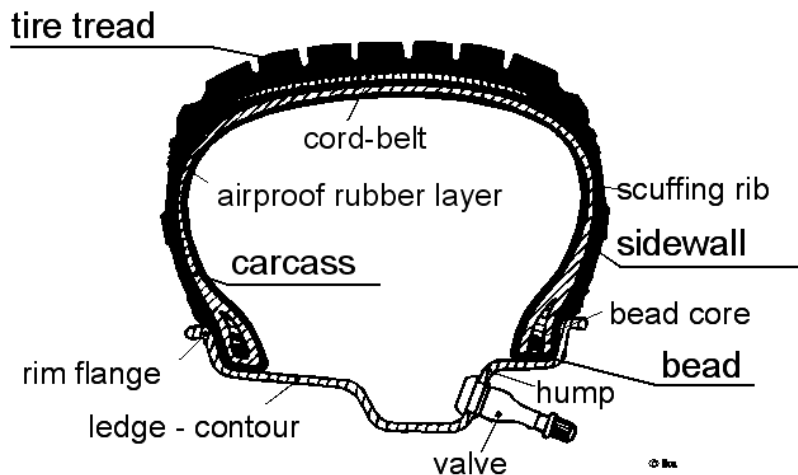


Fig 2.2-2: Section of a tubeless car belted tire

Tire Bead

The primary function of the tire bead is to guarantee a fastening of the tire on the rim. In order to prevent a linear expansion of the tire at the rim contour, one or more bead wires are included in the tire bead. In case of tubeless tires, the tire bead also doubles as a seal which separates the air volume in the tire from the environment.

Sidewall

The sidewall with its skirting serves as a rubber covering for the carcass reaching from the tire bead to the tread. It serves to protect the layers of the carcass against destruction by external influences.

Tread

The tread surrounds the carcass at its outer circumference and maintains frictional or positive-engaged contact between road and tire. Based on the application of the tire, suitable rubber mixtures and profiles are selected. Rubber mixtures and profiles for summer tires, winter tires and all-season tires can be differentiated.

Carcass

The carcass, which is held in tension by internal pressure, forms the supporting structure of a tire. It consists of several fabric layers which are embedded in rubber and isolated to prevent mutual contact. The fabric materials used in the past were Cotton, followed by Rayon. Nylon and Polyester are predominantly used today. The strength of the carcass is determined by number and material of the fabric layers. It is indicated by the PR-number (ply rating), which does not necessarily correspond to the actual number of plies.

The cord angle γ , also denoted as the crown angle, is defined as the angle between the threads of the fabric plies and the centerline of the tire circumference, Fig 2.2-3.

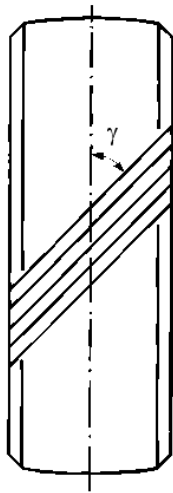


Fig 2.2-3: Definition of cord angle

The cord angle influences the rigidity of the carcass substantially. Furthermore it affects tire characteristics such as rolling resistance, suspension characteristics, high-speed capability and tire slip rigidity (chap. 2.2.4). The cord influence of the cord angle on the stiffness of the carcass in principle is shown in Fig. 2.2-4.

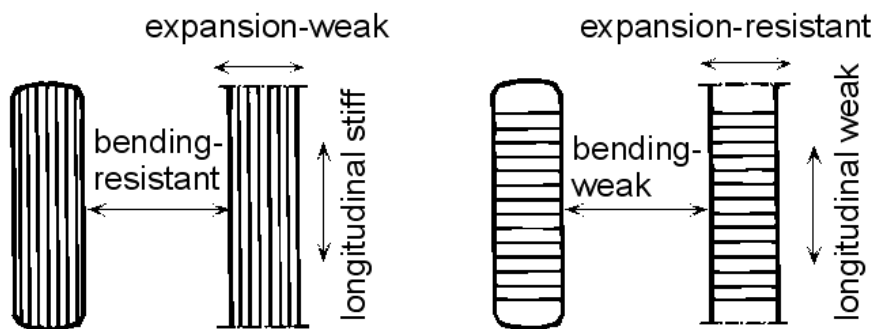


Fig 2.2-4: Influence of cord angle /9/

According to /9/, for the sake of explanation, the tire (illustration on the left) can be unwound and considered as a simple tube (illustration on the right) to describe the influence of the cord angle.

For a cord angle equal to zero, all threads run parallel to the circumference of the wheel, or in the longitudinal direction in case of the tube. The tube length or the tire circumference is determined by the thread length. The tire is hence rigid in the circumferential direction and relatively rigid to lateral forces, while on the other hand a ballooning in the radial direction is possible.

In comparison, when a cord angle of 90° is considered, the threads run perpendicular to the circumference of the wheel. The tube appears to be wound. A ballooning of the tire, e.g. due

to centrifugal forces at high circumferential speeds is prevented. On the other hand, expansion in the circumferential direction of the tire as well as bending from the effect of a lateral force is possible.

In summary the following can be fixed:

Small cord angles:

- rigid tire tread (horizontal)
- soft sidewall (radial)

Large cord angles:

- soft tire tread (horizontal)
- rigid sidewall (radial)

This classification applies approximately to the comparison of different bias ply tires (see chapter 2.2.2.1). In case of radial-ply tires this classification cannot be employed (see chapter 2.2.2.2). Their carcass contains fewer fabric layers, but additional ply belts, which strongly influence the tire characteristics.

2.2.2.1 Bias Ply Tires

Bias ply tires show diagonally crossed fabric layers in their substructure; resulting from this, the denomination of this tire design is dissipated. In normal tires of this type, the primary direction of the cords of the carcass fabric layers intersect the line of the tire's circumference at an angle of 35° - 38° . In high-speed and racing tires, the cord angle approximately amounts to 26° .

Fig. 2.2-5 shows a bias ply tire with intersecting cords and four layers in its substructure. Depending upon the demands on strength, textile fibers or steel cords are used as material for the fabric layers.

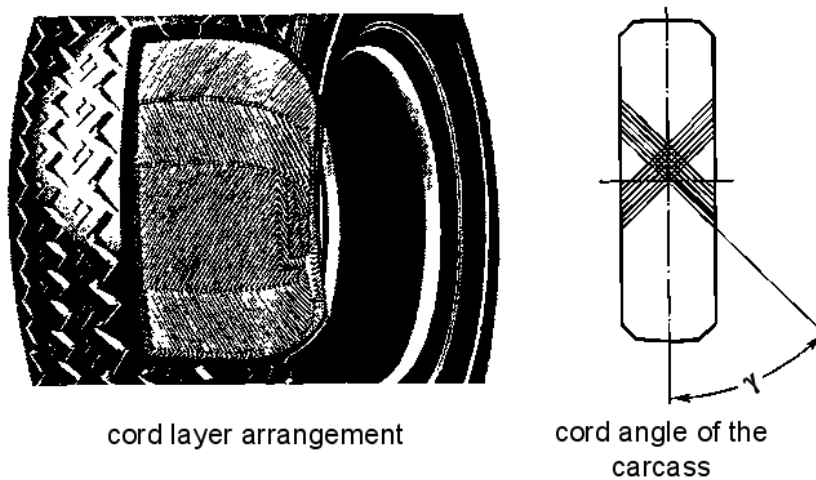


Fig. 2.2-5: Bias ply tire

2.2.2.2 Radial Tires

Radial tires feature an almost obtuse cord angle in the substructure of the carcass, which amounts to between 85° and 90° .

Accordingly, the primary cord direction runs in a direction radial to the tire, hence the name given to the tire.

Bracing plies are present above the layers of the substructure of the carcass in the circumferential direction. Depending on manufacturer and the demand, materials such as polyester cords, steel cords or other materials such as glass fibre and similar materials are used.

The individual bracing plies indicate a cord angle between 6° to 20° to the circumferential line of the tire, fig.2.2-6.

The belt which circumscribes the tire, is limited in its flexibility and distorts the substructure, hardens the tread and is also responsible for its flat shape. This is the reason behind radial car tires generally not exceeding an aspect ratio of 0.82.

A reduction of weight as a result of the smaller aspect ratio of the radial tire in comparison to the bias ply tire has a positive effect on ride comfort and driving safety.

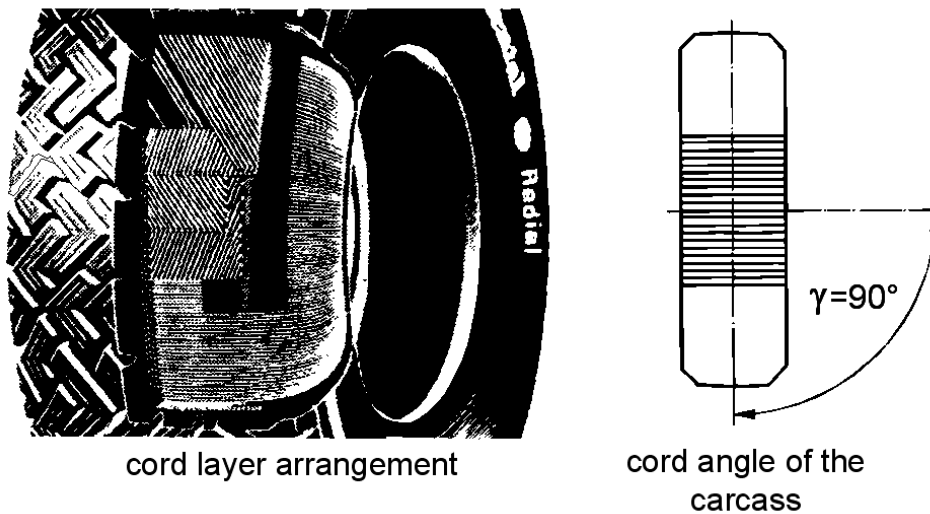


Fig. 2.2-6: Radial-ply tire (belted tire)

The carcass which consists of the substructure and bracing ply, allows for the optimisation of the tire characteristics within certain limits independent from each other.

Radial tires consist of fewer fabric layers in their substructure and hence contain lower quantities of rubber in the sidewall as compared to bias plies. This results in a reduced radial rigidity of the carcass. Rigidity of the tread obviously increases by using belts. Due to the uniform distribution of pressure at the center of tire contact patch, fig.2.2-7, the usable friction coefficient is higher, i.e. larger circumferential as well as lateral forces can be transferred between tire and road.

A lower rigidity of the sidewalls implies that the radial tire in its rolling process converts a smaller proportion of its deformation energy into heat. Higher rigidity of the tread also results in reduced flexing energy in the area of the tread. As a result of the lower rolling-resistance power, the operating temperatures of radial tires are lower than those of bias plies under identical conditions. Hence, the stability at high-speeds is better and the achievable performance, higher.

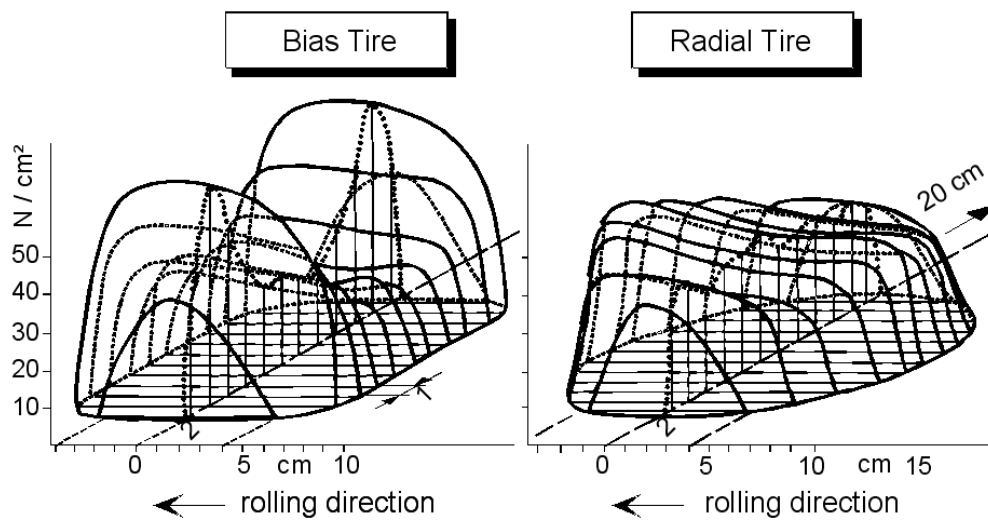


Fig. 2.2-7: Pressure distribution in the contact area of straight ahead rolling tires of different designs / 15 /

2.2.3 Transfer of Forces in Circumferential Direction

The area of tire contact with the road is called the Tire Contact Patch. The physical and chemical processes which enable force transmission take place here. The transfer of forces results from adhesion and positive engagement.

- Adhesion: Adhesion in the contact surface between road and tire.
- Positive Engagement: interlocking of tire and road surface by the intrusion of irregularity (e.g. granulation of road surface) into tire rubber or a plastic road surface (off-road surface) into the negative profile of the tire.

According to the classical law of friction (Coulomb) the maximum force transferred by the tire contact patch is directly proportional to the wheel load. The proportionality factor between frictional force F_R and wheel load G_R is called coefficient of friction μ :

$$F_R = \mu \cdot G_R \quad (2.2-1)$$

This relationship only applies to the combination of materials considered at the tire (e.g. concrete-rubber), if the coefficient of friction μ is assumed as the dependent variable in a set of influencing factors.

Due to the elastic characteristics of the rubber material in the tread, circumferential forces can be transferred only in combination with rotational slip, i.e. a speed difference between the circumferential speed v_R of the wheel and driving speed v .

The following definitions of rotational slip are used for acceleration and braking, which result in positive values for $1 \geq \lambda \geq 0$.

$$\lambda_A = \frac{r_{\text{dyn}} \cdot \omega_w - v}{r_{\text{dyn}} \cdot \omega_w} \quad (v \geq 0, \omega_w \geq 0, r_{\text{dyn}} \cdot \omega_w \geq v) \quad (2.2-2)$$

$$\lambda_B = \frac{v - r_{\text{dyn}} \cdot \omega_w}{v} \quad (v \geq 0, \omega_w \geq 0, r_{\text{dyn}} \cdot \omega_w \leq v) \quad (2.2-3)$$

Fig.2.2-8 shows the relationship between rotational slip and utilized friction for the transfer of circumferential forces on different road surfaces / 33 /.

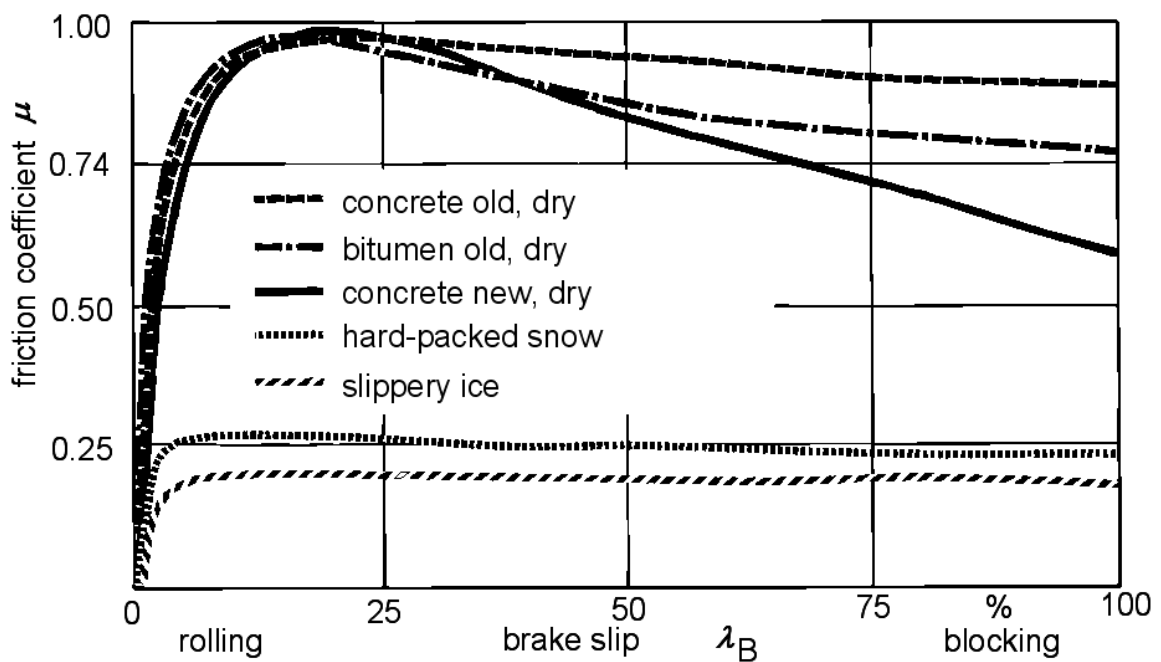


Fig.2.2-8: Relationship between rotational slip and friction coefficient for circumferential forces acting on a pneumatic tire

On roads which offer good grip, the utilized friction coefficient initially rises with increasing slip up to a maximum value and then declines to the sliding coefficient at a slip of 100%. On slippery roads the maximum coefficient of friction and the sliding coefficient only differ marginally from each other.

The relationship between rotational slip and frictional coefficient in the circumferential direction depends not only on the condition of the road surface, but also on the condition of the tire.

In addition to tire design (see above) the tread layout also plays a significant role. The primary task of the tire tread is to maintain contact between the road and tire in case of dirt or

wet conditions. In the following section, the influence of the tread pattern on the coefficient of friction μ for dry and wet roads will be discussed.

Influence of Tread on the Coefficient of Friction μ for *Dry* Roads:

Experiments show that the transferable forces increase with decreasing tread depth and driving speed on clean, dry road surfaces, fig.2.2-9.

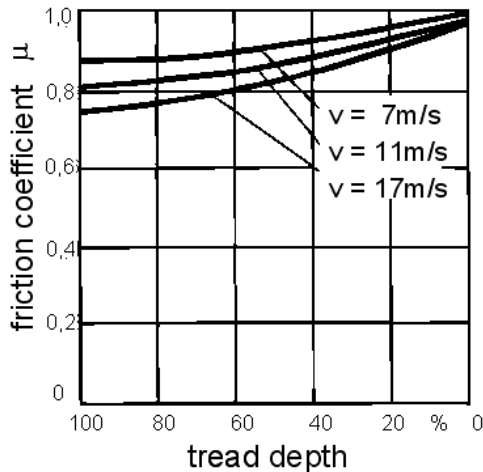


Fig.2.2-9: Friction coefficient as a function of driving speed and tread depth on dry roadways

A possible explanation can be seen in the fact that decreasing tread depth causes the surface pressure to be spread uniformly on the surface of the individual tire profile elements, such that the total amount of sheer stress on the entire tire-contact length results in a higher grip. A smaller driving speed has a similar effect since the centrifugal forces which cause an upward deformation of the tread become smaller. The road-contact area of the tire hence becomes marginally larger for the same total load. In case of radial tires, the upward deformation of the contact surface is largely prevented by the radial belt.

Influence of the Tread on the Coefficient of Friction μ for *Wet* Roads:

The tire tread enables road contact on wet roads by displacing the fluid. The tread pattern of the tire has to take up a part of water or displace it from the area of road contact. The water volume displaced is proportional to the velocity v and the film thickness of the water z_F .

$$\dot{Q} \sim v \cdot z_F \quad (2.2-4)$$

Increasing driving speeds reduce the time available to produce road contact. A wedge of water is formed between tire and road, which intrudes into the tire contact patch at increasing velocity and reduces the contact surface between tire and road, fig.2.2-10.

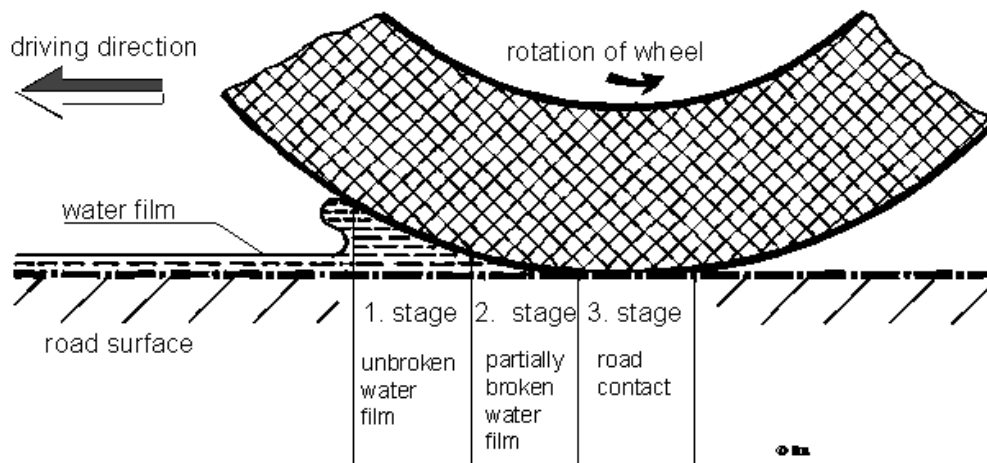


Fig.2.2-10: Displacement of a water film from the contact area between tires and roadway

The transferable horizontal forces in the tire contact area fall, since a part of the wheel load is transferred in the vertical direction, similar to a hydrodynamic bearing. Only the remaining part in conjunction with the locally usable friction coefficient contributes to the transfer in horizontal direction. The phenomenon of floating of the tire on the water wedge is called „Aquaplaning“.

In Fig 2.2–11 the dependence of the maximum friction coefficient for braking on the driving speed and level of the water film is shown using a steel-belted tire (measurement on internal-roller test bench) as example. Fig.2.2 –12 shows the influence of tread depth.

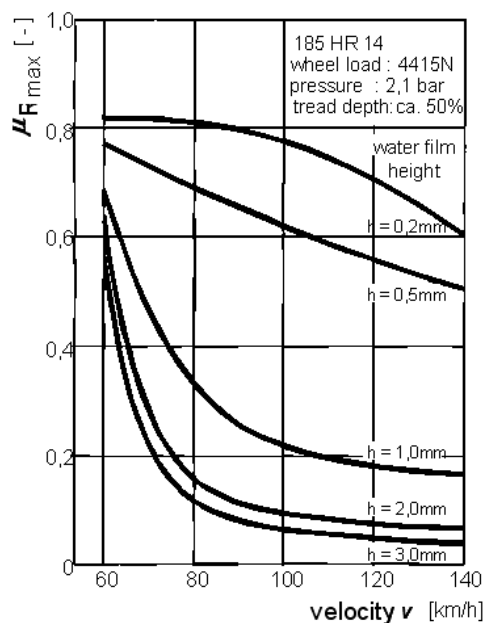


Fig.2.2-11: Friction coefficient for braking force as a function of driving speed and water film thickness on the road / 16 /

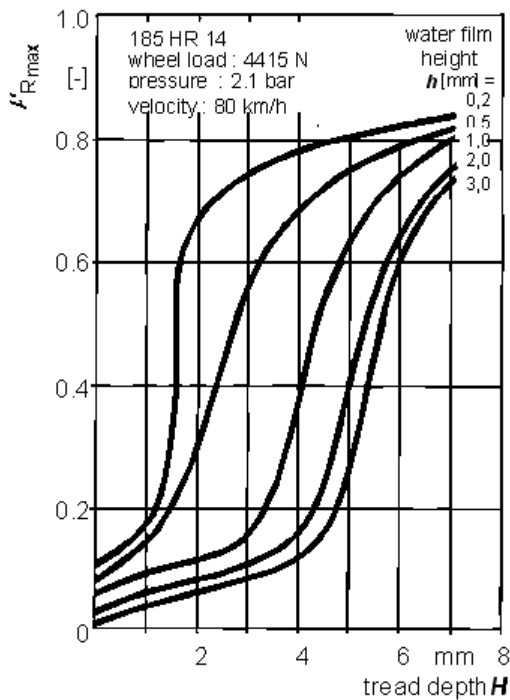
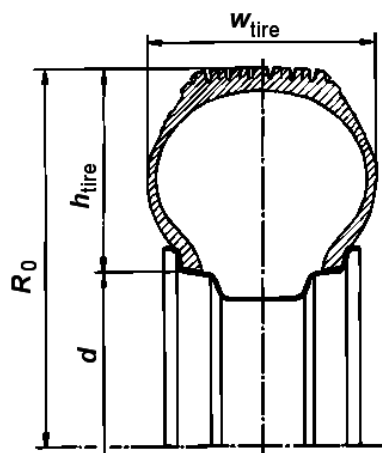


Fig 2.2-12: Friction coefficient for braking force as a function of tread depth and water film thickness on the road / 16 /

With progress in the development of motor vehicles, the demand on load-carrying capacity and load transfer characteristics of tires is constantly increasing. The development of wide tires with a reduced aspect ratio (Fig 2.2-13) allows a reduction of tire diameter for a constant load-carrying capacity.

$$x = \frac{h_{\text{tire}}}{w_{\text{tire}}} \cdot 100\%$$



(aspect ratio)

Fig.2.2-13: Aspect ratio

Even after introduction of radial tires at the beginning of the 60`s, the trend towards a further reduction of the aspect ratio remains. This reduction in aspect ratio is not associated with reduced external diameters, but rather with increased rim diameters, which facilitate the accommodation of high-performance wheel brakes.

Smaller aspect ratios offer the advantage of uniform and reduced surface pressures in the tire contact patch as a result of the larger footprint. This enables better force transfer between the tire and road.

Furthermore the appearance of the vehicle as a result of the reduced ground clearance meets with the contemporary sense of styling.

The disadvantages of wider tires include the increased danger of aquaplaning on wet roads as well as reduced spring and damping properties. Since the improved force transfer in the tire contact area improves the driving performance of the vehicle substantially, the disadvantages of these tires are either accepted (e.g. compromising comfort in favor of better driving performance in sports cars) or reduced as far as possible by additional measures (e.g. target-oriented design of the tire tread for reduction of the danger of aquaplaning).

2.2.4 Force Transmission in Lateral Direction

2.2.4.1 Lateral Forces and Aligning Torque by Tire Slip

A rolling wheel exclusively moves under the influence of circumferential forces towards the intersecting straight line of the plane of the wheel and the road. If a lateral force acts on the wheel, an angle is formed between the direction of movement of the wheel and this intersecting straight line. This angle is called the Slip Angle α , fig.2.2-14.

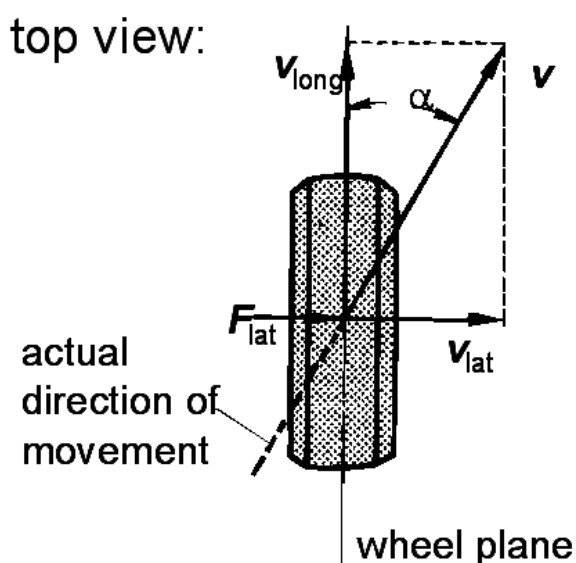


Fig.2.2-14: Definition „Slip Angle“

The reason behind this tire slip is a continuous lateral deflection of the rolling tire in the range of the tire contact area under the effect of the lateral force transferred between tire and road.

Only by this deflection of the elastic tire material, shear stresses which are necessary for transferring the lateral force can be established in the tire contact area. In analogy to rotational slip, the tire slip is also called transverse slip. A detailed illustration of tire deformation when transferring side forces is possible on the basis of fig.2.2-15.

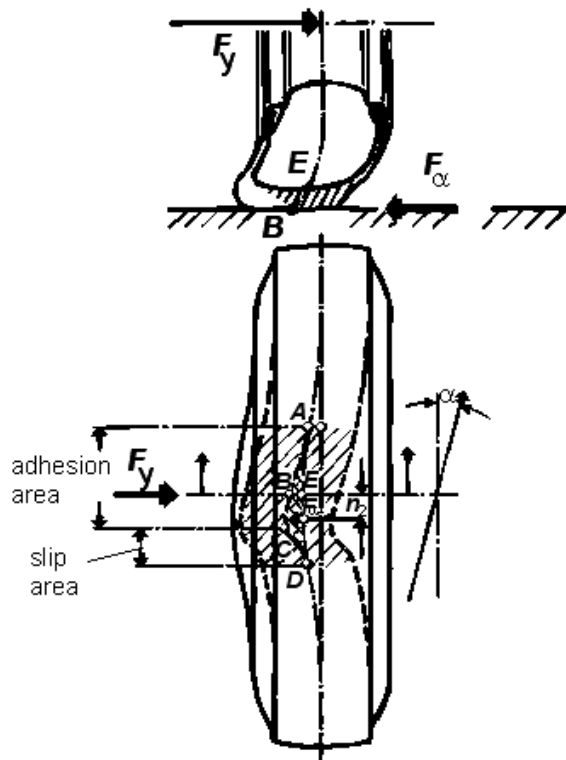


Fig.2.2-15: Deflection of the rolling tire by a lateral force F_y

The non-deflected part of a rotating tire is deformed gradually while contact between tire surface and road is set, as represented in fig.2.2-15 (upper picture).

In the tire contact area, the center line of the tire body is moved from the wheel plane into the position AED (fig.2.2-15, lower picture). The circumference of the tread in the tire contact area comes into contact with the road along the line ABCD and is increasingly deformed along A to C. Here the friction coefficient between rubber and road is sufficiently large in order to prevent the rubber from returning to its mean position. Behind point C, the deflection results in a shear stress which is so large that the friction on the road is exceeded, resulting in the deflected portion of the contact patch elastically returning to its mean position at point D.

The line AC runs at an angle to the wheel plane. It indicates the direction of motion of the wheel, since the surface of the tire adheres to the road within this area. The angle between the plane of the wheel and the line AC is identical to the slip angle α .

The surface included between the lines AED and ABCD is a measure for shear deformation of the protective rubber over the tire body and for the local distribution of shear forces in the tire contact area. The sum-total of shear forces result in the Cornering Force F_α .

As this force acts in the center of gravity of the surface, about caster n_2 behind the wheel center, an Aligning Torque M_α results:

$$M_\alpha = F_\alpha \cdot n_2 \quad (2.2-5)$$

The relationship between slip angle α and cornering force F_α depends on several parameters. In particular the wheel load G_W has a large influence on size of the cornering force for a constant slip. Fig.2.2-16 indicates a corresponding tire performance map for a passenger car tire. It was determined on a test bench.

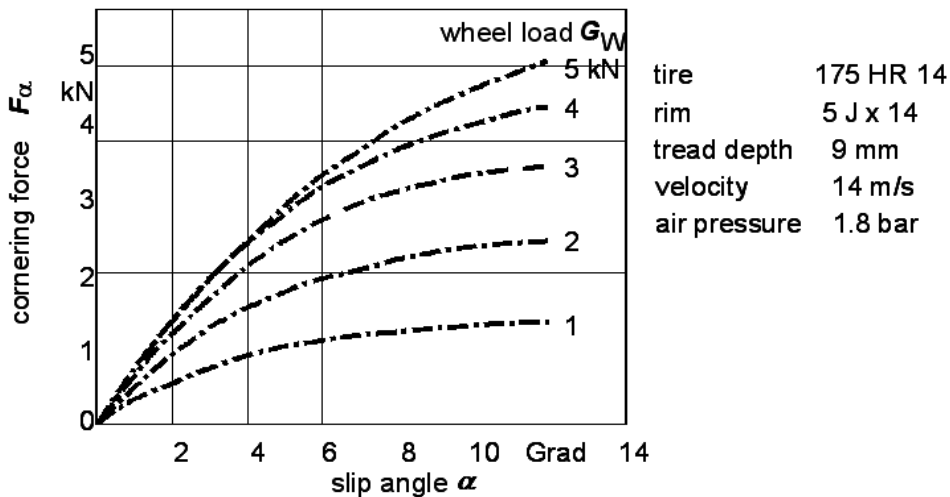


Fig.2.2-16: Cornering force subject to the slip angle (wheel load as a parameter)

With another illustration of this diagram, fig.2.2-17, it becomes clear that not only the relationship between F_α and α shows a degressive distribution at a constant G_W , but also the dependence between F_α and G_W at α =constant.

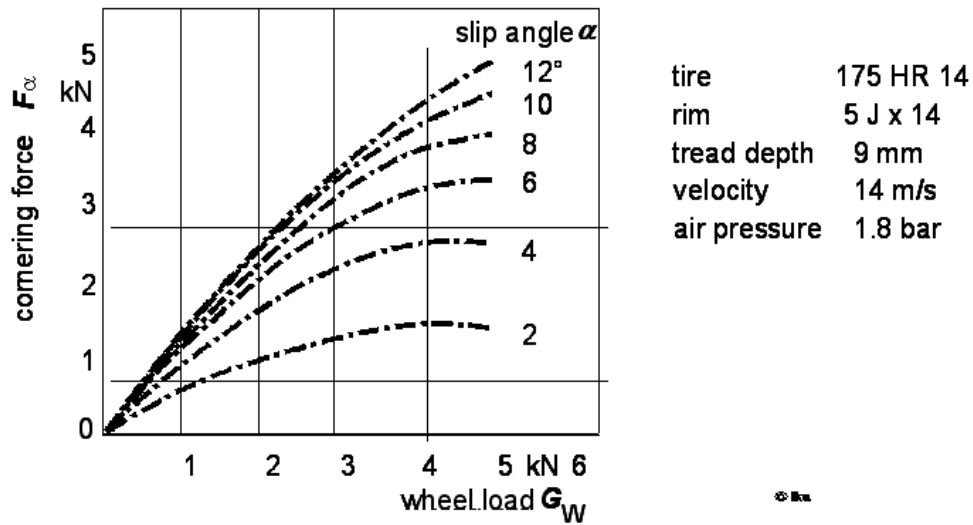


Fig.2.2-17: Cornering force subject to the wheel load (slip angle as a parameter)

Influence of the tire inflation pressure on the transfer behavior of lateral forces of the exemplary tire is shown in Fig.2.2-18. The measured values of the cornering force indicate maximum values for a certain air pressure, for which the tire design is optimized.

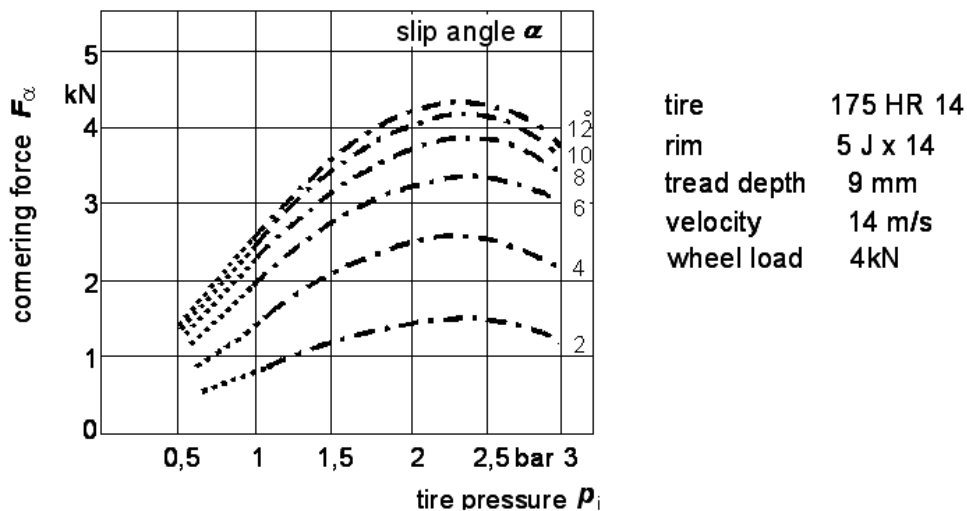


Fig.2.2-18: Cornering force subject to the tire inflation pressure (slip angle as a parameter)

Fig.2.2-19 shows the tire performance map for aligning torques. The magnitudes of the aligning torques depend on the respective specific magnitudes of adhesive and sliding friction in the tire contact area (see fig. 2.2-15).

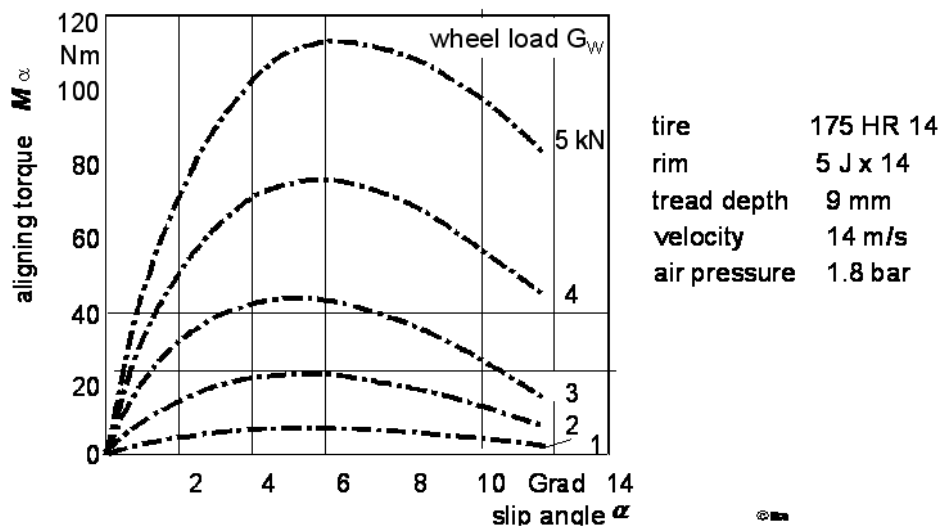


Fig.2.2-19: Aligning torques M_α subject to the slip angle (wheel load as a parameter)

The so-called GOUGH diagram provides a summarised representation of side force and aligning torque characteristics of a tire, fig.2.2-20. In a characteristic operating point of the tire specified by the current wheel load G_w and the current slip angle α , the resulting lateral force as well as the aligning torque and the tire caster n_2 can be read off here (cp.fig.2.2-15).

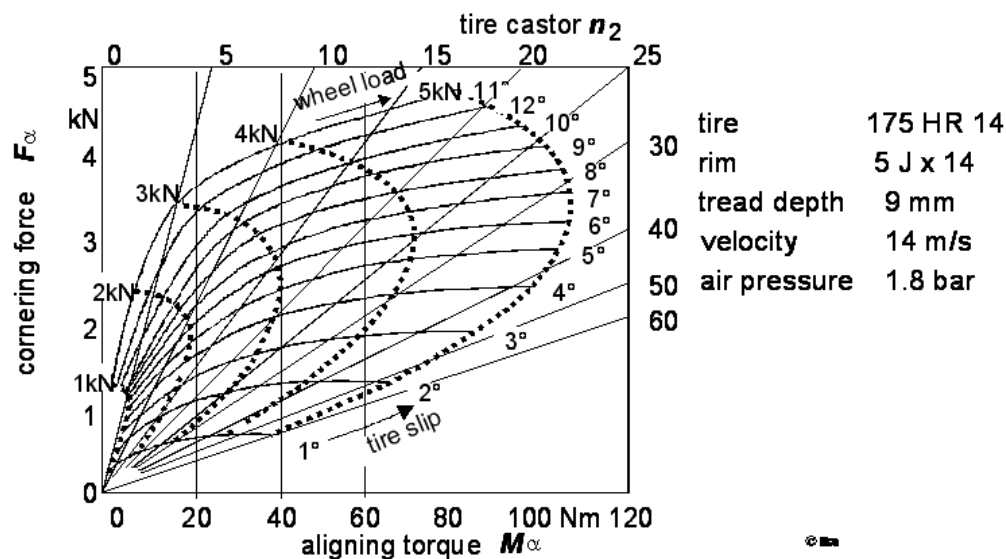


Fig.2.2-20: Tire performance map by GOUGH /19

2.2.4.2 Lateral Forces and Aligning Torques generated by Wheel Camber

The camber angle γ is defined as the angle between the wheel plane and the normal of the road in the transverse plane of the automobile. One differentiates between positive and negative camber, fig.2.2-21.

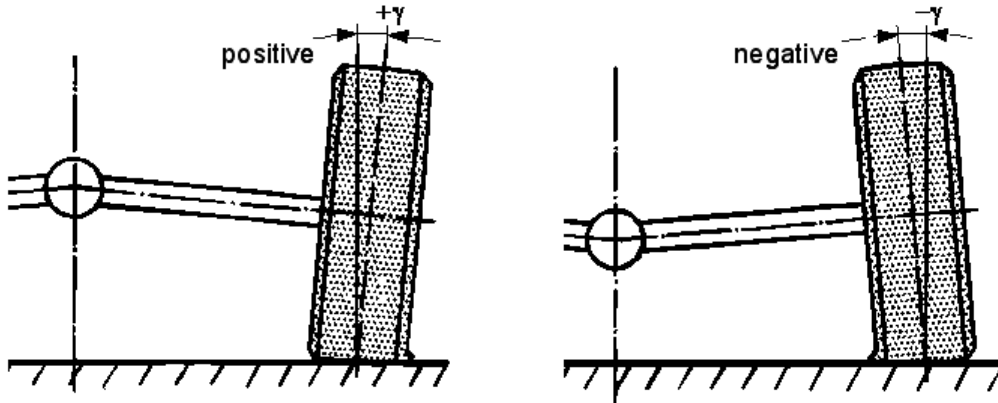
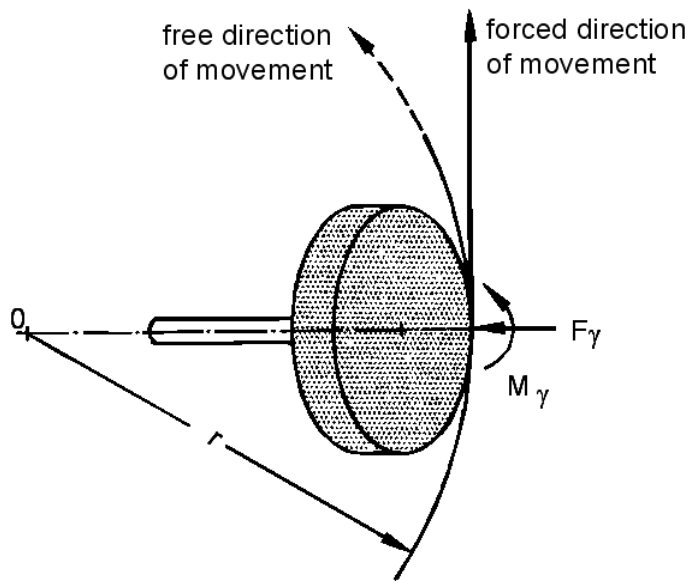


Fig.2.2-21 : Definition wheel camber

A freely rolling wheel running under camber would move on a circular path around the center of the trajectory O . As a result of the wheel suspension, the wheel is forced into straight-ahead direction. Thereby the camber force F_γ and a camber torque M_γ is developed, fig.2.2-22.

Fig.2.2-22 : camber force F_γ and camber torque M_γ

The value of the camber force F_γ increases approximately linearly with the camber angle up to $\gamma=10^\circ$ at a constant wheel load. At a constant camber angle the camber force changes proportional to the wheel load. As is evident from fig.2.2-23, the forces and torques resulting from wheel camber are very small compared to those resulting from tire slip.

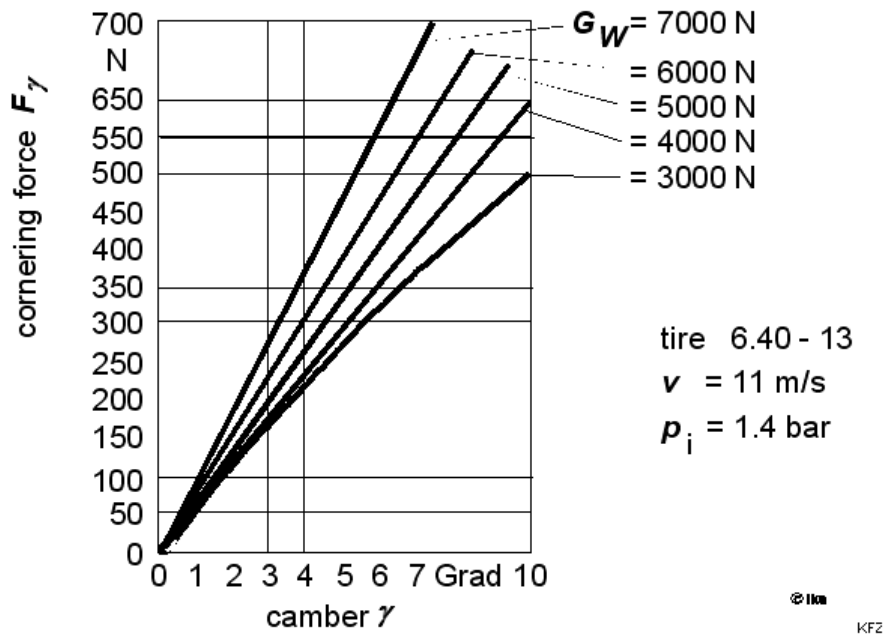


Fig.2.2-23: Cornering force F_γ subject to the camber angle for different wheel loads

2.2.5 Superposition of Lateral and Circumferential Forces

In reality, circumferential forces as well as lateral forces are usually transferred simultaneously from the tire to the roadway.

In fig. 2.2-24 the resulting lateral force F_α when a wheel is subjected to a simultaneous traction or braking force is indicated for different slip angles α . The characteristic map was recorded on a tire test bench.

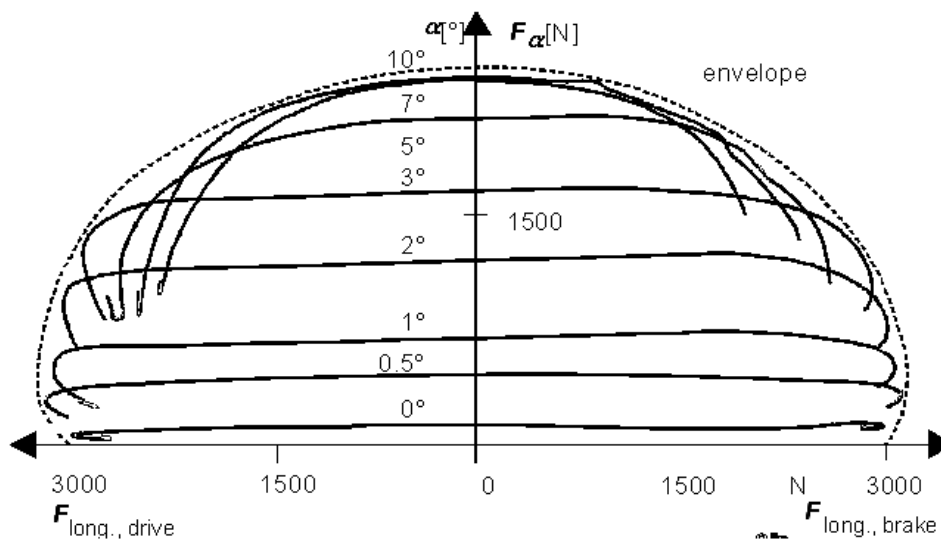


Fig.2.2-24: Characteristic map for lateral force, traction (Krempel graph) / 26 /, tire 165 SR 15, tread 60 %, Rim 4 x 15, $G_W = 3000$ N, $p_i = 1.8$ bar, $v = 14$ m/s

It is clear from the hemispherical curve, that the larger the circumferential force F_C becomes, the smaller is the maximum transferable lateral force F_{α} . Conversely, the larger the lateral force F_{α} that is required for cornering, the lower is the maximum allowable circumferential force F_C .

The curves of constant tire slip α indicate particularly for the larger tire slip angles, a decrease of the cornering force at increasing circumferential force F_C , i.e. with increasing rotational slip λ .

The functional relationship of the Krempel-chart is described in the following:

With the rotational slip λ as a parameter the tire performance map, the characteristic on the top right-hand side of fig 2.2-25 results. Its characteristic line at $\lambda = 0$ corresponds with the illustration in fig.2.2-16, but continues in the range of larger tire slip angles.

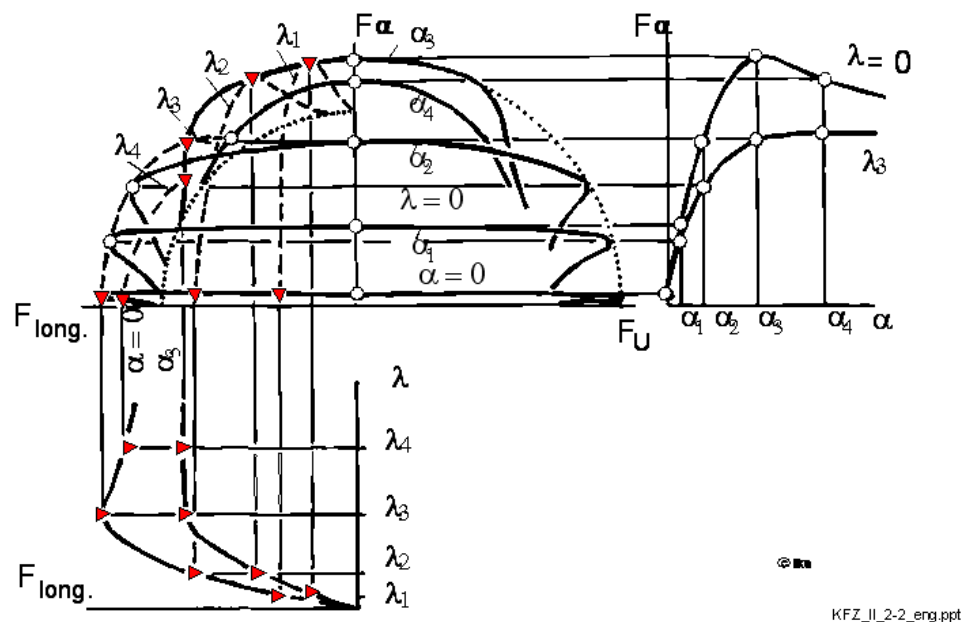


Fig.2.2-25: Superposition of tire forces, lateral forces and circumferential forces / 41 /

At the beginning of section 2.2.4.1, it was already mentioned that the tire slip in analogy to rotational slip can also be understood as transverse slip. Thereby, for the relationship between rotational slip λ and circumferential force F_C with the tire slip α as a parameter, a corresponding representation to the figure on the top right results in the figure at the lower left, fig.2.2-25.

If both fields are transferred into one diagram, which again represents the lateral force as a function of the circumferential force, the reason behind the curves of constant tire slip angle curving backwards in fig. 2.2-24 becomes clear. The curves initially become tangential to the hemisphere with increasing rotational slip and then huddle against the inner ellipse of sliding friction with further increase of slip. In fig. 2.2-25 curves of constant slip λ are indicated in

analogy, which once again points towards the formal equivalence of rotational slip and tire slip or transverse slip and the law of superposition. Another representation of the relationship between lateral forces and circumferential forces is shown in fig. 2.2-26. Here a characteristic map of lateral force and traction is indicated as a function of the rotational slip λ_B . This is of interest e.g. from the point of view of brake-force regulation (ABS).

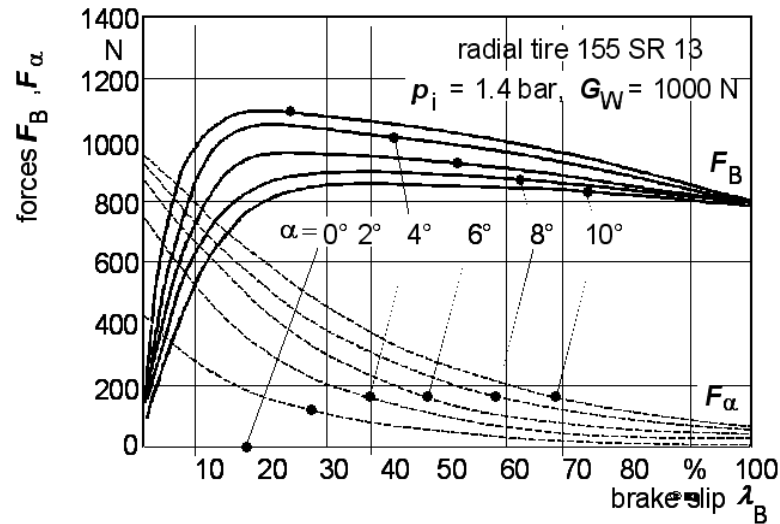


Fig.2.2-26: Lateral force – traction map subject to the brake slip λ_B

2.2.6 Transient Tire Behavior

The tire characteristics described in the preceding paragraph are strictly speaking only applicable to steady-state conditions, i.e., for very slow temporal changes in the considered influencing parameters.

Due to the nonlinearity of the tire characteristics and the run-in process in the tire contact area for changes in the operating parameters, for normal driving, the tire characteristics differ from those described by the characteristic map.

Fig. 2.2-27 shows the influence of nonlinearity when the operating parameters are temporally varied using the example of a harmonic wheel load fluctuation.

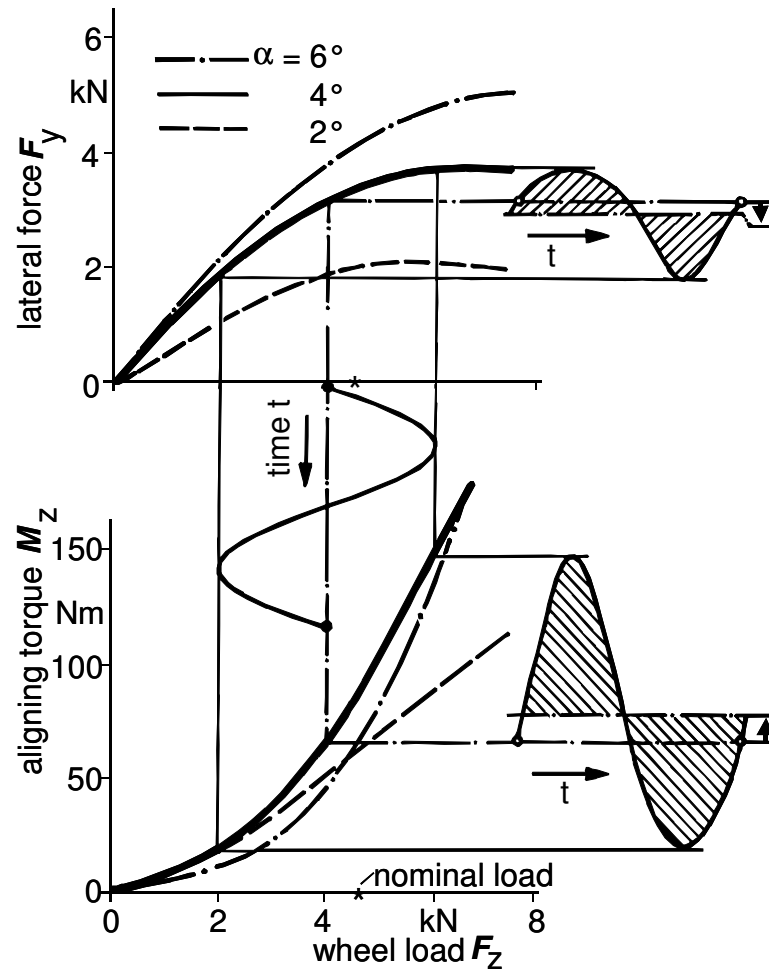


Fig.2.2-27: Determination of the quasi-static loss of lateral force and changes of the aligning torque as a result of harmonic wheel load fluctuations on the basis of static characteristic lines (PC-tires 185/70 R 14, $p_i = 2$ bar, $v = 20$ km/h) / 27 // 43 /

Due to the degressive F_y - F_z -trend, the mean lateral forces are smaller due to wheel load fluctuations when compared to the static values. In case of the aligning torque M_z , an amplification is noticed compared to the static values due to the usually progressive M_z - F_z -lines.

The influence of the run-in processes in the tire contact area as a result of a harmonic modification in the slip angle is shown in Fig. 2.2-28. With increasing steering frequency, a hysteresis loop is formed at first, which results from a phase shift between tire slip angle (steering angle) and lateral force. With further increasing steering frequency, the maximum value of the slip angle passes through so quickly, that the achieved lateral force is only a part of the maximum value which is achieved at low steering frequencies.

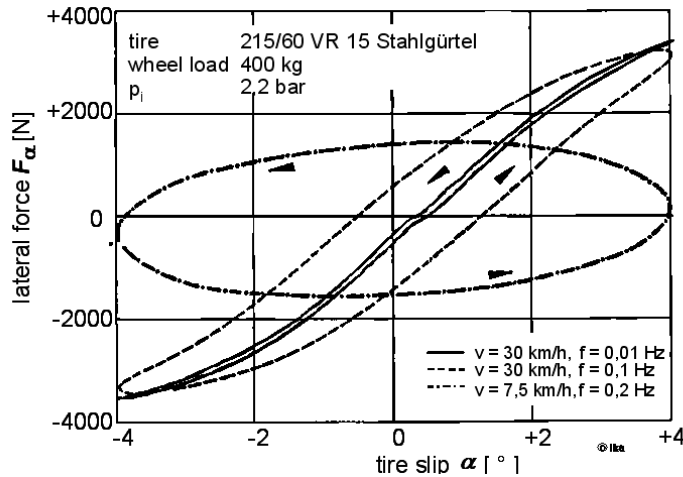


Fig.2.2-28: Lateral forces as a function of slip for sinusoidal excitation at different velocities and frequencies

The run-in processes in the tire contact area take place faster at increasing wheel speeds. Accordingly, for a constant steering frequency, the phase shift between slip angle and lateral force as well as the weakening of amplitude of the lateral force reduces with increasing driving velocity, fig.2.2-29 and fig.2.2-30.

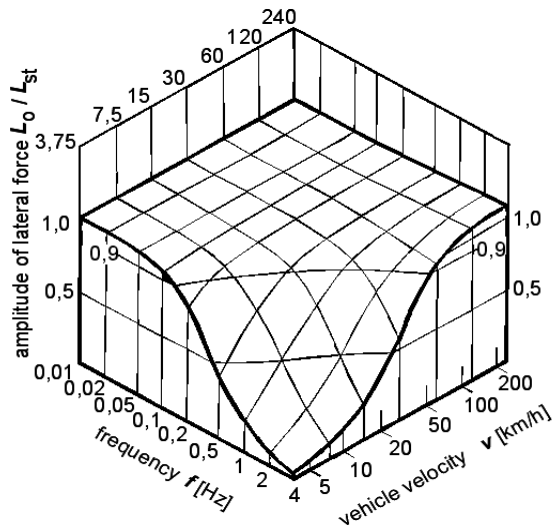


Fig. 2.2-29: Amplitude, frequency and velocity (215/60 VR 15, amplitude of slip 1°, $F_R = 400$ kg, $p_i = 2.2$ bar)

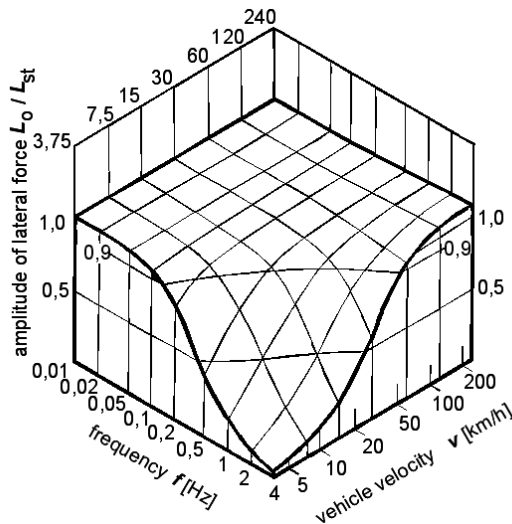


Fig. 2.2-30: Phase angle, frequency and velocity in spatial representation (tire data like fig. 2.2-29) / 42 /

In the theoretical investigations of vehicle driving dynamics using mathematical simulation models, the tire characteristics are often represented in the form of characteristic maps for steady-state operating conditions. The temporal behavior is simulated using delay elements. As an example, the approach developed by Böhm is presented as follows / 45 /:

$$F_{\alpha} + \frac{c_{\alpha}}{v \cdot c_{Ly}} \cdot \frac{dF_{\alpha}}{dt} = c_{\alpha} \cdot \alpha \quad (2.2 - 6)$$

With: F_{α} = cornering force

c_{α} = stiffness of tire slip

α = slip angle

v = driving speed

c_{Ly} = transverse stiffness of the tire contact area in relation to the rim

Using a linear formulation, the model considers a transverse displacement of the tire contact area over the rim. As a result, the wheel and tire indicate differing slip angles to the road in the transient condition, which in turn again corresponds to the steady-state condition ($dF_{\alpha}/dt = 0$).

Another transient tire model is the Schlippe/Dietrich Model. This model takes into account not only the transverse motion as a dynamic degree of freedom, but also the rotation of the tire contact area in relation to the rim / to 45 /:

$$F_{\alpha} + \frac{c_{\alpha}}{v \cdot c_{Ly}} \cdot \frac{dF_{\alpha}}{dt} = c_{\alpha} \cdot \alpha - \frac{c_{\alpha} \cdot r_{Lx}}{v} \cdot \frac{d\alpha}{dt} \quad (2.2-7)$$

With: r_{Lx} = half tire-contact length of the tire

Using the software tool MATLAB, the simulated functions of frequency response related to the Böhm and Schlippe/Dietrich models are shown in fig. 2.2-31.

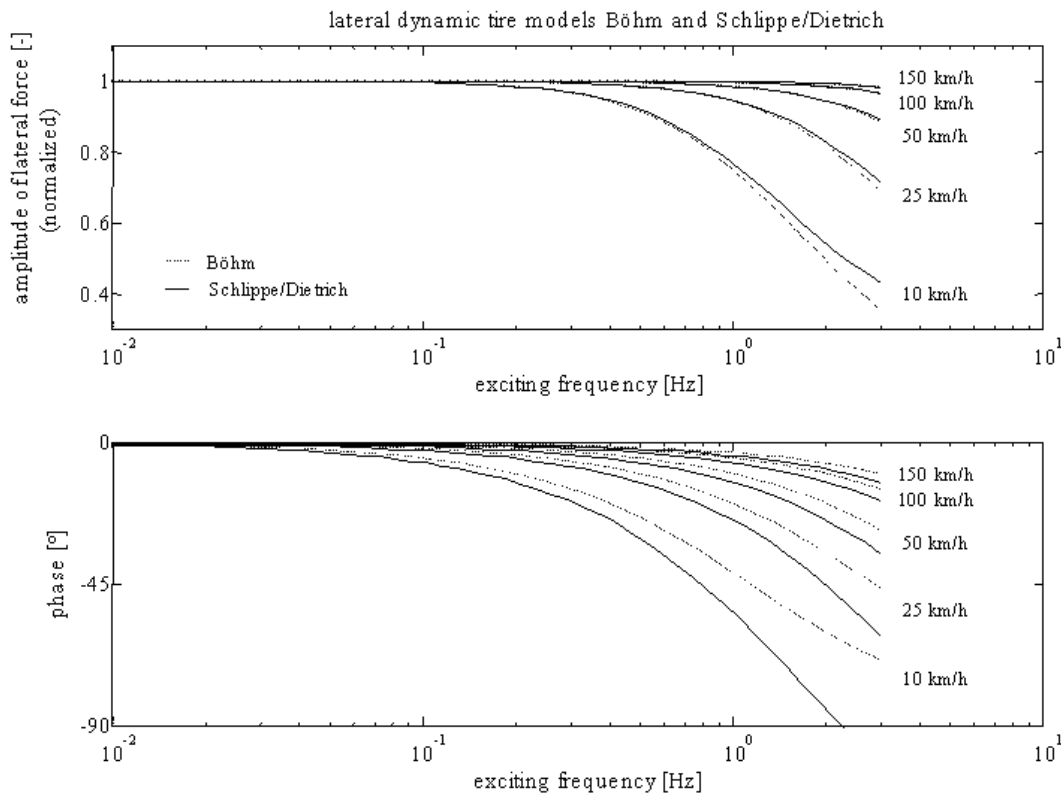


Fig.2.2-31: Tire behavior of transient tire models for variation of driving speed

The phase responses expose the differences the formulation of the two models. As a result of the rate element ($T_v = c_{\alpha} r_{Lx}/v$, s.eq. 2.2-7) larger phase shifts with increasing driving speed are indicated in the Schlippe/Dietrich model as against the Böhm model. The amplitude responses however show an almost identical characteristic.

Consequently, the influence of the parameters tire-contact length (r_{Lx}) and the transverse stiffness between the tire contact area and the rim (c_{Ly}) are included for a more realistic formulation of the Schlippe/Dietrich model shown in fig.2.2-32.

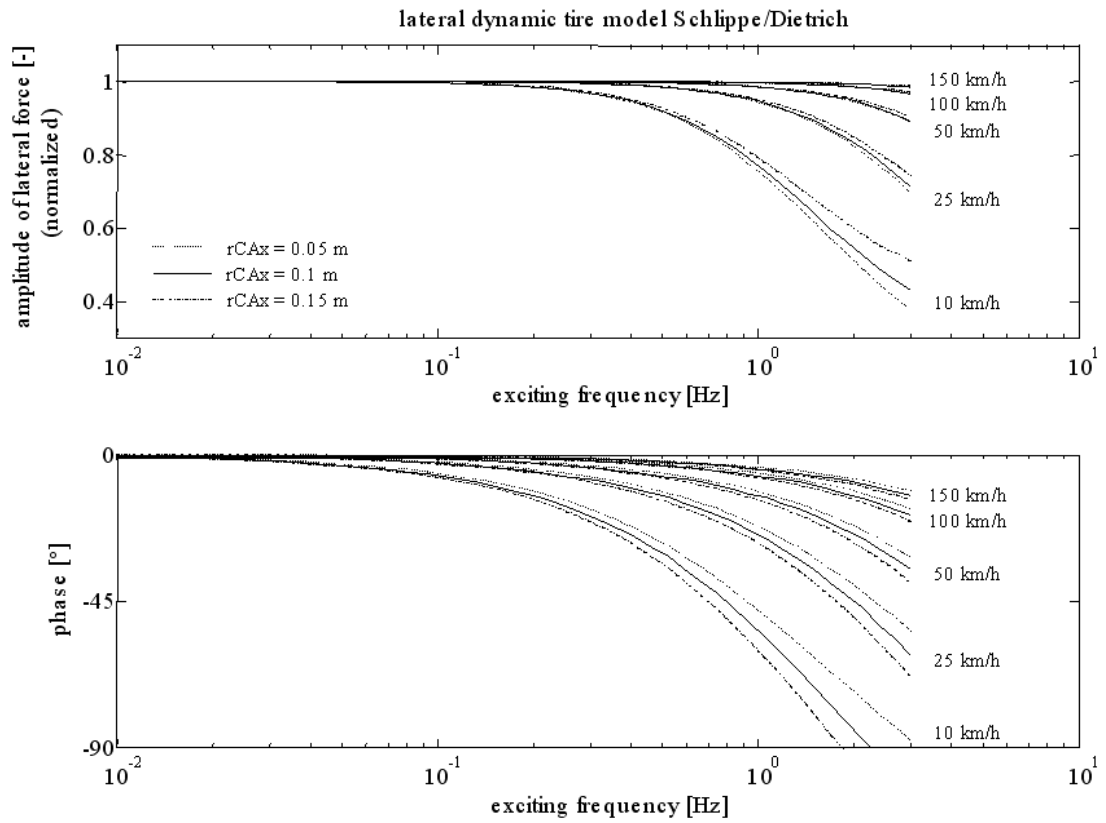


Fig.2.2-32: Transient tire behavior

Contents

2	Lateral Dynamics (Driving Stability)	33
2.3	Single Track Vehicle Model	33
2.3.1	Steady-State Cornering	36
2.3.2	Transient Behavior	42
2.3.3	The Vehicle as an Element in a Control Loop	47
2.3.3.1	Static Behavior of the Control Loop Vehicle	47
2.3.3.2	Dynamic Behavior of the Control Loop Vehicle	48
2.4	Four-Wheel Vehicle Model	55
2.4.1	Model Formulation	55
2.4.2	Test Procedures and Assessment Criteria for Vehicle Handling	58
2.4.3	Parametric Study of Steering Behavior (Passenger Car)	60
2.4.3.1	Height of Center-of-Gravity	65
2.4.3.2	Location of the Center-of-Gravity	70
2.4.3.3	Roll Axis	71
2.4.3.4	Anti-roll Suspension Distribution	72
2.4.3.5	Camber and Toe Angle	74
2.4.3.6	Traction (Drive Concept)	81
2.4.3.7	Auxiliary Rear-Axle Steering	83
2.4.4	Influence of Longitudinal Dynamic processes on Lateral Dynamics	89
2.4.4.1	Acceleration in Corners	90
2.4.4.2	Load Changes in Cornering	91
2.4.4.3	Braking during Cornering	95
2.4.4.4	Braking on Roads with Lanes of Differing Coefficients of Friction (μ -split)	96

2 Lateral Dynamics (Driving Stability)

2.3 Single Track Vehicle Model

To understand the driving dynamics of motor vehicles, theoretical knowledge of the mechanics of the vehicle motion is a prerequisite.

Theoretical investigations of driving dynamics are today usually executed using simulation programs, for which a complex equivalent mechanical model forms the basis for further discussion.

However, in order to depict the basic relationships of driving dynamics, simplified vehicle models are better suited, since the number of degrees of freedom which are considered remain in a manageable range.

A simplified description of the lateral dynamics of vehicles is possible using the single track vehicle model as shown in Fig 2.3-1 .

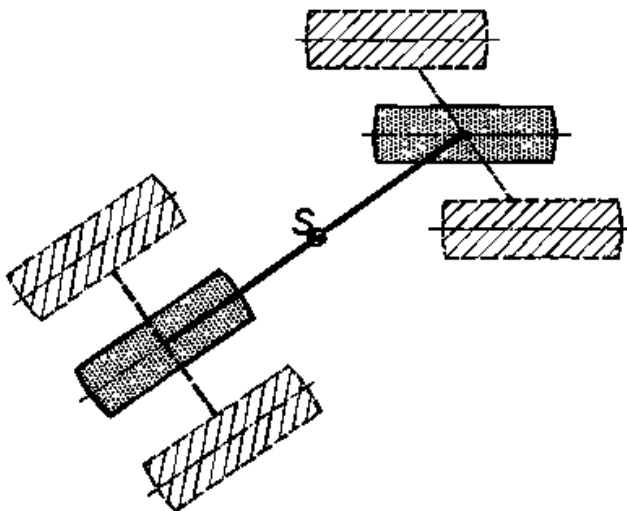


Fig 2.3-1: Single Track vehicle model

The tire contact points, where the lateral forces acting on the vehicle are responsible for course holding are cumulatively indicated for each axle. Longitudinal forces in the tire contact point as well as wheel load fluctuations, are not considered. The height of the center of gravity is zero.

For analytical considerations, the equations of motion for the single track model are linearized, i.e. only small angles with $\sin \alpha \sim \alpha$ and $\cos \alpha \sim 1$ are considered and a linear tire behavior is assumed.

The linearization of the tire characteristics achieved by the declaration of a tire slip stiffness C_α which characterizes the relationship between the tire lateral force and the tire side slip angle α at a constant wheel load:

$$C_\alpha = \frac{F_\alpha}{\alpha} \quad (2.3-1)$$

This linearization is considered sufficiently accurate upto tire side slip angles of 3° , since beyond this point, the errors become excessive as a result of the degressive characteristic. The side slip rigidity not only depends on the wheel load and the inflation pressure, but to a large extent also on the type of tire, Fig 2.3-2.

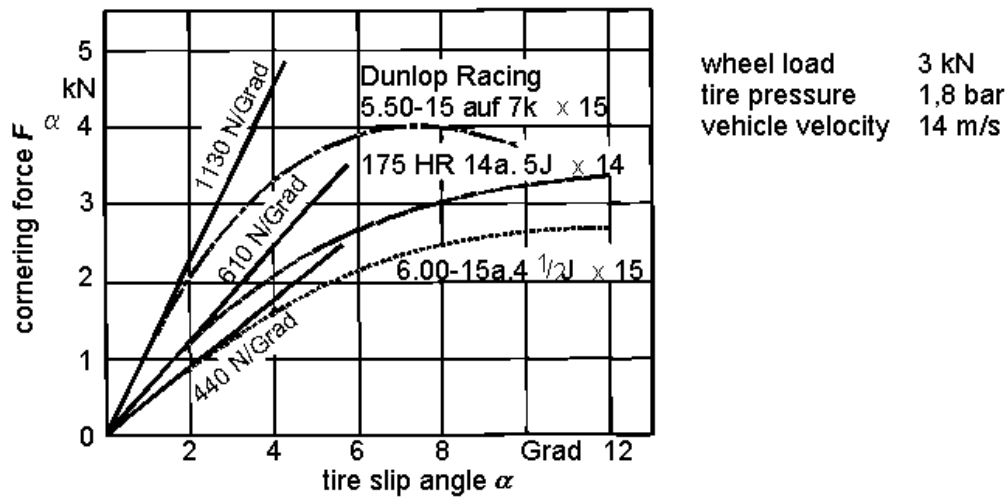
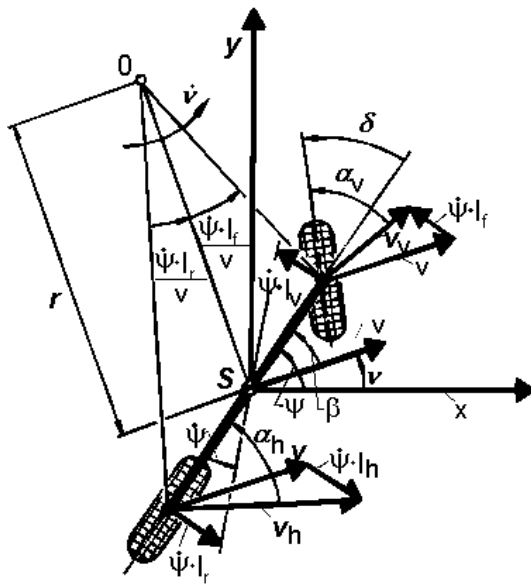


Fig 2.3-2: Linearized Side Slip rigidity C_α for different tires

In spite of these simplifications, the Single Track Vehicle Model not only provides a view of fundamental relationships associated with vehicle dynamics, but also useful results from the point of view of trends in order to influence individual vehicle parameters such as wheel base, weight distribution and tire characteristics.



- v = vehicle velocity
 r = radius of curve (at the moment)
 \dot{v} = angular velocity of center of mass
 $\dot{\psi}$ = yaw velocity
 ψ = yaw angle
 β = sideslip angle
 δ = steering angle

Fig 2.3-3: Single Track vehicle model

Based on the specified assumptions, two equations of motion can be drawn up in relation to the linearized single track vehicle model.

1. Newton's equation of motion for the vehicle lateral direction:

$$m \cdot a_y = F_{sf} + F_{sr} \quad (2.3-2)$$

2. Law of angular momentum about the z-axis at the vehicle's center of gravity

$$\theta \cdot \ddot{\psi} = F_{sf} \cdot l_f - F_{sr} \cdot l_r \quad (2.3-3)$$

The force of inertia acting at the vehicle center of gravity $m \cdot a_y$ corresponds to the centrifugal force resulting from the instantaneous road curvature:

$$m \cdot a_y = m \cdot \frac{v^2}{r} = m \cdot \frac{v}{r} \cdot \dot{v} \cdot r = m \cdot v \cdot (\dot{\psi} - \dot{\beta}) \quad (2.3-4)$$

with: v = driving velocity

r = curve radius (instantaneous)

\dot{v} = angular velocity of vehicle's center of gravity around the curve

$\dot{\psi}$ = yaw rate (angular velocity of the vehicle around its Z-axis)

$\dot{\beta}$ = rate of change of side slip angle (angular change between velocity vector in the vehicle center of gravity and vehicle longitudinal axis)

The tire side forces are given by:

$$F_{sf} = c_{sf} \cdot \alpha_f \quad (2.3-5)$$

$$F_{sr} = c_{sr} \cdot \alpha_r \quad (2.3-6)$$

Note: Instead of tire slip rigidity c_{α} , a tire slip rigidity c_s is applied, in which the elasticities of the wheel guides are considered. This influences the vehicle reactions substantially.

Assuming small side slip angles β considering the geometrical relations as follows (viz. Fig 2.3-3 below).

$$\alpha_f = \delta + \beta - \frac{l_f \cdot \dot{\Psi}}{v} \quad (2.3-7)$$

$$\alpha_r = \beta + \frac{l_r \cdot \dot{\Psi}}{v} \quad (2.3-8)$$

with: ψ = yaw angle (angle between vehicle longitudinal axis and x axis)

β = Side Slip angle (angle between vehicle longitudinal axis and velocity vector in the center of gravity)

α = Tire Slip angles at wheel (angle between wheel circumferential direction and velocity vector at tire contact point)

δ = Steering angles at the wheel (angles between wheel circumferential direction and vehicle longitudinal axis)

2.3.1 Steady-State Cornering

The steady state cornering of a road vehicle is characterized by the fact that apart from the driving speed v , the yaw velocity $\dot{\Psi}$ and the side slip angle β are also constant, i.e., $\ddot{\Psi} = 0$, $\dot{\beta} = 0$.

Instead of angular momentum (eqn. 2.3-3), in this case, a torque equilibrium can be formulated around the front and rear tire contact point.

$$F_{sf} \cdot l = m \cdot a_y \cdot l_r \quad (2.3-9)$$

$$F_{sr} \cdot l = m \cdot a_y \cdot l_f \quad (2.3-10)$$

from 2.3-5 and. 2.3-6:

$$c_{sf} \cdot \left(\delta + \beta - \frac{l_f \cdot \dot{\Psi}}{v} \right) = \frac{l_r}{l} \cdot m \cdot a_y \quad (2.3-11)$$

$$c_{sr} \cdot \left(\beta + \frac{l_r \cdot \dot{\Psi}}{v} \right) = \frac{l_f}{l} \cdot m \cdot a_y \quad (2.3-12)$$

Since in steady-state cornering $\dot{\beta} = 0$, it follows (eqn. 2.3-4):

$$\dot{\Psi} = \frac{v}{r}$$

After resolving equations 2.3-11 and 2.3-12 for β and equating, a further transformation results in:

$$\delta = \frac{l}{r} + \frac{m}{l} \cdot \left(\frac{l_r}{c_{sf}} - \frac{l_f}{c_{sr}} \right) \cdot a_y \quad (2.3-13)$$

A substantial statement about the behavior of a vehicle during cornering can be derived from this equation.

The necessary steering angle for cornering consists of one part which depends only on geometrical data (l/r) (Ackermann angle) and a second part which characterizes the influence of lateral acceleration. To the steering angle which is necessary at low velocities ($a_y \sim 0$) an addition is to be made at higher speeds ($a_y > 0$) which can either increase or decrease the steering angle, as the case may be.

To increase $\left(\frac{l_r}{c_{sf}} > \frac{l_f}{c_{sr}} \right)$

To decrease $\left(\frac{l_r}{c_{sf}} < \frac{l_f}{c_{sr}} \right)$

In the exceptional case $\left(\frac{l_r}{c_{sf}} = \frac{l_f}{c_{sr}} \right)$, no modification of steering angle, as a function of a_y , is required.

This regularity is of special importance for the interactions between actions of the driver and vehicle handling in the control loop consisting of the driver and vehicle. While driving along curves, the driver has to set a steering angle, which depends not only on the curve radius, but additionally on the present lateral acceleration.

The dependence of the steering angle on the lateral acceleration can be attributed to the fact that the respective slip angles which are created on the front and rear axles as a result of a side force, deviate from one another.

The difference in side slip angles in the single track model is as follows:

$$\alpha_{fv} = \delta + \beta - \frac{l_f \cdot \dot{\Psi}}{v} \quad (2.3-14)$$

$$\alpha_r = \beta + \frac{l_r \cdot \dot{\Psi}}{v} \quad (2.3-15)$$

$$\Delta\alpha = \alpha_f - \alpha_r = \delta - \frac{l \cdot \dot{\Psi}}{v} \quad (2.3-16)$$

with $v = \dot{\Psi} \cdot r$:

$$\Delta\alpha = \delta - \frac{l}{r}$$

$$\text{with (eqn. 2.3-13):} \quad \Delta\alpha = \frac{m}{l} \cdot \left(\frac{l_h}{c_{sv}} - \frac{l_v}{c_{sh}} \right) \cdot a_y \quad (2.3-17)$$

Equation 2.3-13 can also be interpreted in such a way that the steering angle which has to be set by the driver in order to drive through a curve, must contain a portion in addition to the geometrical part l/r , which is a function of the necessary side slip angle difference $\Delta\alpha$ (eqn. 2.3-16). The dependence of the necessary side slip angle difference on lateral acceleration is determined by vehicle and tire parameters. The dependence of the steering characteristics of a vehicle, on these parameters is called "Self-Steering Response".

In reference to the influencing parameters (implying the parameters of eqn. 2.3-17 for the linearized single track vehicle model) which are of considerable significance, it should be kept in mind that the scope for the design of these parameters is considerably limited by the defined vehicle concept. Hence, the effect of the self-steering response must be taken into account at a very early phase of vehicle development.

Since the driver has to compensate the side slip angle difference with the steering angle δ , it can be considered as a quantifiable measurement variable for the assessment of the steering characteristics. It forms the basis for the classical definition of over-steer and under-steer according to OLLEY (1940) / 31 /.

$$\text{Over-steer} \quad \Delta\alpha = \alpha_f - \alpha_r < 0$$

$$\text{Neutral} \quad \Delta\alpha = \alpha_f - \alpha_r = 0$$

Under-steer

$$\Delta\alpha = \alpha_f - \alpha_r > 0$$

According to this definition, a vehicle driving in a circular track is said to under-steer if it requires larger steering angles and over-steer if it requires smaller steering angles when compared to a vehicle which indicates neutral handling, as in Fig 2.3-4.

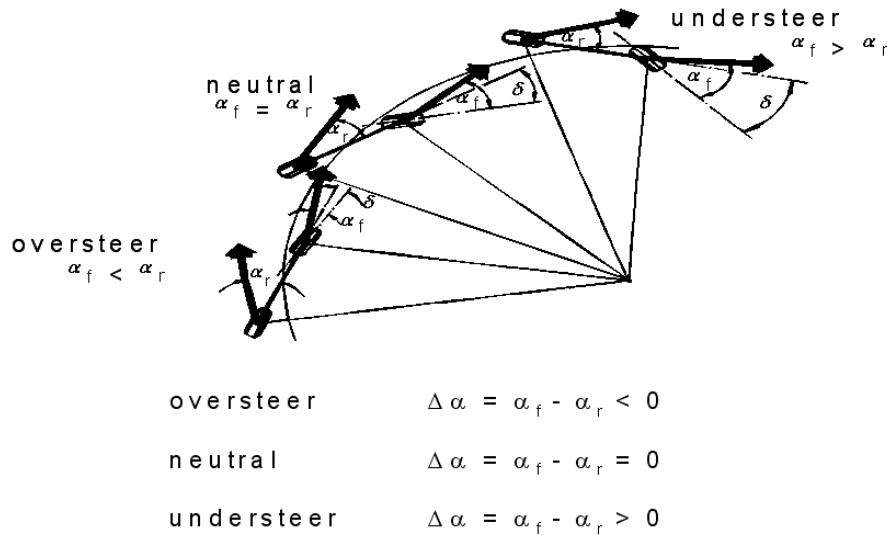


Fig 2.3-4: Characteristic driving behavior according the definition of Olley

If equation 2.3-13 is presented in the form of a diagram, the basic effects of the front and the rear side-slip rigidity and the axle load distribution can be discussed, Fig 2.3- 5 and Fig 2.3- 6:

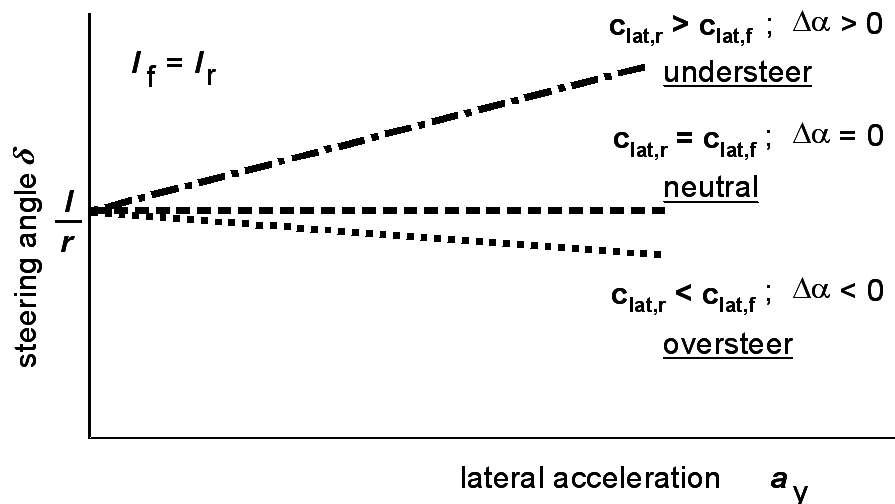


Fig 2.3- 5: Steering angle characteristic of the Single Track model with variation of the side slip rigidity. (curve radius $r = \text{const.}$)

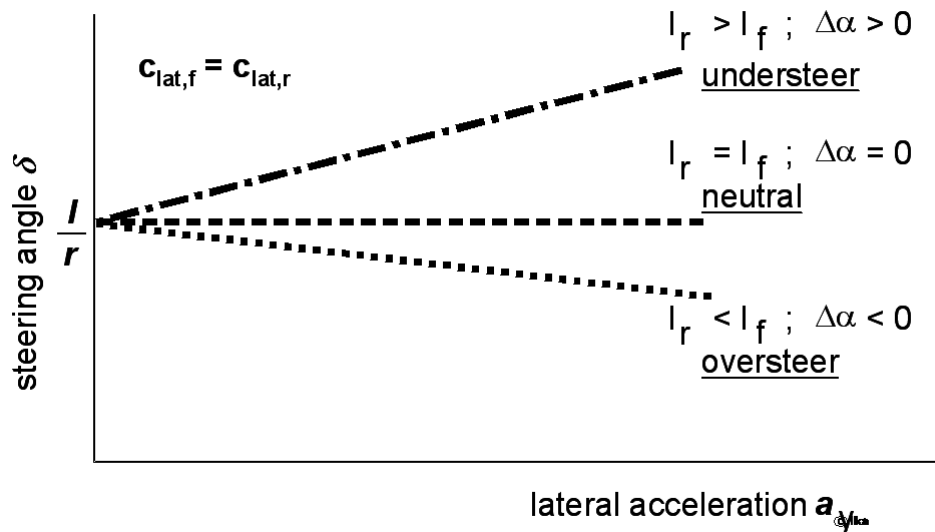


Fig 2.3- 6: Steering angle characteristic of the Single Track model with variation of the axle load distribution (curve radius $r = \text{const.}$)

In the evaluation of the self steering response, the instantaneous value of the slope $d\delta/da_y$ is more important than the absolute values of slip angle difference or rather the steering angle.

The definition of the self-steering behavior according to Olley, is hence useful only for small lateral accelerations, in which the vehicle and tire characteristics can be linearized with sufficient accuracy.

During higher lateral accelerations, the effective slip rigidity changes in the respective operating points of the tires (viz. Fig 2.3-1). Thus the linear relationship between the side slip angle difference and the lateral acceleration, in other words, the necessary steering angle and the lateral acceleration does not exist any more. The sign of the slope $d\delta/da_y$ does not correspond necessarily to the sign of the side slip angle difference.

Fig 2.3- 7 shows an appropriate curve of the steering angle over lateral acceleration . Instead of classifying the self-steering response into the areas understeer, neutral and oversteer, as in the definition of Olley, the classification based on the sign of the gradient $d\delta/da_y$ became generally accepted.

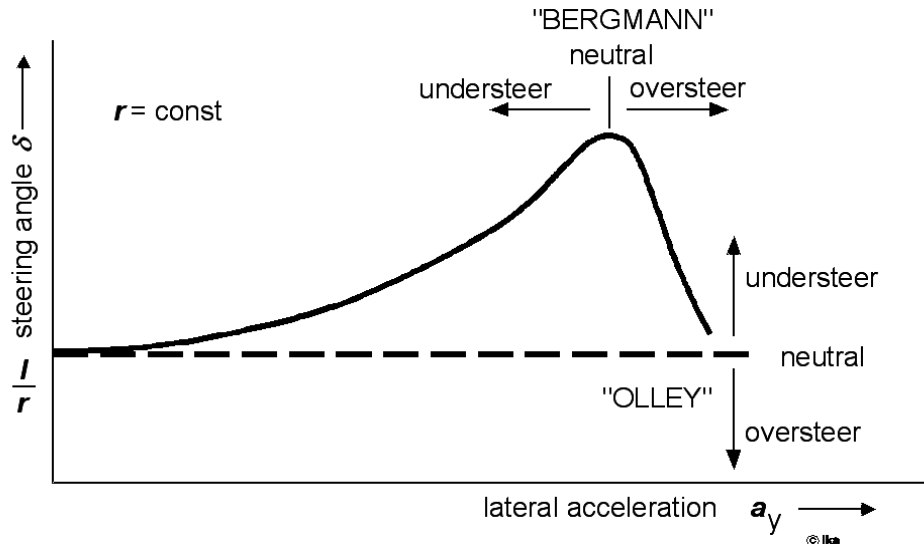


Fig 2.3- 7: Different definitions of the steering behavior

Definition of the steering behavior according to Bergmann from the year 1965: / 3 /

$$d\delta / da_y > 0 \quad \Rightarrow \quad \text{Understeer}$$

$$d\delta / da_y = 0 \quad \Rightarrow \quad \text{Neutral}$$

$$d\delta / da_y < 0 \quad \Rightarrow \quad \text{Oversteer}$$

Within the linear area the results of both definitions match.

As described by eq. 2.3-13, the important relation between steering behavior and vehicle/tire parameters, is also applied in differential form under non-linear tire characteristics.

$$\text{With} \quad F_{sf} = \int_0^{\alpha_y} c_{sf}(\alpha) d\alpha \quad (2.3-18)$$

$$F_{sr} = \int_0^{\alpha_h} c_{sr}(\alpha) d\alpha \quad (2.3-19)$$

one also receives here:

$$\frac{d\delta}{da_y} = \frac{m}{l} \cdot \left(\frac{l_r}{c_{sf}(\alpha_f)} - \frac{l_f}{c_{sr}(\alpha_r)} \right) \quad (2.3-20)$$

Depending on the actual operating points of the tires, or the resulting tire slip rigidity at front and rear axle, the following relations apply:

$$c_{sr}(\alpha_r) \cdot l_r > c_{sf}(\alpha_f) \cdot l_f \quad \text{Understeer}$$

$$c_{sr}(\alpha_r) \cdot l_r = c_{sf}(\alpha_f) \cdot l_f$$

Neutral steering behavior

$$c_{sr}(\alpha_r) \cdot l_r < c_{sf}(\alpha_f) \cdot l_f$$

Oversteer

On reaching the max. lateral acceleration a_y , the friction limit is exceeded, first at the front axle in an understeering vehicle and at the rear axle in an oversteering vehicle i.e. the slip angle rises uncontrolled at the axle concerned.

As a result, in an understeering vehicle, the side slip angle β reduces, leading to a relative drop of the tire slip angle α_h on the rear axle. The associated decrease of lateral force at the rear axle causes the vehicle to stabilize in a large curve radius with low lateral acceleration .

In the oversteering vehicle, a quick rise of the slip angle at the rear axle causes an increase of the side slip angles β and thus a relative enlargement of the slip angle α_f on the front axle. The associated increase in the lateral force increases the tendency of the vehicle to spin. A stabilization of the vehicle is possible only in a larger curve radius by the quick reduction of the steering angle by the driver. The accurate reduction of the steering angle may however be realized only with considerable difficulty by a normal driver. Hence, an inherent understeering tendency is aimed at in the layout of the self-steering response.

2.3.2 Transient Behavior

In order to make statements about the transient behavior of road vehicles, the equations of motion introduced in paragraph 2.3 for the linearized single track vehicle model are substituted into one another. From eqn. 2.3-2 and eqn. 2.3-3 and eqn. 2.3-4, eqn. 2.3-5, eqn 2.3-6 the following results:

$$m \cdot v \cdot (\dot{\psi} - \dot{\beta}) = c_{sf} \cdot \left(\delta + \beta - \frac{l_f}{v} \cdot \dot{\psi} \right) + c_{sr} \cdot \left(\beta + \frac{l_r}{v} \cdot \dot{\psi} \right) \quad (2.3-21)$$

$$\Theta_z \cdot \ddot{\psi} = c_{sf} \cdot \left(\delta + \beta - \frac{l_f}{v} \cdot \dot{\psi} \right) \cdot l_f - c_{sr} \cdot \left(\beta + \frac{l_r}{v} \cdot \dot{\psi} \right) \cdot l_r \quad (2.3-22)$$

eqn . 2.3-21 can be resolved for yaw velocity: $\dot{\psi}$

$$\dot{\psi} = \frac{m \cdot v \cdot \dot{\beta} + c_{sf} \cdot (\delta + \beta) + c_{sr} \cdot \beta}{m \cdot v - c_{sr} \cdot \frac{l_h}{v} + c_{sf} \cdot \frac{l_v}{v}} \quad (2.3-23)$$

Under the prerequisite, $v = \text{const}$, one receives by derivation:

$$\ddot{\psi} = \frac{m \cdot v \cdot \ddot{\beta} + c_{sf} \cdot (\dot{\delta} + \dot{\beta}) + c_{sr} \cdot \dot{\beta}}{m \cdot v - c_{sr} \cdot \frac{l_r}{v} + c_{sf} \cdot \frac{l_f}{v}} \quad (2.3-24)$$

As a result, yaw velocity $\dot{\psi}$ and yaw acceleration $\ddot{\psi}$ can be replaced in Eqn. 2.3-22:

$$\begin{aligned} \ddot{\beta} + \left(\frac{c_{sf} + c_{sr}}{m \cdot v} + \frac{c_{sf} \cdot l_f^2 + c_{sr} \cdot l_r^2}{v \cdot \Theta_Z} \right) \cdot \dot{\beta} \\ + \left(\frac{c_{sr} \cdot l_r - c_{sf} \cdot l_f}{\Theta_Z} + \frac{c_{sf} \cdot c_{sr} \cdot l^2}{\Theta_Z \cdot m \cdot v^2} \right) \cdot \beta \\ = \left(\frac{c_{sf} \cdot l_f}{\Theta_Z} - \frac{c_{sf} \cdot c_{sr} \cdot (l_f \cdot l_r + l_r^2)}{\Theta_Z \cdot m \cdot v^2} \right) \cdot \delta - \frac{c_{sf}}{m \cdot v} \cdot \dot{\delta} \end{aligned} \quad (2.3-25)$$

Hence, a non-homogeneous linear differential equation of 2nd order for the side slip angle β results. The steering angles δ and the steering angular velocity $\dot{\delta}$ appear as disturbance variables in the inhomogeneous part of this equation (in real vehicles, additional disturbances are road undulations and wind forces). The homogeneous part of the differential equation represents the motion equation of a simple oscillator with damping.

$$\ddot{\beta} + A \cdot \dot{\beta} + B \cdot \beta = 0$$

$$\underbrace{\quad}_{2 \cdot D \cdot \omega_e} \quad \underbrace{\quad}_{\omega_e^2}$$

Thus, a road vehicle can execute motion in the form of damped oscillations about its vertical axis. By a comparison of the coefficients in the differential equation for β , the undamped natural frequency ω_e and the damping rate D result:

$$\omega_e = \sqrt{\frac{c_{sr} \cdot l_r - c_{sf} \cdot l_f}{\Theta_Z} + \frac{c_{sf} \cdot c_{sr} \cdot l^2}{\Theta_Z \cdot m \cdot v^2}} \quad (2.3-26)$$

$$D = \frac{\frac{c_{sf} + c_{sr}}{m \cdot v} + \frac{c_{sf} \cdot l_f^2 + c_{sr} \cdot l_r^2}{\Theta_Z \cdot v}}{2 \cdot \omega_e} \quad (2.3-27)$$

$$\omega_{e \text{ m.D.}} = \sqrt{1 - D^2} \cdot \omega_e \quad (2.3-28)$$

Although above parameters are obtained from a differential equation for the side slip angles β , they are designated as yaw natural frequency and yaw damping rate. This purely formal step is taken due to the fact that both the side slip angle and the yaw angle describe a

motion of the vehicle around the vertical axis. Therefore, an oscillation about this axis consists of only one frequency and one damping rate¹ for both angles.

Fig 2.3- 8 shows the typical pattern of yaw natural frequency and yaw damping. The diagrams are based on the following vehicle specifications:

$$\begin{array}{llll} L & = & 2,5 \text{ m} & m & = & 1300 \text{ kg} \\ I_f & = & 1,3 \text{ m} & \Theta_z & = & 1960 \text{ kgm}^2 \\ I_r & = & 1,2 \text{ m} & c_{sf} & = & 30000 \text{ N/rad} \end{array}$$

The side slip stiffness of the rear wheels c_{sr} is varied, so that a total of three vehicles with differing steering behaviors result:

$$c_{sr} = 30000 \text{ N/rad}: \quad c_{sr} \cdot I_r < c_{sf} \cdot I_f = \text{oversteer}$$

$$c_{sr} = 35000 \text{ N/rad}: \quad c_{sr} \cdot I_r > c_{sf} \cdot I_f = \text{understeer}$$

$$c_{sr} = 40000 \text{ N/rad}: \quad c_{sr} \cdot I_r > c_{sf} \cdot I_f = \text{understeer}$$

¹ (The mathematical proof for the above statement follows from a view of the angle of the curve ν , which consists of the difference of yaw angles ψ and side slip angles β (see Fig 2.3-3):

$$\nu = \psi - \beta$$

Accordingly the derivatives of the angles are given by:

$$\dot{\nu} = \dot{\psi} - \dot{\beta}$$

$$\ddot{\nu} = \ddot{\psi} - \ddot{\beta} \quad \text{eg.} \quad \ddot{\psi} = \ddot{\beta}$$

If the curve angular acceleration is neglected ($\ddot{\nu} = 0$). With the help of these relations the side slip angles β can be replaced by the yaw angles ψ in Eqn. 2.3-25. One then receives again an inhomogeneous linear differential equation of 2nd Order:

$$\ddot{\psi} + A \cdot \dot{\psi} + B \cdot \psi = X_1 \cdot \delta + X_2 \cdot \dot{\delta} + Y_1 \cdot \nu + Y_2 \cdot \dot{\nu}$$

In the inhomogeneous part of this equation, apart from the motion quantities of the steering angles δ the curve angles also appear as disturbance variables. The natural frequency and the damping rate of the homogeneous proportion remain however unchanged.)

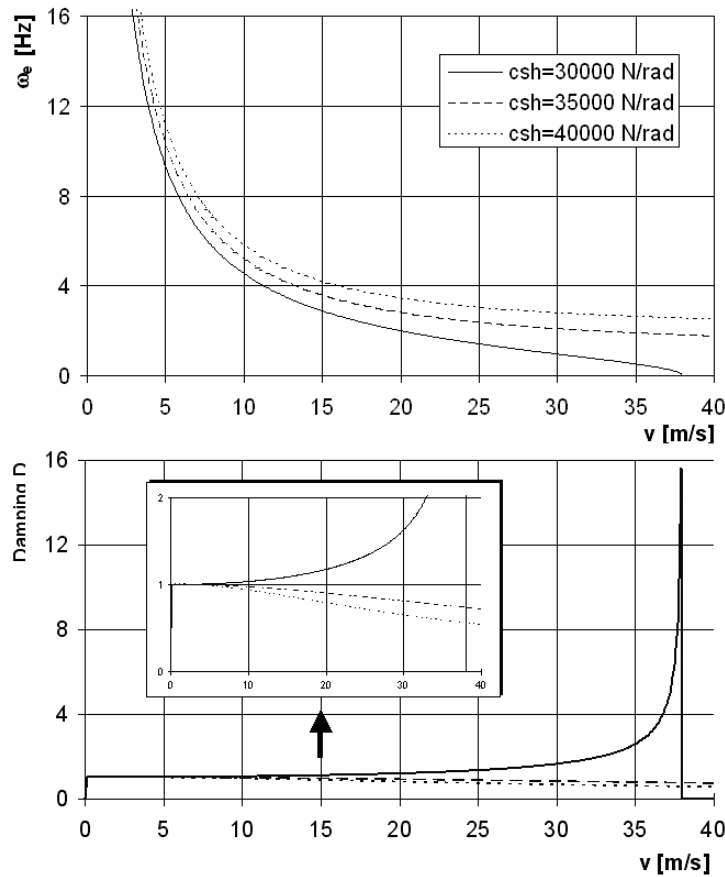


Fig 2.3- 8: Yaw natural frequency and yaw damping as function of the driving speed

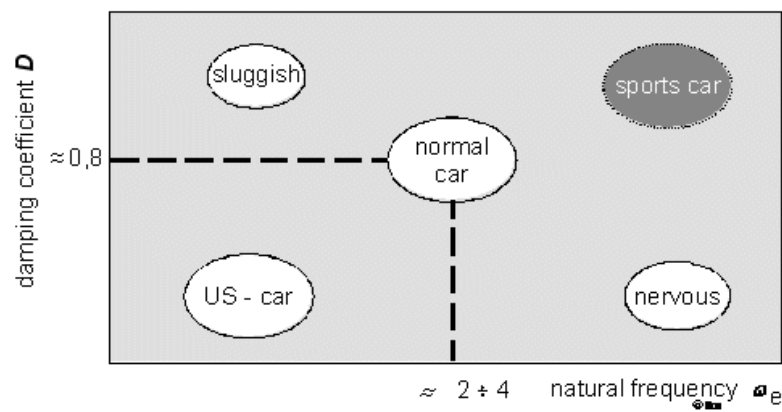
In understeering vehicles ($c_{sf} \cdot l_r > c_{sf} \cdot l_f$) the yaw damping decreases with the driving speed.

For oversteering vehicles ($c_{sf} \cdot l_r < c_{sf} \cdot l_f$), a critical driving speed v_{crit} exists, with which the undamped yaw natural frequency becomes zero or the yaw damping D becomes negative (viz. Eqn. 2.3-26 or Eqn. 2.3-27). The yaw does not fade away after exceeding this critical driving speed. The vehicle loses its cornering stability and begins to spin.

By appropriate design of the vehicle, the critical driving speed can be set to a very large value that it cannot be reached or it does not exist at all. (understeering vehicle).

However, in extreme driving conditions, the operating points of the tires can change (high demand for traction due to a combination of lateral and longitudinal forces, unfavorable wheel load changes), in which the instantaneous slip rigidity takes values which leads to "dynamic oversteering" / 45 /. At correspondingly high driving speeds, the limit of cornering stability can be exceeded.

The target for vehicle construction from the point of view of steering behavior can generally be indicated by the need for a quick response to steering angles, wherein no overshooting takes place. Fig 2.3-9 shows the relationship between the demands placed on vehicle design and the system parameters yaw natural frequency and yaw damping.



$V = 20 - 30 \text{ m/s}$

Fig 2.3-9: Vehicle characteristic as a function of the yaw damping and the yaw natural frequency ($v = 20 - 30 \text{ m/s}$)

Since the influencing vehicle parameters are also determined taking into account the specifications of other vehicle characteristics (suspension characteristics, pay-load carrying capacity, engine arrangement), an optimum design is not possible for each vehicle concept.

The reaction of the vehicle to steering movements is dealt with in more detail in the following section.

2.3.3 The Vehicle as an Element in a Control Loop

At the beginning of chapter 2 it was mentioned that the relationship between driver inputs and vehicle reaction can be understood as a closed control loop process.

Therefore the steering behavior of the linearized single track vehicle model is to be examined based on the reaction of the vehicle considered as a control loop for variations in the control variable or input variable represented by the steering angle δ . The yaw velocity $\dot{\psi}$ and lateral acceleration a_y are considered as output variables from the control loop vehicle.

2.3.3.1 Static Behavior of the Control Loop Vehicle

For the description of the static behavior of the vehicle control loop, the relationship between steering angle δ and lateral acceleration a_y for steady state cornering of the linearized single track model, deduced in section 2.3-1 and eq. 2.3-13 is considered.

As is common in control engineering, the output variable $\dot{\psi}$ is referred to the input variable δ . With $1/r = \dot{\psi} / v$ and $a_y = v \cdot \dot{\psi}$, the transformation of Eqn. 2.3-13 results in:

$$\left(\frac{\dot{\psi}}{\delta} \right)_{\text{stat.}} = \frac{v}{l + \frac{m}{l} \cdot \left(\frac{l_r}{c_{sf}} - \frac{l_f}{c_{sr}} \right) \cdot v^2} \quad (2.3-29)$$

$$\left(\frac{\dot{\psi}}{\delta} \right)_{\text{stat.}} = \frac{v}{l + \frac{d\delta}{da_y} \cdot v^2} \quad (2.3-30)$$

The relation $\dot{\psi} / \delta$ is denoted as the steady-state yaw amplification factor. Fig 2.3- 10 shows the dependence of the yaw amplification factor on the driving speed v for vehicles with different self-steering responses (eqn 2.3-20).

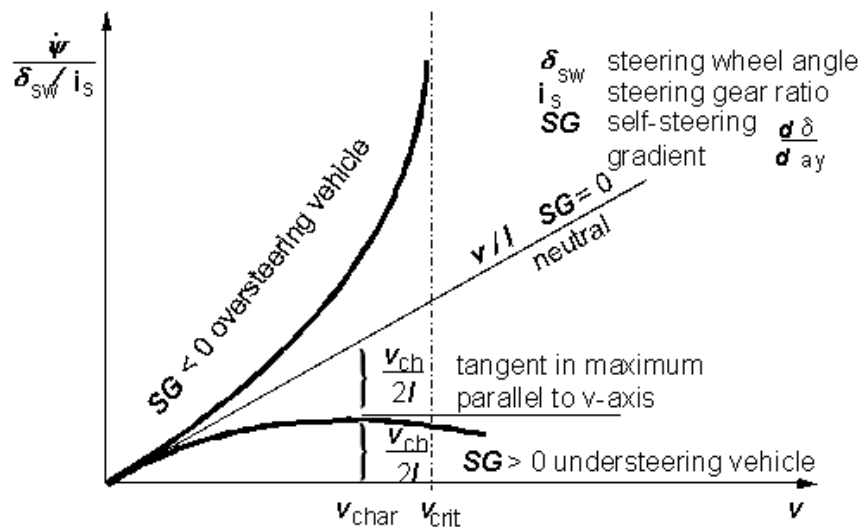


Fig 2.3- 10: Yaw amplification factor as function of the driving speed / 45 /

The meaning of the critical velocity v_{crit} was already described in the preceding section. On reaching the critical velocity, the steering sensitivity of an oversteering vehicle tends to infinity, which implies that the vehicle can no longer be stabilized.

The curve for the steering sensitivity of the understeering vehicle indicates a maximum value. The appropriate driving speed is called characteristic velocity V_{char} . Using V_{char} , eqn. 2.3-30 can be written in another form for the steady-state yaw amplification factor :

$$\left(\frac{\dot{\psi}}{\delta} \right)_{stat.} = \frac{v}{l \cdot \left(1 + \frac{v^2}{v_{char}^2} \right)} \quad (2.3-31)$$

Today's passenger cars are designed in such a way that max. steering sensitivity is at a driving speed between $v_{char} = 65$ km/h and 100 km/h. The necessary understeer tendency can be estimated using Eqn 2.3-30

2.3.3.2 Dynamic Behavior of the Control Loop Vehicle

For an analysis of the dynamic behavior of the vehicle as a control element, one refers to the differential equations of motion for the linearized single track vehicle model in section 2.3.2, Eqn. 2.3-21 and Eqn. 2.3-22.

After a Laplace transformation / 32 /, the equations of motion can be substituted into one another and after a few transformations, the transfer function of yaw velocity results / 45 /:

$$\frac{\dot{\psi}}{\delta} = F(s) = \left(\frac{\dot{\psi}}{\delta} \right)_{\text{stat.}} \cdot \frac{1 + T_z \cdot s}{1 + \frac{2 \cdot D}{\omega_e} \cdot s + \frac{1}{\omega_e^2} \cdot s^2} \quad (2.3-32)$$

with: s : Laplace transform

$(\dot{\psi} / \delta)_{\text{stat}}$: Steady-state yaw amplification factor

T_z : Counter time constant

ω_e : Undamped yaw natural frequency

D : Yaw damping

Yaw natural frequency ω_e and yaw damping rate D were already introduced in section 2.3-2.

One finds the counter time constant T_z similar to ω_e and D by comparison of coefficients:

$$T_z = \frac{m \cdot v \cdot l_f}{c_{sr} \cdot l} \quad (2.3-33)$$

From the point of view of control engineering, the linearized single track vehicle model reacts to steering angle input with a yaw motion similar to a control loop consisting of a series connection of a PT2 and a PD element.

The Laplace transformation of the equations of motion can be resolved in such a way that the transfer function of lateral acceleration can be determined / 45 /:

$$\frac{a_y}{\delta} = F'(s) = \left(\frac{a_y}{\delta} \right)_{\text{stat.}} \cdot \frac{1 + T_1 \cdot s + T_2 \cdot s^2}{1 + \frac{2 \cdot D}{\omega_e} \cdot s + \frac{1}{\omega_e^2} \cdot s^2} \quad (2.3-34)$$

with: $(a_y/\delta)_{\text{stat}}$ Steady-state amplification factor for lateral acceleration :

$$T_1 = \frac{l_h}{v} \quad \text{Time constant:}$$

$$T_2 = \frac{\Theta}{c_{sh} \cdot l} \quad \text{Time constant}$$

In section 2.3-2, the relationship between yaw natural frequency, yaw damping and transient steering behavior of a vehicle was clearly represented (Fig 2.3- 10). The application of these two system parameters however only partially describes the steering behavior and the parameters are not directly measurable. Due to this reason, in order to derive an objective

evaluation, the approach commonly used in control engineering, which involves the evaluation of the behavior of a control loop on the basis of its reactions to special input signals is generally accepted.

With the linearized single track vehicle model, the vehicle reactions can be determined analytically, by using the Laplace transformation of the time-function for the input signal in Eqn. 2.3-31 and later executing an inverse transformation into the time domain, which provides the appropriate time-function of the output signal. In real vehicles, the vehicle reactions are experimentally determined.

The "Stepped steering input" (step function of input signal) and "Sinusoidal steering input" (frequency response determination) are the most important driving test maneuvers. Fig 2.3-11 shows the characteristic of yaw velocity and lateral acceleration for a stepped steering input.

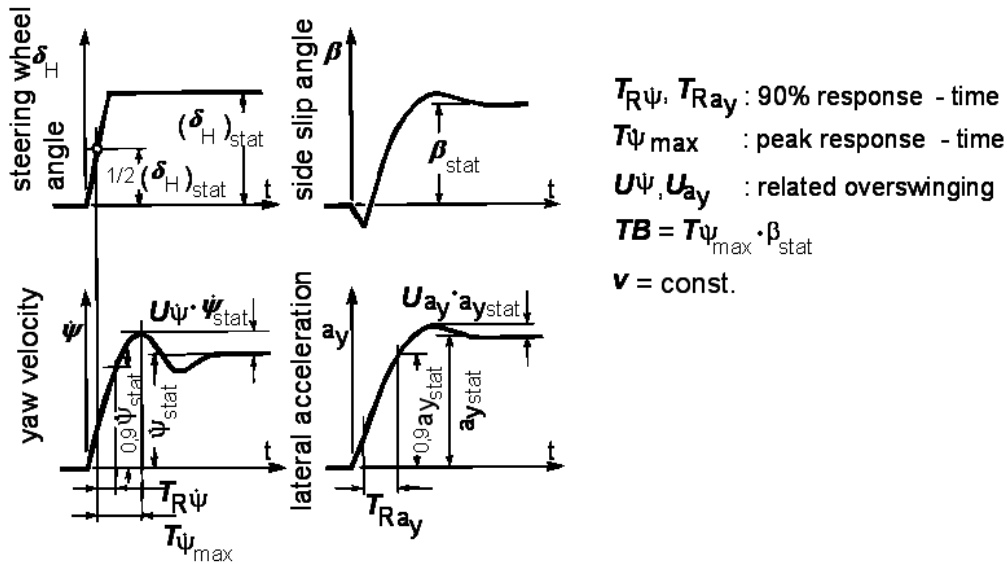


Fig 2.3- 11: Time function of the vehicle motion quantities at step steer 5 /

In the design of a vehicle, a compromise has to be made between the need for a quick response to steering inputs and the increasing demand for a small overshoot in the motion quantities. In today's passenger cars, the values of response time lie between 200 ms and 400 ms / 45 /as represented in Fig 2.3- 12.

For a sinusoidal steering angle input, the transfer function of the yaw velocity ψ for the linearized single track vehicle model (Eqn. 2.3-32) takes the following form:

$$F(i \cdot \omega) = \left(\frac{\psi}{\delta} \right)_{\text{stat.}} \cdot \frac{1 + T_z \cdot i \cdot \omega}{1 + \frac{2 \cdot D}{\omega_e} \cdot i \cdot \omega - \frac{\omega^2}{\omega_e^2}} \quad (2.3-35)$$

The amplitude ratio $\hat{\psi}/\hat{\delta} = |F(i\omega)|$ is hence frequency dependent. The same applies to the frequency response of lateral acceleration, which results from Eqn. 2.3-34:

$$F'(i\omega) = \left(\frac{a_y}{\delta} \right)_{\text{stat.}} \cdot \frac{1 + T_1 \cdot i\omega - T_2 \cdot \omega^2}{1 + \frac{2 \cdot D}{\omega_e} \cdot i\omega - \frac{\omega^2}{\omega_e^2}} \quad (2.3-36)$$

Additionally in each case, a frequency dependent phase shift φ occurs between the sinusoidal output signal and the sinusoidal input signal.

$$\varphi(i\omega) = \arctan \frac{\text{Im}(F(i\omega))}{\text{Re}(F(i\omega))} \quad (2.3-37)$$

From the point of view of the frequency response, a vehicle should be designed in such a way, that on the one hand the drop of the amplitude response of lateral acceleration does not take place at low frequencies (significant from the point of view of steering reaction for quick steering inputs), and on the other hand, the peak of the amplitude response for yaw velocity is not too high / 2 /.

Further, the phase shifts in both phase responses should be as small as possible up to high frequencies (since this would place an increased dependence on the abilities of the driver as the controller). The coupling of the transfer functions of yaw velocity and lateral acceleration however permits only a compromise between these demands / 37 /.

Frequency response functions simulated using MATLAB are shown in the following figures. Here, a variation of the driving speed v , the yaw inertia moment θ and the slip rigidity of the rear axle c_{sh} was undertaken.

- **Variation of the Driving Speed V :**

In Fig 2.3- 12, the frequency response functions (amplitude response or amplification and phase response) for variation of the driving speed are presented. For frequencies of $\omega = 0$ steady-state conditions prevail. The amplitude increments then read:

$$\left(\frac{\dot{\psi}}{\delta} \right)_{\text{stat.}} = \frac{v}{1 + \frac{d\delta}{da_y} \cdot v^2} \quad (2.3-30)$$

$$\left(\frac{a_y}{\delta} \right)_{\text{stat.}} = \frac{v^2}{1 + \frac{d\delta}{da_y} \cdot v^2} \quad (2.3-38)$$

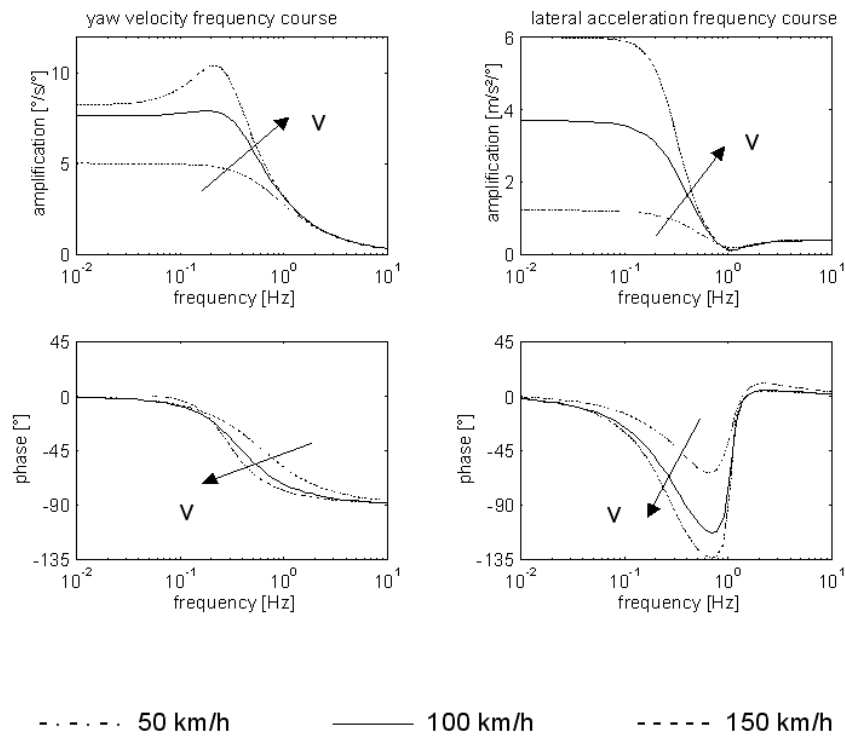


Fig 2.3- 12: Frequency response functions under variation of the driving speed V

As shown in Fig 2.3- 12, with increasing velocities, there is a higher steady-state amplification. From the respective initial values, the amplitude curves drop steeply and asymptotically tend to a limit value at high frequencies.

From the phase responses, it can be inferred that the phase lag, and hence the vehicle reaction to steering angle inputs, becomes larger with increasing driving speed.

Variation of the Yaw Moment of Inertia θ

Fig 2.3- 13 shows the results of the frequency response analysis for variations in the yaw moment of inertia θ

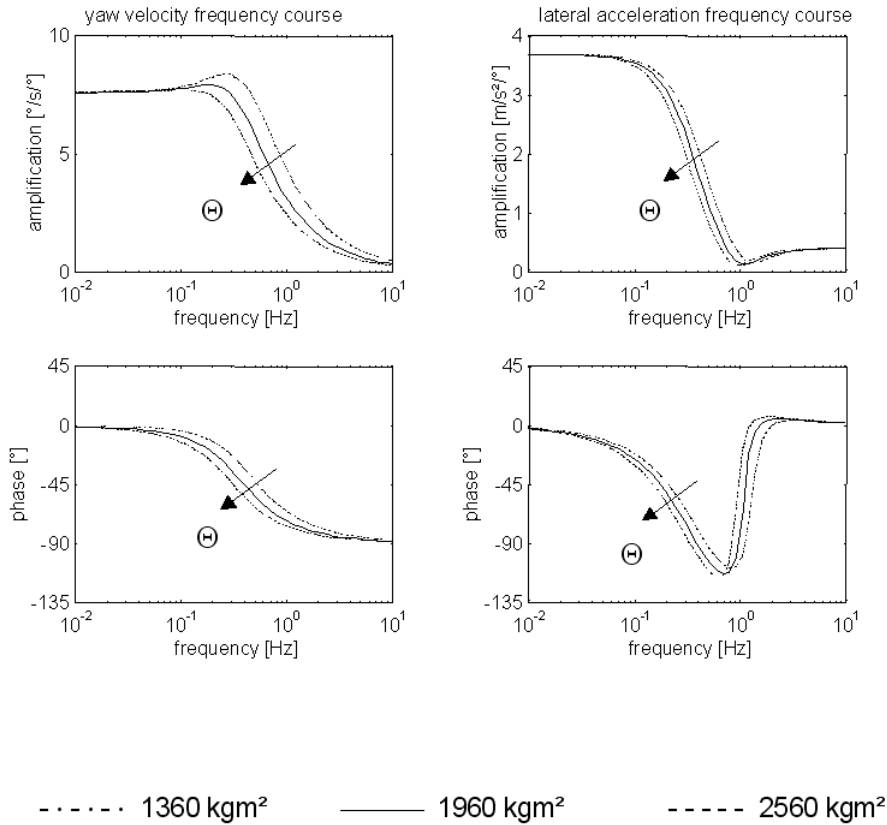


Fig 2.3- 13: Frequency response functions under variation of the yaw moment of inertia

According to the eqn. 2.3-30 and 2.3-38, the yaw moment of inertia does not have an influence on the steady-state amplification ($\omega = 0$). For higher excitation frequencies, with increase of the yaw moment of inertia, the amplitude maximas move to lower frequencies, i.e. the amplitude responses drop for high yaw moments of inertia at low frequencies and move again asymptotically towards a limit value.

The phase responses also show a clear influence of the yaw moment of inertia on the phase angles. With increasing yaw moment of inertia, as expected, the vehicle reactions become more sluggish, leading to a higher lag.

- **Variation of the Tire Side Slip Stiffness of the Rear Axle c_{sr} :**

The following figure explains to what extent the understeer tendency of the test vehicle affects the frequency response functions, Fig 2.3- 14.

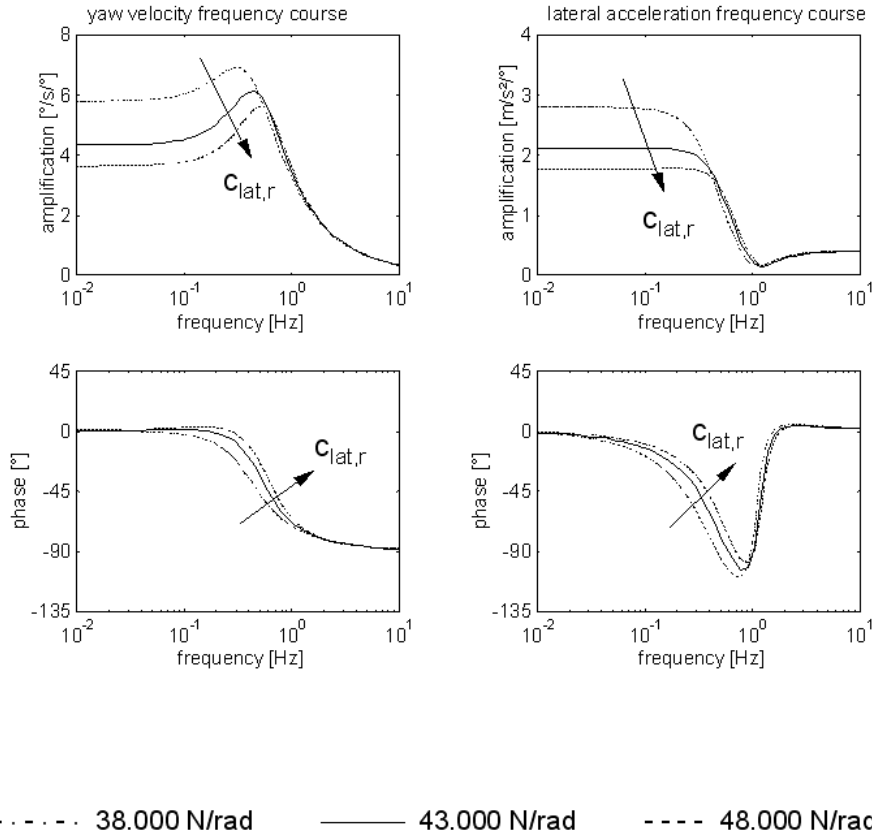


Fig 2.3- 14: Frequency response functions under variation of the tire side slip stiffness of the rear axle c_{sr}

With increasing understeer tendency ($c_{sr} \uparrow$) smaller amplifications of the steady-state amplitude and smaller phase lags are noticed. Referring to the earlier formulated demand, that the drop of the amplitude response of lateral acceleration should not begin at too low frequencies, indicates that a heavily understeering vehicle has the best handling. However, the most pronounced resonance peak shows up in the amplitude response of the yaw velocity for this vehicle.

During the evaluation of the simulation results, it must however be noted that the analytical solutions for the linearized single track vehicle model may not accurately correspond to the frequency responses of real vehicles, since the motion of real vehicles is influenced by a large number of nonlinearities.

In particular, the non-linear tire characteristics, which indicate a frequency response, influence the transient steering behavior substantially, as described in section 2.2.6.

2.4 Four-Wheel Vehicle Model

In addition to basic investigations about the stability behavior of the vehicle control system, the single-track vehicle model dealt with so far, already permitted a qualitative study of the influences of some vehicle parameters, e.g., the effect of the location of the center of gravity or of different front or rear cornering stiffness (side slip stiffness) on understeer and oversteer.

The driving stability of real motor vehicles is determined by a multitude of further parameters, with the height of the center-of-gravity, anti-roll suspension rates and wheel suspension kinematics constituting major factors of influence. When the stability limit with respect to driving dynamics is approached, the lateral dynamic response of a vehicle will increasingly be influenced by the drive concept.

Investigations about the dependence of steering behavior and driving stability on these parameters require the replacement of the linearized single-track vehicle model by a three-dimensional four-wheel vehicle model, which above all also includes a more precise representation of the nonlinear tire characteristics.

2.4.1 Model Formulation

Section 2.3 contains the linearized equations of motion for the single-track vehicle model and an analysis of the influence of the vehicle parameters on steering behavior and course stability on the basis of these equations. The system of equations describing the motion of a three-dimensional four-wheel vehicle model cannot be analyzed due to its complexity. Hence, for the following parametric study, the simulation model of a complete vehicle is generated using ADAMS.

In order to create a vehicle computer model, the individual components of the vehicle have to be described at first. The ADAMS database consists of each part being characterized by its mass, the coordinates of its center of gravity and its moments of inertia around the three primary inertial axes. Points are indicated on each component, where various parts are to be linked by joints along with the forces acting on them.

The various types of joints are available in a "library", with the number of the degrees of freedom being stated for each joint.

A similar procedure is used for forces. From a list of linear forces for example, general spring-and-damper elements or compression-only forces can be selected for the modeling of stoppers or collision points.

By means of self-written FORTRAN subroutines, random nonlinearities can be included in the calculation, in addition to the standard elements for forces and motion. Hence, for example, tire characteristics can be fully described by means of measured maps (see Section 2.2.4.1). Fig. 2.4-1 shows the ADAMS model of a complete vehicle.

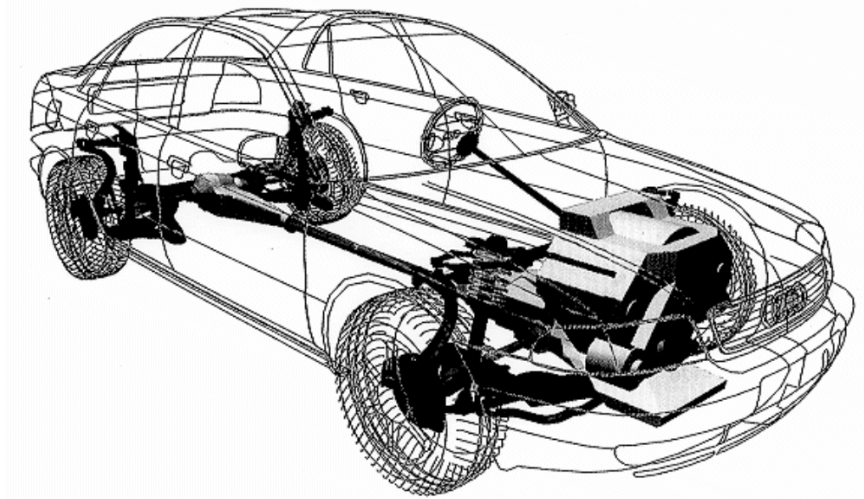


Fig. 2.4-1: ADAMS model of a complete vehicle for driving-dynamics simulations (Audi A8)

The vehicle on which the following simulation is based is clearly simpler than the very complex model shown in Fig. 2.4-1. Wheel-suspension elasticity, for example, is neglected for the number of influencing parameters to be reduced and interpretation of the calculating results to be facilitated.

The tire performance maps, on which the calculations are based, are shown in Fig. 2.4-2 and Fig. 2.4-3.

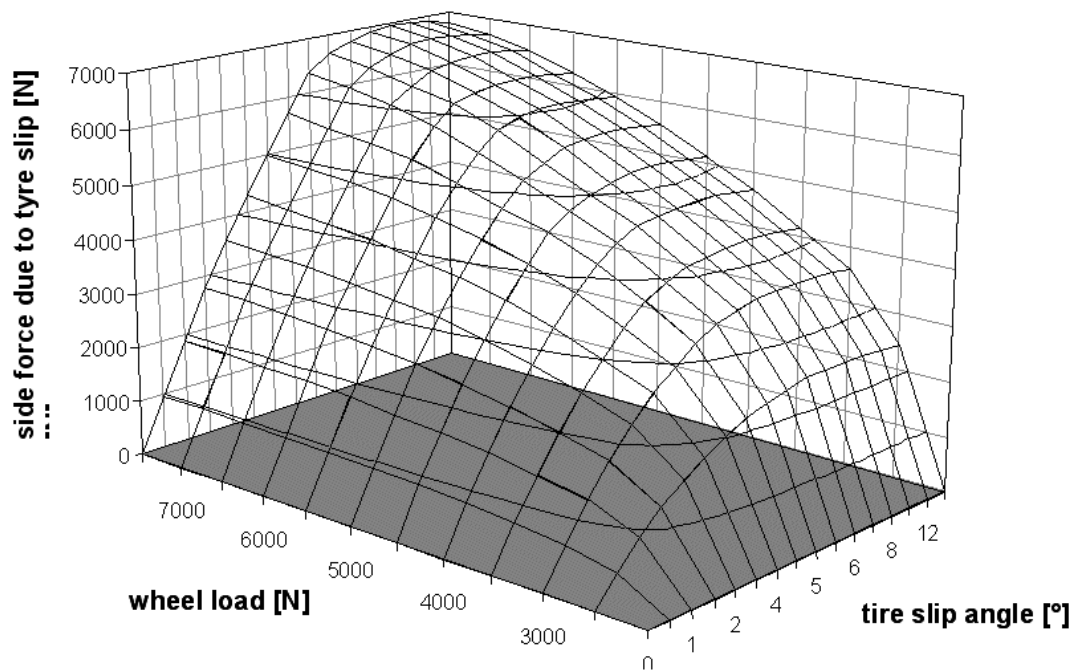


Fig. 2.4-2: Lateral force over slip angle (parameter wheel load) and over wheel load (parameter slip angle)

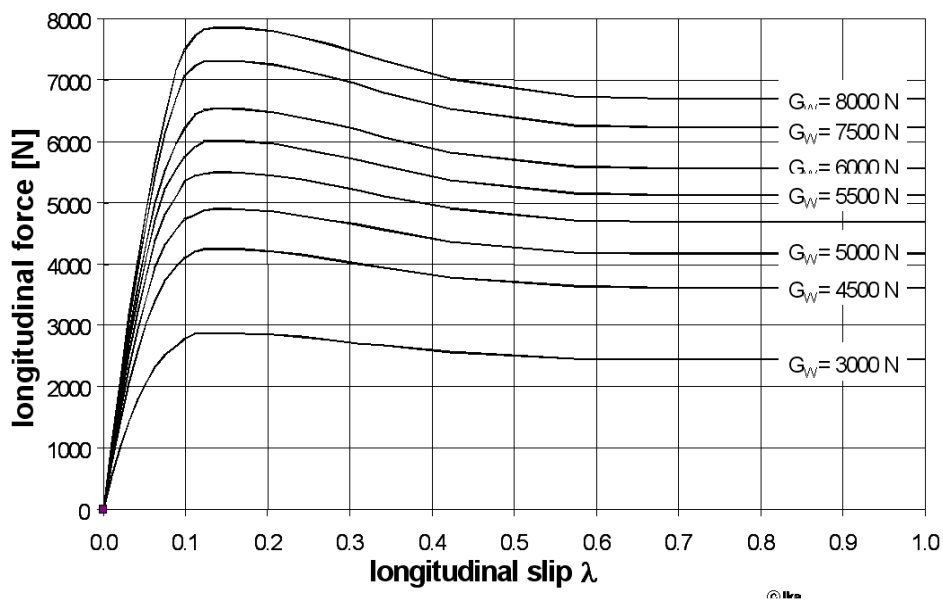


Fig. 2.4-3: Radial force over rotational slip, for wheel loads of $G_R = 3000, 4500, 5000, 5500, 6000, 6500, 7500, 8000$ N

An approximate consideration of transient tire behavior for quick variations in the tire slip angle is achieved using a 1st order delay for the tire slip angles. The delay time is calculated in relation to a specified run-in period of the tire and the instantaneous wheel circumferential speed.

Wheel caster is considered using a predetermined map, from which the aligning torque around the normal to the road through the axis of rotation of the wheel is obtained by interpolation based on the instantaneous wheel load and the slip angles.

The steering inputs required for the simulation are specified as time functions or set via a PID controller in relation to a specified desired course. Traction forces are also specified as a time function, so that a characteristic for the desired velocity is obtained.

ADAMS hence allows the calculation of vehicle motion during the most diverse driving maneuvers and offers the advantage of the variations of the vehicle parameters with relative ease within arbitrary limits, in contrast to driving tests.

2.4.2 Test Procedures and Assessment Criteria for Vehicle Handling

The use of the simulation techniques allow for the investigation of handling characteristics (operating behavior) of vehicles in the most diverse driving situations on the basis of purely theoretical investigations.

Many test procedures have been developed for the assessment of handling characteristics, Fig. 2.4-4.

The bulk of the test procedures reflect ideal driving maneuvers. Fig. 2.4-4 also shows test procedures which originate from the testing methods used in control engineering (stepped steering input, sinusoidal steering) and classifies them into the main driving maneuvers.

Test procedures which provide information on the behavior of the "vehicle control system" within the closed driver-vehicle loop (see Section 2.3.3) are referred to as "closed-loop" driving maneuvers (e.g. lane-changing test). The evaluation decisively depends on the adaptation of the "control system vehicle" to the abilities of the driver-controller.

In contrast, those test procedures where changes in the controlled-variable are specified in advance in the form of time functions (e.g. sudden steering-angle change), i.e. where the motion of the vehicle has no effect on the driver's actions, are referred to as open-loop driving maneuvers. These test procedures, above all, provide insights into the stability behavior of the vehicle control system and the system's susceptibility to external disturbances (e.g. crosswind).

main driving situation	driving manoeuvre	closed loop	open loop
cornering behaviour	steady state cornering (self-steering prop.)	-	+
	load-alteration effect	+	+
	non stat. cornering	+	+
	braking in curve	+	+
	aquaplaning	+	+
straight ahead driving behaviour	tracking stability	+	+
	lane keeping	+	+
	aquaplaning	+	+
	side wind	+	+
	load-alteration effect	+	+
	straight ahead braking	+	+
	drastic steer	-	+
	steering response	+	-
transient response	sudden steering input	-	+
	self alignment	-	+
	turning into curve	+	-
	exiting curve	+	-
	lane change	+	-
	ISO-lane change test	+	-
S bend behaviour	sinusoidal steering	-	+
	slalom	+	-
	wobble (drastic steer and accelerating)	-	+
	reaction- and obstacle avoiding test	+	-

Fig. 2.4-4: Test procedure for the handling of an automobile /35/

Every test procedure provides information on the handling characteristics of a vehicle in a certain discipline. A comprehensive assessment of operating behavior is therefore only possible if all individual results are considered.

The "closed-loop" test procedures in particular, still lack universally accepted assessment criteria that would permit a quantifiable assessment on the basis of measured numerical values. Vehicle tuning is therefore largely dependent on the subjective assessments of experienced test drivers. Moreover, "closed-loop" test procedures are not really suitable for computer simulation, since the mathematical description of the control behavior of humans driving a vehicle is still rudimentary. Investigations involving the use of driving simulators are however exceptions, since the driver is included in the computer simulation as a real element.

2.4.3 Parametric Study of Steering Behavior (Passenger Car)

As a further extension on the results presented in Section 2.3 on the basis of a linearized single-track vehicle model, this section deals with a parametric study conducted using the above-described ADAMS kinematics four-wheel model, which allows the categorization of individual design measures and their effects on steering behavior.

The test procedures used include "steady-state cornering" under the class of "open-loop" driving maneuvers for the description of steady-state steering behavior and the "stepped steering input" for the description of transient steering behavior (steering response) and stability behavior (yaw decay):

- "Steady-state Cornering"

Cornering radius $R = 40\text{m} = \text{const.}$

Driving speed $v = 0\text{-}20\text{ m/s}$

The driving speed v is increased slowly enough so that steady-state conditions of motion prevail at any point in time. The desired values for driving speed and cornering radius are set with the aid of PID controllers via the driving forces and the steering-wheel angle δ_H .

- "Stepped Steering Input"

driving speed $v = 27.8\text{ m/s} = \text{const.}$

steering wheel angular velocity $\dot{\delta}_H = 300\text{ }^\circ/\text{s}$

The step function of the steering-wheel angle δ_H is approximated by a steep ramp function, Fig. 2.4-5.

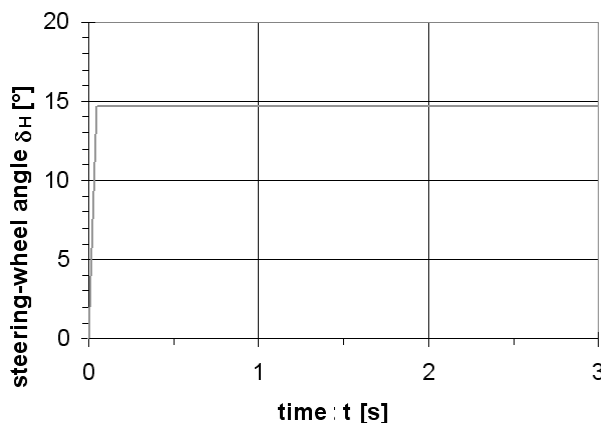


Fig. 2.4-5: Ramp function of the steering-wheel angle δ_H

The maximum steering-wheel angle δ_H is set to a value such that the lateral acceleration during steady-state driving at the end of settling processes amounts to $a_y = 4.0 \text{ m/s}^2$, Fig. 2.4-6.

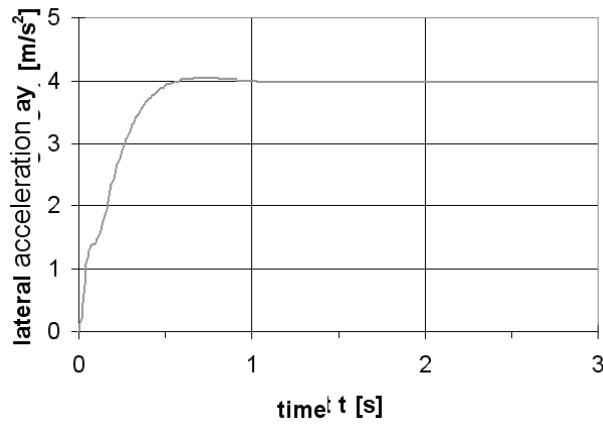


Fig. 2.4-6: Lateral acceleration after transient response

The yaw rate, for example, can then be used to evaluate the simulation, Fig. 2.4-7.

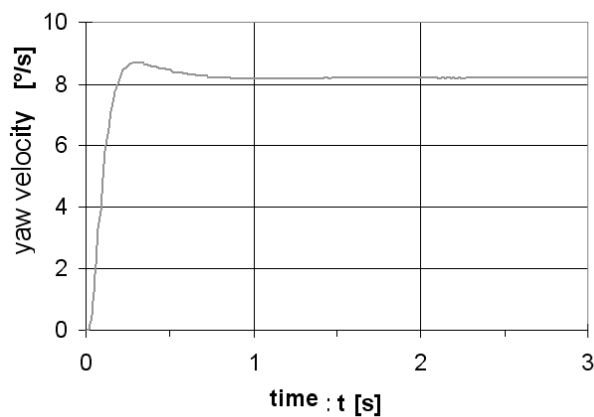


Fig. 2.4-7: Yaw velocity after transient response

- 0-Version of the Test Vehicle:

Fig. 2.4-8 shows the geometric terms and the location of the vehicle coordinate system.

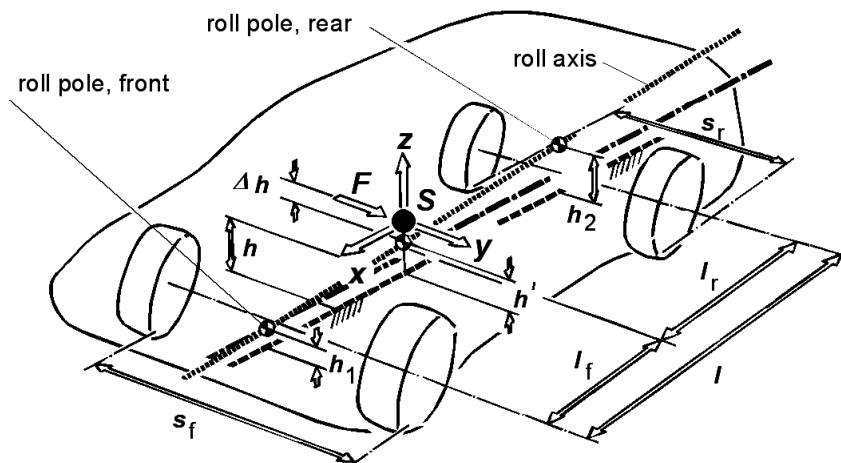


Fig. 2.4-8: Four-wheel vehicle model

Total vehicle mass:	$m_{\text{ges}} = 1678 \text{ kg}$
Wheel mass:	$m_{\text{Rad}} = 35 \text{ kg}$
Wheelbase:	$l = 2680 \text{ mm}$
Front/rear track width:	$s_v = s_h = 1520 \text{ mm}$
Center-of-gravity location (axle-load ratio):	$l_v / l_h = 1080 \text{ mm} / 1600 \text{ mm}$
Center-of-gravity height:	$h = 520 \text{ mm}$
Roll-center heights:	$h_1 = h_2 = 0 \text{ mm}$
Driven axle:	front axle
Tires (figs 2.4-2 - 2.4-4):	Michelin MXT 195/65 R15, 2 bar

Fig. 2.4-9 shows the simulation results for the zero version at steady-state cornering. The following parameters are considered for the description of steady-state steering quality:

Steering wheel angle: $\delta_H = f(a_y)$

Sideslip angle: $\beta = f(a_y)$

Roll angle: $\varphi = f(a_y)$

Yaw angle velocity: $\dot{\psi} = f(a_y)$

The lateral forces and the vertical forces of all four wheels are plotted against lateral acceleration.

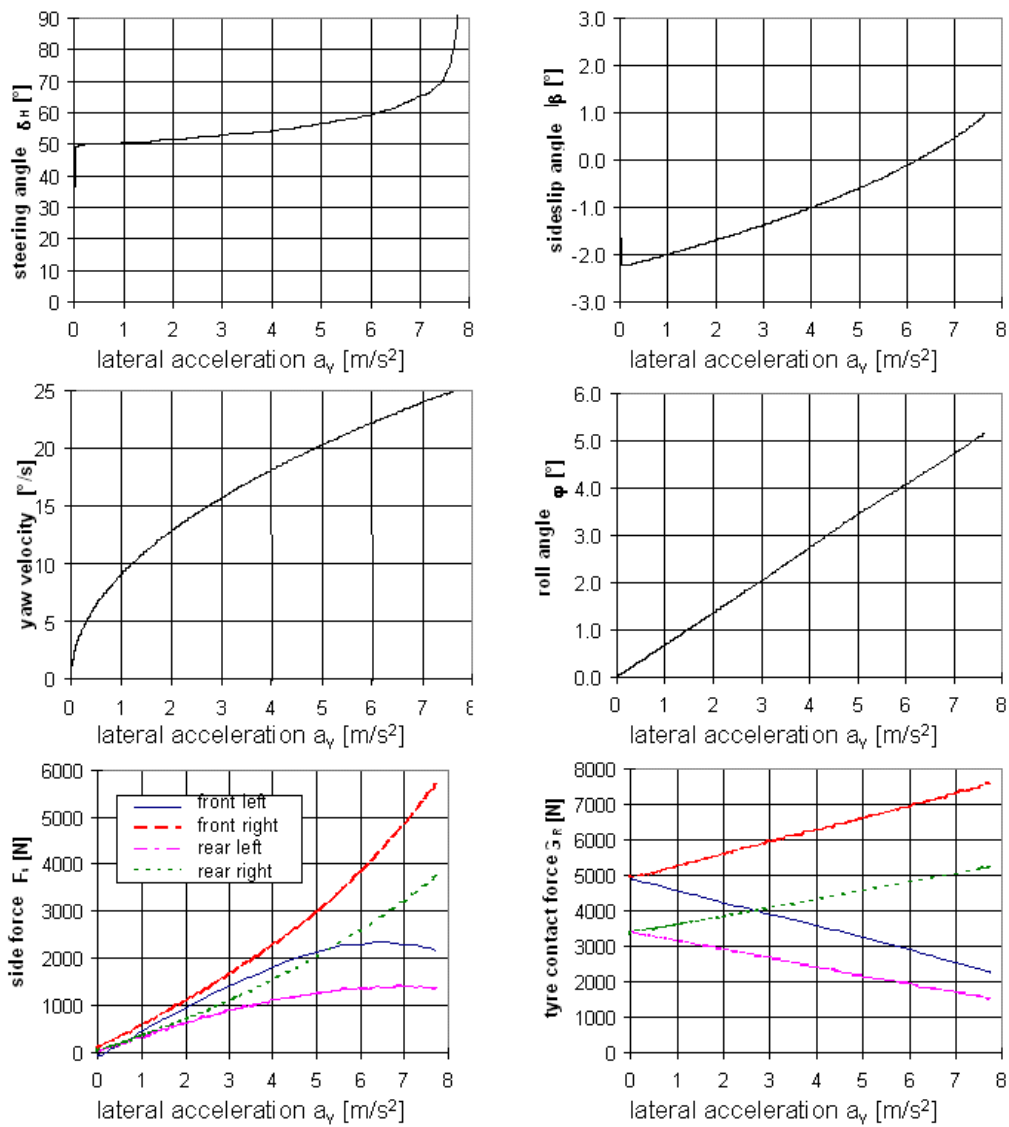


Fig. 2.4-9: Simulation results of steady-state cornering (left turn)

The main objective of steady-state cornering is to determine the steering-wheel angle δ_H as a function of lateral acceleration a_y . The initially linear and then progressively increasing steering-wheel angle together with increasing lateral acceleration is characteristic for the steering wheel angle function in the 0-version. That is, the 0-version displays an increasingly understeering steady-state steering behavior as lateral acceleration increases.

According to equation 2.3-20, the linear part of the characteristic line can be described by the self-steering gradient EG:

$$EG = \frac{1}{i_s} \cdot \frac{d\delta_H}{da_y} - \frac{d\delta_A}{da_y}$$

The steering ratio i_S can be determined on the basis of the steering-wheel angle measured during driving in the absence of a lateral force ($\delta_{HA} = 50^\circ$) and the Ackermann angle $\delta_A = l/R = 2.68\text{m} / 40\text{m} = 3.84^\circ$:

$$i_S = \frac{\delta_{HA}}{\delta_A} = 13$$

Since the Ackermann angle δ_A for the drive $R = \text{const.}$ is constant, its derivative with respect to lateral acceleration equates to zero, while the self-steering gradient can be read off directly from the required steering angle curve considering the steering ratio:

$$EG = 0,0017 \text{ rad/m/s}^2$$

The yaw-amplification factor is another significant parameter for the assessment of vehicle handling, see Fig. 2.3-10. In the linear range for driving dynamics, the following relationship exists between the yaw-amplification factor and self-steering gradient:

$$\frac{\dot{\psi}}{\delta_H / i_S} = \frac{v}{1 + EG \cdot v^2}$$

If the parameters of the zero version are employed in this function, then the relation between yaw-amplification factor and driving speed as shown in Fig. 2.4-10 is obtained.

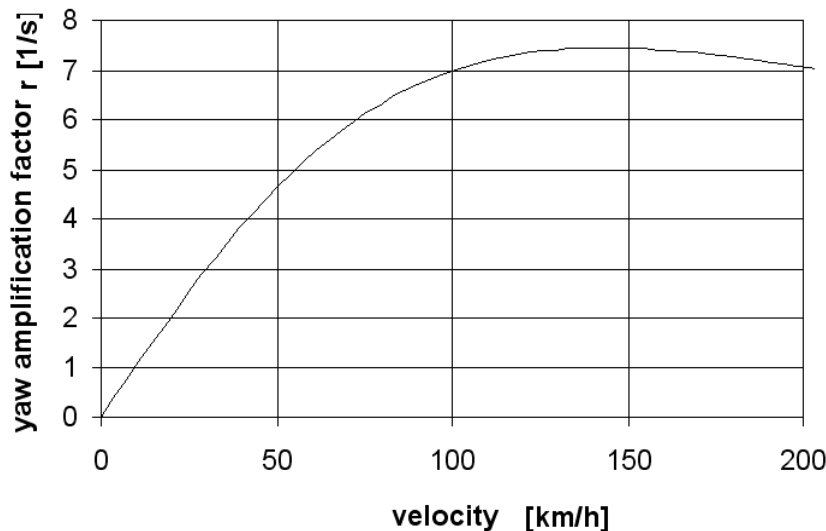


Fig. 2.4-10: Yaw-amplification factor as a function of driving speed

The characteristic line shown in Fig. 2.4-10 is typical for understeering vehicles, see section 2.3.3.1.

Apart from the self-steering response, the steering behavior of a vehicle is significantly determined by the sideslip angle. The sideslip angle characteristic shown in Fig. 2.4-9 starts at a lateral acceleration of $a_y = 0 \text{ m/s}^2$ with the negative value determined by the geometric conditions, which for a single-track model can be calculated as follows:

$$\beta_o = \frac{l_h}{R} = -2.2^\circ$$

With increasing lateral acceleration, a mildly progressive increase of the characteristic of the vehicle sideslip angle is noticed. On the present 40-m radius, the zero transition, which is the point where the vehicle longitudinal axis and the tangent to the cornering radius coincide, occurs at about 6 m/s^2 . Thus a change in the sign of the vehicle sideslip angle only occurs at higher values of lateral acceleration.

In the following section, the vehicle versions listed in Fig. 2.4-11 will be compared with the 0-version.

Version	Parametric Variation
1	center-of-gravity height $h = 0$ instead of $h = 0.52 \text{ m}$
2	center-of-gravity location $l_f/l_r = 0.776$ instead of 0.675
3	roll-center height front axle $h_1 = 0.15 \text{ m}$ instead of 0.0 m
4	stabilizer spring on front axle
5	negative static camber angle on front axle
6	kinematic bump toe-out on front axle $(\delta_f = c \cdot \Delta f, \Delta f = \text{compression})$
7	rear-wheel drive instead of front-wheel drive
8	rear-axle auxiliary steering with homodirectional (parallel) steering angle $(\delta_r = 0,2 \cdot \delta_f)$

Fig. 2.4-11: Overview of parameter variations

2.4.3.1 Height of Center-of-Gravity

To establish a correlation to the single-track vehicle model dealt with before, the location of the vehicle center of gravity is lowered to the height of the road surface in contrast to the realistic location of the 0-version. Fig. 2.4-12 shows the simulation results for both vehicle versions.

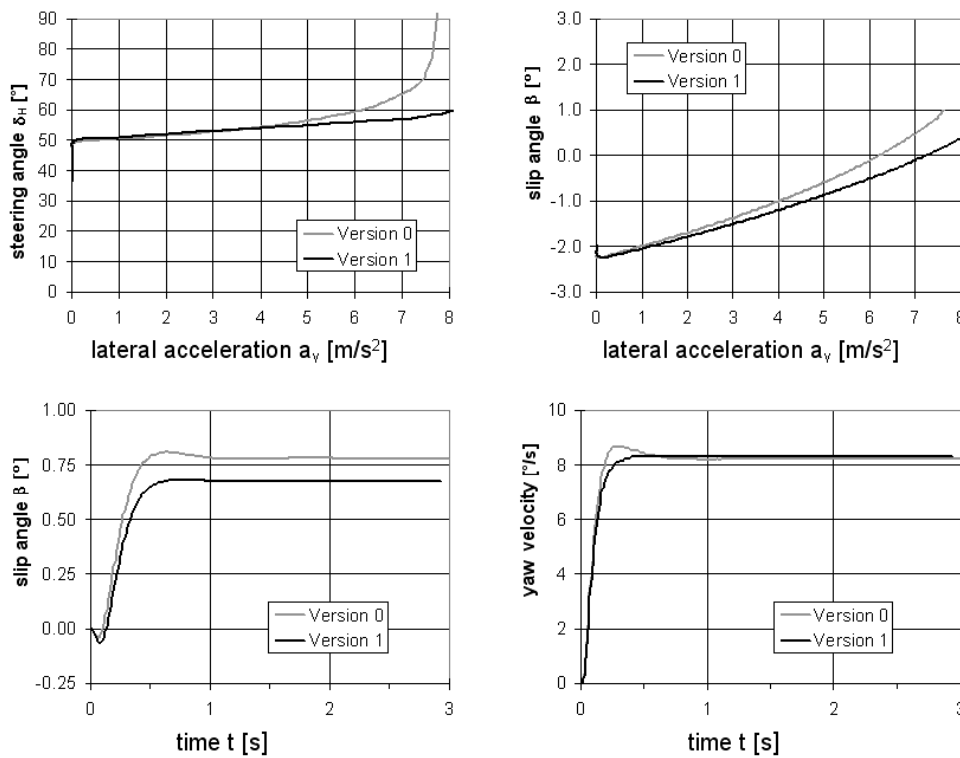


Fig. 2.4-12: Simulation results parameter variation no. 1 (center-of-gravity height $h = 0$)

While the 0-version shows an intensifying understeer tendency ($d\delta/da_y$) in steady-state steering behavior with increasing lateral acceleration, version-1 shows a virtually linear increase in the steering-wheel angle required until the limit is reached (maximum lateral acceleration). The steady-state steering behavior of version-1 thus roughly corresponds to that of a linearized single-track vehicle model. The mild understeer tendency of version-1 despite nearly identical center-of-gravity distances l_f , l_r and identical front and rear tires is due to a slight reduction of the effective side-slip stiffness c_{sf} on the front axle caused by the drive forces required to overcome the forces of rolling resistance and drag (see section 2.3).

In the 0-version, the time function of yaw velocity shows a mild overshoot after the stepped steering input. In version-1, the overshoot is insignificant, which suggests higher yaw damping. Both results are essentially due to the fact that with increasing center-of-gravity height, the effective axle slip stiffness values c_{sf} and c_{sr} on front and rear axles respectively decrease (see eq. 2.3-26 or eq. 2.3-27).

The decrease in side-slip stiffness is caused by the fact that with increasing center-of-gravity height during cornering there will be greater wheel-load differences between the wheels of an axle, which in conjunction with the nonlinearity of the tire characteristics require greater slip angles for the same centrifugal force to be supported. These relations will be described in more detail because of their great significance for steering behavior:

The wheel-load differences between the wheels of an axle during cornering are obtained with the aid of a torque balance around a point on the road surface. For derivation of the relations, the two-track suspension model from section 1.5.2 is used, Fig. 2.4-13.

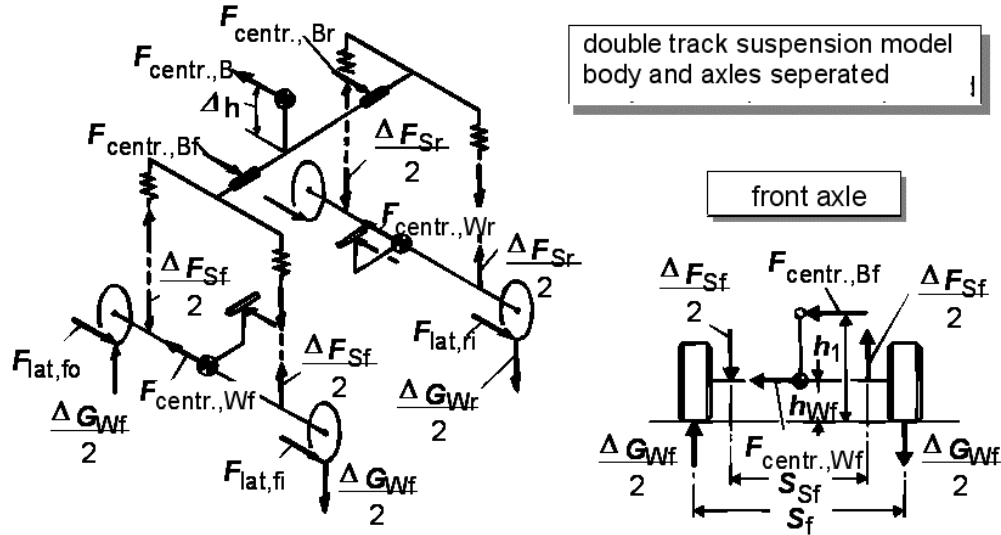


Fig. 2.4-13: Forces acting on the two-track suspension model during cornering

In this model, for the sake of simplification, it is assumed that the position of the roll centers in the vehicle do not change as a result of suspension movement. Considering small angles and linear spring characteristics, it follows:

$$\sum M_{VA} = 0 \quad (2.4-1)$$

$$F_{cf, Bf} \cdot h_1 + F_{cf, Wf} \cdot h_{Wf} + 2 \left(\frac{\Delta F_{Sf}}{2} \right) \cdot \left(\frac{s_{Sf}}{2} \right) - 2 \left(\frac{\Delta G_{Wf}}{2} \right) \cdot \left(\frac{s_f}{2} \right) = 0$$

with:

$F_{cf, Bf} = m_B \cdot a_y \cdot \frac{l_r}{l}$:	Proportion of body centrifugal force supported at the front axle
h_1	:	Front roll-center height
$F_{cf, Wf} = m_{Wf} \cdot a_y$:	Centrifugal force of front-axle mass
h_{Wf}	:	Height of front-axle center of gravity above the road
ΔF_{Sf}	:	Spring-force difference on front axle due to rolling motion
s_{Sf}	:	Front spring-track width
ΔG_{Wf}	:	Front wheel-load difference during cornering
s_f	:	Front track width

The spring-force differential depends on the magnitude of the roll angle φ :

$$\begin{aligned} (\Delta F_{Sf} / 2) &= c_{Bf} \cdot \Delta f + c_{stab,f} \cdot \Delta f_{stab,f} \\ &= c_{Bf} \cdot \varphi \cdot (s_{Sf} / 2) + c_{stab,f} \cdot \varphi \cdot (s_{stab,f} / 2) \end{aligned} \quad (2.4-2)$$

The relation between roll angle φ and body centrifugal force $F_{cf,B}$ was already derived in section 1.5.2:

$$\varphi = \frac{2 \cdot \Delta h}{c_{Bf} \cdot s_{Sr}^2 + c_{Br} \cdot s_{Sr}^2 + c_{stab,f} \cdot s_{stab,f}^2 + c_{stab,r} \cdot s_{stab,r}^2} \cdot F_{cf,B} \quad (2.4-3)$$

From eq 2.4-1 and eq 2.4-2 after transformation, the wheel-load difference is given by:

$$\Delta G_{Wf} = F_{cf,Wf} \cdot \frac{h_{Wf} \cdot 2}{s_f} + F_{cf,B} \cdot \left(\frac{l_r}{l} \right) \cdot \frac{h_1 \cdot 2}{s_f} + c_{Bf} \cdot \varphi \cdot \frac{s_{Sf}^2}{s_f} + c_{stab,f} \cdot \varphi \cdot \frac{s_{stab,f}}{s_f} \cdot s_{Sf} \quad (2.4-4)$$

Accordingly, the wheel-load difference on the rear axle:

$$\Delta G_{Wr} = F_{cf,Wr} \cdot \frac{h_{Wr} \cdot 2}{s_r} + F_{cf,B} \cdot \left(\frac{l_f}{l} \right) \cdot \frac{h_2 \cdot 2}{s_r} + c_{Br} \cdot \varphi \cdot \frac{s_{Sr}^2}{s_r} + c_{stab,r} \cdot \varphi \cdot \frac{s_{stab,r}}{s_r} \cdot s_{Sr} \quad (2.4-5)$$

Thus the wheel load supported on each wheel during cornering can be calculated as:

$$G_{Wfo} = \frac{1}{2} \cdot m_{tot} \cdot g \cdot \frac{l_r}{l} + \frac{1}{2} \cdot \Delta G_{Wf} \quad (2.4-6)$$

$$G_{Wfi} = \frac{1}{2} \cdot m_{tot} \cdot g \cdot \frac{l_r}{l} - \frac{1}{2} \cdot \Delta G_{Wf} \quad (2.4-7)$$

$$G_{Wro} = \frac{1}{2} \cdot m_{tot} \cdot g \cdot \frac{l_f}{l} + \frac{1}{2} \cdot \Delta G_{Wr} \quad (2.4-8)$$

$$G_{Wri} = \frac{1}{2} \cdot m_{tot} \cdot g \cdot \frac{l_f}{l} - \frac{1}{2} \cdot \Delta G_{Wr} \quad (2.4-9)$$

In the present case, the instantaneous-center heights (roll-center heights) h_1 and h_2 equal zero, front and rear body suspension stiffness including stabilizer stiffness are equal, and the spring-track widths correspond to the wheel-track widths (independent wheel suspension).

If the centrifugal-force shares of the wheel masses are neglected, the equations 2.4-4 and 2.4-5 are simplified and become:

$$\Delta G_{Wf} = \Delta G_{Wr} = (c_B + c_{stab}) \cdot \varphi \cdot s \quad (2.4-10)$$

or with equation 2.4-3 and $\Delta h = h$ ($h_1 = h_2 = 0$):

$$\Delta G_{Wf} = \Delta G_{Wr} = \frac{2 \cdot h}{s} \cdot F_{cf,B} \quad (2.4-11)$$

The sum of tire lateral forces on one axle has to counteract the share of the total centrifugal force to be supported here:

$$F_{sfi} + F_{sfo} = F_{Lat,tot} \cdot \frac{l_r}{l} \quad (2.4-12)$$

$$F_{sri} + F_{sro} = F_{Lat,tot} \cdot \frac{l_f}{l} \quad (2.4-13)$$

Under the assumption that the tire slip angles on the wheels of an axle are the same, the required "axle" slip angle will not only depend on the axle load G_A but also on the wheel-load difference ΔG_R on this axle, Fig. 2.4-14.

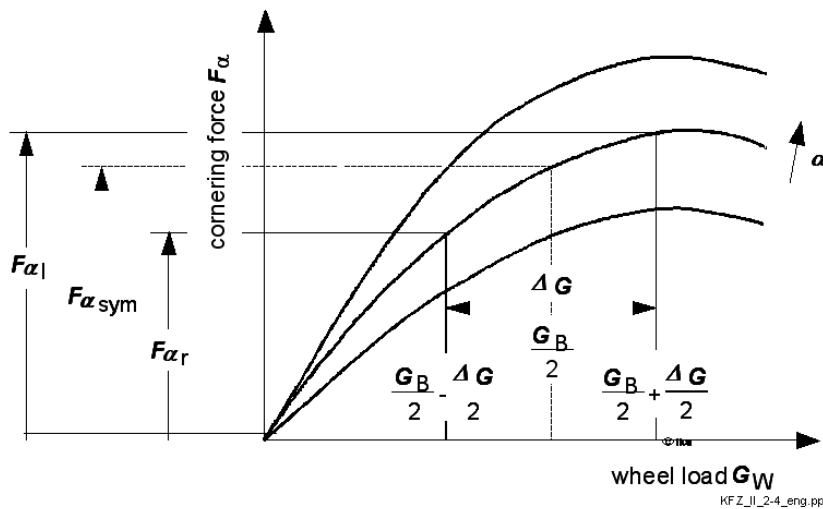


Fig. 2.4-14: Cornering force in relation to the wheel-load difference

If the axle load G_A was symmetrically distributed among both wheels ($G_W = G_A / 2$), each wheel would support half the share of the transverse force $F_{lat,f}$ or $F_{lat,r}$. If wheel-load differences occur on an axle, then the sum of the cornering forces will reach the required amount only in the presence of a wider slip angle (in contrast to $\Delta G_W = 0$) due to the degressive course of the tire characteristic curves $F_\alpha = f(G_W, \alpha = \text{const.})$.

The results of parametric variation-1 can thus be summarized as follows:

With increasing center-of-gravity height h , there will be greater wheel-load differences on front and rear axles during cornering (see equation 2.4-11). Wheel-load differences reduce axle cornering force with constant slip angle, in other words, an increased slip angle is required in order to generate the same cornering force. This corresponds to a reduction of the effective slip stiffness c_s as a result of wheel-load differences (Fig. 2.4-14).

If slip stiffness decreases to the same extent on front and rear axles, as in the present case (version-1 \rightarrow version-0), then an existing oversteer or understeer tendency will be intensified.

2.4.3.2 Location of the Center-of-Gravity

In order to determine the influence of axle-load distribution, a vehicle is compared with the 0-version, whose center of gravity is relocated rearward ($l_f/l_r=0.776$), Fig. 2.4-15.

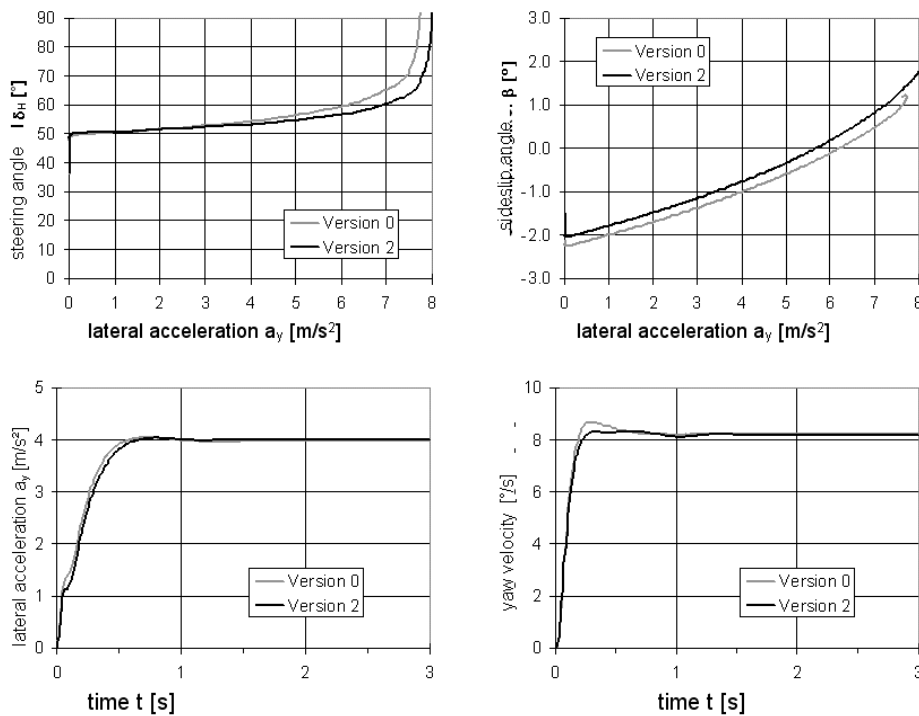


Fig. 2.4-15: Simulation result parametric variation no. 2 (center-of-gravity location $l_f/l_r = 0.776$)

The understeer tendency of the 0-version is reduced by the relocation of the vehicle center of gravity rearwards. The transient behavior of version-2 points to a lower yaw natural frequency and a higher yaw damping compared to the 0-version.

Both results match with the relations (section 2.3) derived with the help of the linearized single-track vehicle model. Due to the degressive nature of the tire characteristics $F_\alpha = f(G_W, \alpha = \text{const.})$, the decrease of the effective slip stiffness c_{sf} on the front axle is not of the same magnitude as the increase of the center-of-gravity distance l_f to the front axle.

2.4.3.3 Roll Axis

The instantaneous axis of rotation of the vehicle body in relation to the road, around which the vehicle body tilts during rolling motion (see section 1.5.2), is referred to as "roll axis" or "instantaneous axis". It constitutes the connecting line of the roll centers on front and rear axle, whose locations are determined by the kinematics of wheel suspension.

In the 0-version, the roll axis runs along the road surface. In version-3, the roll center on the front axle is 0.15 m above the road surface, and the roll axis descends towards the rear axle (see Fig. 2.4-8).

The lever arm Δh of the body centrifugal force around the roll axis is thus smaller in version-3 than in the 0-version:

$$\Delta h \approx h - \left(h_1 + l_v \cdot \frac{h_2 - h_1}{l} \right)$$

As a result the roll angle reduces for the same lateral acceleration. Since all other influencing parameters remain unchanged, a lower wheel-load difference on the rear axle results, equation 2.4-4.

In both vehicle versions, the sum of the wheel-load differences on the front and rear axles have to compensate the same torque resulting from the centrifugal force around the track.

The wheel-load difference on the front axle of version-3 is greater, equation 2.4-5.

As expected, the existing understeer tendency of the 0-version increases with the height of the roll center on the front axle, since the effective slip stiffness values are influenced by the altered distribution of the wheel-load differences, Fig. 2.4-16.

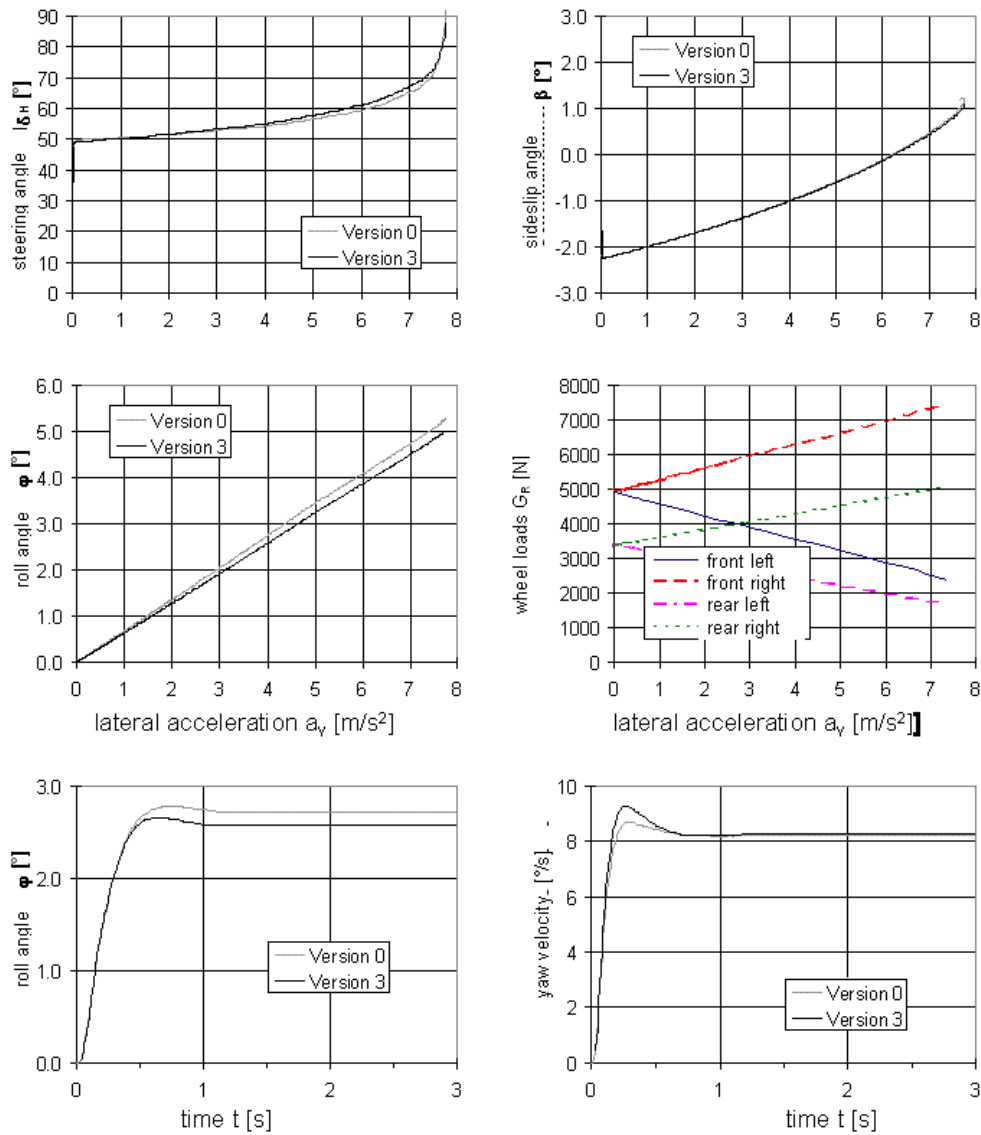


Fig. 2.4-16: Simulation result parametric variation no. 3 (front-axle roll-center height)

2.4.3.4 Anti-roll Suspension Distribution

So far, only vehicle versions with symmetric distribution of anti-roll suspension stiffness have been studied, i.e. the moment resulting from the body centrifugal force is equally supported on the front and rear axles.

In version-4, the stabilizer stiffness on the front axle was increased compared to the 0-version. For the same lateral acceleration, this results in a narrower roll angle ϕ , equation 2.4-3.

With the help of equation 2.4-4 and equation 2.4-5, the influence on the wheel-load differences and thus on steering behavior can be assessed:

The wheel-load difference ΔG_{Wr} on the rear axle decreases, since all influencing parameters in equation 2.4-5 are unchanged, except for the roll angle φ . Accordingly, the wheel-load difference ΔG_{Wf} on the front axle has to increase by the same amount, because – as already described in the influence of the roll-center heights – the sum of the wheel-load differences on front and rear axles depend only on the dimensions of the track widths and the height of the overall center of gravity above the road, and not on the design of the suspension system.

Fig. 2.4-17 shows the influence of the proportion of the wheel load difference dependent on the stabilizer-stiffness on an axle during cornering on the sum of lateral forces.

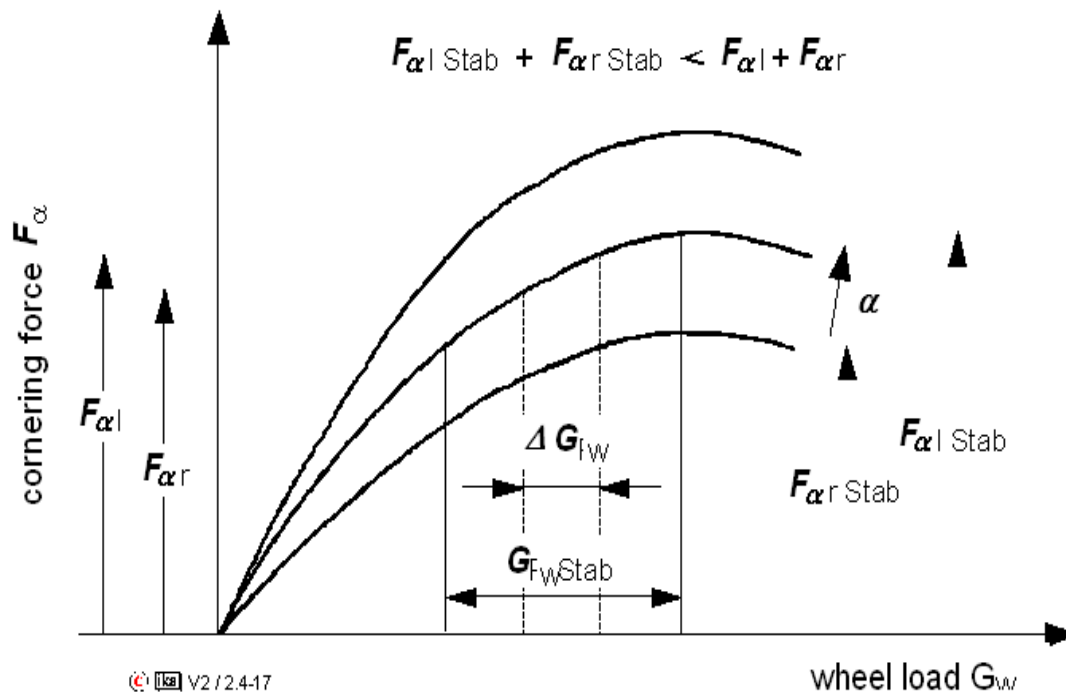


Fig. 2.4-17: Axle cornering forces with/without stabilizer spring

The axle slip angle required to support a certain total lateral force increases with growing stabilizer stiffness, i. e. the effective slip stiffness c_s decreases.

The theoretical considerations are verified by the simulation results. Version-4 shows an intensified understeer tendency compared to the 0-version, Fig. 2.4-18.

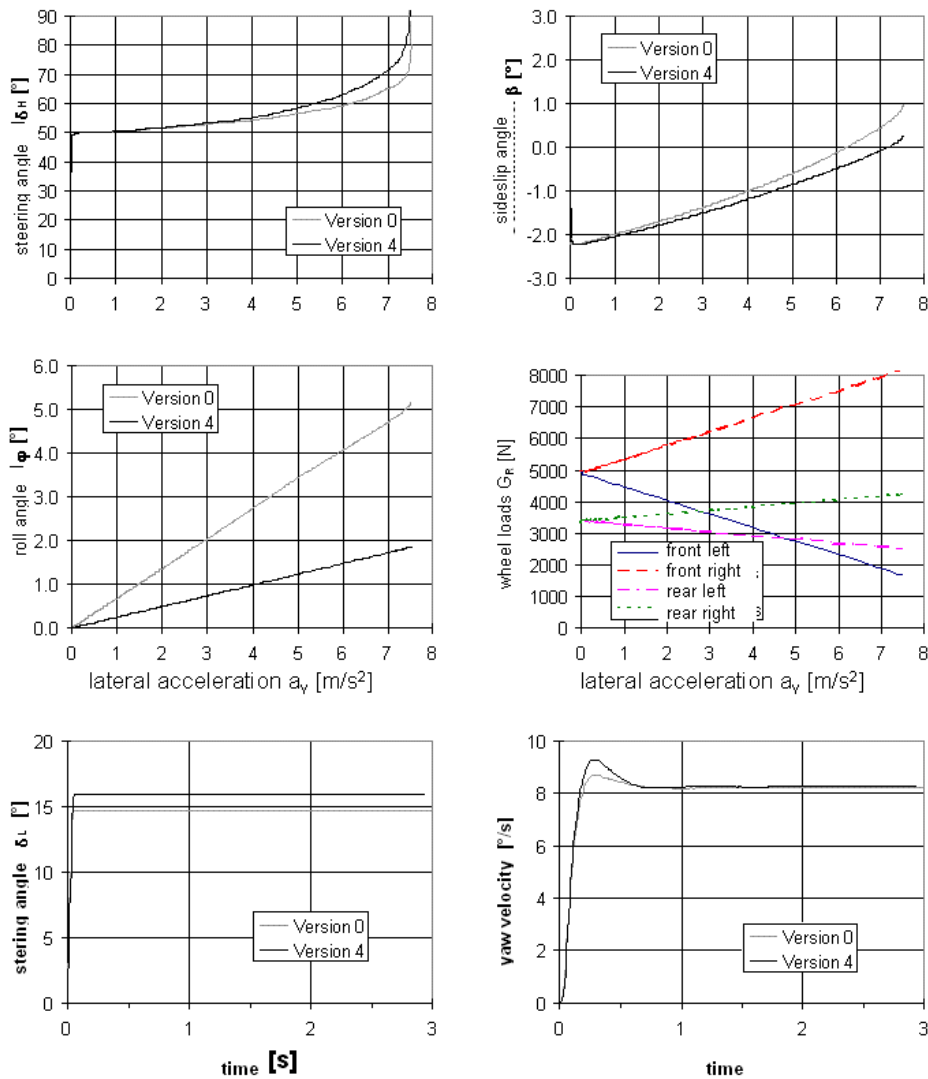


Fig. 2.4-18: Simulation result parametric variation no. 4 (stabilizer on front axle)

Increasing stabilizer stiffness on the rear axle would result in a decreasing understeer tendency. Distribution of total effective stabilizer stiffness between front and rear axles is an important instrument in tuning the steering behavior of an automobile.

2.4.3.5 Camber and Toe Angle

In all parametric variations considered so far, the influence exerted on the steering behavior was in the final analysis due to the nonlinearity of the tire characteristics.

Apart from the tire characteristics, the kinematic and elastic properties of wheel suspensions are of great significance in lateral dynamics.

As a rule, axles - and wheel carriers in the case of independent suspensions – are guided by links (or joints) relative to the body, in a manner that essentially only one degree of freedom of compression is left. Since the links are of a finite length, suspension compression is

associated with changes in the position of the wheel relative to the body, i.e. changes in track width, wheelbase, wheel camber and toe determined by wheel suspension kinematics, Fig. 2.4-19.

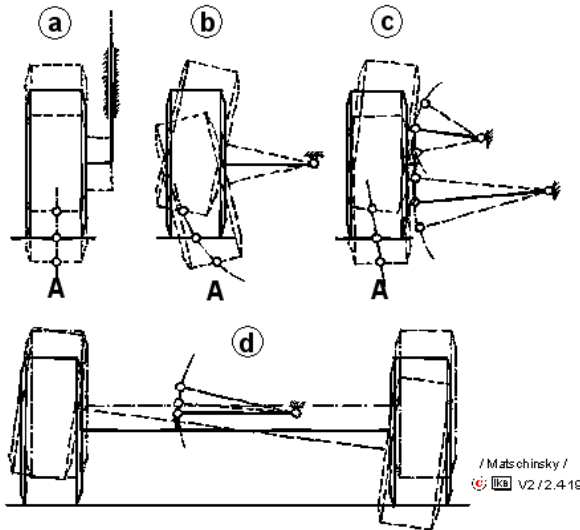


Fig. 2.4-19: Wheel position changes during suspension movement

In order to achieve vibration isolation between wheel suspension components and body, the body-side mounts of these links (pivots) are not designed in the form of rigid bearing journals or ball joints but as rubber-metal elements. The angular flexibility required of the bearing points (pivots) is realized solely by the elasticity of the rubber elements, so that the mounts do not have any clearances and are maintenance-free.

Due to the elasticity of the rubber mounts, changes in the position of the wheel also occur as a result of the forces and torque acting in the tire-contact center of the vehicle.

In comparison to kinematic changes in wheel-position as a consequence of suspension movement, these wheel-position changes are referred to as elastokinematic changes, since they are dependent on wheel suspension kinematics and elasticity.

The kinematic camber-angle variations and the kinematic and elastokinematic toe-angle variations are the most significant changes in the wheel-position from the point of vehicle handling.

In section 2.2.4.2, the absolute camber angle γ of the wheel relative to the road surface was defined. The absolute camber angle γ is composed of the roll angle ϕ of the body and the relative camber γ_{rel} of the wheel relative to the body, Fig. 2.4-20.

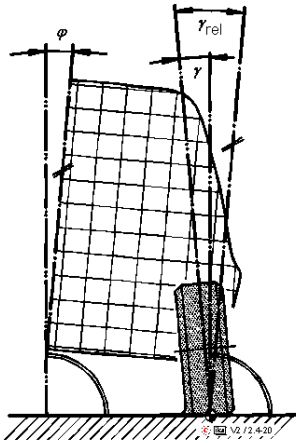


Fig. 2.4-20: Representation of absolute and relative camber angles

Mathematically, the signs assigned to camber angles on left as well as right vehicle sides are not identical. The relative camber is negative if the upper edge of the wheel disk is inclined towards the vertical-longitudinal plane of symmetry of the body. The absolute camber is negative if the upper edge of the wheel disk is inclined towards a plane, which in vehicle longitudinal direction stands vertical relative to the road.

The camber side-forces (see Section 2.2.4.2) caused by the wheel camber and the lateral slip forces overlap and add up as long as the limit for the utilizable friction coefficient for lateral forces is not reached.

During cornering, negative camber angles on the wheels of an axle increase the axle lateral force resulting from a certain axle slip, Fig. 2.4-21.

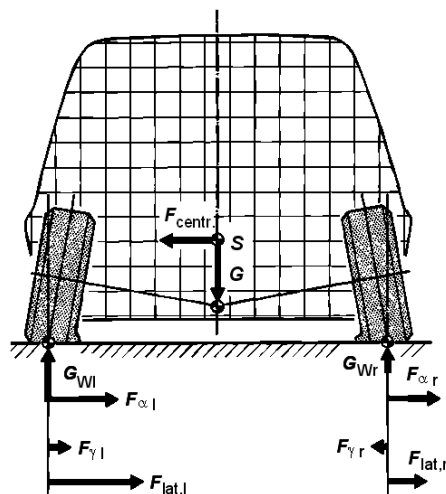


Fig. 2.4-21: Overlap of cornering forces due to slip and wheel camber

Vehicles with an oversteer tendency due to their rear-wheel drive concept usually feature negative camber angles on the wheels of the rear axle, which contribute to an understeer

behavior that is more favorable from the point of view of driving stability. Intensification of the understeer tendency of RWD vehicles requires only minor kinematic camber changes if relatively large negative camber angles are already provided on the rear axle in the design position (ca. -2.0°). The design should also give due consideration to the effect on tire wear.

Fig. 2.4-22 shows the simulation results of version-5 "negative camber angles on front-axle wheels".

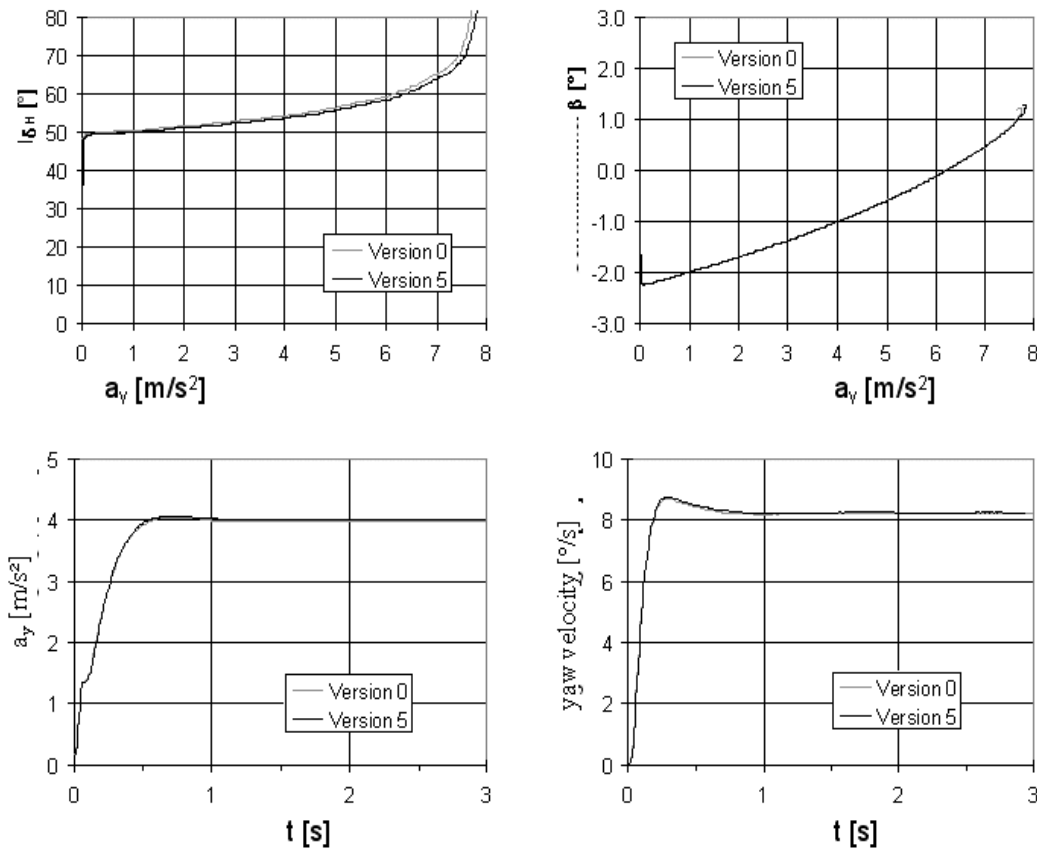


Fig. 2.4-22: Simulation results parametric variation no. 5 (negative camber angles on front-axle wheels)

Due to a camber on the wheels of the front axle, higher lateral forces can be transferred on this axle. The understeer tendency of the 0-version is hence reduced.

With increasing roll angle of the body during cornering, the negative camber angle on the outside wheel effective in the design position however reduces, Fig. 2.4-20. By means of a kinematic wheel-camber change during compression, this decrease in the absolute (negative) camber angle could be compensated.

In the design of the suspension however, the fact that the considerable kinematic camber changes required, result in the straight-running properties being affected must also be taken into account, since these camber changes also become operative as a result of suspension

movements caused by road irregularities and then produce undesired lateral force fluctuations.

Fig. 2.4-23 illustrates the sign conventions for toe angles. Positive toe angles are referred to as toe-in, negative as toe-out. As a rule, a total toe-in angle δ_f is specified for the front axle because the wheel-related toe-in angles depend on the steering angle δ on the front axle.

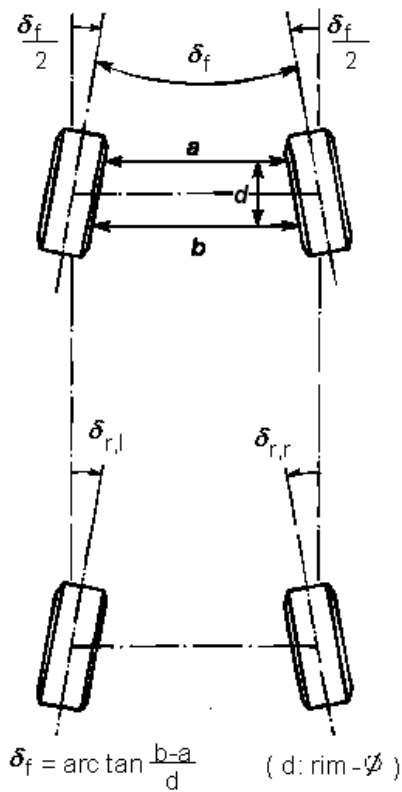


Fig. 2.4-23: definition toe angle

Toe-in angles on the outside wheel or toe-out angles on the inside wheel of an axle increase the tire slip angle operative at a certain axle slip angle and thus the resulting axle lateral force.

On account of a higher wheel load, the lateral-force increase due to the toe-in share of the outside wheel of an axle exceeds the lateral-force loss due to an identical toe-in share of the inside wheel.

A total toe-in angle on the front axle thus causes an increase in the axle lateral force resulting from a certain axle slip angle; a total toe-out angle causes a decrease.

During straight-ahead driving, toe-in angles cause one-sided wear of the tires on their outside shoulders. Static toe-in angles in the design position must hence be small enough for them to be just about compensated by the toe change caused by rolling-resistance forces in combination with the elasticity of the wheel suspension.

Static toe-in angles are consequently not suited for the tuning of steering behavior. In many vehicles, kinematic toe-in change during suspension compression is used to specifically influence steering behavior. For example, in vehicles with a design-related oversteer tendency, the understeer tendency, which aids driving stability, can be intensified by a wheel suspension layout causing toe-out of the front wheels and toe-in of the rear wheels during compression. Such measures can be combined with camber changes, Fig. 2.4-24.

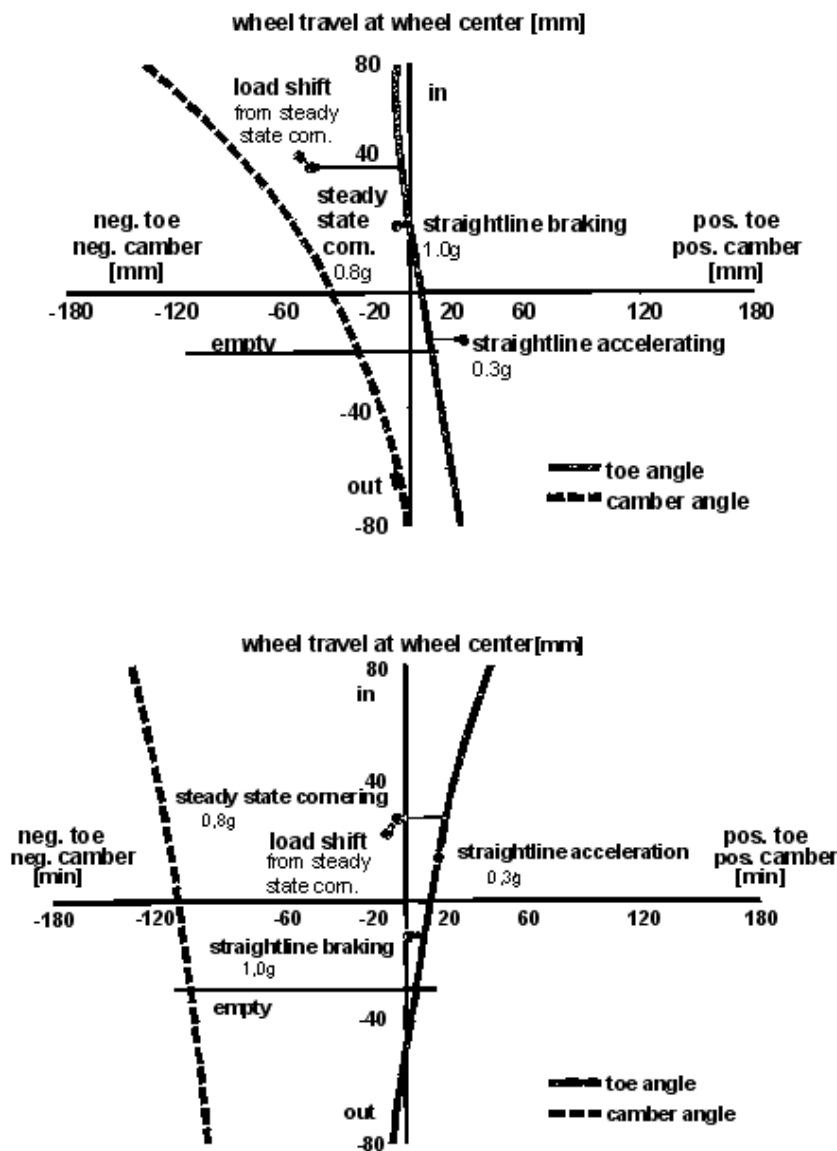


Fig. 2.4-24: Toe-in and camber characteristics (Audi A4, 1995)

The effect on steering behavior is referred to as "roll understeer", Fig. 2.4-25.

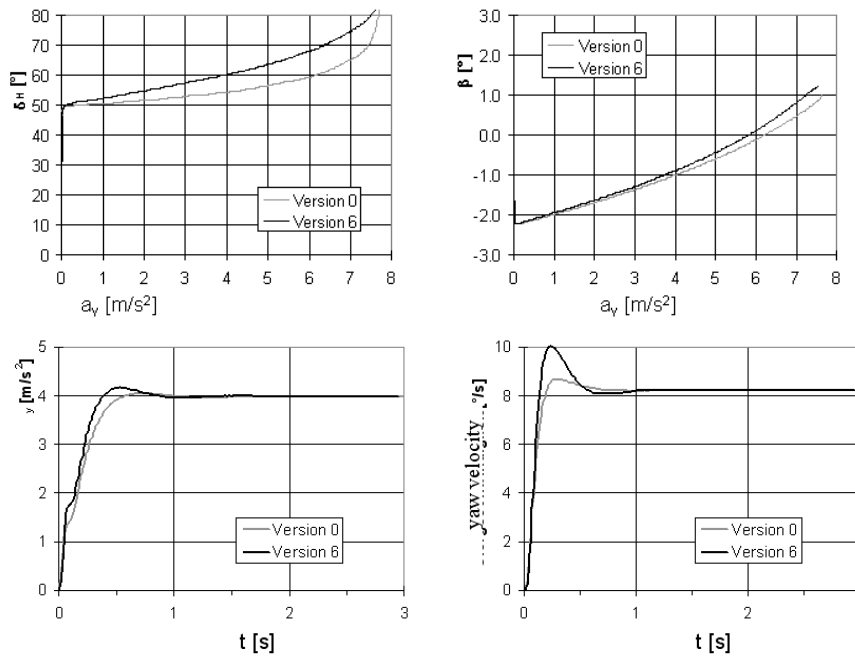


Fig. 2.4-25: Simulation results parametric variation no. 6 (toe-out on the front axle)

Design should take into account the fact that kinematic toe-in changes, especially on the wheels of the rear axle, adversely affects straight-running properties, since suspension movements caused by road irregularity also result in toe-in changes and thus to undesired lateral-force fluctuation / 45 /.

Since changes in toe directly affects tire slip, only a few angular minutes suffice to bring about significant lateral-force variation. Vehicle handling is therefore not only affected by purely kinematic but also by elastokinematic changes of toe.

Suspension layouts designed to fulfill certain elastokinematic properties as a rule require very complex designs of wheel guidance. In many commonly used wheel suspension types, the elastokinematic properties caused by the rubber mounts needed for vibration isolation are therefore accepted, and the effect of the resulting wheel position changes (especially changes in toe) are compensated by targetted kinematic layout, which is almost always easier to realize.

More recent designs however, reflect the increasing efforts to realize a target-specific layout for elastokinematic properties.

The so-called "lateral-force oversteer", for example, can be prevented if the rear-axle wheel suspension is designed in such a manner that the lateral tire force during cornering does not cause toe-out of the outside wheel (which is more decisive for steering behavior as a result of the higher wheel load) / 23 /.

Elastokinematic changes of toe not only occur as a result of the effect of lateral tire forces but also due to the effect of longitudinal tire forces. Criteria for specific design are mentioned in section 2.4.4.

2.4.3.6 Traction (Drive Concept)

It was already mentioned in the parametric variation of the height of the center-of-gravity (version-0 – version-1) that the traction or driving forces required to overcome rolling-resistance force and aerodynamic drag reduce the instantaneous effective side slip stiffness on the driven axle.

For small slip angles, the influence of the circumferential forces on the resulting lateral force is insignificant (see section 2.2.4.2, Fig. 2.2-24, "Krempel Diagram").

At higher values of lateral acceleration however, the slip angles required during cornering reach values at which the simultaneously acting circumferential forces cause a reduction of the resulting lateral force. This reduction of the lateral force has to be compensated by an increased slip angle, which is tantamount to a reduction of the effective side-slip stiffness.

The increase in lateral acceleration during cornering on a constant track radius, not only results in the increase in lateral forces but also the circumferential forces on the driven wheels, since road resistance will increase with increasing driving speed.

As a result of this combined tire load, the axle slip angles required to produce the required lateral forces increase progressively with increasing lateral acceleration. This effect is intensified by the wheel-load differences occurring during cornering.

Therefore, a front-wheel driven vehicle features a steady-state steering behavior with an understeer tendency that increases until the stability limit is reached. A realistically responding vehicle with rear-wheel drive, i. e. a vehicle tuned for understeer by means of a specific layout of mass distribution, roll suspension rate, axle kinematics and tire inflation pressure, can show a trend reversal with regard to steady-state steering behavior, Fig. 2.4-26.

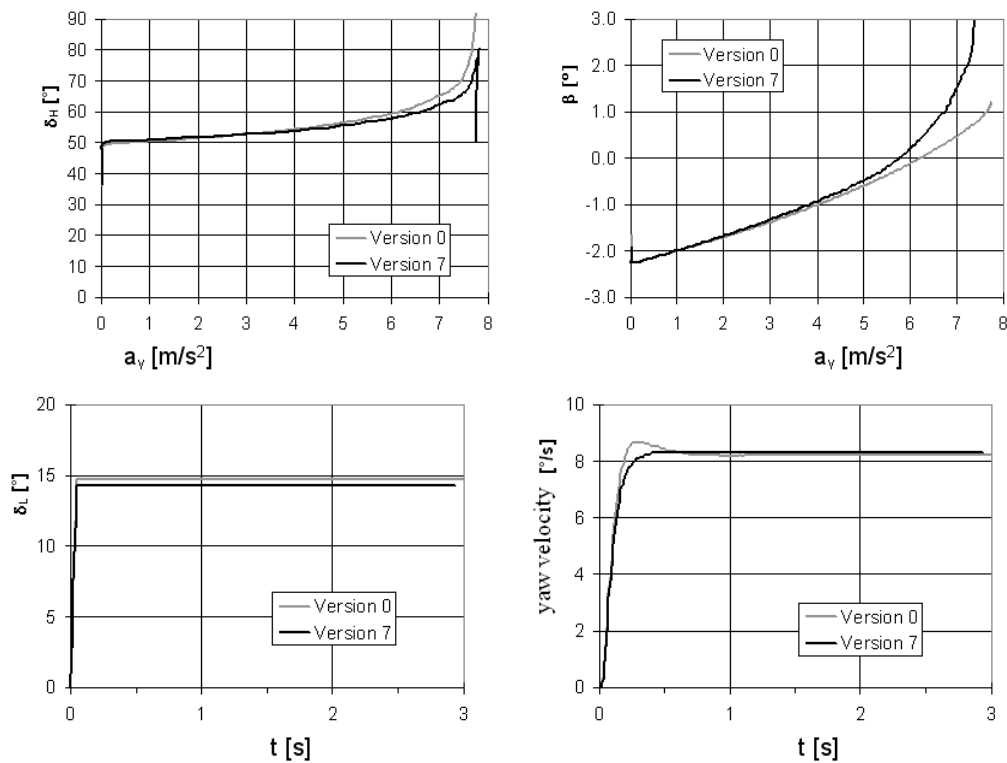


Fig. 2.4-26: Simulation results parametric variation no. 7 (RWD instead of FWD)

The trend reversal in steering behavior occurs when the decrease in slip stiffness on the driven axle as a result of the circumferential forces exceeds the decrease in slip stiffness on the front axle due to increasing wheel-load differences or other tuning measures.

The slip angles required on the rear axle thus bring about a very considerable vehicle side slip angle. Front-axle slip angles corresponding to lateral acceleration require the steering angle to be reduced when the stability limit is approached (see equation 2.3-7, Section 2.3).

If driving speed is increased beyond the stability limit, the FWD vehicle with understeer tendency will drift with the front wheels to the outer edge of the curve. As a result, the track radius driven is increased, lateral acceleration is reduced and the vehicle regains stability.

The RWD vehicle with trend reversal in steady-state steering behavior analyzed here however, drifts with the vehicle tail to the outer edge of the curve when the stability limit is reached and hence turns into the curve. Consequently, lateral acceleration increases further, and if the driver does not promptly reduce the steering angle at this point, the vehicle will spin around its vertical axis and lose control. Understeering on the stability limit is easier for the driver to control.

Of course, these statements only apply if the driving forces required to maintain the driving velocity are constant. Vehicle behavior as a result of load reversal or braking during cornering is dealt with in section 2.4.4.

The behavior of AWD vehicles on the stability limit depends on the distribution of the driving torque between the front and rear axles.

The design principle allows somewhat higher lateral acceleration than would be possible for a comparable vehicle with only a single driven axle, since the loads on the tires as a result of force transfer are distributed uniformly between all wheels.

In the tuning of steering behavior, no matter what the drive concept is, it has to be borne in mind that the transition from the stability limit to the range in which it is practically no longer possible to hold the desired course will be more abrupt the closer the maximum achievable lateral acceleration approaches the friction-related, theoretically possible lateral acceleration and hence puts additional pressure on the driver in estimating the approach to this transition.

2.4.3.7 Auxiliary Rear-Axle Steering

With the help of auxiliary rear-axle steering, the steering behavior of a vehicle can be influenced over a wide range.

In the parking mode (low driving speed), the turning circle can be reduced by introducing a steering angle on the rear wheels which is opposite in relation to the steering angle on the front wheels, Fig. 2.4-27.

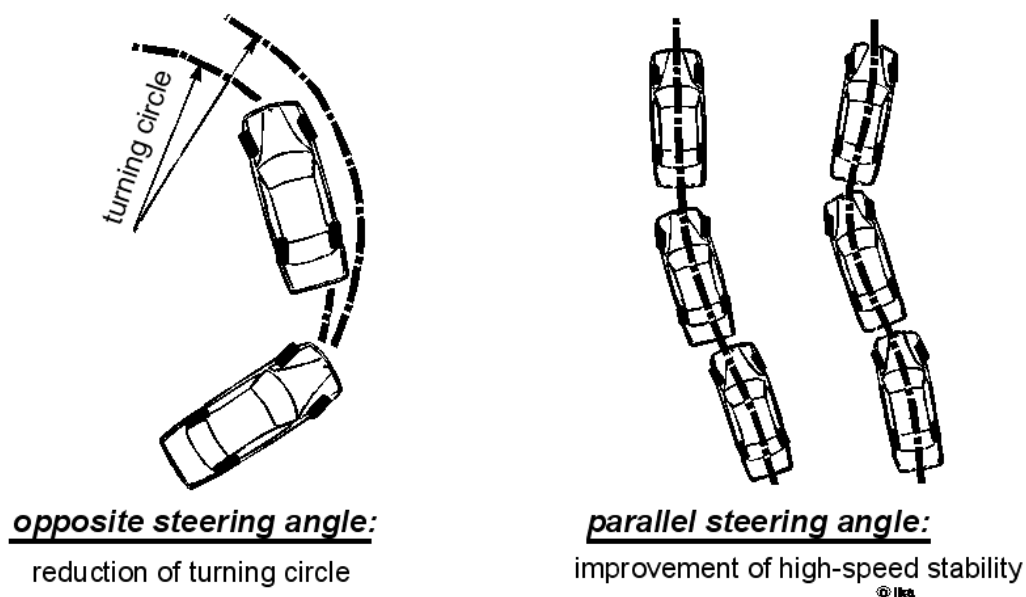


Fig. 2.4-27: Rear-axle auxiliary steering /40/

In a speed range that is interesting from the point of view of driving dynamics, an opposing steering angle on the rear axle will however, reduce the stability.

Transient steering behavior can be influenced positively only by a unidirectional steering angle on the rear wheels. The effect is in a way similar to that of a rear axle whose elastokinematic design is such that the lateral force causes toe-in on the outside wheels.

Compared to such a passive rear-axle steering system, active rear-axle auxiliary steering, however, has the advantage that the build-up of lateral forces takes place immediately and not only after a change of the sideslip angle.

The effect of opposite steering angles on the rear axle on driving dynamics can be assessed on the basis of the following consideration:

In a vehicle without rear-axle steering, a lateral force is initially built up only on the front axle as a result of a quick steering movement by the driver, Fig. 2.4-28.

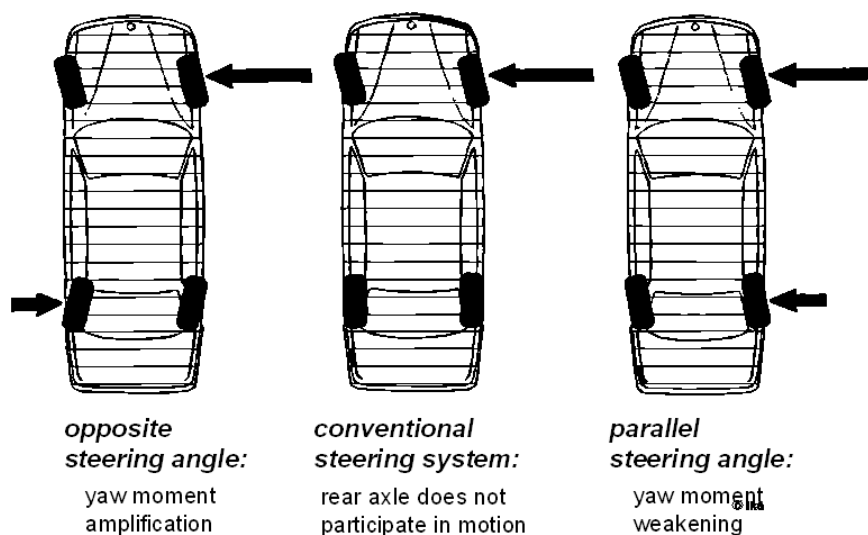


Fig. 2.4-28: Lateral-force buildup immediately after a stepped steering-angle input /40/

Only when the vehicle responds to the excitation with a lateral motion and yaw, will a slip angle also be created on the rear axle. A lateral force will then be built up on the rear-axle which will result in a further increase in lateral acceleration and reduce yaw acceleration to zero (state of equilibrium of steady-state cornering).

In a vehicle with opposite steering on the rear wheels, oppositely directed lateral forces are built up on the front and rear axles immediately after a steering-angle change. The resulting lateral acceleration at this point is hence lower while the yaw acceleration higher than in a vehicle without rear-axle steering. Accordingly, a quick increase in yaw rate is to be expected, which will cause a distinct overshoot, while lateral acceleration will be slower in reaching its steady-state final value.

A more favorable steering response with regard to driving stability involves a quick increase in lateral acceleration in combination with a minor overshoot of yaw rate. This can be achieved if lateral forces are built up on the front and on the rear axle immediately after the

steering-angle change, these forces being directed towards the inside of the curve, i.e., using a unidirectional steering angle on the rear axle. Fig. 2.4-29 shows the simulation results conducted for steady state cornering.

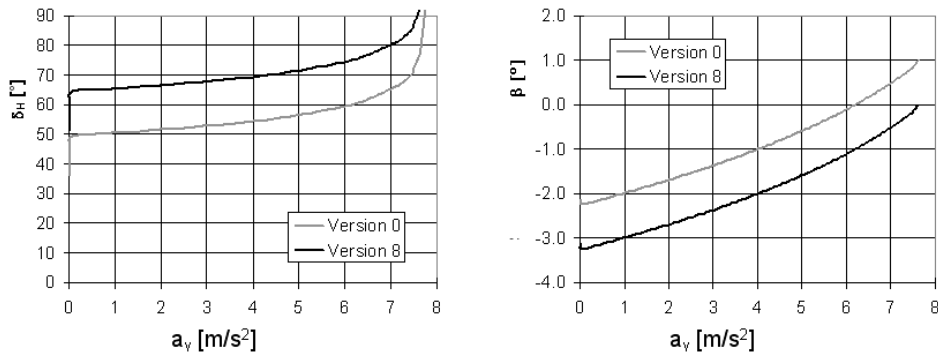


Fig. 2.4-29: Simulation results parametric variation no. 8
(rear-axle auxiliary steering $\delta_r = 0,2 \cdot \delta_f$)

With the help of such elementary considerations, it may be possible to answer questions related to the suitability of a particular direction to the steering angle on the rear axle, but will however, not help in the determination of a suitable functional relation between the steering angle on the front axle and the steering angle on the rear axle.

The following consideration, in the least, provides a theoretically meaningful control strategy for rear-axle steering: The approach towards the stability limits in relation to the driving dynamics of a motor vehicle is usually characterized by significant vehicle sideslip angles being reached very rapidly.

In these situations, the driver's reflexes are often overtaxed, since these vehicle movements along with the steering inputs required to stabilize them are not within the scope of stimulus-response mechanisms experienced by him in everyday traffic /11/.

Therefore, the objective in this case is to fully compensate the vehicle sideslip angles by means of rear-axle steering in a speed range which is of significance from the point of view of driving dynamics and thus to offer the driver a familiar steering behavior which remains virtually unchanged at the stability limit.

The basic derivation of the required functional relation between front and rear steering angles can be determined using the linearized single-track vehicle model.

Considering a rear-axle steering angle, the equations of motion in section 2.3 take the form:

$$m \cdot v \cdot (\dot{\psi} - \dot{\beta}) = c_{sf} \cdot \left(\delta_f + \beta - \frac{l_f}{v} \cdot \dot{\psi} \right) + c_{sr} \cdot \left(\delta_r + \beta + \frac{l_r}{v} \cdot \dot{\psi} \right) \quad (2.4-16)$$

$$\Theta_z \cdot \ddot{\psi} = c_{sf} \cdot \left(\delta_f + \beta - \frac{l_f}{v} \cdot \dot{\psi} \right) \cdot l_f + c_{sr} \cdot \left(\delta_r + \beta + \frac{l_r}{v} \cdot \dot{\psi} \right) \cdot l_r \quad (2.4-17)$$

By substituting the conditions for vehicle side-slip-angle compensation, $\beta = 0$, $\dot{\beta} = 0$ in the two differential equations, the following transfer function is obtained between rear-axle and front-axle steering angles after a Laplace transformation / 11 /:

$$F_{\delta}(s) = \frac{\delta_r(s)}{\delta_f(s)} = P_r \cdot \frac{1 + T_D \cdot s}{1 + T_1 \cdot s} \quad (2.4-18)$$

Vehicle side-slip angle compensation thus requires a transfer function equivalent to that of a PDT_1 element /32/.

- Amplification factor of the proportional part

$$P_h = - \frac{c_{sf} \cdot c_{sr} \cdot l_r \cdot l - c_{sf} \cdot l_f \cdot m \cdot v^2}{c_{sf} \cdot c_{sr} \cdot l_f \cdot l + c_{sr} \cdot l_r \cdot m \cdot v^2}$$

- Time constant of the D-part

$$T_D = \frac{\Theta_z \cdot v}{c_{sr} \cdot l_r \cdot l - l_f \cdot m \cdot v^2}$$

- Delay time constant

$$T_1 = \frac{\Theta_z \cdot v}{c_{sf} \cdot l_f \cdot l + l_r \cdot m \cdot v^2}$$

The vehicle side-slip angle compensation for steady-state driving conditions consequently requires a speed-dependent steering ratio between front and rear axles.

Fig. 2.4-30 gives a qualitative representation of the derived "self-steering characteristic" for steady-state driving conditions (only positive vehicle side-slip angles are compensated).

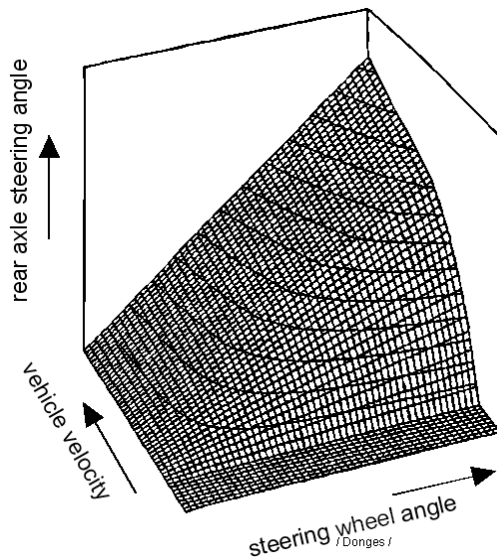


Fig. 2.4-30: Self-steering characteristic of rear-axle auxiliary steering for attitude-angle compensation (stationary) /11/

The vehicle side-slip angle compensation for transient driving conditions also requires a certain time response of its control.

In real vehicles, the influence of the nonlinearity of the tire characteristics, the wheel-suspension kinematics and so on, must be considered. Instead of an analytical approach, a corresponding self-steering map would have to be experimentally determined.

Fig. 2.4-31 shows the effect of vehicle side-slip angle compensation on the transient steering behavior of an automobile on the basis of simulation results of sinusoidal steering.

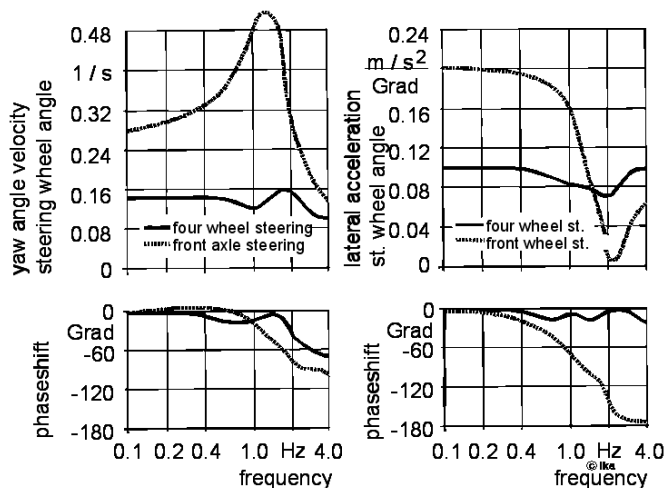


Fig. 2.4-31: Frequency curves of a vehicle with/without vehicle side-slip angle compensation by means of rear-axle auxiliary steering /4/

Driving speed is $v = 150$ km/h. The amplitude of the steering-angle was set in order to achieve a lateral acceleration of $a_y = 4\text{m/s}^2$ for steady-state cornering at $v = 150$ km/h.

In a vehicle with additional rear-axle steering, a larger amplitude of the steering-angle is required, since a lower yaw-amplifying factor (see equation 2.3-30, section 2.3.3.1) results from the unidirectional steering of the rear wheels simply because of the geometrical relations (see equation 2.3-7, equation 2.3-8). The amplitudes of yaw rate and lateral acceleration relative to the steering-angle amplitude are hence lower. This could be compensated by a more direct steering ratio on the front axle.

A vehicle without rear-axle steering shows a distinct resonance peak in the amplitude of the yaw rate in the range of the yaw natural frequency (ca. 1.1 Hz). This points to low yaw damping (due to the high driving speed; see section 2.3.2). The low yaw damping results in after-vibration of the vehicle following steering movements of the driver, which affects driving stability.

In the same vehicle, but with rear-axle steering, the amplitude of the yaw rate is almost independent of the excitation frequency of the steering input. Yaw damping is sufficient enough to adequately damp the yaw oscillation excited by the driver's steering inputs. Yaw excitation is thus less intense in a vehicle with rear-axle steering.

Moreover, the minor phase difference between a steering input and the change of lateral acceleration, i.e. change of course of the vehicle, has a very positive effect on vehicle handling. At a steering frequency of about 1.1 Hz, a value associated with a fast lane-changing maneuver, for example, the change of course and the change of steering-angle in a vehicle without rear-axle auxiliary steering shows a phase shift of about 90° . At the moment when the driver has already turned the steering wheel into the straight-ahead position, the vehicle will just about have reached its maximum lateral acceleration or change of course. The vehicle will change its direction of motion although the driver is no longer steering. This effect is perceived as a "push". In a vehicle with rear-axle auxiliary steering however, the phase shift at this steering frequency amounts to only about 15° .

In addition to the control strategies of the nature described for rear-axle auxiliary steering systems, other control strategies which incorporate the rear-axle steering system in a closed loop for the regulation of desired values of driving dynamics are conceivable. The yaw rate control system in the VW research vehicle IRVW4-Futura /34/ serves as an example. Since these concepts are however of little practical relevance, they will not be dealt with in greater detail.

2.4.4 Influence of Longitudinal Dynamic processes on Lateral Dynamics

The primarily longitudinal dynamic processes

- acceleration
- load changes (releasing the accelerator, declutching)
- braking

usually also lead to lateral dynamic vehicle responses during cornering, which the driver has to compensate by a steering correction.

On roads with sufficient traction, this vehicle response is primarily determined by the dynamic shift of axle-load between front and rear axles, which takes place during acceleration or deceleration, due to a pair of forces consisting of the circumferential forces acting at the wheels and the inertia force acting in the center of gravity of the vehicle and the associated changes in the lateral tire force, Fig. 2.4-32.

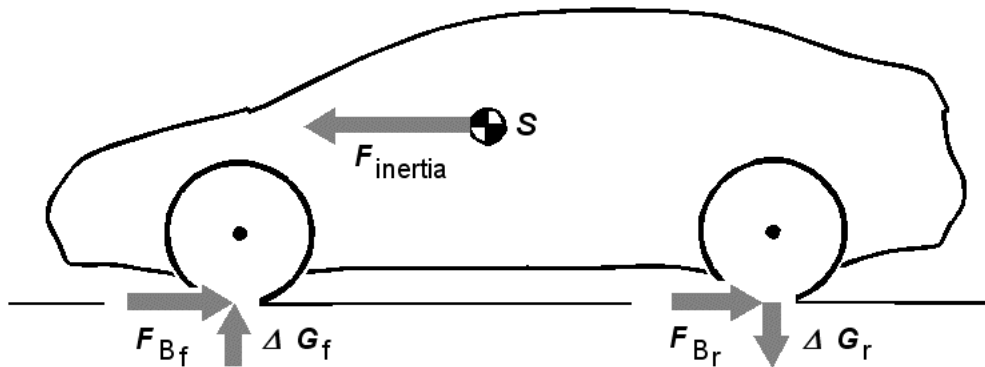


Fig. 2.4-32: Dynamic axle-load transfer during braking

On slippery roads or in the case of very high longitudinal tire forces (high brake power), however, a reduction of the transferable lateral tire forces in the presence of simultaneously acting longitudinal tire forces will have a stronger effect (see section 2.2.5).

Especially during braking, even during straight-ahead driving, a lateral-dynamic vehicle response which has to be controlled by the driver arises when a significant difference in the coefficients of friction is encountered between the left and right lanes (μ -split).

2.4.4.1 Acceleration in Corners

Accelerating leads to a drop of load on the front axle along with a simultaneous increase of load on the rear axle due to a dynamic axle-load transfer. On roads with good traction, both RWD as well as FWD vehicles drift with their front axes towards the outer edge of the curve in the absence of a steering correction, since the resulting axle lateral force on the front axle decreases with the axle load, while the centrifugal force to be supported increases with the driving speed.

FWD vehicles usually require a larger steering correction since the traction forces transferred on the front axle reduce the simultaneously transferrable lateral forces, resulting in the dynamic understeer tendency being additionally intensified.

As a measure for evaluating the vehicle response to accelerating in corners, the yaw rate difference at the point in time Δt is used, which results from the transition from steady state cornering at $R = \text{const.}$ to accelerated cornering, for a constant steering wheel position. Fig. 2.4-33 shows the difference in yaw rate after 1 sec in relation to longitudinal acceleration for various drive concepts.

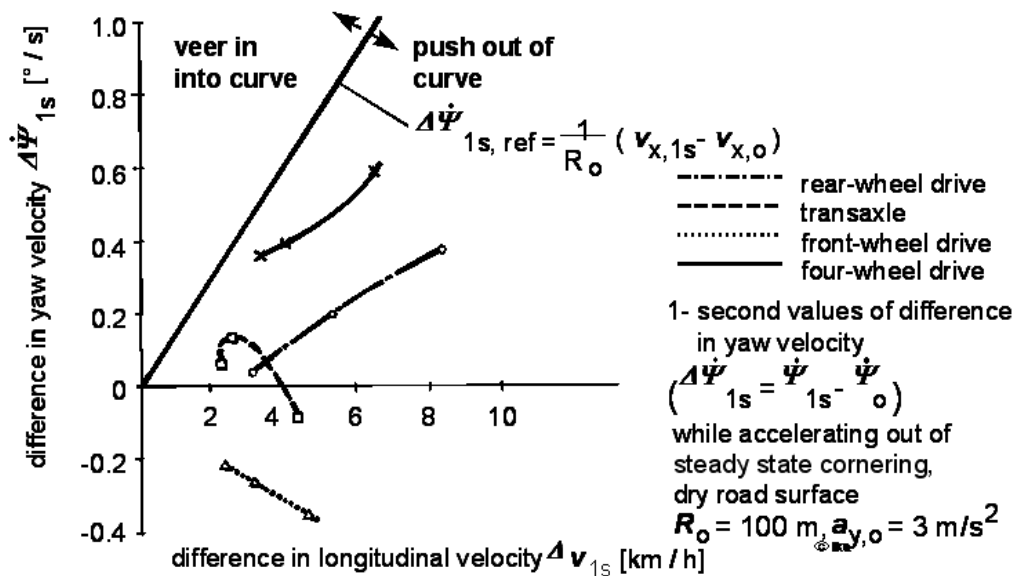


Fig. 2.4-33: Variation of yaw rate for accelerating in corners /37/ on road with good traction

The reference line marks the increase in yaw rate that would result from an increase in driving speed if no deviation from the initial radius takes place during acceleration.

On slippery roads, vehicle reactions are clearly more intense, Fig. 2.4-34. The dynamic oversteer of the investigated RWD vehicle caused by overlapping lateral and longitudinal tire forces results in the vehicle spinning into the initial curve.

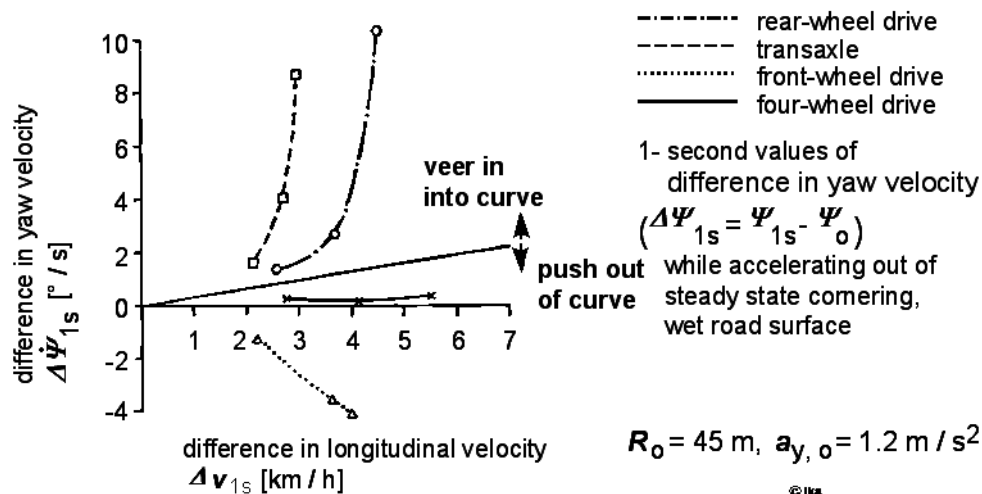


Fig. 2.4-34: Yaw speed variation for accelerating during cornering /37/ on a slippery roadway

The advantages of the distribution of the traction forces between four wheels in the case of AWD become obvious on a slippery road. On a dry road however, the differences are related more to the steady-state steering behavior (minor understeer tendency) than to the drive concept.

2.4.4.2 Load Changes in Cornering

Load-change can be defined as the sudden change in the traction forces caused by abrupt changes in the accelerator-position, during declutching or at the beginning of a gearshift in an automatic transmission.

During cornering, abrupt changes in the circumferential forces on the driven wheels cause a yaw response on the vehicle, which in the absence of a steering correction from the driver would result in the vehicle drifting into the curve. The most violent excitation is caused by the sudden release of the gas pedal, since in this case, the traction forces are not only reduced to zero but are converted into braking forces as a result of the braking torque from the engine.

Since a sudden release of the gas pedal is a natural reflex of a driver entering into a curve too fast or when faced with a progressively sharpening curve, the effects of load-changes during cornering are of paramount importance for active driving safety. A moderate drift of the vehicle into a curve as a result of load-change is considered favorable. It must however not be so severe, that the driver is no longer able to provide the required steering corrections to stabilize the vehicle. The effect of load change results from the superimposition of a number of individual factors, Fig. 2.4-35.

Causes for the effects of load-change Drive concept	Tendency of variation of self-steering response		
	FWD	RWD	AWD
1. Influence of traction			
- Change from drive to circumferential force = 0	↑	↓	-
- Change from circumferential force = 0 to deceleration	↓	↑	-
2. Influence of the shift of wheel-loads on cornering forces	↑	↑	↑
3. Reduction of understeer by reduction of speed	↑	↑	↑
4. Change of a component of the driving-force acting curve inwards	↓	-	↓
5. Kinematic change in the wheel-position due to pitch and roll	Effect depending on suspension design		
6. Elastic change in wheel-position due to changes in wheel circumferential forces	Effect depending on suspension design		
7. Steering torque due to bending angles on drive shaft joints	↑	-	↑
8. Twist due to yaw speed variation	↑	↑	↑
9. Change of lateral-force aligning torque due to change of wheel circumferential forces	↑	↓	-
10. Influence of lateral displacement on the tire contact area	↑	↑	↑

(↑ = oversteer ; ↓ = understeer); AWD with ideal force distribution

Fig. 2.4-35: Causes for the effects of load-changes /6/

forces cause toe-in, then this self-steering effect, which is controlled by the variation in longitudinal tire force, will immediately counter the effect of load-change.

An evaluation of the effect of load change is based on the following criteria: Deviation of the path followed by the center-of-gravity from the initial radius following a load change during steady-state cornering, with fixed steering wheel, Fig. 2.4-37, as well as the associated deviations of the kinematic parameters from the initial values 1 s after the load change (driver's response time).

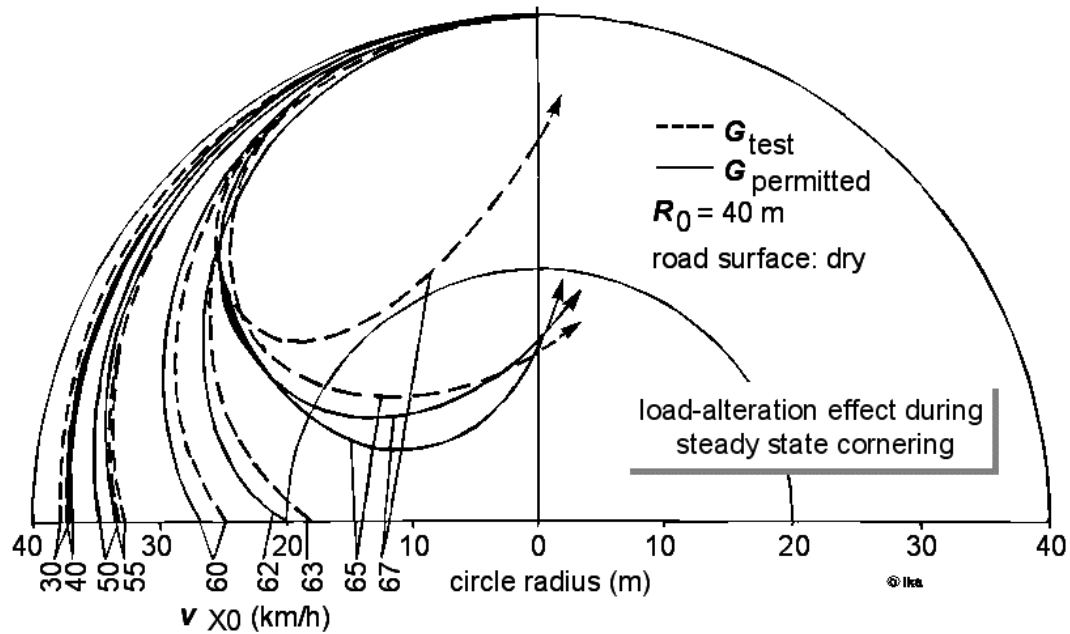


Fig. 2.4-37: Deviation of the center-of-gravity path associated with load alteration /37/

Initial radius and initial lateral acceleration are the parameters varied, Fig. 2.4-38.

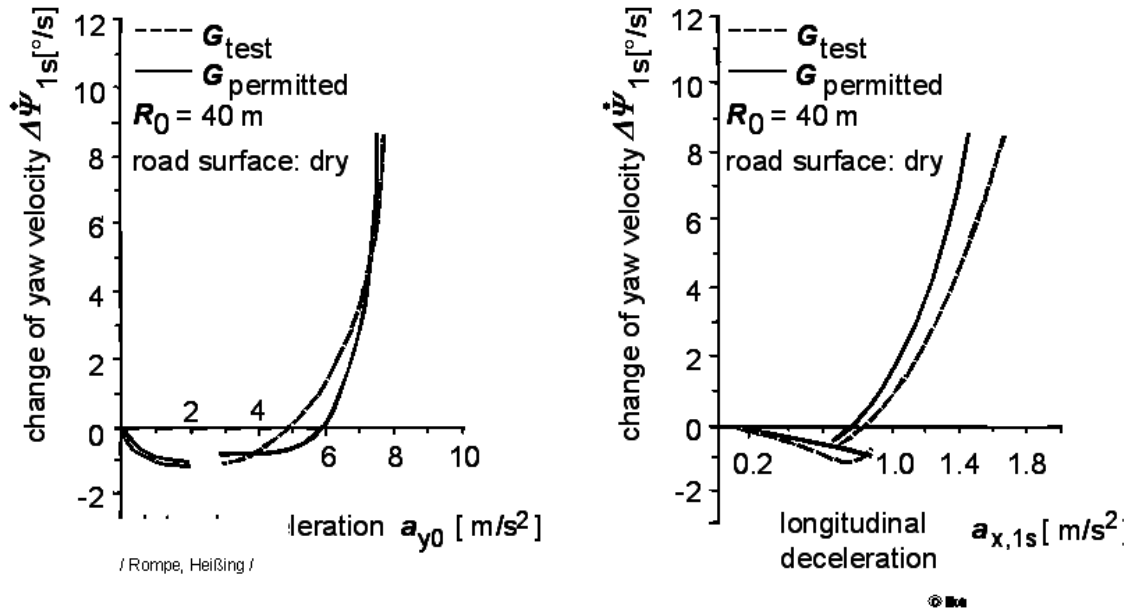


Fig. 2.4-38: Deviation of the yaw rate 1 s after load alteration (FWD vehicle) /37/

2.4.4.3 Braking during Cornering

In the consideration of the response of a vehicle to braking in a curve, one has to differentiate between light to medium deceleration and high deceleration. In case of light to medium deceleration during braking, the consequential effect of load change will be strengthened, i.e. there will be a stronger movement of the vehicle into the curve. As for the load shift, vehicle response is largely determined by the yaw moment induced by oversteer, which is caused by the dynamic shift of axle-load.

In the case of mean to hard deceleration however, the vehicle response will increasingly depend on the influence of the longitudinal tire forces on the simultaneously transferrable lateral tire forces.

Depending on the brake distribution between front and rear axles, two borderline cases of vehicle response must be differentiated. If the rear axle is overbraked during cornering (i.e. the friction coefficient utilized on the rear axle exceeds that of the front axle), then the rear of the vehicle will break away when the friction limit is reached, resulting in the yaw stability of the vehicle being lost. If however, the front axle is overbraked, maneuverability is lost when the friction limit is reached, but the vehicle retains its yaw stability and control over the vehicle may be resumed after releasing the brake.

In order to guarantee yaw stability, an arrangement which provides a safe distance between the curve of the installed brake force distribution and the parabola of ideal brake force distribution for straightline braking should be selected. Brake force controllers which regulate the brake force distribution based on deceleration can also be used. Using an antilock braking system, steering capability can also be retained in the event of hard braking.

As assessment criteria, the values of the motion parameters 1 s after the start of the braking process (driver's response time) for steady state cornering with fixed steering wheel is considered, Fig. 2.4-39.

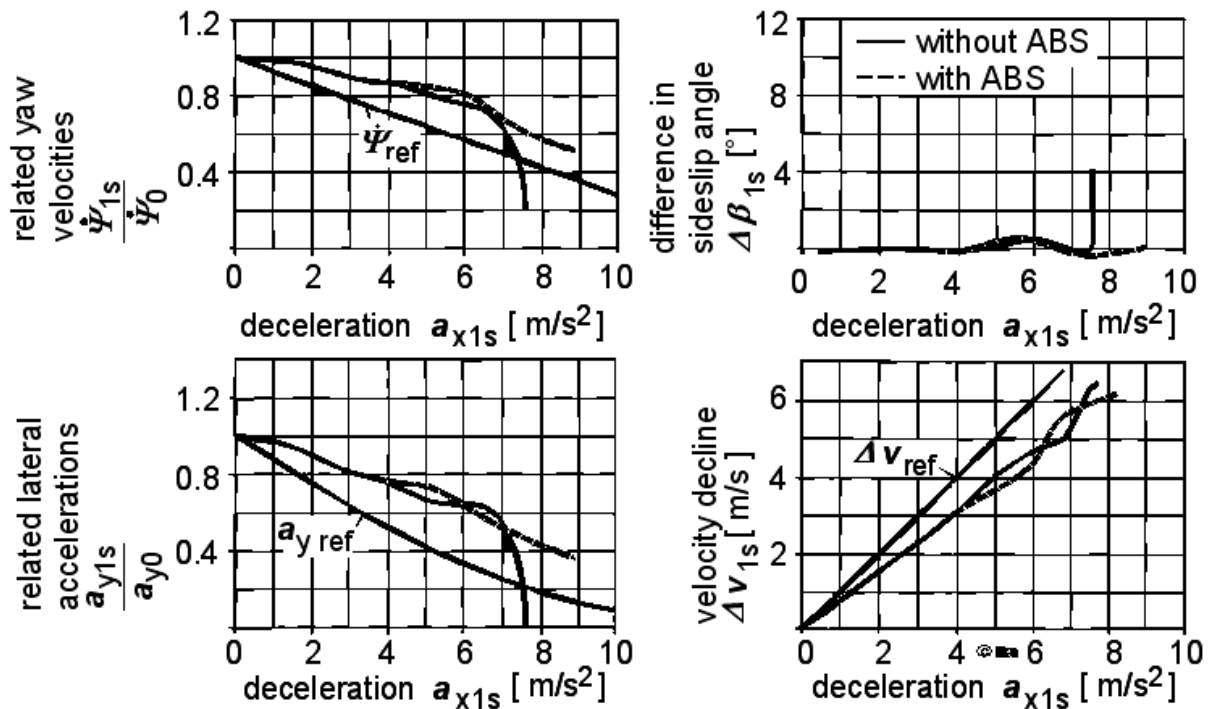


Fig. 2.4-39: Parameters for the description of vehicle response to braking during cornering
/37/

The initial radius, initial lateral acceleration and longitudinal deceleration are parameters which are varied. If these values lie above the reference line with respect to deceleration for exact holding of the initial curve radius, it points to the vehicle drifting into the curve during braking. The limit of maneuverability is characterized by the fact that the lateral acceleration at the beginning of braking drops to zero. The yaw rate in this case drops below the reference line, since the vehicle drifts with its front axle towards the outer edge of the curve.

2.4.4.4 Braking on Roads with Lanes of Differing Coefficients of Friction (μ -split)

Braking on roads with lanes of differing coefficients of friction (e.g. roads with iced edges) results in differing brake forces being induced between right and left sides of the vehicle. This difference in braking force leads to the formation of a yaw moment, which causes the vehicle to spin towards the direction of the lane having a higher coefficient of friction. For this yaw moment to be compensated, a couple composed of a lateral force acting on the front axle and an oppositely directed lateral force acting on the rear axle must be realized, Fig. 2.4-40.

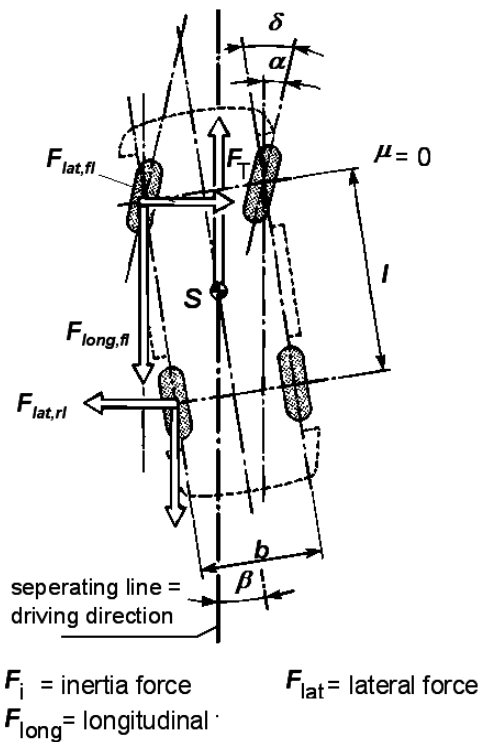


Fig. 2.4-40: Yaw moment balance for braking under μ -split conditions /8/

The slip angle required on the rear axle can only be realized if the vehicle-side-slip angle β is oriented towards the direction of travel during deceleration. On the front axle, a steering angle oriented towards the lane with the lower coefficient of friction is required. Braking stability is improved if the elastokinematics of the wheel suspension are arranged in such a way that the braking force produces a toe-in on the front wheel running on the surface with a higher coefficient of friction, Fig. 2.4-41.

improvement of braking stability under μ -split-circumstances

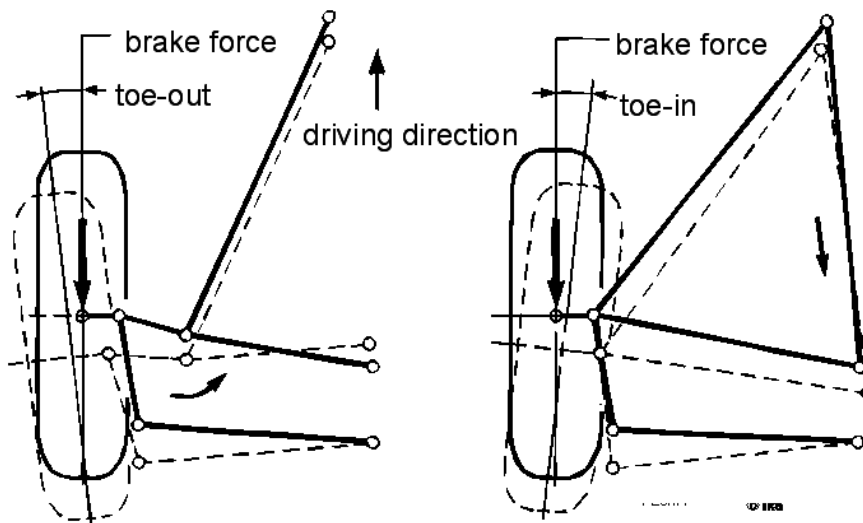


Fig. 2.4-41: Elastokinematic layout of front-wheel suspension for the improvement of braking stability under μ -split-conditions /28/ (right)

Immediately at the beginning of braking, even before the driver's reaction time has lapsed, countersteer is initiated. A yaw moment is already built up which counteracts the yaw rotation caused by the difference in braking forces. However, while tuning the suspension, it should be kept in mind that such a layout assists the vehicle in drifting into the curve.

Another approach to make vehicle handling during braking on μ -split surfaces easier to control by the driver, is to equip vehicles with an antilock braking system (ABS). If the ABS-controlled wheel running on a high-friction surface is initially underbraked, the buildup of the yaw moment caused by the difference in brake force is delayed, allowing for a timely countersteering intervention from the driver. The driving condition is determined by the analysis of the angular acceleration of the wheel during braking. An additional lateral acceleration sensor prevents a response to cornering at high lateral acceleration.

Similar to braking in corners, the deviations of the motion parameters at a certain point in time after the start of braking ($\Delta t = 0.5\text{s}$ or $\Delta t = 1.0\text{s}$) are used as assessment criteria for braking on μ -split surfaces, with the initial driving speed and braking deceleration being used as parameters.

Contents

2	Lateral Dynamics (Driving Stability)	98
2.5	Steering	98
2.5.1	Demands on Steering Systems	99
2.5.1.1	Driver related Demands	99
2.5.1.2	Vehicle-related Demands	101
2.5.2	Characteristic Values for Front Wheel Alignment	102
2.5.3	Steering Kinematics	112
2.5.3.1	Static Steering Layout	112
2.5.3.2	Dynamic Layout of Steering Elements	114
2.5.4	Steering Angle - Steering Torque Diagram	115
2.5.5	Steering Elasticity	116
2.5.6	Components of the Steering System	117
2.5.6.1	Steering Gearbox without Assistance	118
2.5.6.2	Power Steering	120
2.6	Suspensions	124
2.6.1	Basic Suspension Designs	124
2.6.2	Kinematics of Suspensions	126
2.6.2.1	Roll Center	130
2.6.2.2	Brake-Dive and Acceleration-Squat Compensation (Anti-Dive/Anti-Squat)	133
2.6.3	Elastokinematics	135
2.6.4	Requirements to be met by the Suspension	137
2.6.4.1	Handling	138
2.6.4.2	Comfort	140
2.6.5	Rigid Axles	141
2.6.6	Semi-Rigid Axles	145
2.6.7	Independent Suspension	150
2.6.7.1	Swing Axles	150
2.6.7.2	Trailing-Link Suspension	152

2.6.7.3	Semitrailing-Link Suspension	153
2.6.7.4	Double-Wishbone Suspension	156
2.6.7.5	Strut Suspensions.....	159
2.6.7.6	Multilink Wheel Suspensions	165

2 Lateral Dynamics (Driving Stability)

2.5 Steering

In the control loop consisting of the driver and the vehicle, the steering wheel angle forms a control variable, which has to be adjusted by the driver in such a way that a deviation from the desired course remains negligible. However, a clear functional relationship does not exist between the rotation of the steering wheel and the change of direction necessary for a correction of course. This can be attributed, for example, to elasticities in the components of the steering system and the resulting lateral accelerations. The relationship between steering operation and change of driving direction is represented in Fig. 2.5-1.

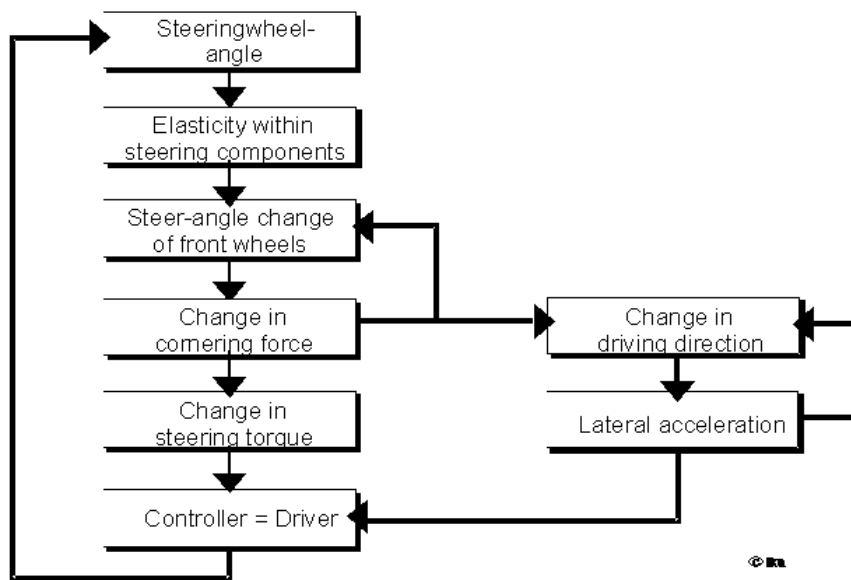


Fig. 2.5-1: Relation between steering actuation and change of driving direction

In order to drive a vehicle, the driver has to constantly analyze the relation between a turn of the steering wheel and the consequential change of driving direction. Apart from visual information (deviation from the desired course), the driver also receives a lot of further feedback, which includes lateral acceleration transmitted over the seat and the steering torque passed on through the steering wheel.

The function of the steering system is not only to convert the steering wheel angle over a clear arrangement into a steering angle at the wheels, but also to provide the driver with feedback about the status of motion of the vehicle.

In the previous sections (chapter 2.2 – 2.4), that part of the control system which dealt with the relation between wheel angle modification and change of driving direction was presented. Here, the demand on the structural component which defines the relation between the steering wheel angle and the steering angle at the wheels will be dealt with.

2.5.1 Demands on Steering Systems

Since humans are integrated into the overall driver – vehicle system via the steering system, the demands on this component are defined by the characteristics of humans and those of the vehicle as shown in Fig. 2.5- 2.

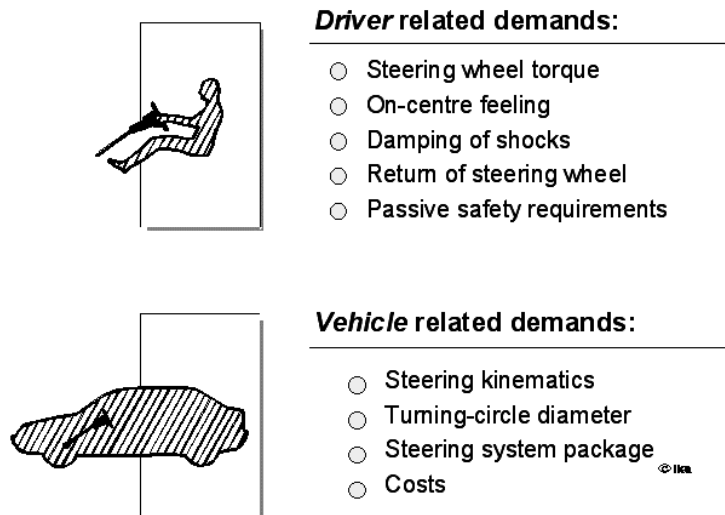


Fig. 2.5- 2: Demands on the steering system

2.5.1.1 Driver related Demands

- Hand Force

The steering moment necessary to turn the steered wheels depends considerably on the driving velocity, Fig. 2.5-3.

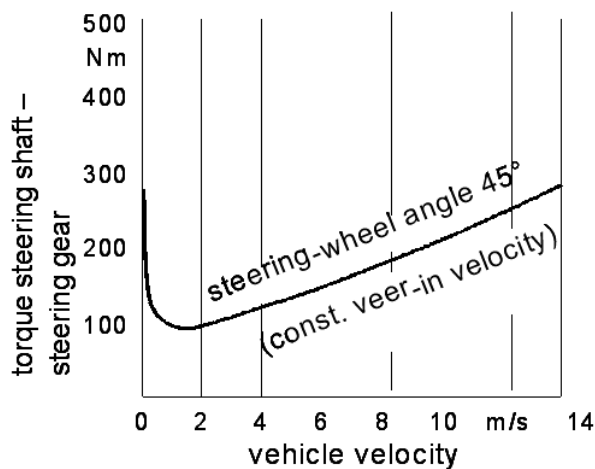


Fig. 2.5-3: Steering resistance as a function of the driving speed (passenger car) /13/

It must be guaranteed that the driver can apply the necessary steering torque in all conditions. The torque necessary for the steering movement is reduced to values which are convenient for the driver over a gear ratio between steering wheel movement and the rotation of the front wheels, Fig. 2.5-4. However, a large steering ratio, not only increases the steering wheel travel, but also the physical strain of the driver.

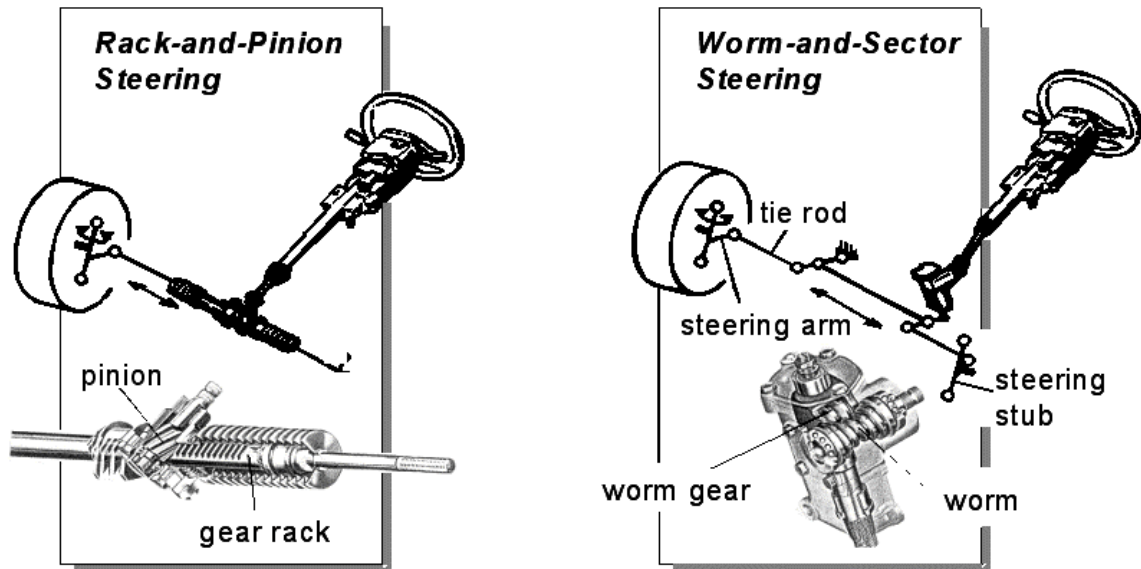


Fig. 2.5-4: Rack and pinion steering, worm and worm-wheel steering

- Sensitivity

The term 'sensitivity' defines the demand for a direct and clearly defined conversion of a turn of the steering wheel into a steering movement of the wheels along with the feedback of forces acting on the wheels. These demands, in the extreme case, prohibit any play in the steering system and cause small elasticities between steering wheel and steering movement of the wheels, as well as small frictional forces in the joints of the steering system.

- Shock Absorption

If an impact affecting the wheels is transmitted undamped to the steering wheel, a steering movement occurs before the driver is able to counterbalance the occurring forces. This implies, that in the interest of a satisfactory steering performance (comfort and safety), high frequency disturbances in the steering system should be damped or even compensated.

- Automatic return of the Steering Wheel

The steering system should remain in the straight-ahead position without the driver's intervention and automatically return to its neutral position after a steering deflection.

- Passive Safety

In the event of an accident, it has to be ensured that the components of the steering system do not penetrate into the passenger compartment and that the steering wheel can sustain an impact of the driver (secondary collision), for example over an impact plate, a deformation element or a slewing device.

2.5.1.2 Vehicle-related Demands

- Steering Kinematics

The steering linkages are placed between the steering gearbox and the steered wheels. The design of these linkages determines the relationship between a turn of the steering wheel and a wheel deflection (fig. 2.5-4). The important boundary conditions in the definition of the kinematics of the linkages are:

- Compression at the wheels or spring actions should not produce any steering reactions (condition for high straight-running stability).
- Slip-free rolling of the tires while cornering with large steering angles (favorable for maneuverability of the vehicle during parking).
- Small toe-in variations with small steering angles (favorable for the build-up of the tire lateral forces for normal cornering).

Width of the vehicle

The necessary width which a vehicle requires during cornering is described by the width of a circular ring. Regulations concerning the width requirement of vehicles are specified by law (StVZO § 32).

- Space requirement of the Steering System

The arrangement of engine-gearbox unit, wheel suspension and steering system is determined on the one hand by the demand for a good economy of space in the front section of the body, and on the other hand, the demand for high impact safety of the vehicle (crash performance) has to be given due consideration when integrating these components into the deformation zone. One criterion for the selection of a certain steering system design is therefore the space requirement in the vehicle and the integration possibility into the fixed package structures.

- Constructional Economy

From the point of view of economy, the structure of a steering element should be as simple as possible.

2.5.2 Characteristic Values for Front Wheel Alignment

With steering movements, the wheels swivel around one wheel-fixed axis of rotation, which is called the 'steering axis' in the following. The position of the steering axis relative to the vehicle body or the road surface is described by the following characteristic values, Fig. 2.5-5:

- Caster Angle: Angle between steering axis and normal to the road in the vehicle longitudinal plane
- Caster Offset: Distance between the point of intersection of the steering axis and the road surface and the ideal center of tire contact in the vehicle longitudinal plane
- Kingpin Inclination: Angle between steering axis and the normal to the road in the vehicle lateral plane (also called the Steering Axis Inclination)
- Kingpin Offset: Distance between the point of intersection of the steering axis and the road surface and the ideal center of tire contact in the vehicle lateral plane (also called Scrub Radius)

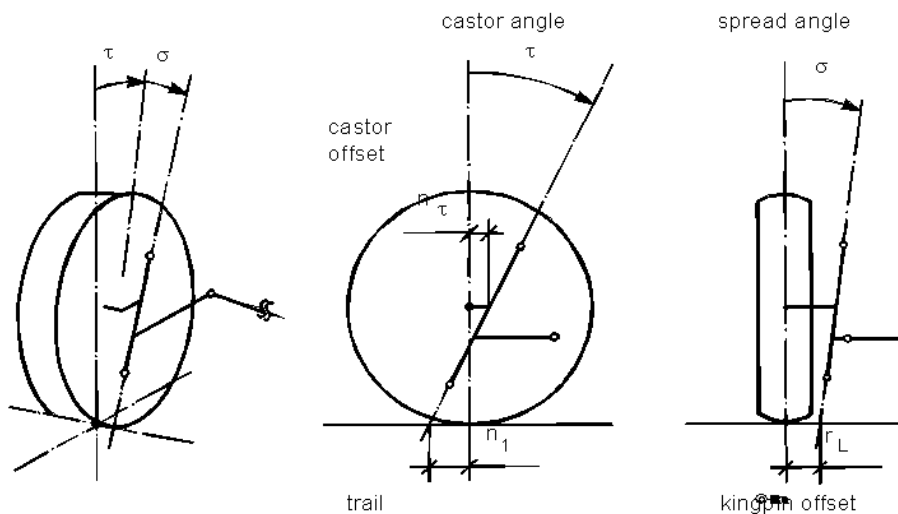


Fig. 2.5-5: Characteristic values for the position of the steering axis

Further characteristics of front wheel alignment for the characterization of the wheel position of the vehicle include the toe-in angle (paragraph 2.4.3.5) and the camber angle (paragraph 2.4.3.5). The position of the steering axis and the wheel alignment in the design position, have a large influence on the characteristics of a steering system. In particular, in order to achieve the driver-specific demands presented in the previous paragraphs, there is a special configuration necessary.

The steering axis is represented by a kingpin only in the case of a rigid truck front axle, Fig. 2.5-6.

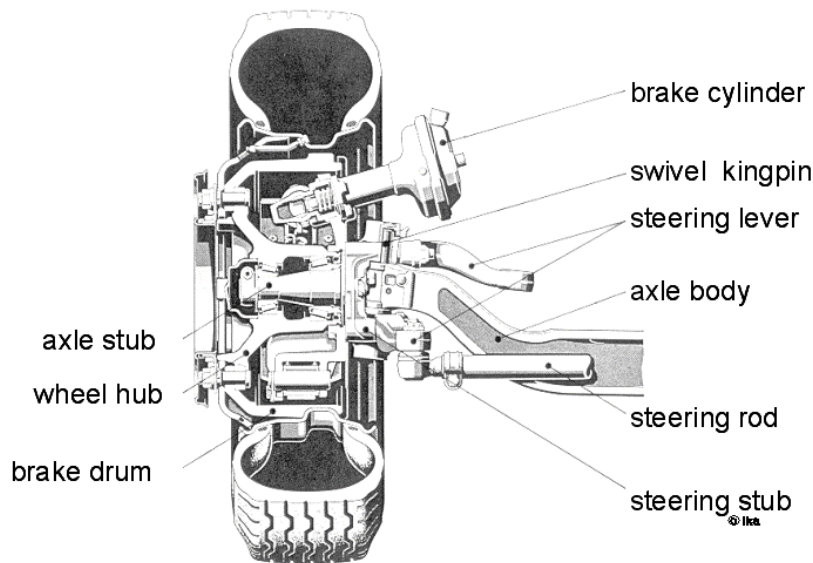


Fig. 2.5-6: Truck front axle (steering stub axle), Mercedes Benz

With modern double wishbone or suspension / shock-absorber strut front axles (McPherson axle) the steering axis passes through the ball-and-socket joint, which connects the wheel carrier to the wishbones, or passes through the upper body-side journal bearing of the suspension / shock-absorber strut, Fig. 2.5-7 (right).

The complete resolution of the axis of rotation fixed in space is shown in Fig. 2.5-7 (left). With this four-link wheel suspension, the line connecting the instantaneous centers of the upper and lower double wishbones represents the instantaneous steering axis. By an appropriate arrangement of the ball and socket joint, this virtual steering axis can be brought in close proximity to the wheel center. This design allows for a significantly shorter, so-called disturbing force lever arm. The disturbing force lever arm represents a decisive measure for the disturbing influences on the steering element as a result of longitudinal forces.

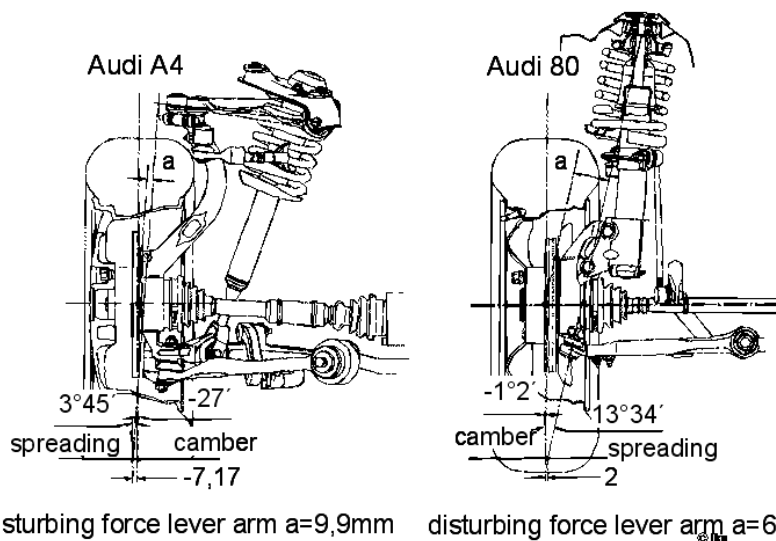
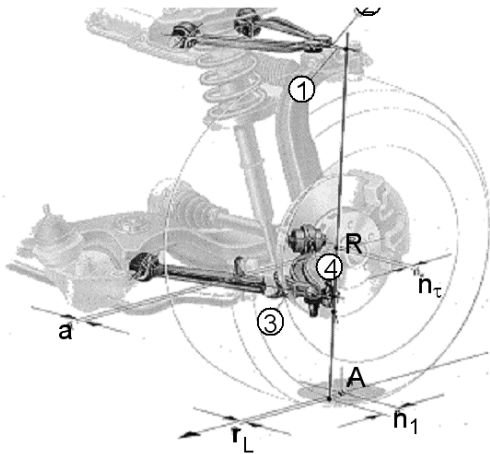


Fig. 2.5-7: Position of the steering axle of four-link wheel suspension and McPherson front axle

Fig. 2.5-8 gives a spatial impression of the displacement of the axis of rotation during steering. By the coupled movement of the two double joints, the motion of the virtual steering axis generates a surface curved to the center of the vehicle.

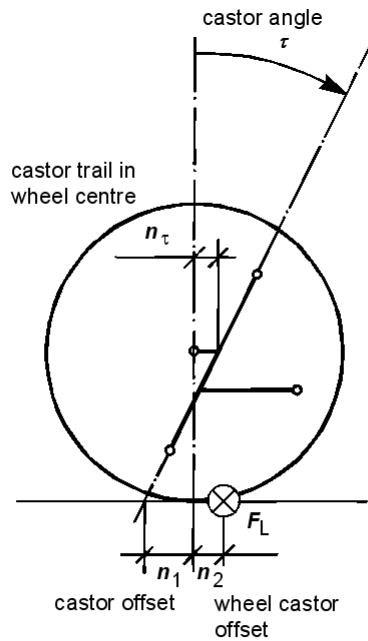


- ①-④ direction of suspension arms
- R wheel centre
- A tyre contact patch

Fig. 2.5-8: Movement of the virtual steering axis while steering, Audi A4

- Caster Angle and Caster Offset

The caster angle and caster trail in the wheel center together determine the resulting caster offset, Fig. 2.5-9.



centrifugal caster: $M = F_L \cdot (n_1 + n_2) \cdot \cos \tau$

Fig. 2.5-9: Wheel caster angle, caster trail in the wheel center, constructional caster offset, tire caster and lateral force.

This constructional offset n_1 is added to the tire caster n_2 (paragraph 2.2.4.1). Lateral forces in the point of wheel contact produce an aligning torque around the steering axis in combination with the caster. The caster moment

$$M = F_s \cdot (n_1 + n_2) \cdot \cos \tau \quad (2.5-1)$$

stabilizes the straight-line characteristic, since it always opposes a deflection of the wheel from the straight-ahead position. While cornering, the caster moment produces a component of the aligning torque, which causes the steering system to return into the straight-ahead position after releasing the steering wheel automatically.

Since the caster moment depends on the forces transferred between tires and road, the driver receives feedback about the traction conditions between tire and road based on the steering torque perceived at the steering wheel, which results from the caster moment.

For the determination of the caster offset, a combination of caster angle and caster trail in wheel center is selected. As a consequence, one has the possibility of arranging the ball-and-socket joints or the support bearing (shock-absorber strut) of the kingpin mounting in such a way, that on the one hand a certain caster offset results, and that on the other hand the clamping friction in the suspension system is small. Additionally, the fact that a positive caster angle causes wheel camber variations, which reduce the understeering tendency of a vehicle during steering has to be taken into consideration.

Caster angle and caster offset are represented as a function of the steering angle in Fig. 2.5-10 for the two exemplary axles shown in Fig. 2.5-7.

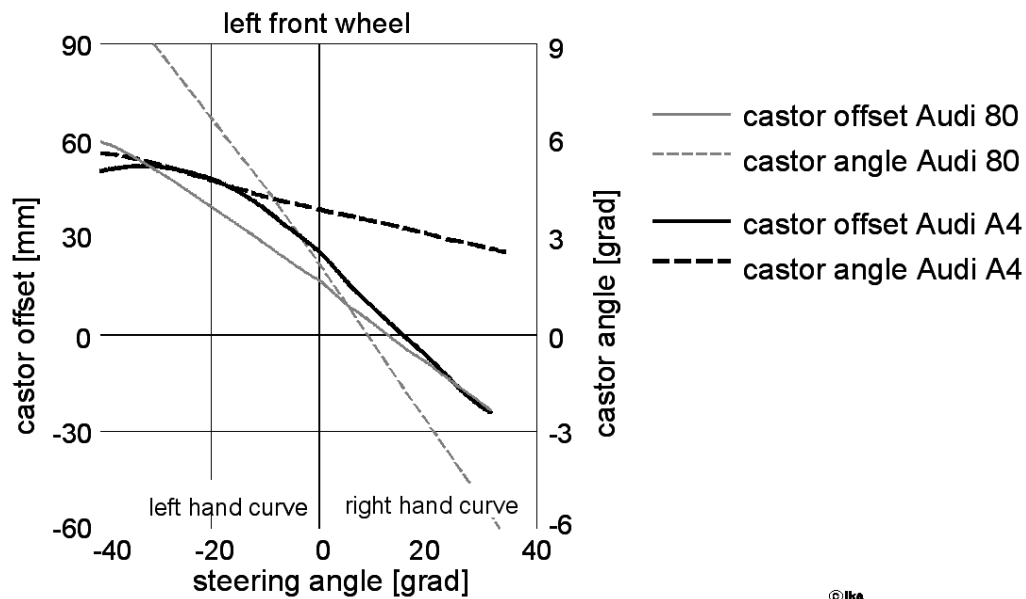


Fig. 2.5-10: Caster angle and caster offset in relation to the steering angle for a four-link wheel suspension and a McPherson axle

In order to avoid a drifting-in effect at the extreme positions of the steering system, the appropriate design of the caster change with the steering angle has to ensure that the sum of inner and outer caster values remains positive, Fig. 2.5-11.

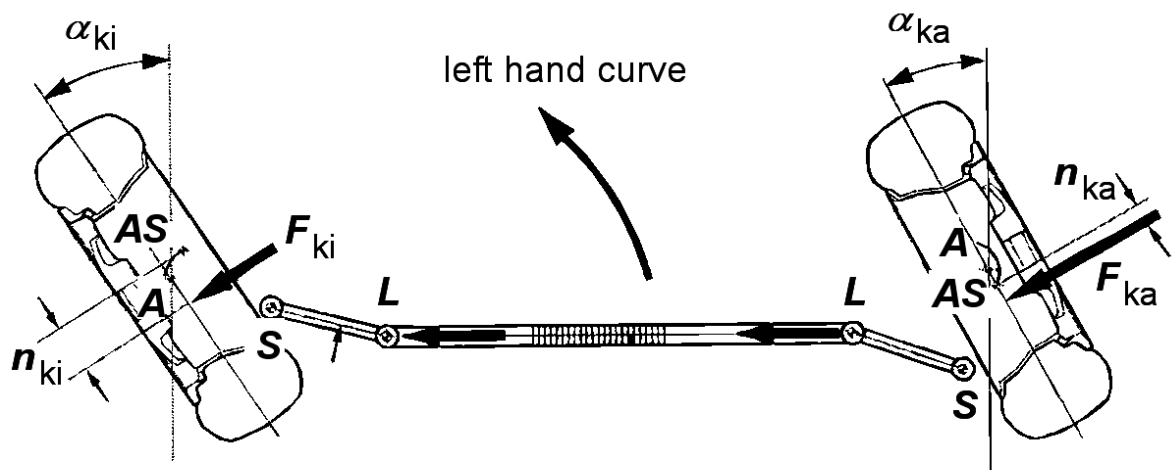


Fig. 2.5- 11: Steering system alignment resulting from the lateral forces

- Kingpin Inclination and Disturbing Force Lever Arm

It is rather difficult to constructionally arrange the steering axis in such a way that the circumferential tire forces do not cause reaction torques in the steering system. The required space for ball-and-socket joints in the rim disc, is needed for the arrangement of the brake system. In case of suspension and shock-absorber strut axles, such a construction cannot be realised based on its constructional principle.

The rolling-resistance forces and the driving forces in front wheel driven axles, act on the wheel carrier at the wheel center line. The resulting reaction torques in the steering system depend on the magnitude of the disturbing force lever arm “a”, Fig. 2.5-12.

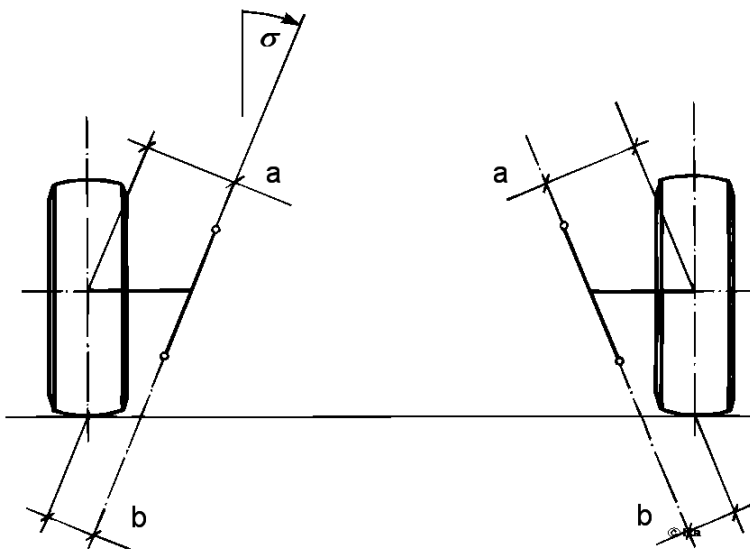


Fig. 2.5-12: Disturbing force lever arms of the longitudinal tire forces in the steering system

During straight-ahead driving (no difference in tire compression, no lateral offset of the tire contact patch) these reaction torques at the right and left wheel are compensated, since the rolling-resistance forces differ insignificantly and the driving torques are almost identical due to the differential conditions.

Contrary to rolling-resistance and drive forces, the braking forces acting on the wheel carrier at the point of wheel contact (external brakes fastened at the wheel carrier) may differ significantly for right and left wheel (μ -split).

In order to reduce the disturbing force lever arm “b” of the braking forces, the steering axis is inclined at a kingpin inclination “ σ ” in the vehicle lateral plane, Fig. 2.5-12. This way, the moment of inertia of the parts of the wheel suspension displaced during steering around the steering axis is smaller, and the tendency of the steering system to flutter is lowered.

The disturbing force lever arm “b” is directly proportional to the scrub-radius (kingpin offset) r_L :

$$b = r_L \cdot \cos \sigma \quad (2.5-2)$$

The inclination of the steering axis at the kingpin angle σ results in two further effects:

- Variation of the Self-Steering Response: With steering movements, wheel camber modifications takes place, which increase the understeer tendency of the vehicle (section 2.4.3.5).
- Weight-induced Self-Alignment: In combination with the lever arm "a", the vertical force F_N produces a weight-induced self-alignment of the steering at the point of wheel contact, which is essential for the automatic return of the steering wheel to the neutral position as well as to avoid the steering from turning during slow travel, since, in this case, there are no lateral forces acting on the tires, Fig. 2.5-13.

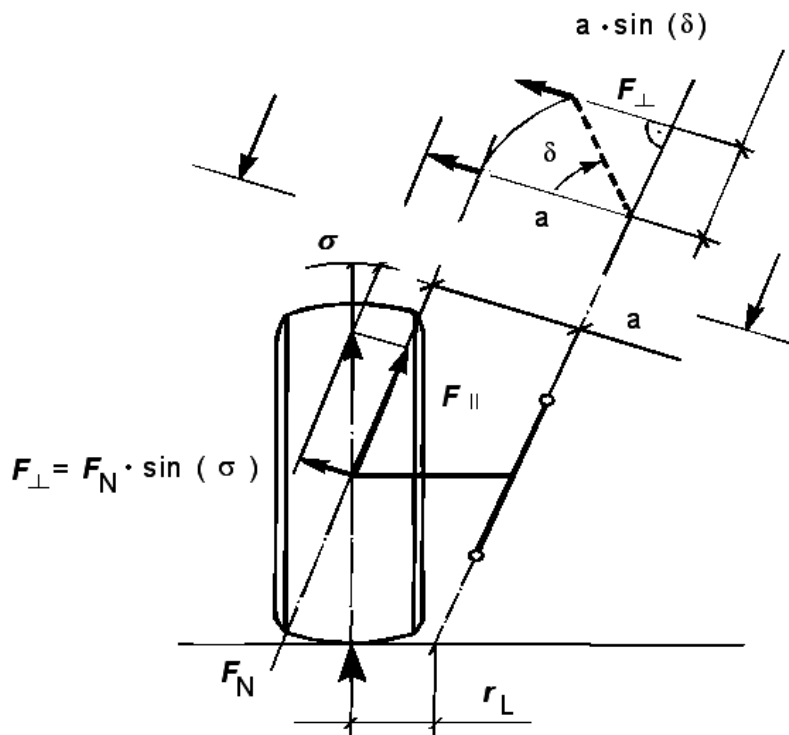


Fig. 2.5-13: Weight-caused self-alignment as a consequence of the spread angle σ

- Kingpin Offset

When the distance between the point of intersection of the steering axis with the road and the center of tire contact measured along the surface of the road is large, the wheel would roll approximately along a circular arc around the point of intersection during steering. Therefore, the distance is called steering kingpin offset r_L or the scrub-radius.

As mentioned above, the kingpin offset should be as small as possible in order to reduce reaction torques in the steering system caused by asymmetrical braking forces. In addition, these reaction torques can be used to influence the driving behavior directly.

On the one hand, it is possible to cause the driver to countersteer early by transmitting the steering torque to the steering wheel. On the other hand, by utilising the inherent elasticities of the suspension, steering linkages and steering column, variations in the steering angle can be induced, which act against the yaw moment caused by the asymmetrical braking force, similar to the elasto-kinematic change of toe as described in section 2.4.4.4 for the improvement of the braking stability.

This can be obtained using a negative kingpin offset. The difference in braking force while braking on a road with differing friction coefficients at the two wheels of an axle, produces a reaction torque in the steering system, which causes the wheels to steer in the direction of the less braked wheel and in this way, produces a countersteer in the correct direction in order to compensate the yaw caused by the asymmetrical braking forces.

The variation of the disturbing force lever arm a and the kingpin offset r_L during the process of steering for the four-link wheel suspension and the McPherson axle (Fig. 2.5-7) is represented in Fig.2.5-14.

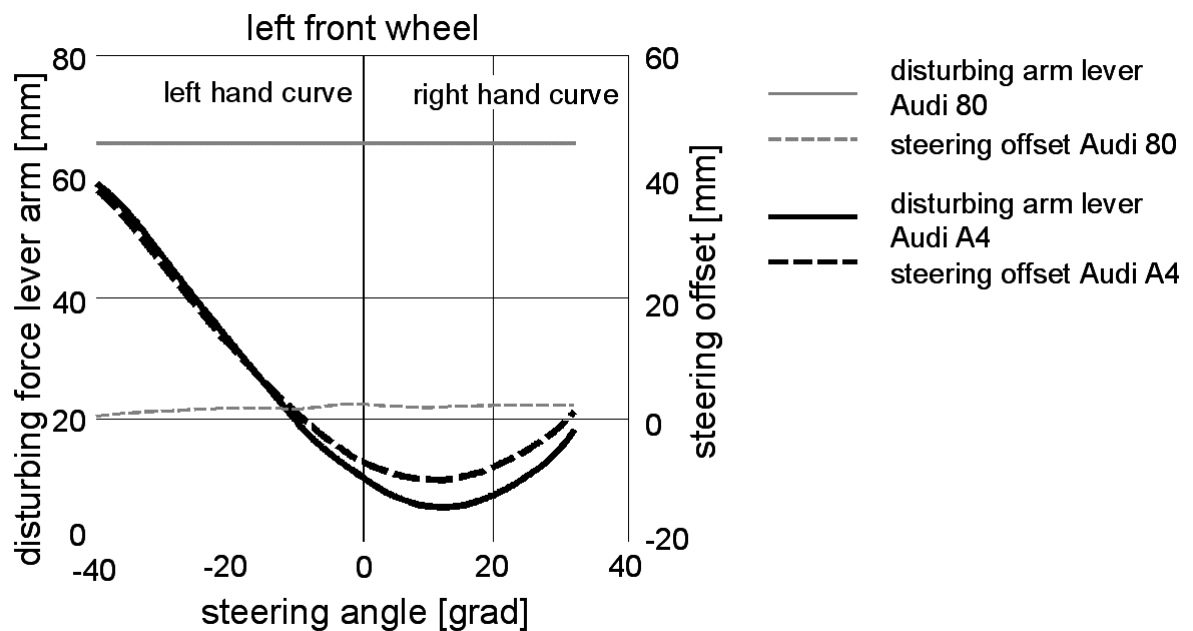


Fig. 2.5-14 : Disturbing force lever arm and kingpin offset in relation to the steering angle for a four-link wheel suspension and a McPherson axle

While the disturbing force lever arm and kingpin offset adopt constructionally determined fixed, invariable values, in case of the conventional McPherson axle, in the four-link wheel

suspension, the respective values tend to increase at the inside wheel and to decrease at the outside wheel.

- Toe-in / Toe-out

The difference between the distance of the rim flange in front of and behind the wheel center line is called toe-in (in case of a negative sign: toe-out) of an axle, Fig. 2.5-15.

Instead of the difference in length, the total toe-in angle can also be indicated: (2.5-4)

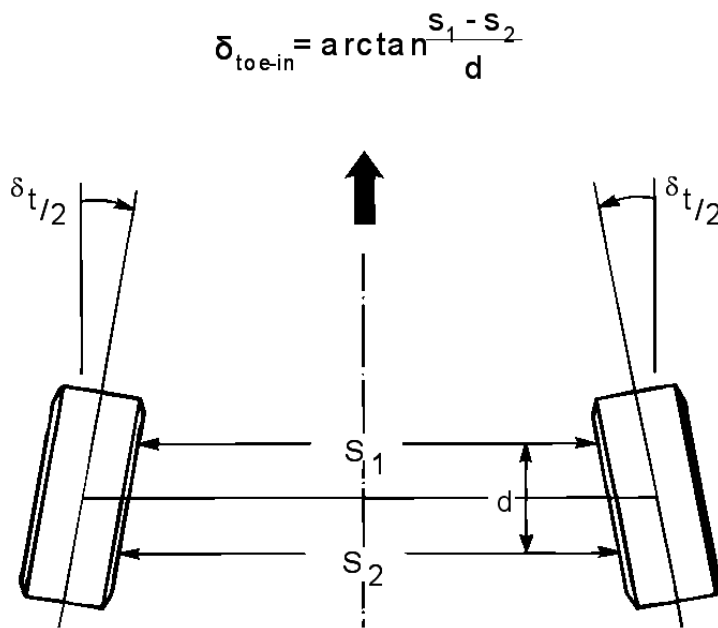


Fig. 2.5-15: Definition of the toe-in

Under the influence of the rolling resistance forces and, in case of driven axles, due to the driving forces, the wheels are pushed into toe-in or toe-out depending on the elasto-kinematics of the wheel suspension. An additional wheel resistance results as a consequence of the toe-in (AE I), and tire wear increases due to continuous tire slip while driving straight ahead.

As a result, a small toe-in is usually set in the design position of the vehicle, which is compensated while traveling straight ahead under normal conditions by the toe-in variation caused by elasticities in the wheel suspension and steering system.

The influence of the kinematic and elasto-kinematic toe-in variation on the handling characteristics was already described in section 2.4.3.5 and 2.4.4.4.

- Wheel Camber Angle

In section 2.4.3.5, the use of static camber angles in the construction position and kinematic camber angle variations in order to influence the handling characteristics was already described.

Camber variations caused by the inclination of the steering axis during steering movements (caster angle and kingpin angle) have also to be considered.

A positive wheel camber angle at the front wheels, intended for the decrease of the kingpin offset in earlier vehicle constructions, cannot be found anymore in modern suspensions. A small kingpin offset is achieved today by a large rim offset, which permits the positioning of the brake disk close to the wheel center plane and, by that, provides a favorable position for the ball-and-socket joints of the steering stub axle mount.

The variation of the wheel camber related to the steering angle for the two exemplary axes from Fig. 2.5-7 is shown in Fig. 2.5-16.

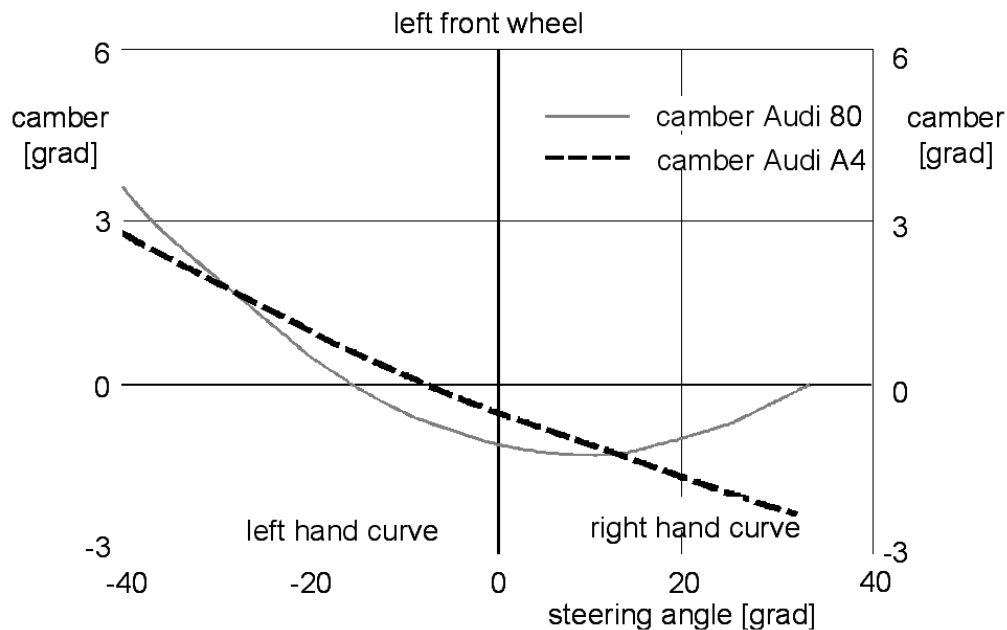


Fig. 2.5-16: Variation of wheel camber while steering for a four-link wheel suspension and a McPherson axle

In order to maintain the lateral force potential while cornering, a positive camber modification takes place on the inside wheel along with a simultaneous negative camber modification on the outside wheel as a function of the steering angle.

2.5.3 Steering Kinematics

The correlation of the steering angles of the wheels to the steering wheel angle and the steering angles of the wheels to each other is described by non-linear relations, since it depends on the instantaneous angle between the components of the steering linkages. This implies that the relationships include angular functions.

As long as the constructional boundary conditions (space, number of joints, steering gear design) permit, these relationships can be designed specifically by the appropriate arrangement and dimensions of the components of the linkage, Fig. 2.5-17.

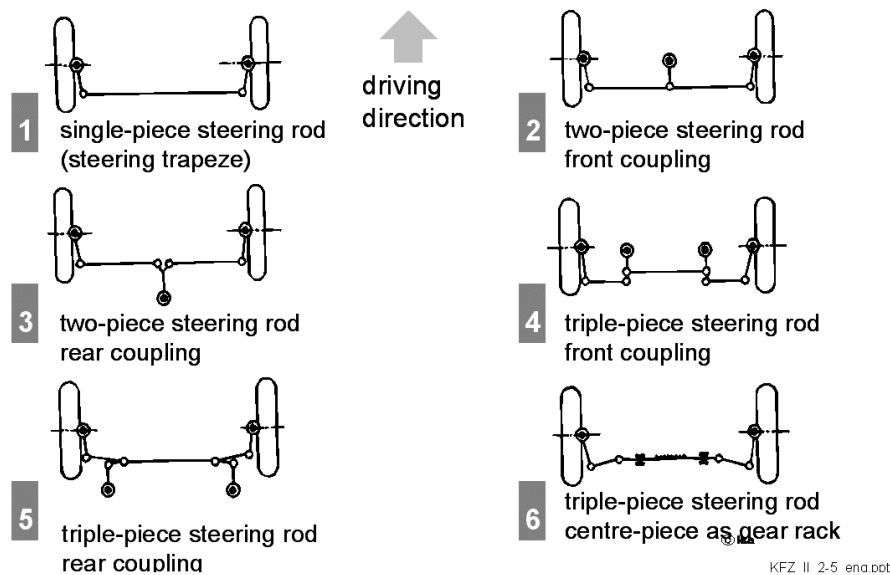


Fig. 2.5-17: Steering linkage configurations /14/

The dimensioning can be made with the consideration of demands on the static (without the influence of the tire lateral force) or dynamic (with the influence of the tire lateral force) steering performance.

2.5.3.1 Static Steering Layout

At low speed cornering, the wheels roll without a tire slip angle and accordingly without any lateral forces, if the projections of the wheel centers intersect at a point, which is the center of the curve (Rudolf Ackermann, 1816), Fig. 2.5-18.

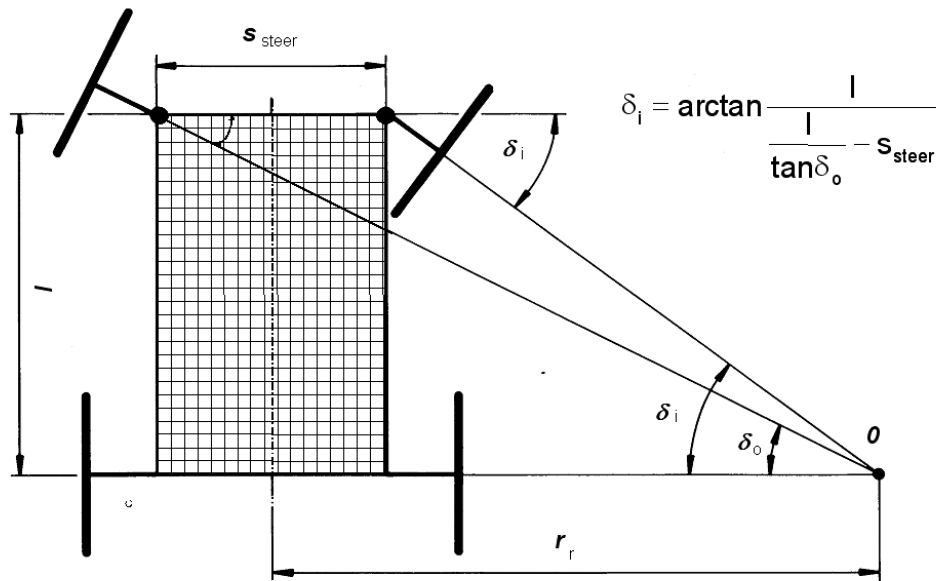


Fig. 2.5-18: Geometrical condition for side slip-free rolling for slow cornering (Ackermann condition)

The geometrical relationships for this rolling of the wheels without forces leads to the following desired functions for the wheel steering angle of inner wheel δ_i as a function of the wheel steering angle at outer wheel

$$\delta_i = \arctan \frac{l}{\frac{l}{\tan \delta_o} - s_{\text{steer}}} \quad (2.5-5)$$

with:

δ_i, δ_o	wheel steering angle
l	wheel base
s_{steer}	kingpin track width
r_r	course radius of the rear axle

While traveling straight ahead, the wheel planes of the steered wheels are placed parallel to each other in the driving direction. A result of the Ackermann condition is that while cornering, the difference in toe angles between outside (δ_o) and inside wheel (δ_i) reaches values in the range of toe-out.

2.5.3.2 Dynamic Layout of Steering Elements

While cornering with high driving speed, tire slip angles occur at the wheels, which result in the wheel lateral forces which are necessary to support the centrifugal force. The curve center is given by the point of intersection of the normal in the direction of motion of the wheels at their respective centers of wheel contact under these conditions, Fig. 2.5-19.

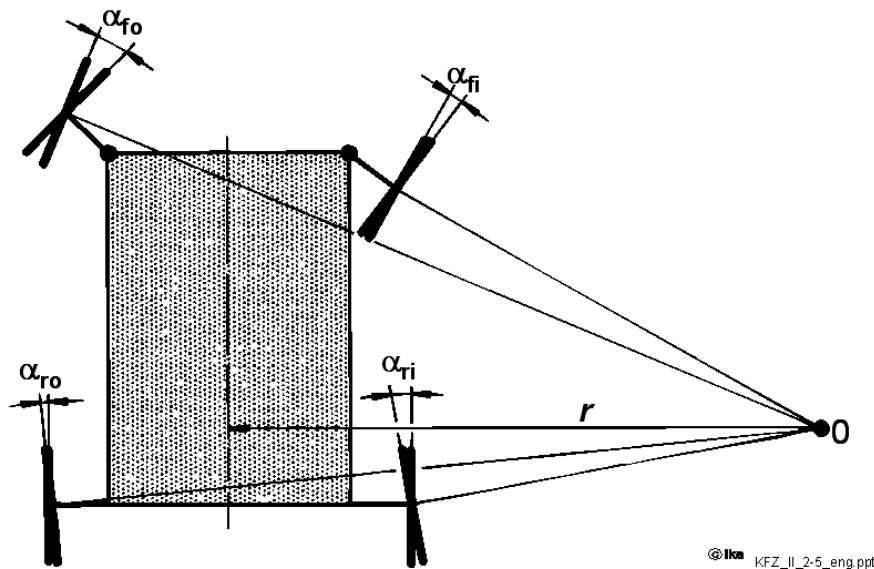


Fig. 2.5-19: Relationship between wheel steering angles, tire slip angles and position of the center of the curve

If the steering kinematics are dimensioned according to the Ackermann condition (Fig. 2.5-18), then the outside tire slip angles are always smaller than the inside tire slip angles.

In order to utilize the same friction coefficient at the outside wheels affected by higher wheel load as compared to the inside wheels, the tire slip angles should be larger at the outside /12/. A real layout of the steering elements therefore requires to diverge from the Ackermann condition such that the wheels are rather steered parallel than with increasing toe-out /29/. A further advantage of this layout is that it can be implemented easier from the point of view of kinematics.

In practice, a parallel steer of the front wheels (real layout) is targeted up to a steering angle of about 20° and only with larger steering angles, an approximation of the Ackermann condition is implemented, Fig. 2.5-20.

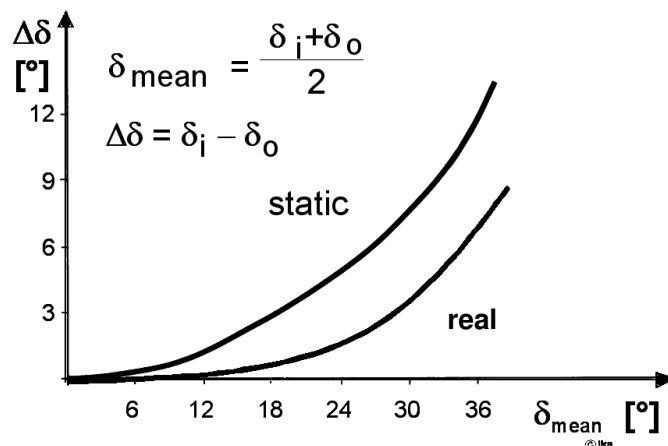


Fig. 2.5-20: Toe-out angle as a function of the mean steering angle for static and real steering element layout

2.5.4 Steering Angle - Steering Torque Diagram

Some important characteristics of a vehicle steering system can be determined by a steering angle – steering torque diagram recorded using a measuring steering wheel.

Fig. 2.5-21 shows the typical characteristic of the steering torque while driving on a sinusoidal course, applied as a function of the steering angle.

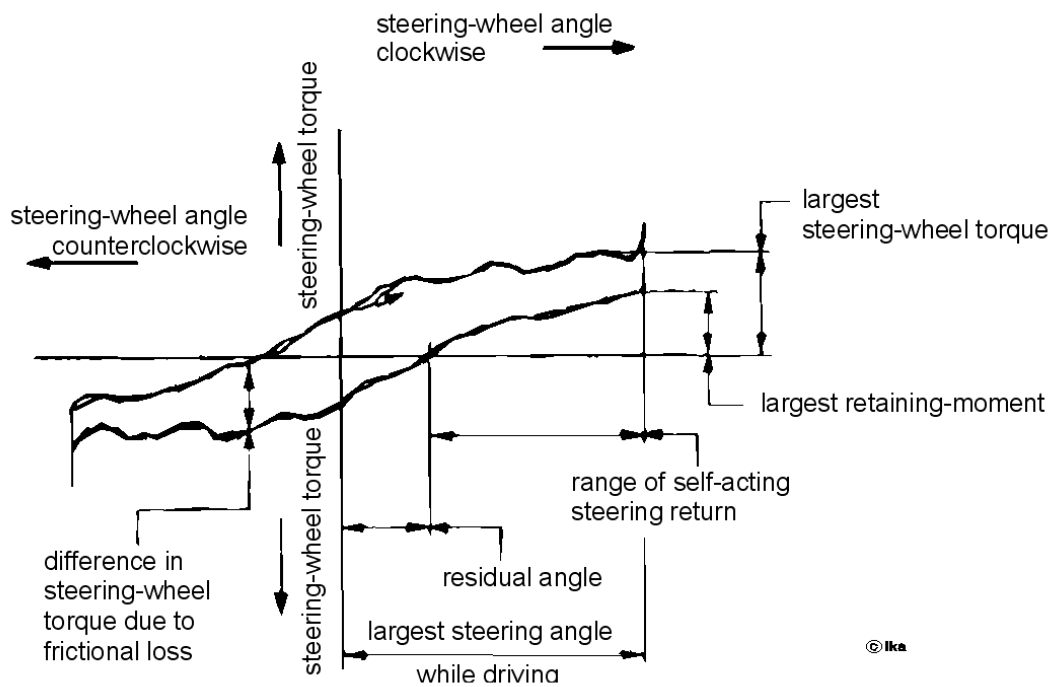


Fig. 2.5-21: Steering angle - steering torque diagram

On the one hand, the diagram gives information about the levels of steering force, while on the other hand, based on the shape of the hysteresis loop, it is possible to estimate the steering “feel” experienced by the driver, which is an important aspect for the assessment of the vehicle’s straight-running properties.

The driver evaluates the steering system as precise, if the steering moment hysteresis loop is small at the zero point (low friction in the steering system) and the rise of the steering moment from the zero position is clearly noticeable (“center point feeling”). In order to keep the overall steering moment level low at the same time, the further characteristic curve of the steering torque in relation to the steering angle should be degressive /39/.

Particularly for the assessment of the straight-running properties, the steering angle - steering torque diagram can also be recorded at high driving speeds for small steering angle amplitudes /10/.

2.5.5 Steering Elasticity

As a consequence of elasticities in the shock-absorbing and noise-insulating rubber bushings of the suspension as well as the component elasticity of the suspension and steering system, an angular loss (play) appears between the rotation of the steering wheel and the resulting wheel angle, whose value depends on the transmitted steering torque. The torsional elasticity of the steering system reduced to the steering column is called steering elasticity. Due to the steering elasticity, the effective steering transmission ratio perceived by the driver, especially at the center position of the steering wheel, deviates from the purely kinematic steering transmission ratio, which depends only on the geometry of the steering gearbox and the steering linkages /39/.

Fig. 2.5-22 shows the steering transmission ratio as a function of the steering wheel angle, influenced by steering elasticity.

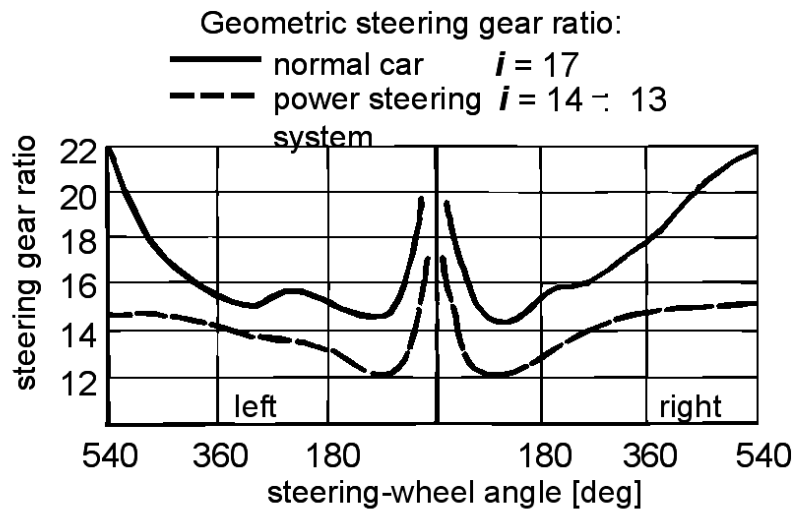


Fig. 2.5-22: Steering transmission ratio influenced by steering torque (measurement on ball rolling plates)

According to Fig. 2.5-22, the geometrical transmission ratio is achieved only for steering wheel angles greater than 30 - 60°. Therefore, with the small steering corrections necessary for straight-ahead driving, a significantly more indirect transmission ratio is effective.

2.5.6 Components of the Steering System

The steering of independently guided front wheels usually consists of the elements specified in Fig. 2.5-23.

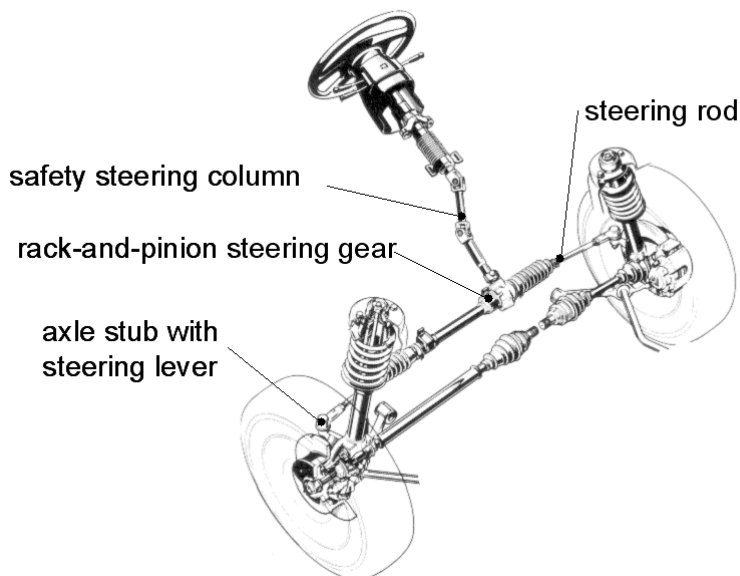


Fig. 2.5-23: Components of the steering system

In the two preceding paragraphs, it was described that small frictional forces and small elasticity in the steering system positively affects the steering feel in straight-ahead driving. However, it should not be ignored that elasticity reduces the sensitivity of the steering system to impacts while driving on unevenness and the presence of a certain amount of self-friction reduces the transfer of vibrations in the steering system to the steering wheel within the range of the wheel natural frequency.

For vibration and noise insulation, often an elastic rubber disc is inserted as a connecting element between steering gearbox and steering column. Steering dampers are not as effective in the suppression of high frequency vibration as in the reduction of impacts and damping of oscillations, which result from the moment of inertia of the steering system reduced to the steering axes and the aligning torque as a result of steering geometry and tire characteristics /29/.

Finally, the only component of the steering that is further dealt with in detail, is the steering gearbox, since a number of the requirements described in this paragraph so far are met by this steering component.

2.5.6.1 Steering Gearbox without Assistance

The torque necessary for steering is reduced to values which can be applied by the driver over the steering gearbox. The steering gearbox has to operate without play and with a low coefficient of friction, in order to fulfil the demands for small physical load on the driver as well as for the sensitivity of the steering system.

Steering gearboxes can be differentiated into rack-and-pinion steering with translatory output and steering gearboxes with rotary output (Fig. 2.5-4).

The tie rods are directly connected to the rack-and-pinion steering by ball-and-socket joints. The fastening takes place either at the front side of the steering rack, Fig. 2.5-24 above, or in the center, Fig. 2.5-24 below, which allows for the use of longer tie rods, resulting in smaller toe variations in case of spring compression.

Steering racks are characterized by a simple construction and a small space requirement. Unfortunately, the design possibilities of the steering kinematics are limited due to the direct fastening of the tie rods, (section 2.5.3). More degrees of freedom are offered by steering gearboxes with rotary output.

Two of the most common steering gearboxes with rotary output are the worm-and-worm wheel steering (Fig. 2.5-25) and the ball-and-nut steering (Fig. 2.5-26).

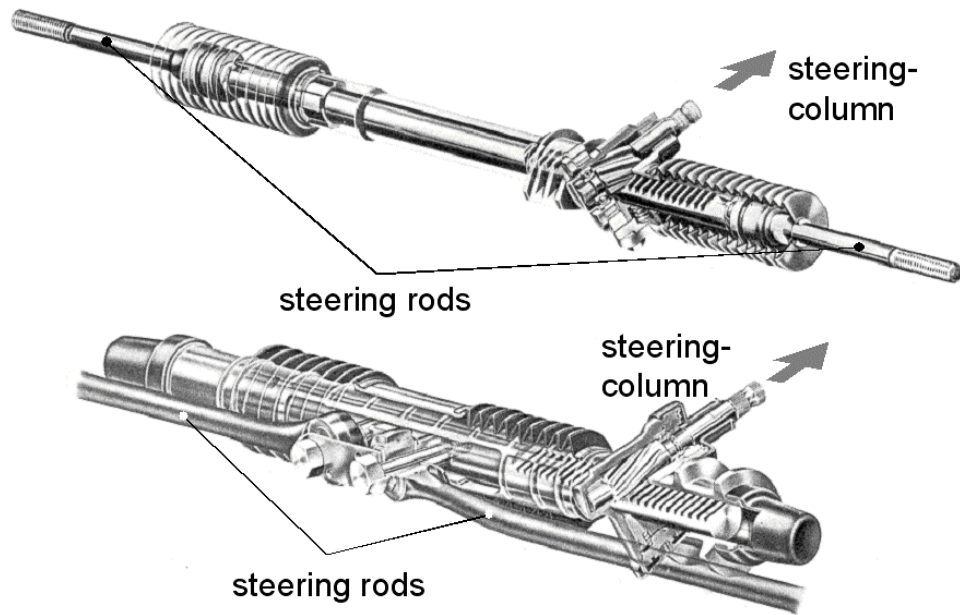


Fig. 2.5-24: Rack-and-pinion steering

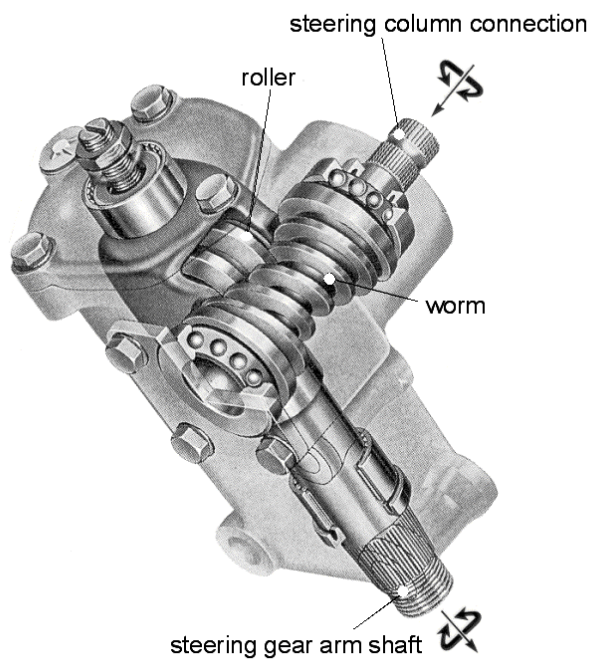


Fig. 2.5-25: Worm-and-worm wheel steering, ZF

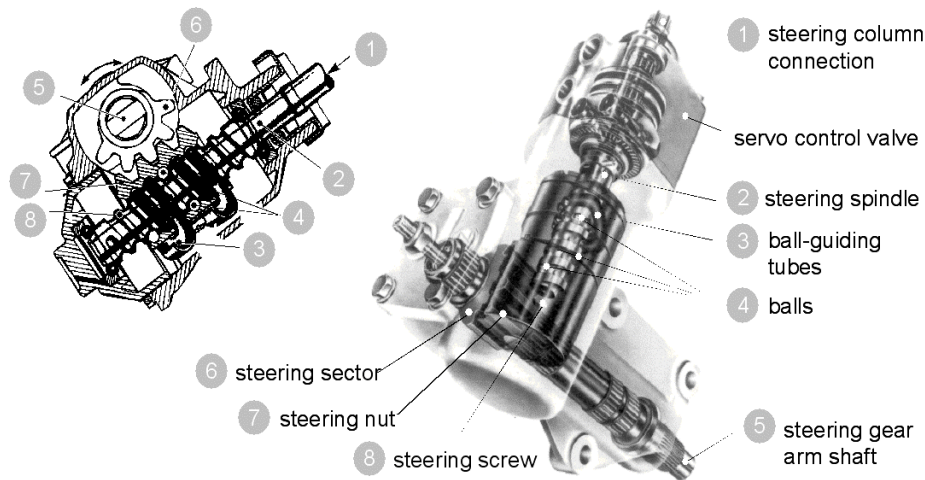


Fig. 2.5-26: Ball-and-nut steering

The worm-and-worm wheel steering consists of a worm gear with the teeth of the worm wheel segments realized as tooth rolls, as a result of which they can roll almost friction-free on the worm.

In the steering gearbox with ball circulation, by turning the steering screw, a steering gear nut which executes only translatory motion is displaced. The steering gear nut meshes with a steering segment, which is located on the output shaft. To decrease friction, the balls rotate in the thread between the steering screw and the steering nut.

2.5.6.2 Power Steering

In order to keep the steering torques in an acceptable range during slow travel, a very indirect steering transmission ratio is necessary for many vehicles, which has an unfavorable influence on the steering behavior at higher driving speeds, since quick steering reactions require large movements of the steering wheel in this case.

The use of power steering enables the configuration of a more direct steering transmission ratio and the reduction of the required steering forces at the same time. The reduction of the physical stress on the driver which is hence realised represents an important contribution for the increase of the active safety. The auxiliary energy necessary for the operation of power steering, is usually produced hydraulically due to the high energy density, by a pump driven by an engine-powered V-belt. Electric-powered servo steering systems are in the development state at present. The functional scheme of a ball-and-nut power steering system is shown in Fig. 2.5-27.

The magnitude of the auxiliary force should be dimensioned in such a way that a proportionality between steering resistance at the wheels and the hand force at the steering wheel is preserved for the operating range (velocities above 3 m/s), since the driver requires feedback of the state of traction between the tires and road. The proportionality factor should be selected in such a way that the road contact is transferred to the driver in a genuine and well perceptible manner, while simultaneously keeping the hand forces required for steering small.

In majority of the cases, the design of the power steering systems represents a compromise between the demand for a high steering assistance while parking and the demand for clear feedback of the steering torques at high driving speeds.

A power steering with speed-dependent steering assistance offers additional degrees of freedom in its design. Here, the proportionality factor of the auxiliary force which is dependent on the steering torque is influenced by an electrically operated solenoid valve in the hydraulic circuit. The control of the solenoid valve is performed by a microprocessor, which receives a driving velocity signal, Fig. 2.5-29.

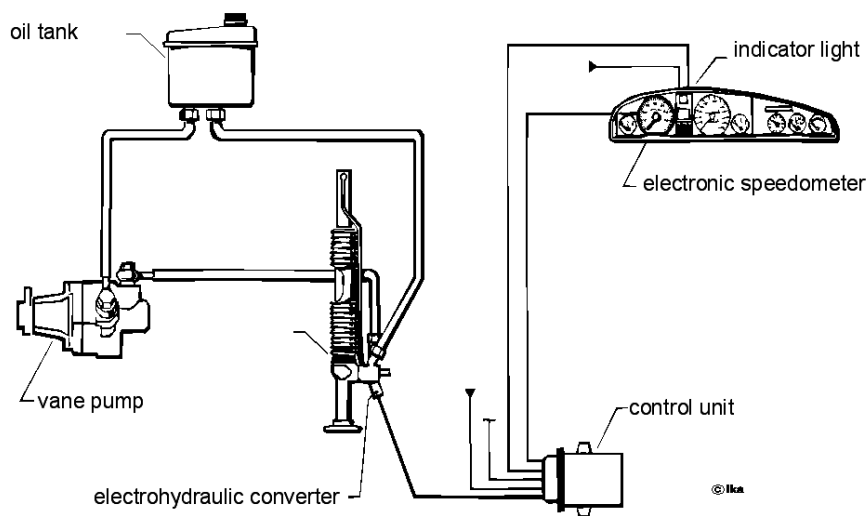


Fig. 2.5-29: Operating principle of the servotronic

In the servotronic, steering assistance decreases with higher driving speed. This dependence enables comfortable parking as well as high speed driving at small steering effort, Fig. 2.5-30.

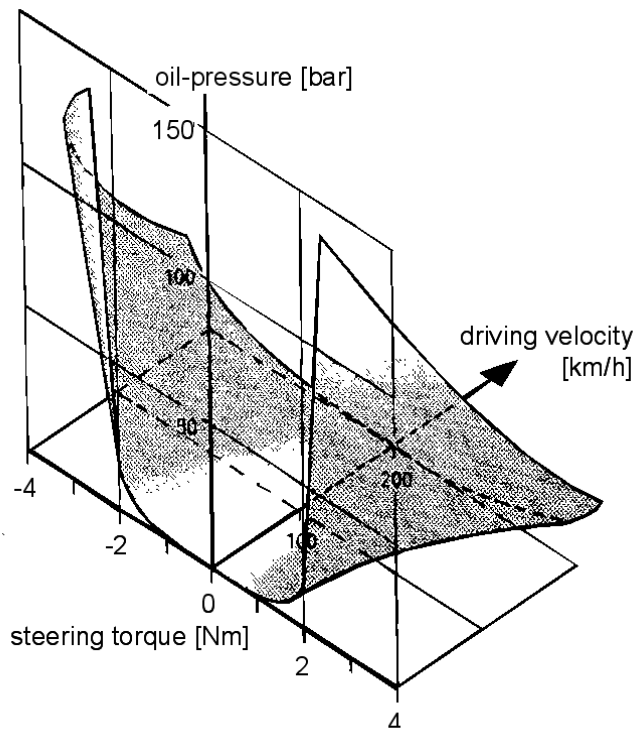


Fig. 2.5-30: Valve characteristic map of the servotronic

The characteristic of the steering torque of the servotronic and the conventional power steering of the predecessor model depending on the lateral acceleration is presented in Fig. 2.5-31. The servotronic features a reduction of the required steering force in comparison to conventional power steering.

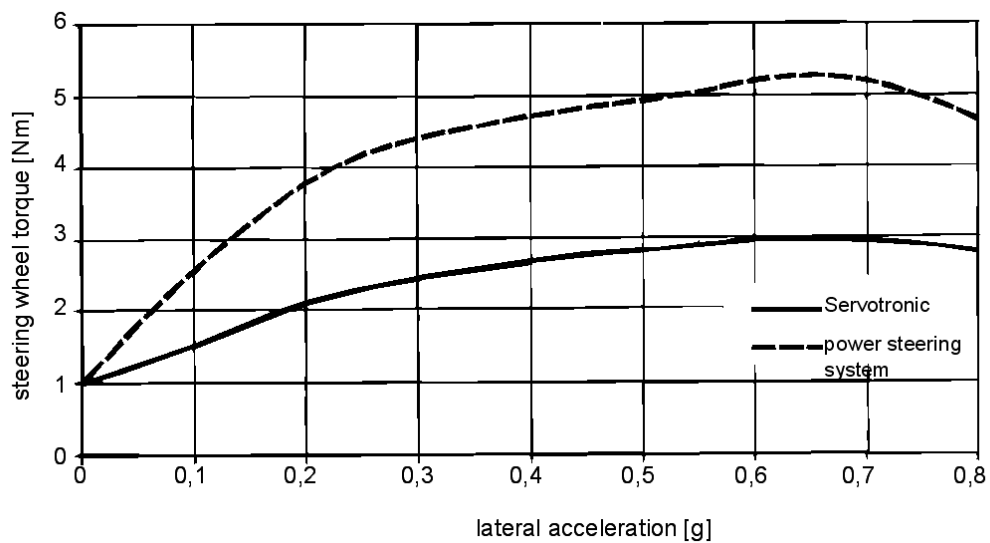


Fig. 2.5-31: Characteristic curve of the steering wheel torque in relation to the lateral acceleration during stationary circular-course driving ($r = 100\text{m}$)

2.6 Suspensions

2.6.1 Basic Suspension Designs

The wheel and body of an automobile are linked to each other via the suspension system. The function of the suspension system is to guide the wheel relative to the body in a manner, which on the one hand allows large vertical compressive displacements, and on the other hand serves to transfer the horizontal tire forces and moments which act in the tire contact center, to the body.

Suspensions can be essentially distinguished into *Independent Suspensions*, *Rigid Axle Suspensions* and *Composite (compound) Axles*.

Relative to the body, the unfastened wheel carrier of *Independent Suspension* possesses six degrees of freedom of movement of a rigid body in space. By means of 5 links with ball joints at both ends, these degrees of freedom are cancelled, except for the degree of freedom for compression. In steerable independent wheel suspension systems, one of the links takes the function of a tie rod. Wishbone arms can be formed by the combination of two links (e.g. double-wishbone suspension), Fig. 2.6-1.

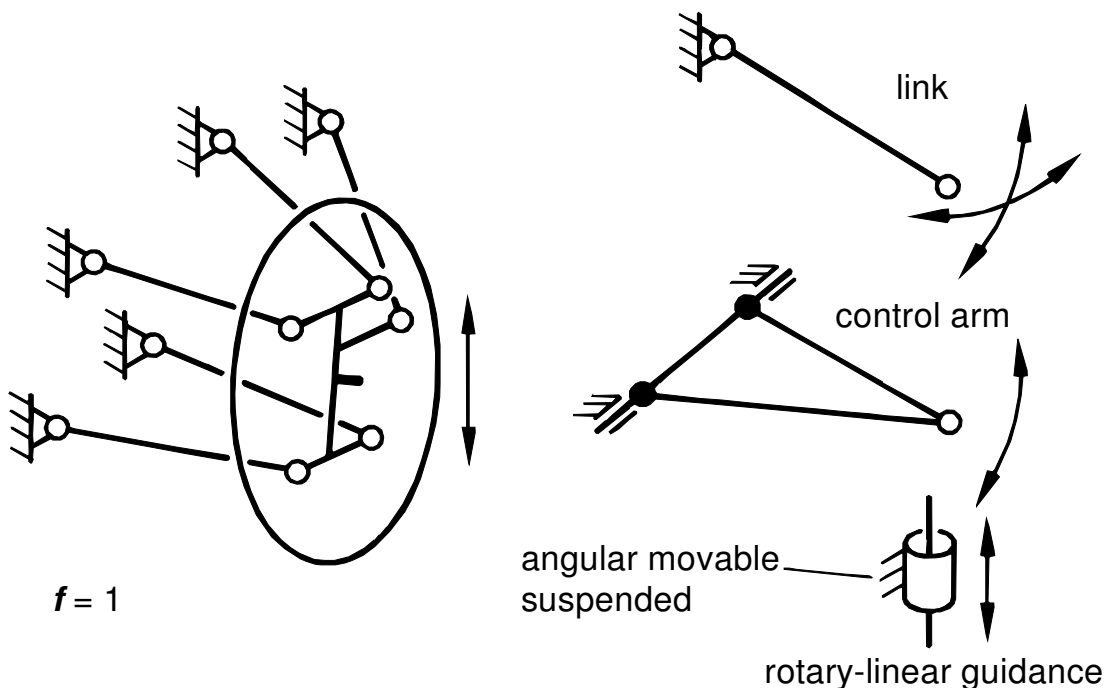


Fig. 2.6-1: Schematic of independent wheel suspension

A link may be replaced by a twist-sliding guide representing a link of infinite length (suspension strut, damper strut suspension). The axes of rotation of the links may coincide (e.g. semi-trailing link wheel suspension).

A *Rigid Axle* is characterized by a rigid connection between the two wheel carriers. For differing compression travels of the two wheels to be possible, the rigid axle must possess 2 degrees of freedom relative to the body (vertical and rolling motion around the vehicle longitudinal axis). Consequently, four links are required for 4 of the originally 6 degrees of freedom to be cancelled, Fig. 2.6-2.

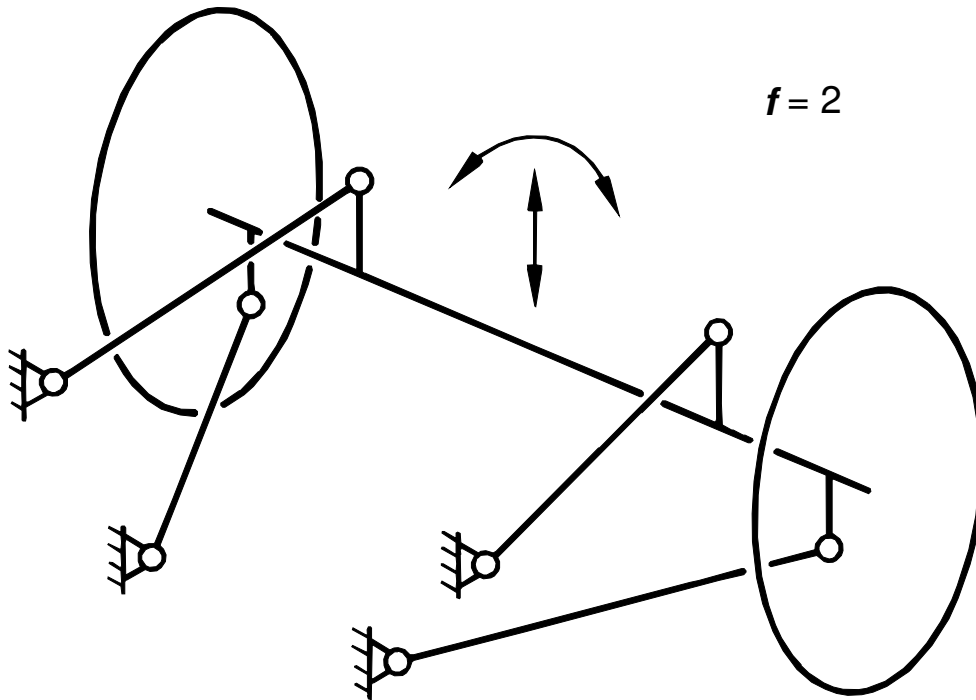


Fig. 2.6-2: Schematic of a rigid axle

Here, too, the links can be arranged in the most diverse way or combined to form control arms. Unlike independent wheel suspensions, rigid axle suspensions are often kinematically overdefined (overrigid)/29/.

Rigid axles guided by leaf springs, for example, possess two degrees of freedom due to the elasticity in the spring attachments.

Axles whose wheel carriers are not rigidly connected to each other but are also not capable of completely independent spring movements are called *Composite Axles*.

The layout as shown in Fig. 2.6-3, with the wheel carriers, which are directly attached to the body, being connected by means of a twisting-sliding guide, is not a general case but one of many possible designs often used.

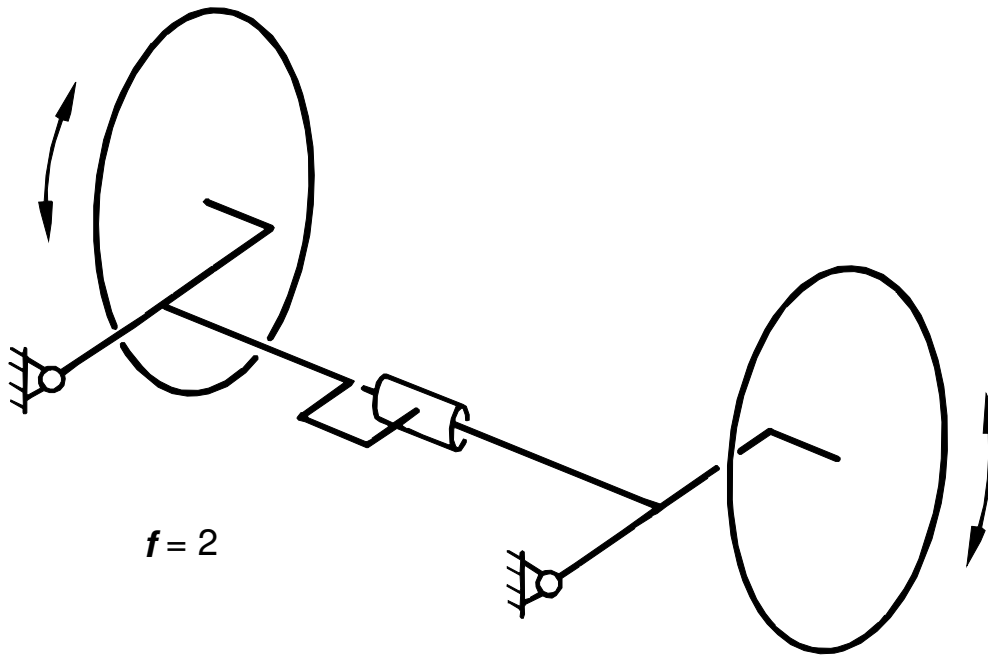


Fig. 2.6-3: Composite (compound) axle, schematic

In the practical application of this version, a torsion section is used instead of the twist-sliding guide. Due to the absence of the sliding degree of freedom, the twist-sliding guide is substituted by the elasticity of rubber mounts at the fastening points (pivots) on the body.

2.6.2 Kinematics of Suspensions

The preceding section described how the degrees of freedom of movement of the wheel relative to the body are cancelled by the wheel suspension, except for the degree of freedom of compression. Since the struts or links guiding the wheel are of a finite length, the wheel carrier will as a rule perform a three-dimensional movement during compression.

If this movement corresponds to the most general movement of a body in space, it can then be denoted as "instantaneously fastened" at any point in time, i.e. as a movement around an instantaneous axis of rotation in space with a displacement in axial direction, and we speak of a "three-dimensional suspension", Fig. 2.6-4.

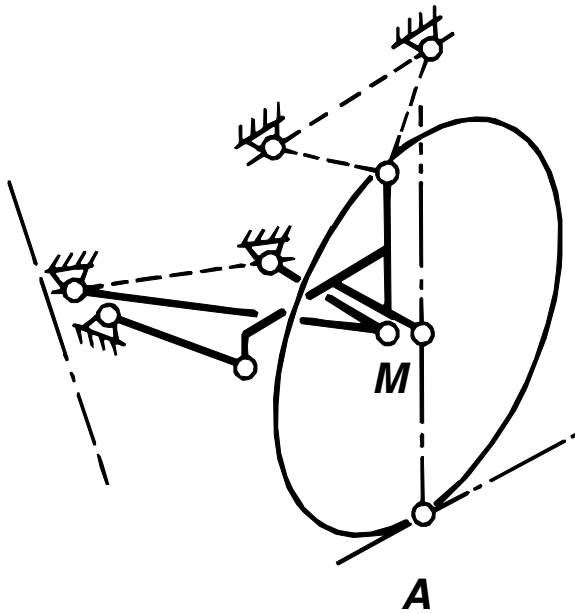


Fig. 2.6-4: "Three-dimensional" Suspension

If the movement of the wheel carrier can be considered as a pure rotation around an instantaneous axis of rotation at any point in time, whose orientation relative to the body changes but nevertheless always runs through a point fixed on the body, then one speaks of a "spherical suspension", Fig. 2.6-5.

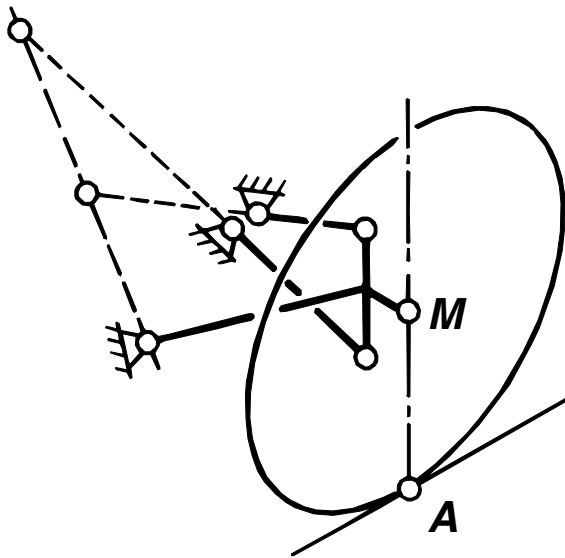


Fig. 2.6-5: "Spherical" suspension

If the wheel carrier at any point in time executes pure rotation around an instantaneous axis of rotation, which changes its position but maintains its orientation relative to the body (parallel displacement), one speaks of a "Plane Suspension", Fig. 2.6-6.

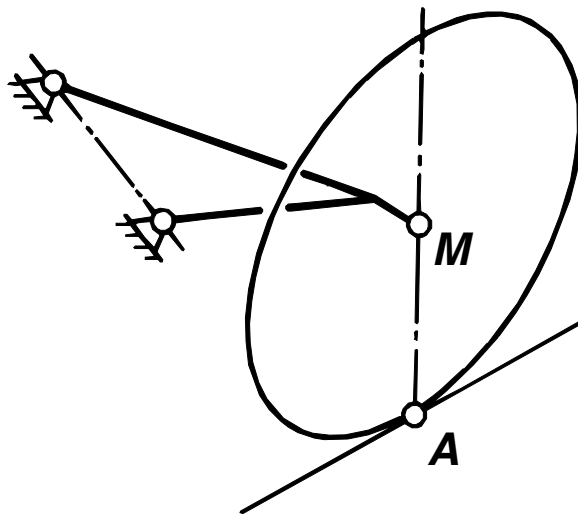


Fig. 2.6-6: "Plane" suspension

A body-fixed instantaneous axis of rotation constitutes the kinematically simplest case (e.g. trailing-link suspension) as a special form of the "Plane" suspension.

Depending on the kinematics of the suspension, changes in the wheelbase, track width, camber angle and toe-angle of the wheel relative to the body or the road take place. The influence of these kinematic changes of the wheel position on vehicle handling was described in section 2.4.

If the position of the instantaneous axis of rotation for a certain compressed position is known, then the wheel-position changes for small suspension movements can be characterized around this initial position. All points on the wheel carrier move tangential to the circular arcs around the instantaneous axis of rotation.

In three-dimensional suspensions, the velocity components of the translational movement in the direction of the axis of rotation must also be considered.

Fig. 2.6-7 illustrates the relation between the position of the instantaneous axis of rotation and wheelbase or track changes during suspension movement using the example of a plane semitrailing-arm wheel suspension.

The points of intersection (penetration points) of the instantaneous axis of rotation through the planes of projection appear here in the respective views as instantaneous centers of rotation (L, Q).

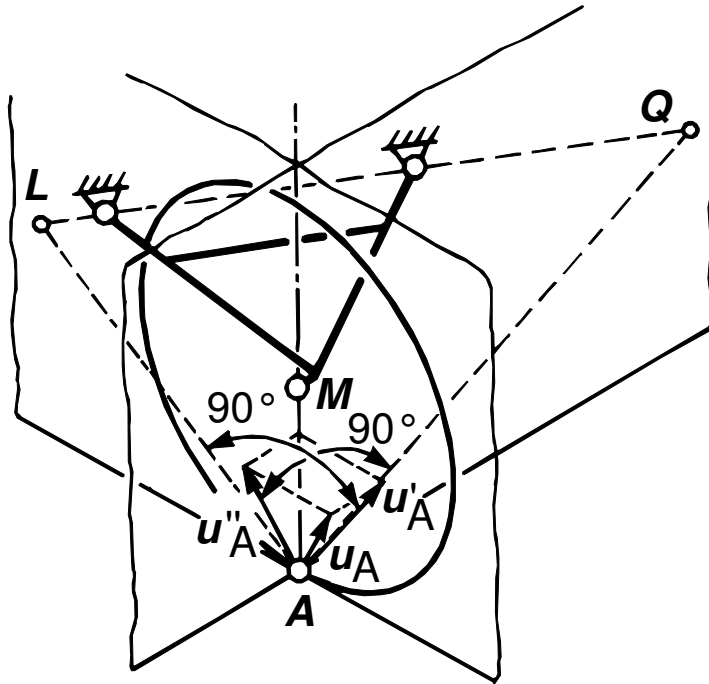


Fig. 2.6-7: Wheelbase and track changes in a plane semitrailing-arm wheel suspension

The position of the instantaneous axis of rotation not only determines wheel-position changes for small suspension displacements, but also the transfer of forces between the tire contact center and body.

In plane and spherical wheel suspensions, forces whose lines of action intersect or run parallel to the instantaneous axis of rotation, do not produce a torque around the axis of rotation and are transmitted to the body without suspension movement. In three-dimensional wheel suspensions however, a torque is produced as a result of forces acting in the direction of the axis of rotation, if the instantaneous pitch is not zero.

These relations determine the position of the roll center of an axis and the magnitude of brake-dive and acceleration-squat (described later).

In spherical and plane wheel suspensions, a torsional equilibrium of the components of forces acting around the point of intersection (penetration point) of the instantaneous axis of rotation can be established by the respective planes of projection (instantaneous center/velocity pole) separately for longitudinal and transverse views.

In three-dimensional wheel suspensions, the points of intersection are not identical to the longitudinal or transverse center, because the displacement in axial direction must also be considered.

"Equivalent poles" can be determined if the velocity components of suspension movement are known in the respective views from two points on the wheel carrier. The instantaneous

center to be determined then corresponds to the intersecting point of the perpendiculars to the velocity directions in these two points (polar projections), Fig. 2.6-8.

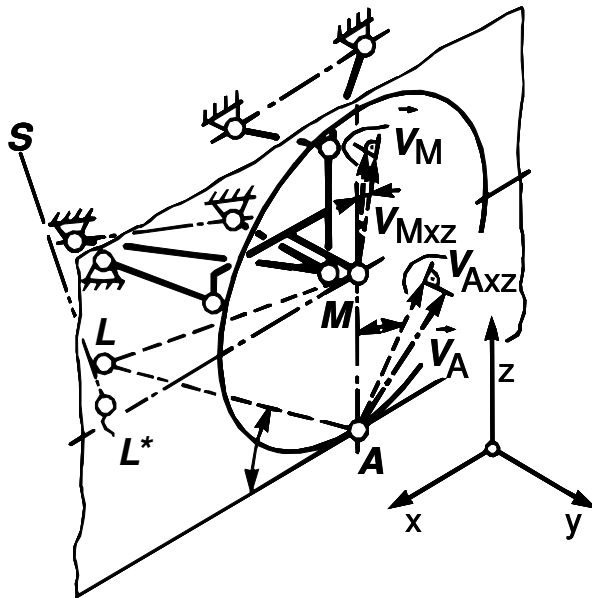


Fig. 2.6-8: "Equivalent center" in longitudinal plane of a three-dimensional wheel suspension

2.6.2.1 Roll Center

Fig. 2.6-9 illustrates by means of a plane double-wishbone suspension (here with parallel axes of rotation in vehicle longitudinal direction), the additional forces acting at the tire contact centers during cornering compared to the static state of rest (for wheel-specific body spring rates, see section 1.3.2.3).

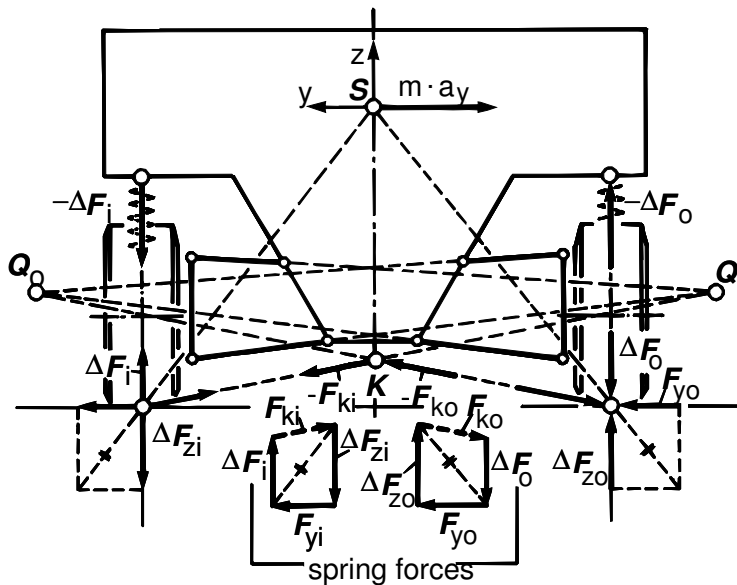


Fig. 2.6-9: Force transmission between tire contact centers and body during cornering (plane double-wishbone suspension)

Lateral acceleration and therefore wheel-load differences and roll angle are assumed to be insignificant. Since in steady-state cornering, a moment balance is again setup at the instantaneous centers (points of intersection of the instantaneous axis of rotation through the plane of projection), the resultant forces acting additionally at the tire contact centers during cornering (wheel-specific suspension forces assumed) can only be directed towards the instantaneous axes of rotation (or instantaneous centers).

Assuming small wheel-load differences, the lateral tire forces are of the same magnitude, and the resulting lateral force on the axle will act in the virtual point K on the body while the vertical components of the resultants at the tire contact centers cancel each other.

Since the lines of action of the resultants at the two tire contact centers pass through their respective instantaneous centers, these lines of action match with the polar projections of the velocity vectors in the tire contact centers. The virtual point K (since compression travel is to be the same) now represents the collective instantaneous center for oppositely phased suspension movement, assuming the body to be fixed, Fig. 2.6-10.

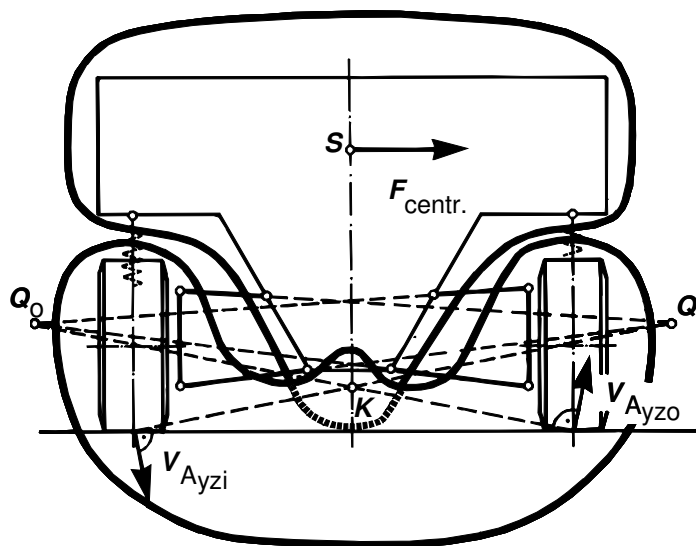


Fig. 2.6-10: Instantaneous center for oppositely phased suspension movement

Rolling motion is the kinematic reversal of this oppositely phased suspension movement. The point K is therefore also the instantaneous center for body roll relative to the road surface. This roll center was already introduced in section 1.6.1, though simplified as an assumed body-fixed hinge point (fulcrum).

In most real wheel suspensions, the position of the roll center is significantly altered as a result of suspension movement.

A simple determination of this change in position during cornering is not possible, since the magnitude of suspension displacement for the inside and outside wheels can only be assumed at low lateral accelerations. This can be easily understood if, for example, a kinematically simple swing axle is considered, Fig. 2.6-11.

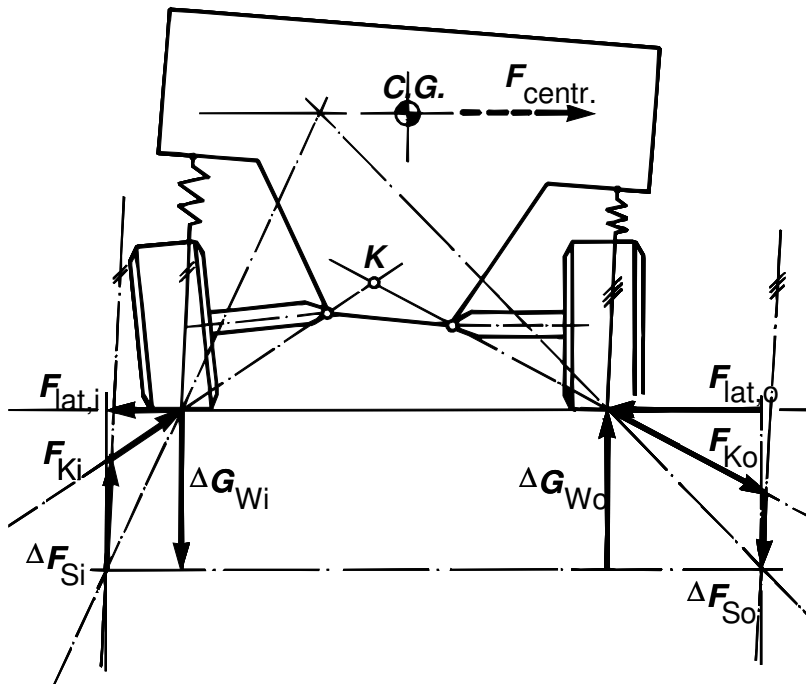


Fig. 2.6-11: Position change of the roll center during cornering (double-jointed swing axle)

In this independent suspension, the instantaneous axis of rotation of the wheel carrier relative to the body passes through the actual pivoting points (\rightarrow instantaneous centers) at any point in time and is thus fixed with respect to the body.

In the ideal case, the distribution of the lateral tire forces between the inside and outside wheels correspond to the relationship between lateral force, wheel load and slip angle determined by the tire performance maps. On the outside wheel, the torque resulting from the change in wheel load around the associated instantaneous center for the motion of the wheel-carrier relative to the body (pivot) is largely compensated by the torque of the tire lateral force. Therefore, the change in spring force bringing about torque balance is much smaller on the outside wheel than on the inside wheel, where nearly the entire torque of the change in wheel load around the instantaneous center has to be supported by a change in spring force.

As a result of this asymmetry of forces, rebound on the inside wheel during cornering will be much more pronounced than compression on the outside wheel. This effect is referred to as the "bottoming-out effect" /29/.

In older vehicles with swing-axle type rear axles and a roll center high above the road, this bottoming-out effect was feared, since the center of gravity of the vehicle was elevated during cornering and this not only impaired vehicle handling in these vehicles which already had relatively high centers of gravity, but could even result in the loss of rollover stability.

It can be demonstrated that the bottoming-out tendency reduces considerably, the lower the height of the roll-center is and the quicker the roll center height drops during parallel

compression of the body. In modern suspension systems, this is realized by means of a target-specific kinematic layout.

2.6.2.2 Brake-Dive and Acceleration-Squat Compensation (Anti-Dive/Anti-Squat)

During braking and acceleration, an axle-load shift takes place as a result of a pair of forces consisting of the forces at the tire circumference and the forces of inertia acting at the vehicle center of gravity, Fig. 2.6-12.

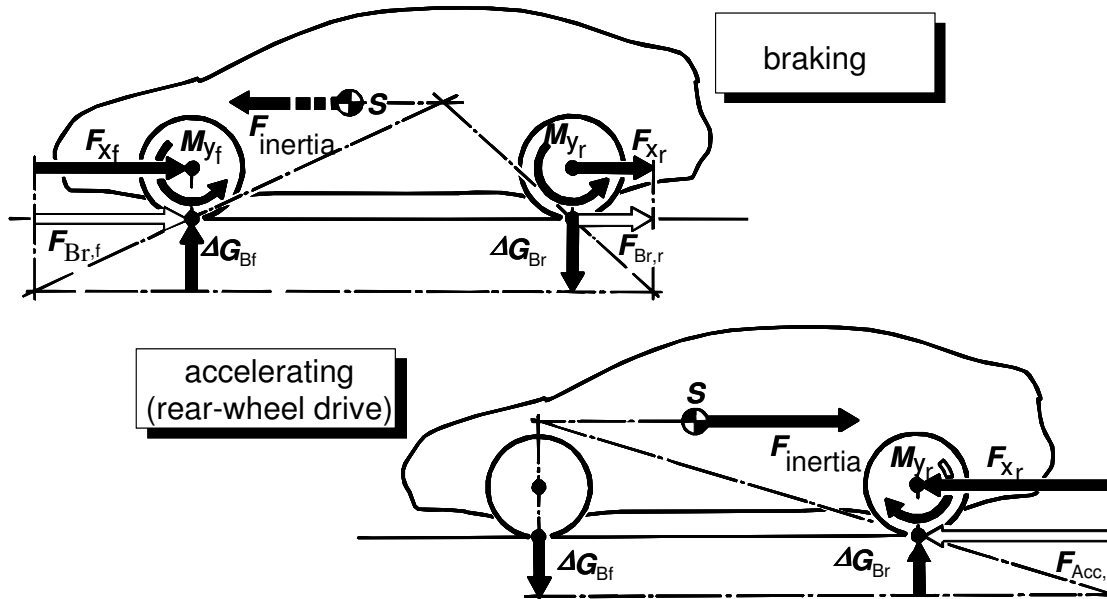


Fig. 2.6-12: Forces acting on the wheel carrier during braking or accelerating

In contrast to the static position of rest, a longitudinal force F_x and a wheel-load difference ΔG_W act on the wheel carrier in the center of rotation of the wheel.

During propulsion, the torque $M_y = F_x \cdot R_{dyn}$ in most wheel suspension systems is supported directly on the body via the drive shafts and therefore has no effect on the reaction forces in the wheel suspension (Exception: rigid axle with integrated differential gear).

During braking with the usual "external brakes" however, the torque M_y acts on the wheel carrier, because it supports the brake torque via the brake caliper. The reaction forces in the wheel suspension then correspond to a force F_x acting at the tire contact center on the wheel carrier. (Exception: "internal brakes", where the brake torque is supported via the propeller shaft on brake disks with brake calipers mounted in the differential gear).

The torque of the forces around the longitudinal pole of the suspension acting additionally on the wheel carrier during braking or accelerating has to be compensated by the torque of the spring-force change ΔF_F . Fig. 2.6-13 illustrates the relationship for braking (wheel-specific spring rates).

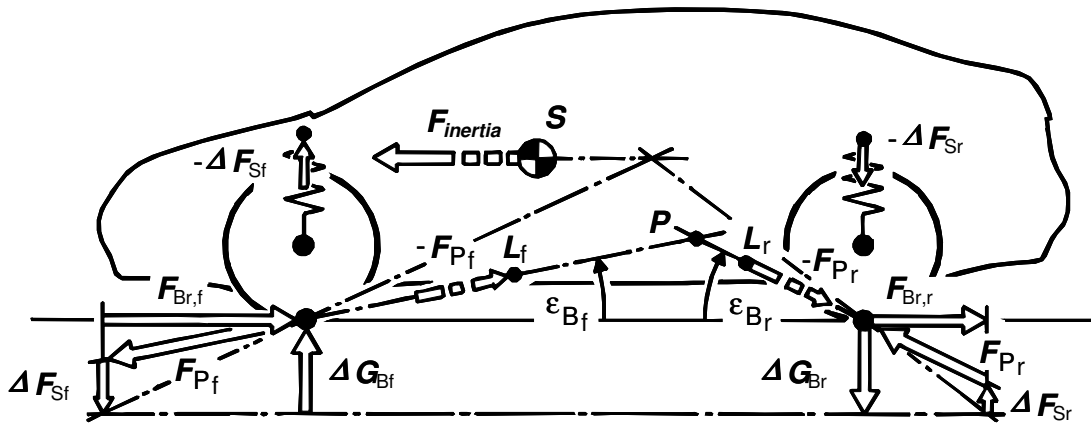


Fig. 2.6-13: Force transmission between tire contact centers and the body during braking

The intensity of brake-dive, i.e. compression of the front axle and rebound of the rear axle, depends on the (instantaneous) position of the longitudinal center. If the position of the longitudinal center agrees with the line of action of the resultant force from the brake force and the wheel-load differences in the tire contact center, then no suspension movement occurs during braking, and one speaks of "complete braking-torque compensation" on the axle considered. For design reasons, such a layout is very difficult to realize in practice. The quality of partial braking-torque compensation can be described with the help of the braking support angle ϵ .

The braking support angle ϵ_{tats} actually realized by wheel suspension design is determined by the angle between a straight line passing through tire contact center and longitudinal center and the horizontal, see Fig. 2.6-13.

The optimum support angle ϵ_{opt} corresponds to the angle between the line of action of the resultant F_{res} in the tire contact center and the horizontal:

$$\text{front: } \tan \epsilon_{\text{opt.f}} = \frac{h}{l} \cdot \left(1 + \frac{1}{F_{B,f}/F_{B,r}} \right) \quad (2.6-1)$$

$$\text{rear: } \tan \epsilon_{\text{opt.r}} = \frac{h}{l} \cdot \left(1 + \frac{F_{B,f}}{F_{B,r}} \right) \quad (2.6-2)$$

F_{Bv}/F_{Bh} brake-force distribution (see vehicle I)

h center-of-gravity height

l wheelbase

A torque balance around the instantaneous center at the design position of the vehicle provides as a measure of the quality of braking-torque compensation that proportion of the

wheel-load transfer during braking that is supported by the wheel suspension without suspension movement:

$$X \cdot \Delta G_f \cdot l_f = F_{B,f} \cdot h_f \quad (2.6-4)$$

l_v horizontal distance

h_v vertical distance, footprint center – longitudinal center

X "braking-torque compensation" (anti-dive)

$$\begin{aligned} \text{rather: } X &= \frac{F_{B,f}}{\Delta G_f} \cdot \frac{h_f}{l_f} \\ &= \frac{1}{\tan \epsilon_{\text{opt.}}} \cdot \tan \epsilon_{\text{real}} \cdot 100\% \end{aligned} \quad (2.6-5)$$

Sometimes the so-called dive factor T is used to characterize braking-torque compensation (anti-dive):

$$S = 1 - \frac{\tan \epsilon_{\text{real}}}{\tan \epsilon_{\text{opt}}} \quad (2.6-6)$$

Identical to braking, suspension movements during acceleration can also be described by the indication of the "acceleration squat compensation" (anti-squat) X of the driven axle.

Fig. 2.6-14 shows the supporting angles acting during acceleration for a driven rear axle with independent suspension:

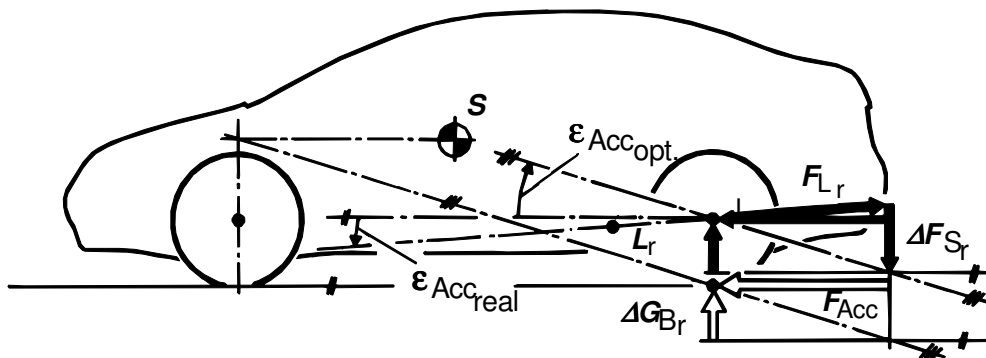


Fig. 2.6-14: Force transmission between footprint center and body during acceleration

2.6.3 Elastokinematics

Road irregularity not only causes vertical but also horizontal shock forces at the tire contact center.

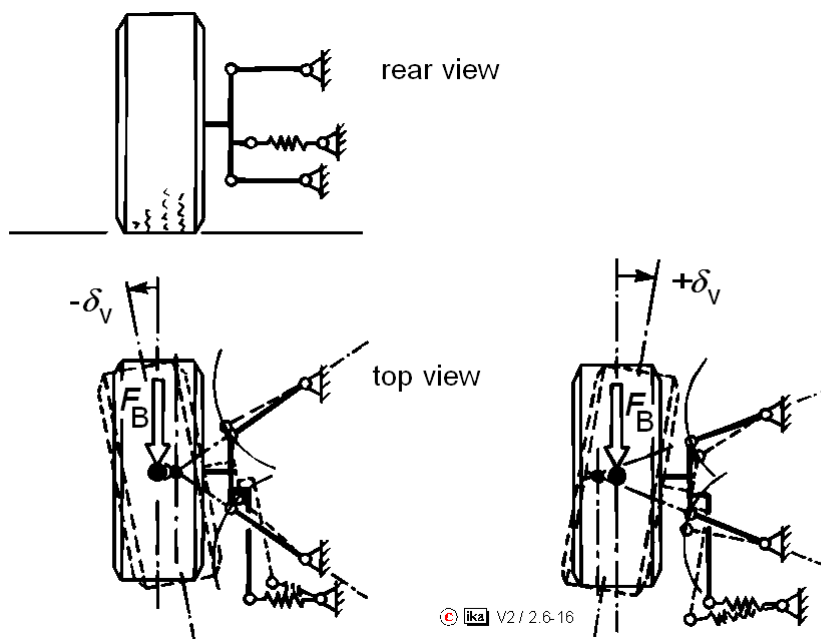


Fig. 2.6-16: Elastokinematics of a five-link wheel carrier with elastic tie rod

Depending on the position of the virtual steering axis, either toe-in or toe-out is caused on the wheel by the radial force due to the elasticity. The great importance of such wheel-position changes for vehicle handling was already described in sections 2.4.3.5 and 2.4.4.4.

Fig. 2.6-16 shows that not every suspension design that makes sense from the point of view of kinematics will also allow favorable elastokinematic tuning. High levels of ride comfort require high levels of elasticity of the wheel suspension, above all in vehicle longitudinal direction. To avoid negative influences affecting vehicle handling, the tire forces acting on the wheel in different directions must not cause any undesired steering angles.

Wheel suspensions that to a large extent fulfill the most diverse requirements regarding kinematic and elastokinematic properties usually require a rather complex design featuring a multitude of potential influencing factors. For practical reasons, optimum configuration of the geometry of the layout of struts and links and the tuning of the elasticity of the rubber mounts are carried out with the aid of corresponding computer programs.

2.6.4 Requirements to be met by the Suspension

The kinematic and elastokinematic properties of suspension systems described in the preceding paragraphs significantly influence vehicle handling (driving safety) and the ride comfort of a vehicle.

In addition to the requirements resulting from these relationships, suspension design also has to fulfill requirements for economy from the point of view of manufacturing cost and compatibility with the overall vehicle design.

This section summarizes the assessment criteria for suspension designs to be derived from the requirements, Fig. 2.6-17.

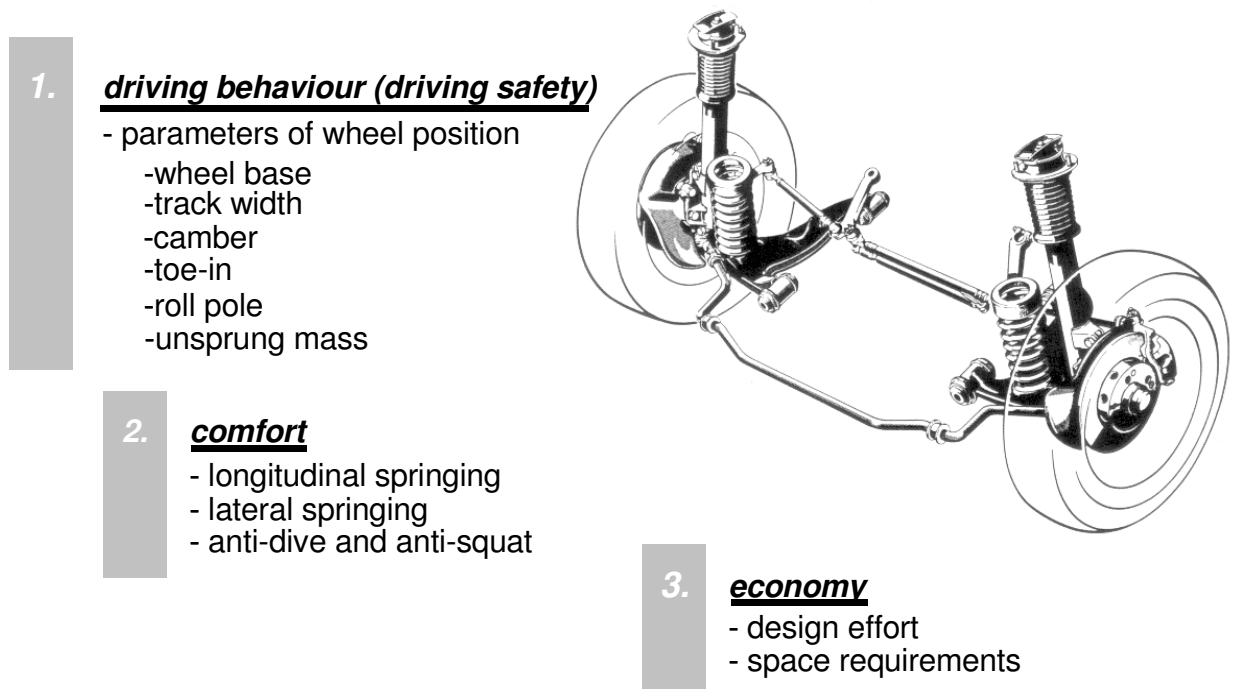


Fig. 2.6-17: Assessment criteria for wheel suspensions

2.6.4.1 Handling

a) Wheel Elevation Curves

The wheel elevation curves describe the position of a wheel relative to the body (superstructure) or the road surface subject to the compression position of the wheel (see Fig. 2.4-19). Wheel position is characterized by the following parameters:

- Track width
- Wheelbase
- Camber angle
- Toe angle (toe-in)

• Track width

Track changes during compression movement of the wheels force lateral movement of the tire contact areas and hence lead to fluctuations of the lateral tire forces, which have a negative effect on the straight-running properties of the vehicle. Moreover, tire wear is

increased due to the lateral movement of the tire contact areas. Therefore, kinematic track changes should be as limited as possible.

- Wheelbase

Wheelbase changes of the magnitude as they occur during compression movement of the wheels do not significantly influence the steering behavior of a vehicle. A wheelbase change which takes place in such a way, that the wheel when passing over a bump simultaneously also responds to the horizontal impact force (oblique suspension) to a certain extent, along with the compression movement, has a positive effect on ride comfort. Major kinematic wheelbase changes however, lead to torsional vibrations in the drive train due to speed fluctuations of the wheels during suspension movement on driven axles, and also affect the quality of the signals for ABS control picked up by speed sensors on the wheels /29/.

- Camber and Toe Angles

Kinematic camber-angle variation and kinematic and elastokinematic toe-angle variation considerably affect vehicle handling, see sections 2.4.3.5 and 2.4.4. The requirements to be met by wheel suspension design derived from this fact cannot be summarized in a generalized form, because they vary according to vehicle concept (location of the center-of-gravity, driven axle) and intended application. Wheel suspension concepts allowing a target-specific kinematic and elastokinematic design, e.g. multi-link suspensions, are as a rule superior to those whose design permit only limited room for design, e.g. rigid axles.

b) Roll Center

The position of the roll center and its position change during cornering are directly related to the kinematic wheel-position changes during suspension movement, see section 2.6.2.1. Wheel elevation curves and lateral-force suspension between tire contact centers and the body can therefore not be optimized independently and separately. A compromise is required between the

- dimension of the centrifugal force lever arm Δh , see section 1.6.1,
- intensity of the bottoming-out effect, see Fig. 2.6-11,
- track and camber changes during suspension movement, see Fig. 2.6-10.

For such a compromise, further factors have to be considered if these kinematic effects in the vehicle lateral plane due to the wheel suspension concept are linked to kinematic effects in the vehicle longitudinal plane and in the plane of the road. These are:

- dive and squat compensation, cf. Fig. 2.6-13, 2.6-14,
- wheelbase and caster changes during suspension movement, see Fig. 2.6-7,

- toe-angle changes during suspension movement.

c) Unsprung Mass

The term unsprung mass refers to those components of the suspension system that are only suspended on the tire suspension (tire springs) and not on the body suspension (body springs), i.e., wheel-hub, wheel-bearing unit, brake disk, wheel carrier, brake caliper, plus proportionately the masses of links, struts, springs, dampers, tie rods, propeller shafts, etc. The amount of unsprung mass should be as small as possible in view of low dynamic wheel-load fluctuations and a good road grip of the wheels (driving safety).

2.6.4.2 Comfort

a) Longitudinal and Lateral Springs

Longitudinal and lateral springs refers to the compliance of the suspension to horizontal impact forces caused by road irregularities. The transfer of these impact forces to the body is thus dampened, resulting in a positive effect on vibration comfort. The compliance of the suspension is achieved by the use of rubber elements at the mounting points on the body. Impact forces in vehicle longitudinal direction can also be absorbed by means of the so-called transverse spring action. A transverse spring action is said to be present when the horizontal impact forces directed towards the wheel axis result in the compression movement of the wheel.

The inclined spring action is based on the same principle as anti-dive. By the appropriate design of the kinematics of wheel guidance, the elevating curve of the wheel center in the vehicle transverse plane is inclined backwards relative to the vertical. One component of the body spring force hence acts in the vehicle longitudinal direction, Fig. 2.6-18.

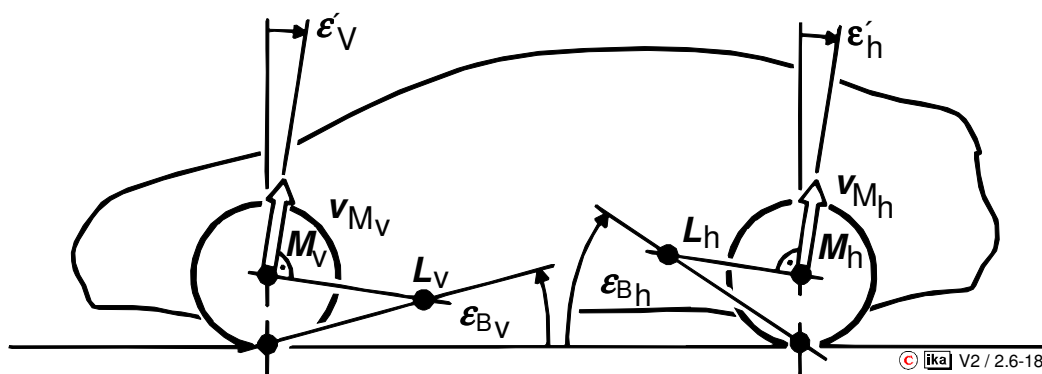


Fig. 2.6-18: Inclined suspension angle and braking support angle

b) Vibration and Noise Insulation

Radial tires with their stiff bracing belt, are particularly excited by road irregularities to into relatively high-frequency vibrations, which are transmitted to the wheel suspension. In order to keep these vibrations away from the body and to suppress the transfer of structure-borne noise, a relatively high degree of longitudinal elasticity of the wheel suspension is necessary. This can be achieved by the use of large-volume rubber mounts at the mounting points of the suspension to the body. To avoid adverse effects on vehicle handling, the suspension should be designed in a manner that no unfavorable elastokinematic wheel-position changes are caused, see Fig. 2.6-16.

c) Brake-Dive and Accelerating-Squat compensation (Anti-Dive/Anti-Squat)

By the design of suspension kinematics in such a way that a component of the longitudinal forces in the tire contact center is directed towards the elevating curve during suspension movement, makes it possible for the braking-induced compression of the front axle / rebound of the rear axle to be less intense than it would be in the case of a purely vertical-force variation (axle-load shift) in conjunction with wheel-specific spring rates.

This form of anti-dive reduces the pitching motion of the body (angular movement around the vehicle lateral axis) during braking and thus has a positive effect on suspension comfort. Moreover, a complete compression of the springs is avoided during extreme braking.

Anti-squat can also be realized identical to anti-dive. In case of a single driven axle, the components of the longitudinal-force which influence compression are only available on the driven axle, and hence a complete compensation is not possible here, see Fig. 2.6-14.

In most suspension concepts, the braking support angle, accelerating support angle and oblique suspension angle (see Fig. 2.6-18) cannot be selected independently and are closely linked to the wheel elevation curves. Particularly in the case of steered wheels, attention must be paid to the fact that the design in view of favorable support angles must not result in considerable caster changes, since they have an adverse effect on the steering quality, see section 2.5.2.

2.6.5 Rigid Axles

Rigid axles distinguish themselves based on the low constructional effort required and favorable possibilities for assembly onto the body. To guarantee freedom of movement of the axle shaft during compression, the spatial requirements of rigid axles which are placed transverse across the underside of the vehicle floor, is relatively high for large suspension displacements.

The opposed influence on suspension movements of both wheels has a negative effect on the dynamic wheel-load variations. Particularly in the case of driven axles with integrated differential, mass coupling is also effective in addition to kinematic coupling.

Axle guidance relative to the body in vehicles with leaf springs usually takes place over the spring leaves, Fig. 2.6-19.

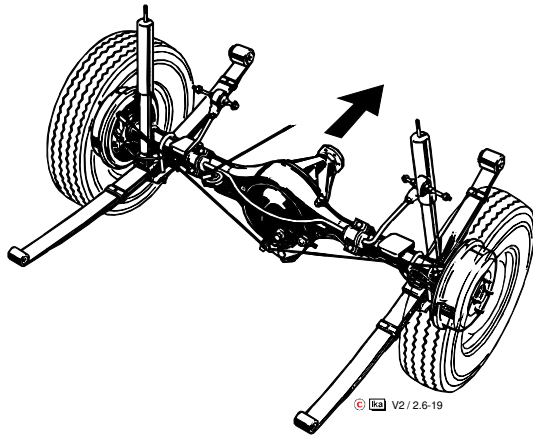


Fig. 2.6-19: Automobile rear axle guided by leaf springs (Ford Capri)

Rigid axle suspensions guided by links are rarely statically determinate, Fig. 2.6-20.

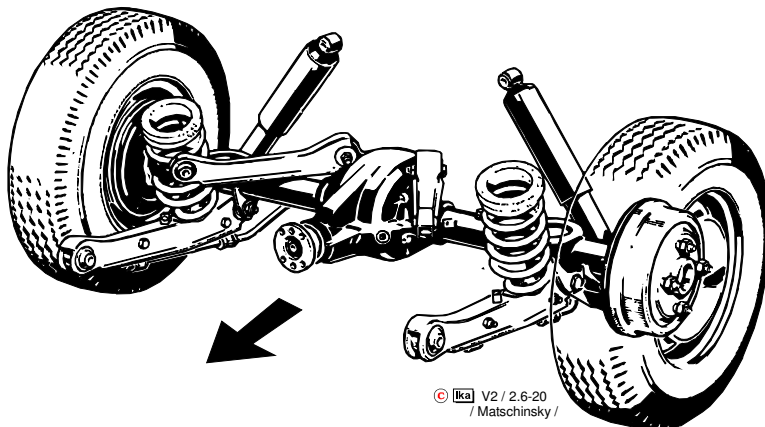


Fig. 2.6-20: Statically determinate suspension of an automobile rear axle (Ford Taunus)

Statically indeterminate mounts are selected as a rule, due the convenient fastening possibilities onto the body or less spatial requirement, Fig. 2.6-21.

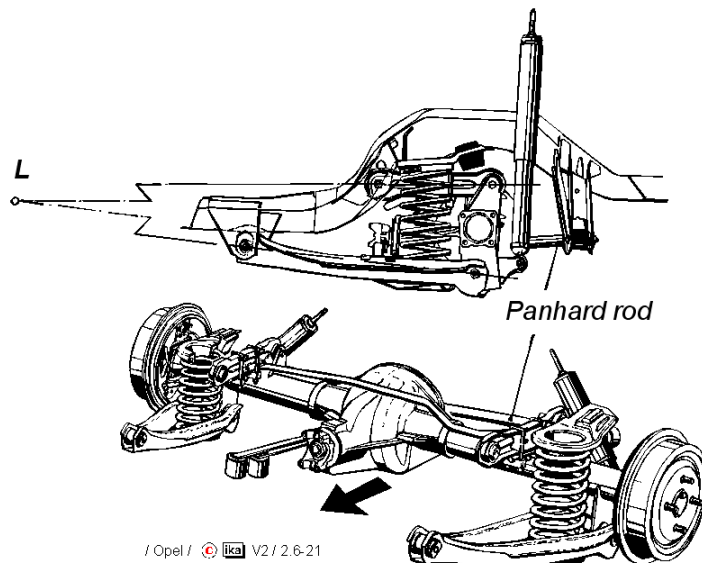


Fig. 2.6-21: Statically indetermined suspension of an automobile rear axle (Opel Rekord)

The transverse guidance of the suspension is realised either using a so-called Panhard rod (see Fig. 2.6-21), or a Watt linkage, Fig. 2.6-22.

The Panhard rod should be as long as possible, for transverse offset of the axle during suspension movement to be kept as low as possible, since this would have a negative effect on straight-running properties.

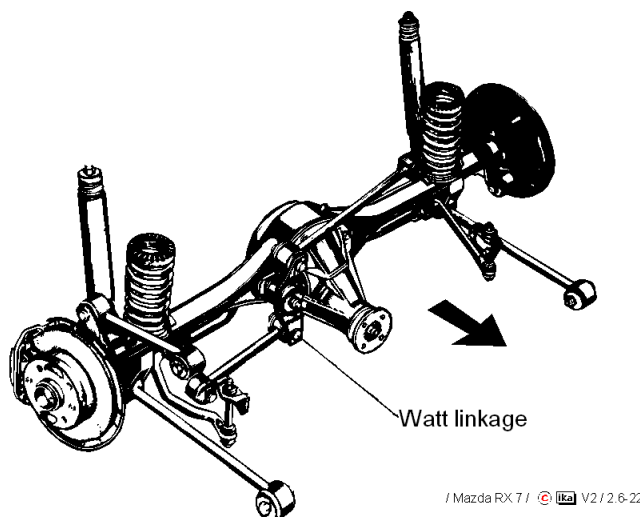


Fig. 2.6-22: Transverse control of a rigid rear axle of an automobile by means of a Watt linkage (Mazda RX 7)

The position of the roll center agrees with the virtual point of transfer of lateral forces between axle and body. For rigid axles suspended on leaf springs, the roll center is located at the height of the spring-mounting points on the body. In case of the transverse suspension consisting of Panhard rod, the roll center lies at the height of the (horizontal) Panhard rod; while for the Watt linkage, at the height of the middle hinge.

Depending on the type of longitudinal guidance, anti-dive and anti-squat can be realized, (see Fig. 2.6-21), and toe-angle variations during rolling motion of the body can be influenced, Fig. 2.6-23.

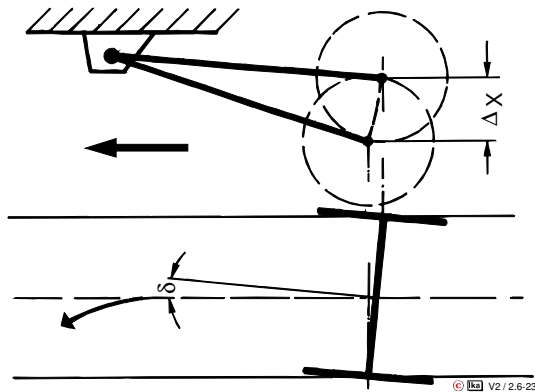


Fig. 2.6-23: Toe-angle variation on a rigid axle for oppositely phased suspension movement (roll steer)

The relative camber angles in rigid axles always correspond to the roll angle, the absolute camber-angle variations are hence always zero (except for deviations due to differing tire deflections).

The so-called Drawbar Axle represents a special type of mount on the body, where one of the mounting points is designed as a ball joint which directly links axle and body, Fig. 2.6-24

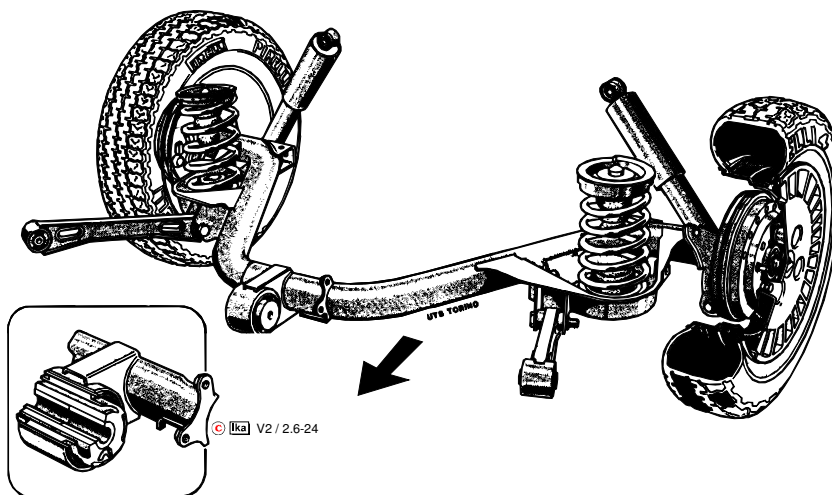


Fig. 2.6-24: Rigid automobile rear axle designed as a Drawbar Axle (Lancia Y10)

The DeDion-Axle (Albert DeDion, 1899) represents a special form of a driven rigid axle, where the two wheel carriers are linked by a rigid carrier but the differential gear is fixed to the body and linked to the wheels via drive shafts, Fig. 2.6-25. In this axle design, the wheel-load difference occurring in rigid axles with integrated differentials, in response to the propeller shaft torque is absent and the amount of unsprung masses is smaller, but these advantages are offset by the disadvantage of considerable design effort.

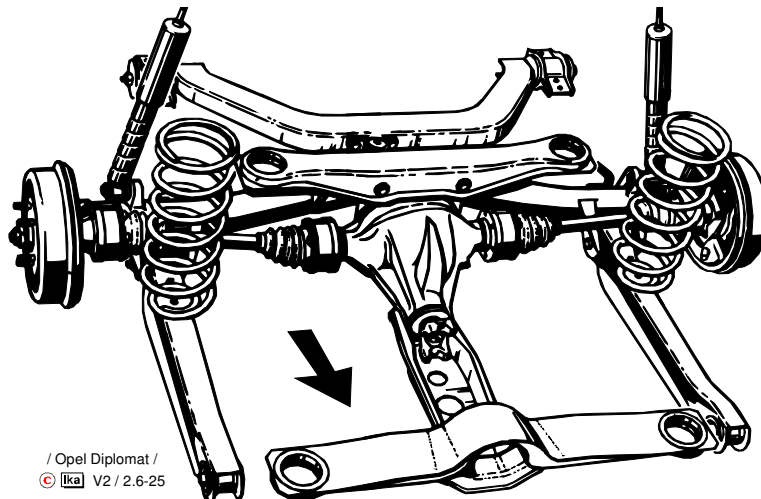


Fig. 2.6-25: De Dion Rigid Axle (Opel Diplomat)

2.6.6 Semi-Rigid Axles

The semi-rigid axles used today in many FWD vehicles as rear axle represents a special version of compound axles, see section 2.6-1.

All semi-rigid axles are characterized by a very simple design and therefore very cost-efficient production. Based on design, one distinguishes between Torsion Crank Axle (flex arm suspension), Twist Beam Rear Axle (semi-independent suspension) and Twist Beam Rear Axle (semi-independent suspension) with rearward displaced cross member.

The Torsion Crank Axle (flex arm suspension) is the oldest design, Fig. 2.6-26.

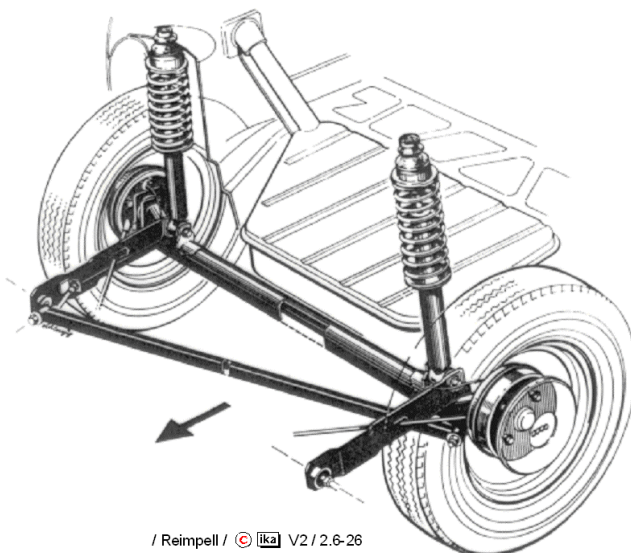


Fig. 2.6-26: Torsion crank axle (Audi 80, 1972)

Similar to a rigid axle, the two wheel carriers are firmly linked to each other by means of a bending-resistant but torsionally weak section.

Longitudinal axle control is effected via longitudinal links welded to the cross member. During roll movement, the cross member is distorted and thus functions as a stabilizer spring.

Transverse axle control is effected by a Panhard rod, which can also run diagonally underneath the vehicle floor if this provides a more favorable mounting point for force application on the body, see Fig. 2.6-26.

The body springs are mounted over spring carriers hinged to the axle tube. The kinematic properties of the torsion crank axle largely correspond to those of a rigid axle. The positions of the longitudinal centers are determined by the positions of the mounting points of the longitudinal links on the body. The position of the roll center depends on the location of the Panhard rod.

By contrast, the Twist-Beam Rear Axle largely has the kinematic properties of a trailing-link suspension, Fig. 2.6-27.

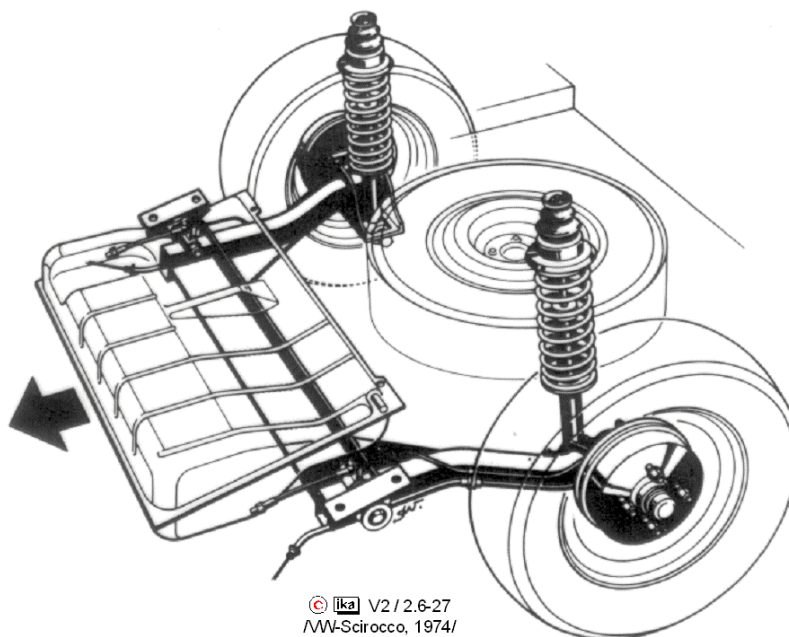


Fig. 2.6-27: Twist-beam rear axle (VW Scirocco, 1974)

This semi-rigid axle consists of two bending and torsion-resistant longitudinal links connected to each other at the height of the mounting points on the body by means of a bending-resistant but torsionally weak cross member welded to the links.

The space required by the axle shaft which is also compressed in the torsion crank axle can be used otherwise in the twist-beam axle.

The use of the connecting section (cross member) considerably simplifies the mounting of the trailing links on the body compared to trailing-link independent suspension. The use of torsion bars however, is not favourable. The body springs are mounted over spring carriers (spring brackets) hinged to the wheel carrier. During oppositely phased suspension movement, the cross member between the links is distorted and thus acts as a stabilizer spring.

Fig. 2.6-28 shows the twist-beam rear axle of the Audi A4 as another example. A stabilizer in front of the axis of rotation of the axle body is provided for additional reduction of roll angle. Due to its position, the stabilizer simultaneously increases transverse stiffness of wheel guidance.

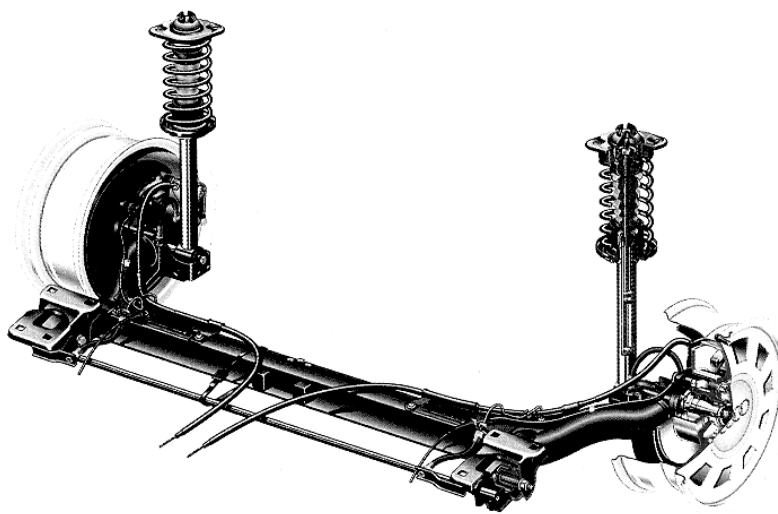


Fig. 2.6-28: Twist-beam rear axle (Audi A4, 1994)

The design of the Twist-Beam Rear Axle with Rearward-Displaced Cross Member corresponds to that of the twist-beam rear axle, however the connecting section (cross member) of the trailing links is not arranged at the mounting points on the body, but displaced backwards, Fig. 2.6-29. Twist-beam rear axles are often also referred to as semi-independent or cross-member-type suspensions. The twist-beam rear axle is today the standard solution in vehicles such as the Ford Fiesta and the VW Polo.

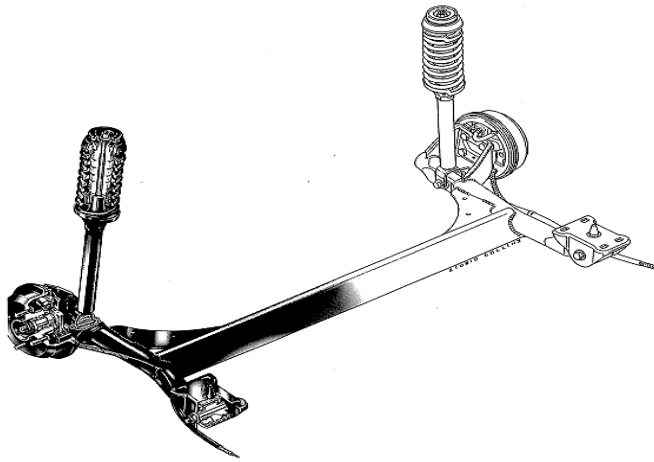


Fig. 2.6-29: Twist-beam rear axle with rearward-displaced cross member (Ford Fiesta, 1995)

When this axle was introduced in the Audi 50, the arrangement of the cross member was probably intended to provide more space for the fuel tank in front of the axle, so that there could be more legroom in front of the rear bench seat.

However, this axle type also proved to have favorable kinematic properties. During parallel spring action, the twist-beam rear axle with rearward-displaced cross member behaves like a trailing-link axle; and during roll, like a semi-trailing link axle.

The virtual rotation axes (pivot axes) of the links run through the pivoting points of the trailing links on the body and through the shear center of the cross member distorted by oppositely phased suspension displacement. In contrast to the twist-beam rear axle, cornering will therefore be associated with relative camber changes, which will reduce the absolute, positive camber angle of the outside wheel, and the roll center is not at the level of the road surface, Fig. 2.6-30.

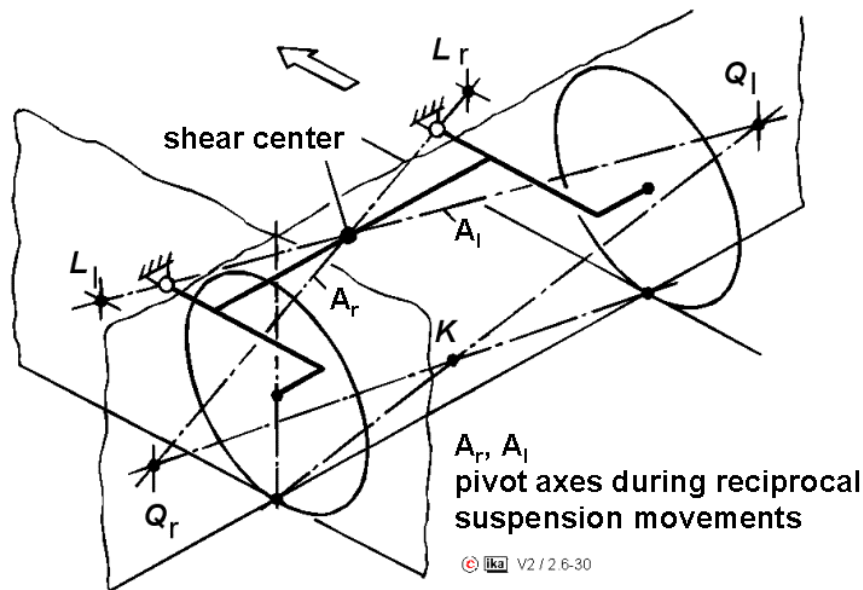


Fig. 2.6-30: Geometry of the twist-beam rear axle with rearward-displaced cross member with roll springing

The twist-beam rear axle with rearward-displaced connecting section is more widely used nowadays than the twist beam rear axle. Lateral forces at the tire contact centers produce a force couple at the axle mounts on the body, which consists of a traction force on the outside bearing acting in vehicle longitudinal direction and a corresponding pressure force on the inside bearing.

The use of soft rubber mounts for suspension comfort, results in an elastokinematic toe-angle variation producing an oversteer effect, which negatively affects the steering behavior of the vehicle during transient driving maneuvers.

This effect can be suppressed by the use of so-called track-aligning bearings. Their design is such that the effect of an axial lateral force results in radial displacement. During cornering, elastic deformation of the bearings is compensated by the reaction forces at the mounts (pivot points), Fig. 2.6-31.

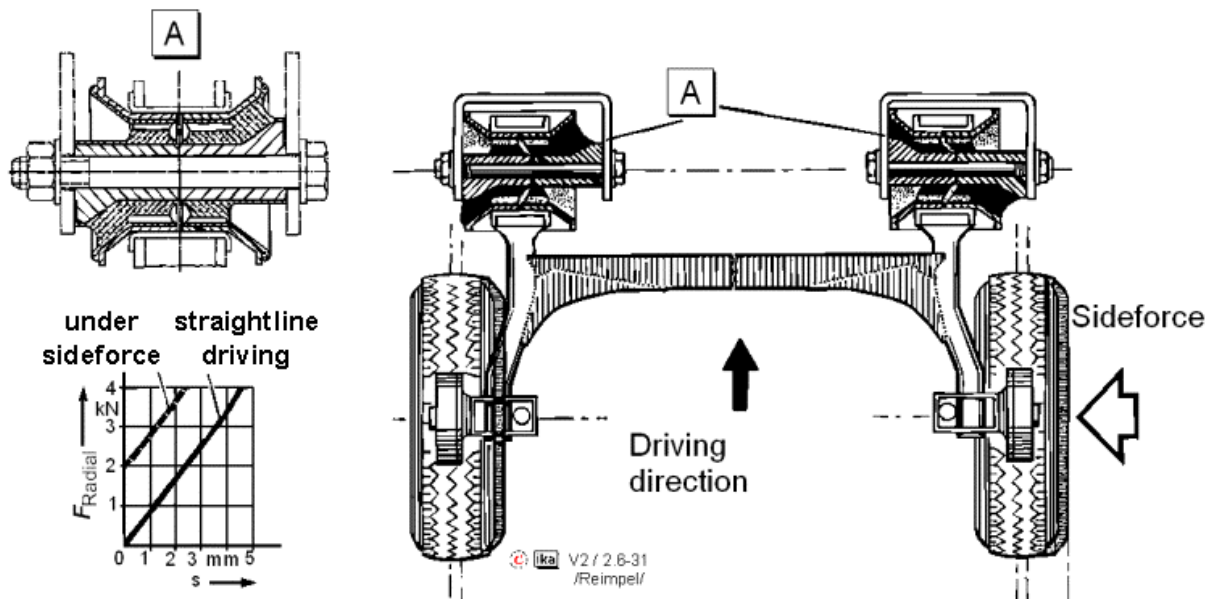


Fig. 2.6-31: Mode of operation of track-aligning bearings on the twist-beam rear axle (with rearward-displaced connecting section) of the VW Passat /33/

2.6.7 Independent Suspension

2.6.7.1 Swing Axles

A swing axle consists of two rigid axle halves hinged to the body in the center of the vehicle. The longitudinal forces are usually supported over tensile members (trailing links), Fig. 2.6-32.

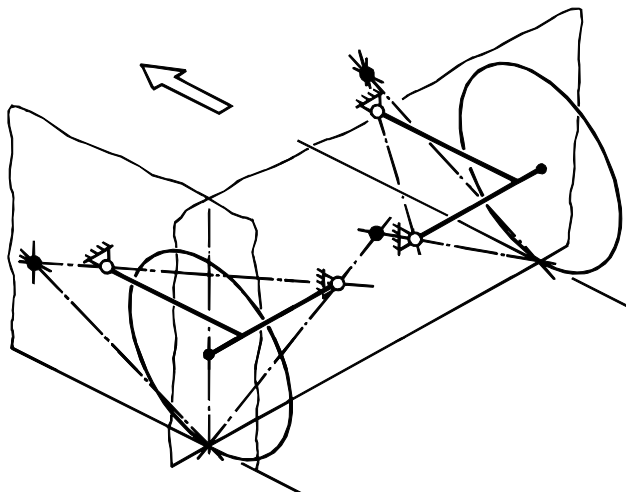


Fig. 2.6-32: Geometry of the double-jointed swing axle

Since the 1930s, the double-jointed swing axle has often been used for driven axles as a moderately complex independent wheel suspension system with a relatively low amount of

unsprung masses. Anti-dive and anti-squat can be realized by the target-specific arrangement of the struts. The drive-shaft joints to the right and left of the differential serve as linking points to the body, Fig. 2.6-33.

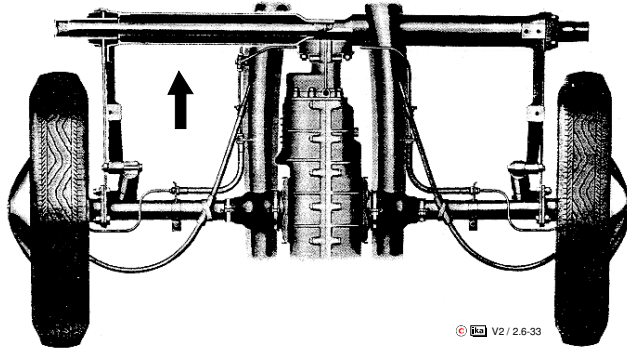


Fig. 2.6-33: Double-jointed swing axle with torsion-bar and longitudinal guidance via torsionally weak trailing links (VW Beetle) (view from above)

The kinematics of this suspension is largely determined by this type of linkage. Suspension movement is associated with significant camber-angle and track changes. The roll center is located high above the road, and the axle therefore has a tendency for a distinct bottoming-out effect, see Fig. 2.6-11.

On account of these drawbacks, this axle design is no longer used today. The single-jointed swing axle (Edmund Rumpler, 1903), with its relatively more favorable kinematic properties and reduced camber and track changes due to the increased swing-arm radius and its (body-fixed) lower roll center, also no longer meets the demands which have to be fulfilled today by suspensions for driven axles, Fig. 2.6-34.

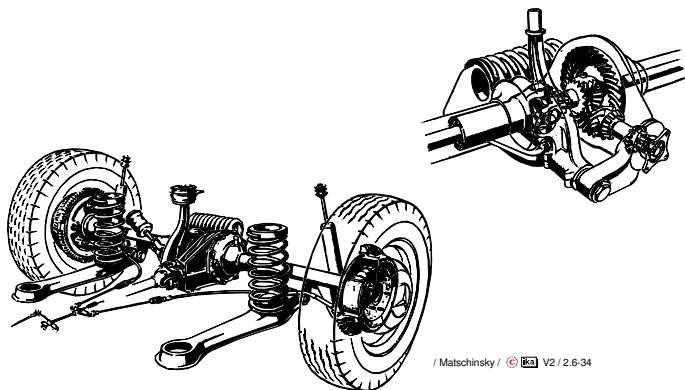


Fig. 2.6-34: Single-jointed swing axle with compensating spring. Lateral-force suspension is effected via the vertical pendulum joint suspension and the strut obliquely hinged to it (MB 220, 1959)

2.6.7.2 Trailing-Link Suspension

Trailing-link suspension systems (or trailing-link or crank axles) are characterized by the fact that the wheels are independently guided by links arranged in vehicle longitudinal direction, with the axis of rotation being oriented in vehicle transverse direction, Fig. 2.6-35.

Trailing links (axis of rotation of the link in front of axis of rotation of wheels in driving direction) are often used for the guidance of non-driven rear wheels.

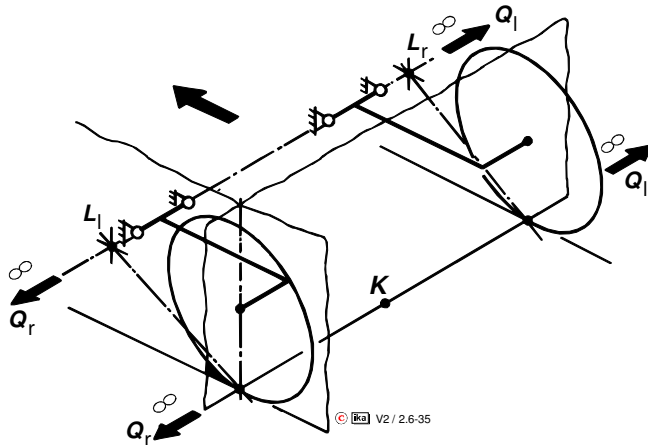


Fig. 2.6-35: Geometry of trailing-link suspension

Pure trailing-link suspension is no longer used on front axles, since the angular displacement of the link is associated with the steering-knuckle pin changing its inclination (Citroën 2CV), i.e., kinematic caster angle changes occur, which have a negative effect on steering quality.

In combination with torsion-bars, trailing-link suspension is characterized by the very little space required and favorable mounting points on the lower longitudinal members (door sill) that are ideal for force application on the body, Fig. 2.6-36.

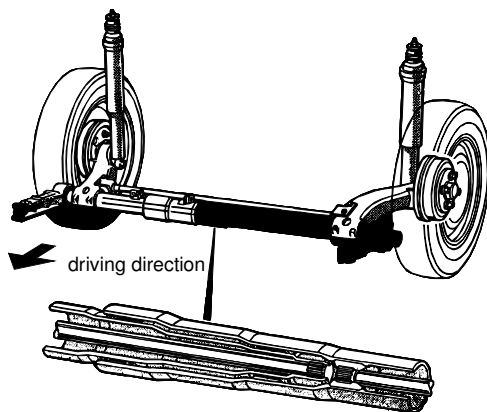


Fig. 2.6-36: Trailing-link rear-wheel suspension with torsion-bar (Renault 9, 11)

The trailing links are subject to bending as well as torsion and must therefore be constructed of a considerable cross section. Due to the orientation of the axes of rotation of the links, neither kinematic toe-in changes and camber-angle variation nor track changes occur.

On account of body roll, the absolute camber angle of the outside wheel during cornering is always positive. Moreover, due to the elasticity in the link mounts, the tire lateral force causes toe-out on the wheel. Both effects minimize the understeer tendency of a vehicle. This is the reason why trailing-link suspension is preferred for the rear axles of FWD vehicles.

According to the wheel control kinematics, the roll center lies on the road surface, see Fig. 2.6-35.

The longitudinal centers crucial for anti-dive, constitute the points of intersection of the axes of rotation of the links through the wheel disk plane and are thus body-fixed points.

In FWD vehicles, the brake force on the rear axle is relatively low. Full braking-torque compensation on the rear axle thus requires a wide angle of braking support, which in turn requires a large vertical distance between longitudinal pole and tire contact center or an accordingly small horizontal distance, see Fig. 2.6-13.

The vertical distance in trailing-link suspension is limited by spatial constraints. The determination of the length of the link requires the fact to be considered that progressiveness of wheel-related spring rates increase with decreasing link length.

2.6.7.3 Semitrailing-Link Suspension

The Semitrailing-Link Suspension which is nowadays often used as a driven rear axle, constitutes a further development of the driven swing axle.

As an additional component, the semitrailing-link suspension features a wheel-carrier-side drive-shaft joint, so that the motion of the axis of rotation of the wheel-carrier relative to the body does not necessarily have to run through the body-side joint on the differential, Fig. 2.6-37.

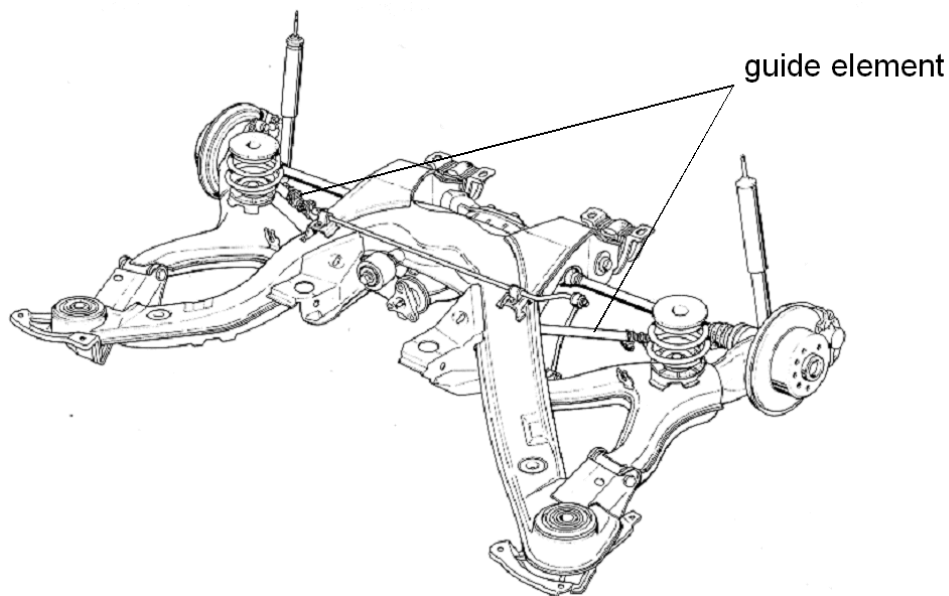


Fig. 2.6-37: Semitrailing-link suspension of a powered rear axle of an automobile (Opel Omega, 1994)

Compared to the swing axle, the semitrailing-link suspension offers much more room for the design of the wheel elevation curves or the longitudinal and transverse poles. For favorable kinematic properties to be realized in modern designs, the projection of the axis of rotation of the link on the transverse plane of the vehicle is inclined by the so-called apex angle β ; while its projection on the plane of the road is inclined by the so-called sweep (angle) α , Fig. 2.6-38.

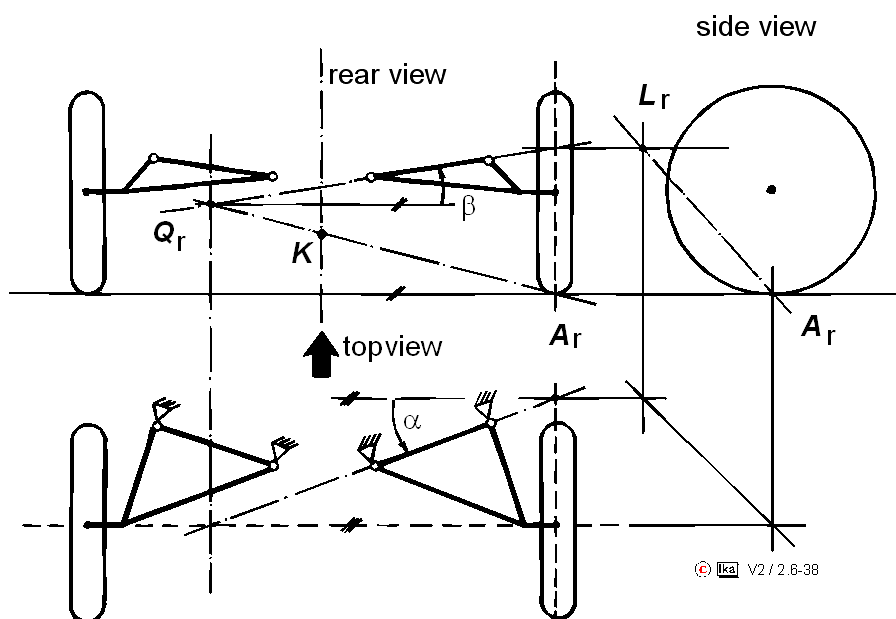


Fig. 2.6-38: Geometry of semitrailing-link suspension

The locations of the longitudinal and transverse poles can be determined graphically, see Fig. 2.6-38. The difference between camber angle γ and apex angle β (magnitude: $\pm 3^\circ$) decisively influences toe-angle variation during suspension movement [29]. The magnitude of kinematic toe-angle variation and the height of the roll center above the road surface are essentially determined by the sweep (angle) α (magnitude: $10 - 25^\circ$).

An additional feature of the semitrailing-link suspension of the Opel Omega shown in Fig. 2.6-37 is represented by a guidance element that is fixed to the chassis subframe and the wheel carrier and supports the wheel forces. This way, load is taken off the wishbone-arm.

Location and orientation of the element are calculated in such a way that only minor changes in toe-in can occur on the wheels during driving. This improves the lateral-force stability of the axle.

A semitrailing-link suspension system with additional degrees of freedom of design is represented by the worm-and-nut-steered rear axle used in the 5 and 7 series of BMW until the model years '96 / '94.

Each semitrailing link has an additional short link fixed to it, which causes axial displacement of the semitrailing link on its rotation axis during suspension movement, Fig. 2.6-39. Plane semitrailing-link suspension is thus turned into three-dimensional wheel suspension with body-fixed instantaneous axis of rotation, see section 2.6.1.

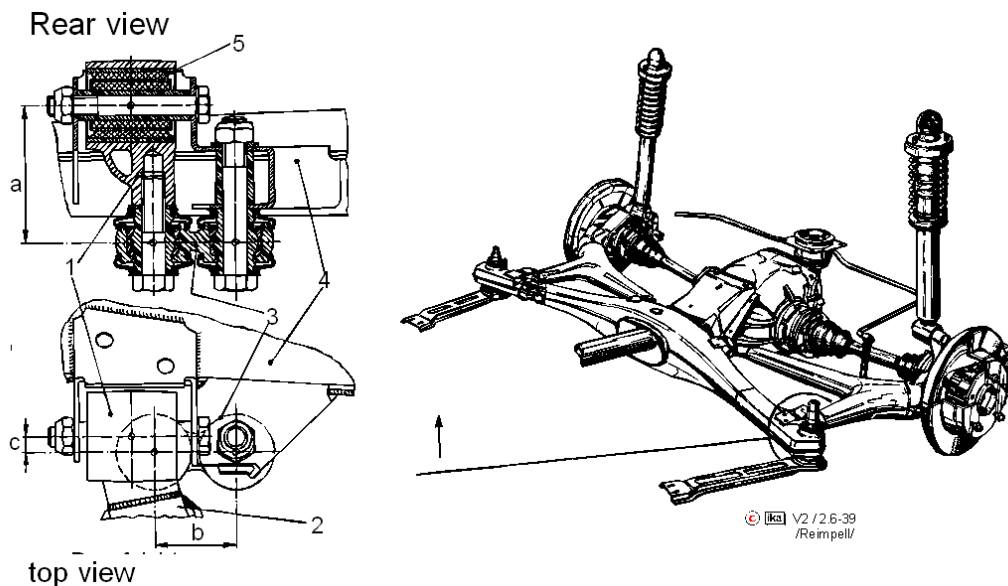


Fig. 2.6-39: "Fastened linkage rear axle" (BMW 5, 7 up to MY '96 / '94) /33/

In the present example, use of the extra link allowed the sweep angle to be reduced for an increase of braking and accelerating support angles without compromising on the change of position of the roll center during cornering, which is favorable from the point of view of preventing of the bottoming-out effect (see Fig. 2.6-11).

Fig. 2.6-40 shows the semitrailing-link rear axle of the VW Sharan as an example for a non-driven rear axle.

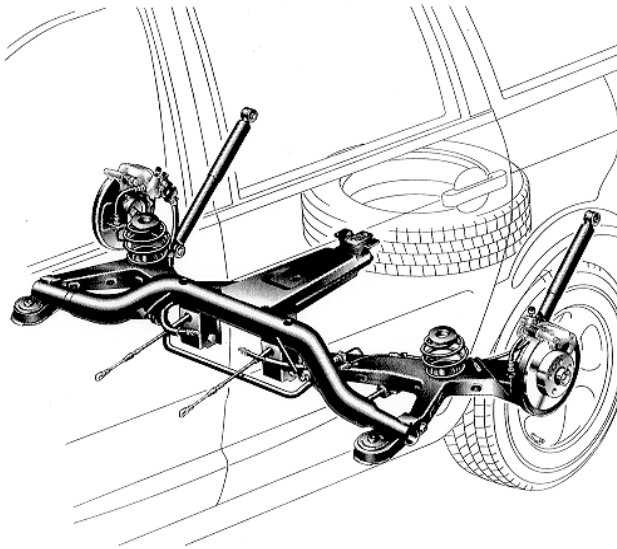


Fig. 2.6-40: Non-driven semitrailing-link rear axle (VW Sharan, 1996)

Miniblock springs permit axle placement under the low loading floor without restricting the width of the loading area. For packaging reasons, the rear-axle dampers are mounted in a rearward-inclined position.

2.6.7.4 Double-Wishbone Suspension

In double-wishbone suspension, the wheel carrier is not hinged directly to the body but forms a kinematic four-link chain along with the body and two wishbone arms, Fig. 2.6-41.

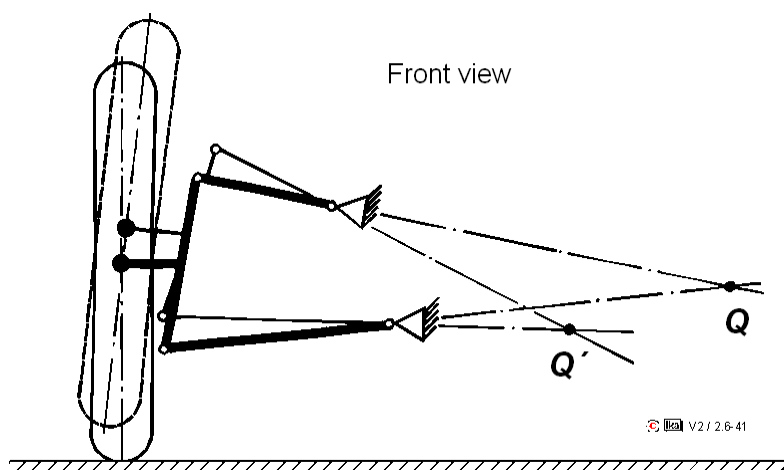


Fig. 2.6-41: Geometry of plane double-wishbone suspension

Depending on the position of the axes of rotation, plane (parallel rotation axes), spherical (intersecting rotation axes) or three-dimensional (skew rotation axes) wheel suspension is obtained (see section 2.6.1).

As a result, the wheel elevation curves, the position of the roll center and the magnitude of anti-dive and anti-squat can be varied over a wide range, Fig. 2.6-42.

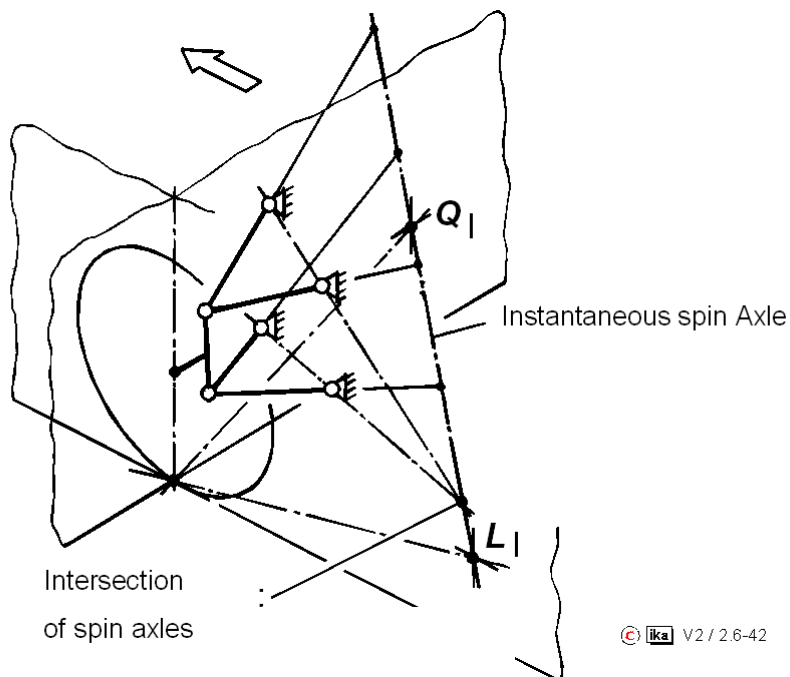


Fig. 2.6-42: Geometry of spherical double-wishbone suspension

In conventional double-wishbone suspension, the relatively high forces at the mounting joints on the body are disadvantageous. On the one hand, they result from the small vertical support base for the brake and reaction torque of the tire forces acting on the wheel carrier; on the other hand, from the usually high spring ratios (see section 1.3.2.3).

Due to the High forces at the joints, wishbones as a rule, are not directly mounted onto the body structure but to a chassis subframe which links both wheel suspensions and thus relieves the body structure of internal forces.

The chassis subframe and body are mostly linked over noise and vibration isolating rubber elements.

Modern double-wishbone suspensions often feature an upper wheel carrier ball joint extending far beyond the wheel disk, so that the vertical support base is extended. This does away with the need for a chassis subframe. The axes of rotation of the links are usually three-dimensionally arranged, so that certain kinematic properties can be realized, Fig. 2.6-43.

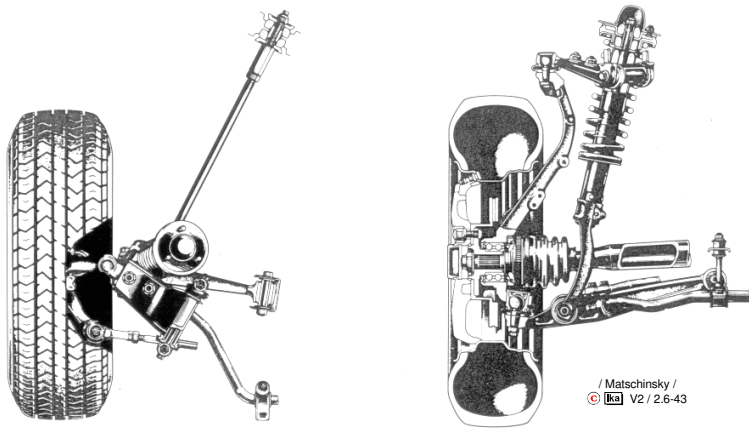


Fig. 2.6-43: Three-dimensional double-wishbone suspension of a powered front axle (Honda Prelude)

Occasionally, the double-wishbone suspension is also used on non-driven front axles. Fig. 2.6-44 shows the front axle of the Mercedes Benz E-Class (1995) as an example.

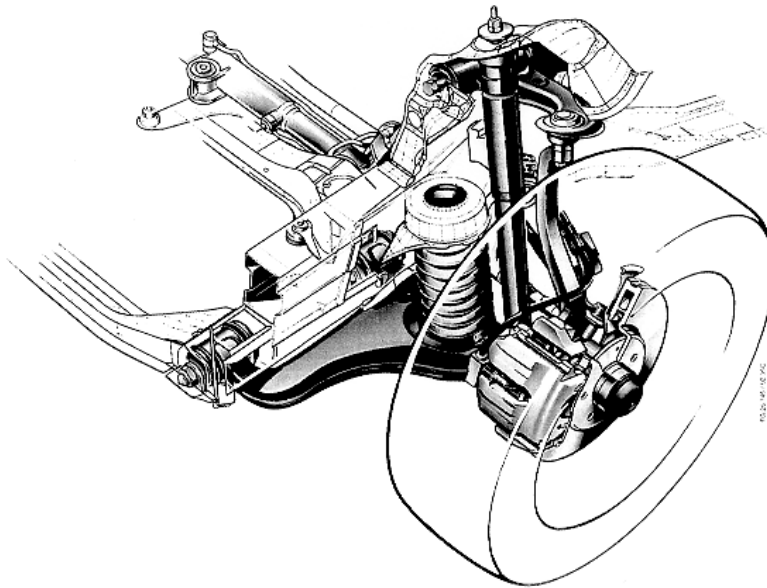


Fig. 2.6-44: Double-wishbone front axle (Mercedes Benz E-Class, 1995)

In spite of the considerable design expenditure, double-wishbone suspensions are also used in rear axles. Their design offers clear advantages especially in very powerful vehicles because of the numerous kinematic and elastokinematic design possibilities compared to other axle concepts. Fig. 2.6-45 shows the "center-point-guided" spherical double-wishbone suspension of the BMW Z1.

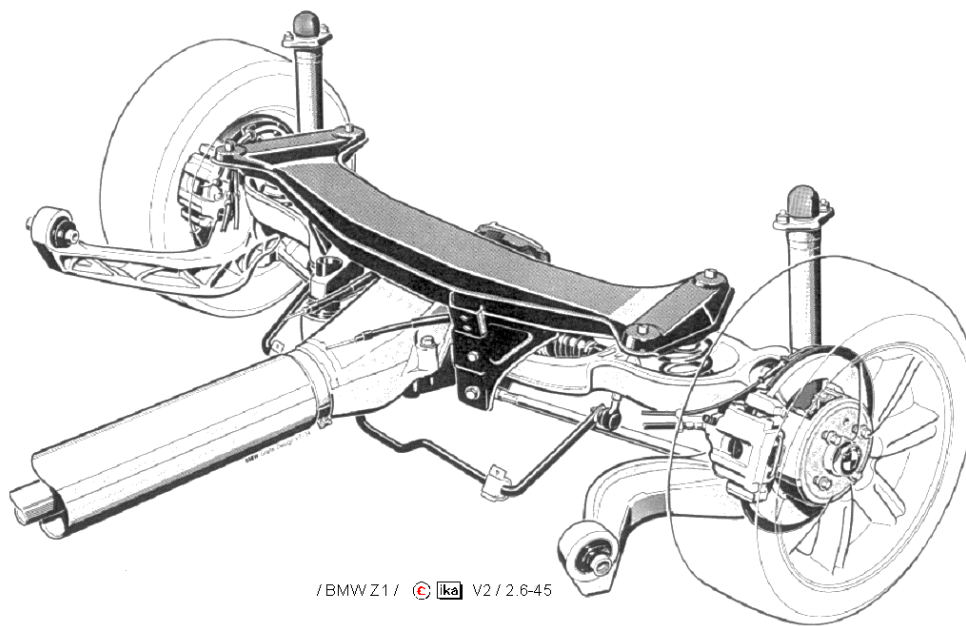


Fig. 2.6-45: "Center-point-controlled" spherical double-wishbone suspension of the driven rear axle of the BMW Z1

The wheel-guiding components of the central-link rear axle are composed of a longitudinal link as a third link in addition to the two transverse links (wishbones) arranged one above the other. The longitudinal link is elastically fastened to the body. The wishbones are linked over rubber mounts to a rear-axle bracket, which is elastically fastened to the body. The three links thus form a spherical guidance.

This design permits a clear distribution of the tasks among the links (with the longitudinal link mainly responding to longitudinal forces and the wishbones mainly responding to the lateral forces), which facilitates separate tuning of longitudinal and transverse dynamics.

A rear axle with nearly identical kinematics is also found in the BMW 3 Series since '91.

2.6.7.5 Strut Suspensions

In the 70s, the double-wishbone suspension was largely replaced by spring-strut-type suspension (Fiat, 1926) as a suspension concept for front axles.

The kinematics of strut suspensions corresponds to that of a double-wishbone suspension in which the upper wishbone is of infinite length or has been replaced by a sliding guide. In the strut suspensions which have been realized, this sliding guide corresponds to the telescopic shock absorber whose casing is firmly fixed to the wheel carrier and whose shock-absorber rod is also used for wheel guidance.

Compared to double-wishbone suspension, the advantages of the strut suspension include the reduced design expenditure and the reduced requirements in space at the level of the wheel axles, which can be utilized especially in FWD automobiles with transversally mounted engine-transmission units.

In the determination of the kinematics of wheel guidance, strut suspensions offers less room for design when compared to double-wishbone suspensions.

In the strut suspension concept according to the McPherson principle (Earl McPherson, 1945), the lower transverse arm is made up of a wishbone and a stabilizer, Fig. 2.6-46.

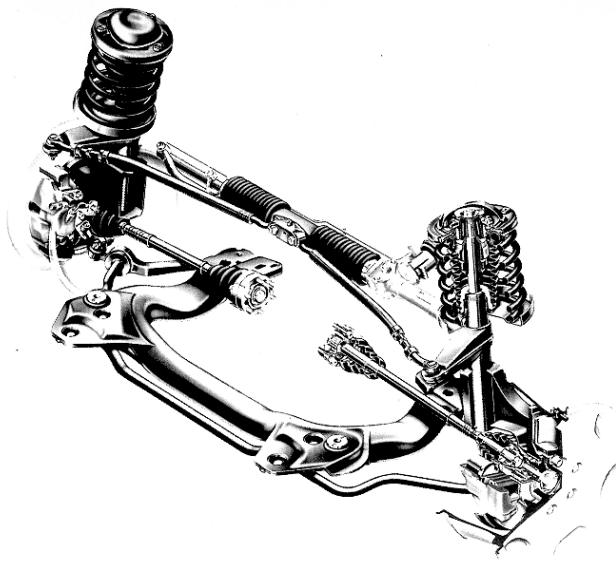


Fig. 2.6-46:McPherson front axle (Audi 100, 1991).

Similar designs with other wishbones are nowadays also referred to as McPherson axles /33/. Fig. 2.6-47 shows the McPherson front axle of the VW Polo (1995). While in the Audi 100 the stabilizer also performs a wheel-guidance function, this function is effected in the VW Polo by a lower triangular transverse-arm. Similar designs are nowadays found in all compact-size automobiles.

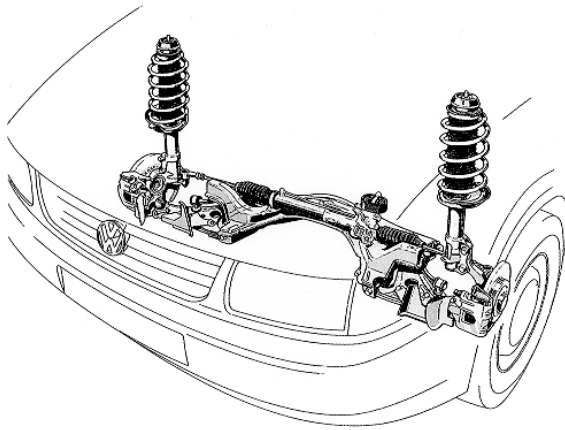
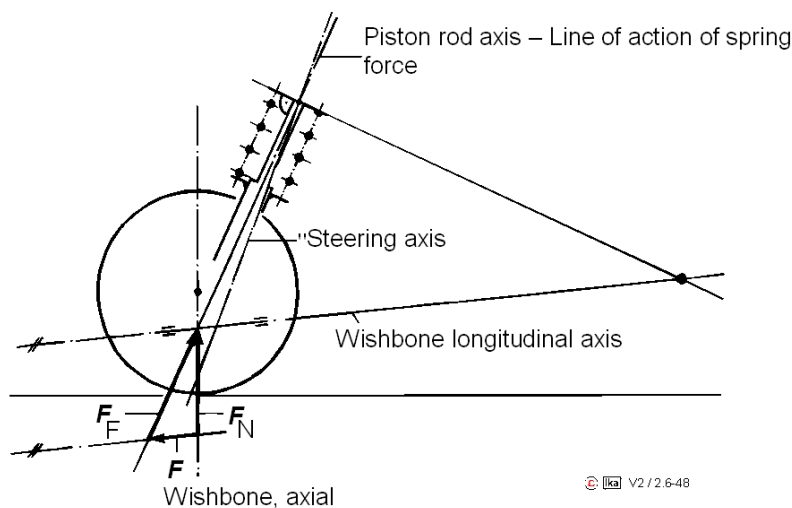


Fig. 2.6-47: Strut suspension (VW Polo, 1995)

Inclination of the damper piston rod in the vehicle lateral plane, in order to influence the roll pole, is limited on the one hand by the inner tire flank and on the other hand by the position of the steering-axis being determined by the mounting point of the upper suspension-strut, see Fig. 2.5-12.

Inclination of the damper rod in the vehicle longitudinal plane, in order to influence the longitudinal pole, is limited by the fact that on the one hand a certain position of the steering axis (caster angle) is to be realized and on the other the clamping force in the piston rod guide of the damper is to be minimized. This clamping force results from the difference in alignment between the line of action of the spring force with the point of intersection of the line of action of the vertical force in the tire contact center and the line of action of the axial force of the wishbone arm, Fig. 2.6-48.



© V2 / 2.6-48

Fig. 2.6-48: Reduction of the clamping force in the piston rod guide of the strut suspension through alignment of the line of action of the spring force, vehicle longitudinal plane

Reduction of the clamping forces in the piston rod guide, which adversely influence spring response, is also achieved by the inclination of the axis of the body springs relative to the damper tube in the vehicle transverse plane.

Clamping force is minimized by the alignment of the line of action of the spring force with the point of intersection of the line of action of the vertical force at the tire contact center and the line of action of the force at the transverse link, Fig. 2.6-49.

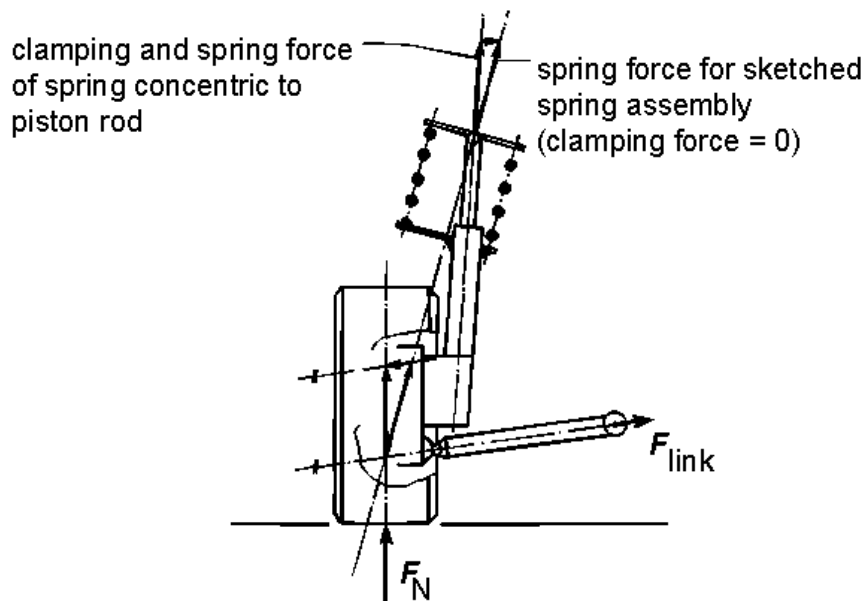


Fig. 2.6-49: Reduction of the clamping force in the piston rod guide of the strut suspension by the alignment of the line of action of the spring force, vehicle transverse plane

The placement of the body springs above the wheel is necessary for the damper tube to run alongside the wheel as closely as possible and for an acceptable kingpin angle to be realized. By means of a target-specific design of the transverse-link mounts in strut suspension, longitudinal elasticity of wheel guidance, which is favorable for suspension comfort can be achieved without unfavorable elastokinematic toe-angle changes, Fig. 2.6-50.

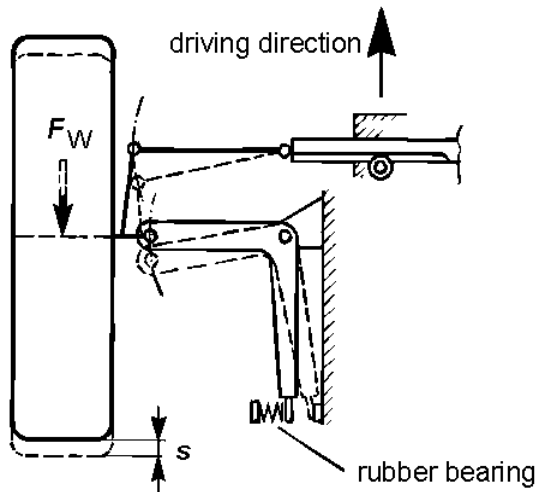


Fig. 2.6-50: Elastokinetically tuned strut-type front axle

The front axles of the current BMW 5 and BMW 7 series can be considered as further developed traditional strut-type suspension, Fig. 2.6-51.

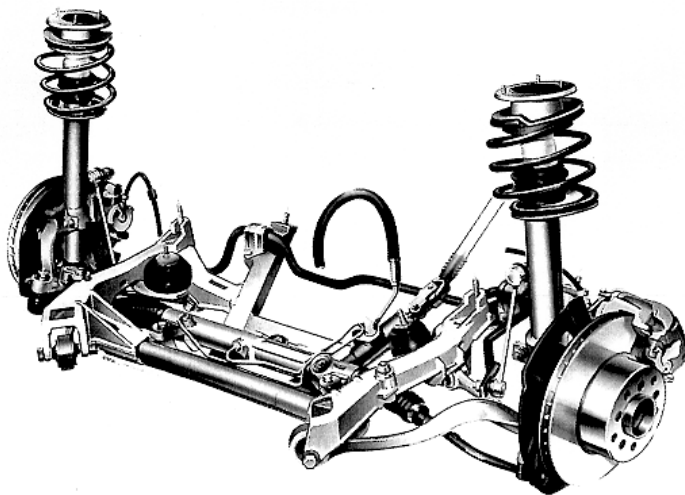


Fig. 2.6-51: Double-jointed strut-type front axle with ideal steering axis (BMW 5, 1996)

Substitution of the lower wishbone by two struts is the common hallmark of these axle concepts. For the steering axis, this results in a virtual point of intersection in the plane of the lower wishbone, which on the one hand causes a minor steering offset, which increases with the steering angle, as well as a disturbing force lever arm, and on the other hand permits a larger brake disk to be installed due to a minor wheel offset, Fig. 2.6-52.

Point of intersection of the virtual steering axis at lower wishbone plane

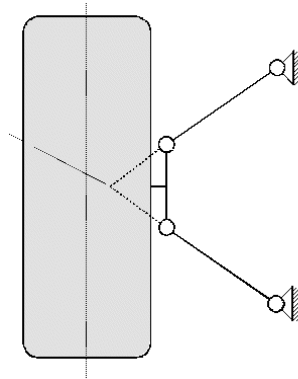


Fig. 2.6-52: Point of intersection of the virtual steering axis

The fact that the front-axle bracket is an aluminum weld assembly is another special feature of the axle design shown in Fig. 2.6-52. Compared to the preceding model, the axle is characterized by a weight reduction of 5.4 kg.

Damper strut suspension, where the spring force of the body suspension is transferred to the wheel carrier via the ball joint of the transverse link, is also a further development of strut-type suspension, Fig. 2.6-53.

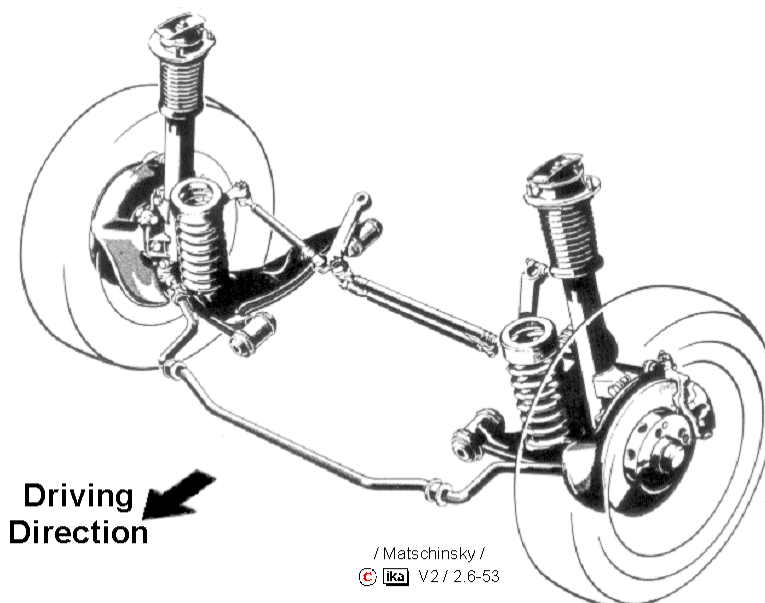


Fig. 2.6-53: Damper strut front axle (MB 190)

In addition to a somewhat reduced overall height, this design offers the advantage that caster angle and longitudinal center can be determined without consideration of the clamping forces in the piston rod guide of the damper caused by the spring force, see Fig. 2.6-48.

2.6.7.6 Multilink Wheel Suspensions

Realization of a wheel suspension system that meets high riding-comfort requirements and at the same time offers favorable handling characteristics is possible if kinematic and elastokinematic properties are specifically tuned and matched, see Fig. 2.6-16.

The larger the number of variable parameters, the larger are the number of aspects which can be considered in the design process. Consequently, a multilink axle offers optimum conditions.

A suspension system whose design follows the basic concept of three-dimensional wheel guidance, with the wheel carrier being linked to the body via 5 links, is referred to as multilink suspension, see Fig. 2.6-1. Design of such a suspension system can be based on a wide range of objectives.

Fig. 2.6-54 shows the four-link front axle of the Audi A4. In this axle type, the wheel is controlled via four rod-shaped links, the tie rod and the suspension strut. Due to the independent guidance elements, the design principle of the A4 axle includes great potential from the point of view of the optimization of comfort and kinematic properties.

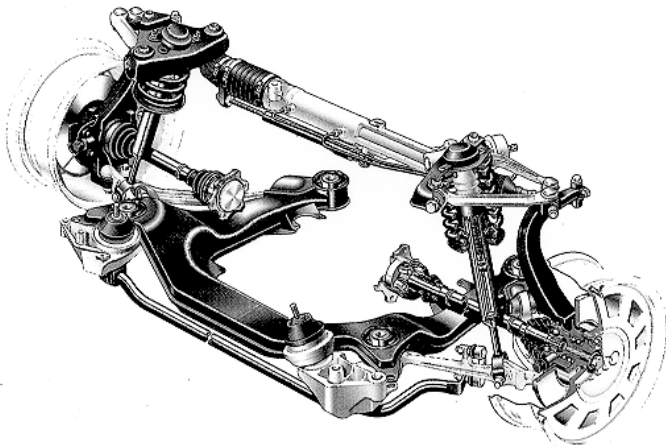


Fig. 2.6-54: Four-link front axle (Audi A4, 1994)

The large support base between upper and lower link plane is the characteristic feature of the design of the four-link front axle of Audi. It is the source of a high camber stiffness.

The four links are linked to the swiveling bearing via low-friction ball joints. A bearing bracket featuring rubber-metal mounts (silent bearings) carries the two upper links as well as the spring and shock-absorber mounts. The spring and shock-absorber mounts are functionally separated from each other. Even the supplementary spring (bump stop) is supported over the bearing bracket directly at the body, so that it is possible to tune the shock-absorber mount exclusively to the shock-absorber forces. The shock absorber features an internal stop spring that supports kinematic anti-squat control.

The axle spring is arranged concentrically around the damper. With its forked end, this spring-and-damper assembly is supported over a rubber-metal bearing by the front lower link, the supporting link. The rearward lower link, the guidance link, only supports the link forces and essentially determines elastokinematic longitudinal control of the wheel. For optimum tuning of the tire comfort and vibrational behaviour of the axle, it features a technically complex rubber-metal bearing with hydraulic damping.

The rack-and-pinion steering along with external end of the tie rod is rigidly bolted to the body above the transmission and thus very close to the plane of the upper link. This allows a relatively precise geometric arrangement between tie rod and link for precise toe-in kinematics.

The virtual steering axis (see Fig. 2.5-8) is an outstanding hallmark of this axle design. With a narrow kingpin angle, it is located near the wheel center and supports a small disturbing force lever arm for driving forces, which plays an important role in FWD automobiles.

While multilink suspensions are still the exception on the front axle, they are more widely used on the rear axle. Fig. 2.6-55 shows the five-link rear axle of the Chevrolet Corvette in a rear view from below.

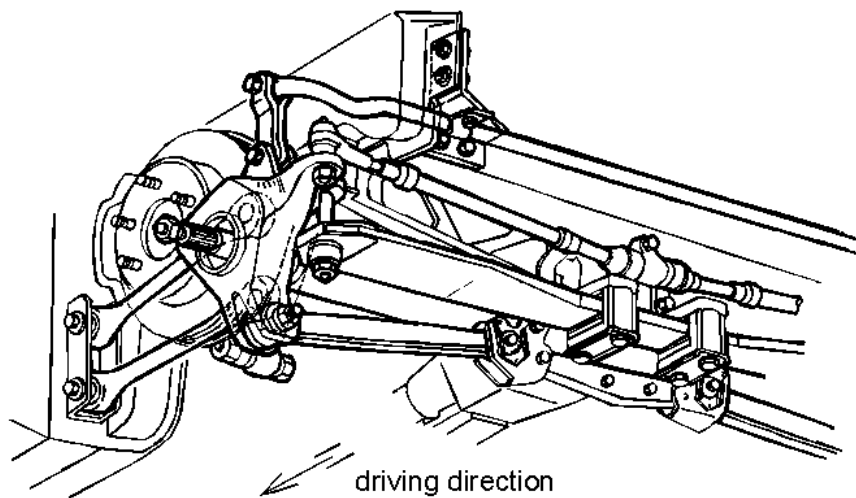


Fig. 2.6-55: Five-link rear axle (Chevrolet Corvette, 1983)

In the "Corvette", longitudinal forces and braking torque are essentially supported over two tension/compression members arranged in the vehicle longitudinal direction. The appropriate dimensioning of the components facilitates the realisation of lightweight design.

The angular position of the links in relation to each other in the vehicle longitudinal plane decisively determines the position of the longitudinal pole, i.e. the magnitude of anti-dive or anti-squat.

The transverse guidance of the wheel carrier is realised over another tension/compression member arranged in vehicle transverse direction and the axle drive shaft, which is also used as a tension/compression member and features joints both on the body end as well as the wheel carrier end.

The positions of the transverse centers or the roll center are essentially determined by the angular position between the jointed shaft and the transverse strut in the vehicle transverse plane.

A fifth adjustable strut arranged behind the axle performs the same function as the tie rod on a steering axle. A plastic transverse leaf spring, which is decoupled from the forces of wheel guidance by means of a short tension/compression member, is employed for body suspension. In order to suppress undesired elastokinematic toe-angle changes, the rubber mounts at the joints of this suspension must be relatively stiff. The associated negative effects on riding comfort are accepted in view of the intended purpose of the axle (sports car).

In the multilink rear suspension system of the Mercedes-Benz model series W 201 and W 124, the wheel carriers are each linked to the body via 5 links (or struts), Fig. 2.6-56.

Four of the links essentially only support tension/compression forces; one link also transmits the spring and damper forces to the wheel carrier. The upper and lower pairs of links each perform the function of a wishbone. The fifth link, which is located roughly at the level of the center line of the wheel, functions as a tie rod.

In the top view, the intersecting point of the lines of action of the upper pair of links is located on the outside of the wheel center plane; while that of the lower pair of links is located on the inside. The position of the "steering axis" hence determined, see Fig. 2.6-16, results, for example, in the longitudinal forces causing elastic toe-in changes to be compensated by kinematic toe-in changes, so that there is zero elastokinematic change of toe-in.

The side view reveals an angular position of the body-end "rotation axes" relative to the "triangular transverse links" formed by the upper and lower pairs of links.

The positions of the transverse centers which are hence decisively influenced result in a braking-dive compensation of 60% and an accelerating-squat compensation of 67%, see section 2.6.2.2. The use of a subframe allows the use of additional rubber elements for noise and vibration isolation between axle (incl. differential) and body. Moreover, this also simplifies vehicle production, since the complete axle can be pre-assembled as a system.

In the kinematic and elastokinematic design of suspension systems, a maximum number of influencing possibilities are available if those links which exclusively cancel only one of the six degrees of freedom of the wheel carrier relative to the body, are used. It is not absolutely necessary for all 5 links to be arranged between wheel carrier and body. If it is taken into

account that the individual links are subject to bending not exclusively by the spring/damper forces, then further possibilities of arrangement open up.

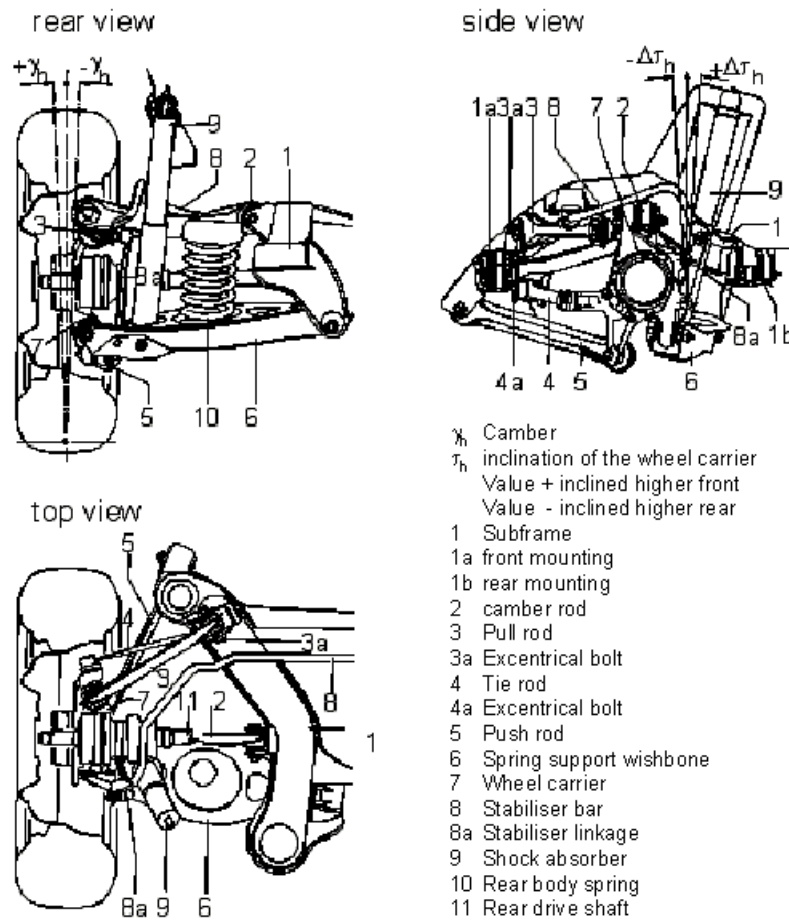


Fig. 2.6-56: Multilink rear suspension MB 190 /33/

Fig. 2.6-57 shows the multilink rear suspension system of the BMW 5. The rear-axle bracket (aluminum tube welded assembly) is mounted to the body by four large-volume rubber mounts (silent bearings) for optimum noise and tire comfort. Even though this is associated with a relatively soft suspension, optimum tracking has been achieved thanks to an intelligent arrangement of the links. As a result, the kinematics as well as elastokinematics are tuned in such a way as to prevent, for example, adverse steering-angle changes during braking deceleration or acceleration.

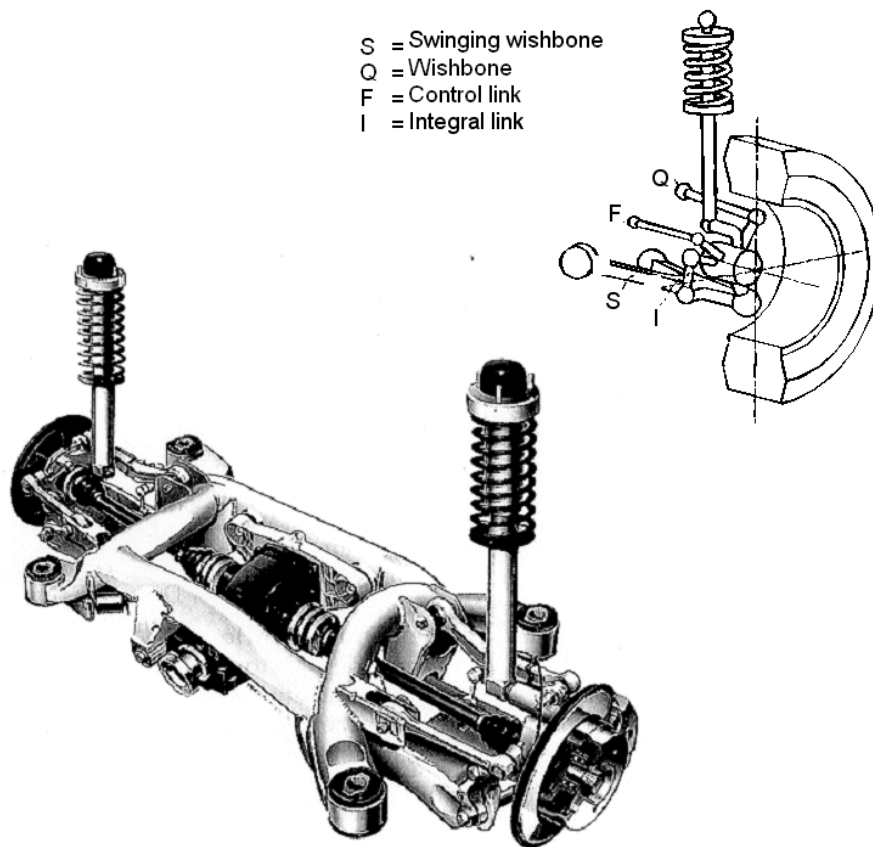


Fig. 2.6-57: Multilink rear suspension (BMW 5, 1996)

Literature

- /1/ Adomeit, G. Umdruck zur Vorlesung Dynamik I und II, Inst.
für allg. Mechanik der RWTH Aachen, 1989
- /2/ Bantle; M. Fahrwerksauslegung und Fahrverhalten des
Porsche 928, ATZ 1977
Braess, H.-H.
- /3/ Bergman, W. The Basic Nature of Vehicle Understeer-
Oversteer, SAE-Paper 957 B, 1965
- /4/ Berkefeld, V. Theoretische Untersuchungen zur
Vierradlenkung, Stabilität und Manövrierbarkeit

Vortrag auf der HDT-Tagung T-30-930-056-9

Allrad-Lenksysteme bei PKW 11/89
- /5/ Bismis, E. Testverfahren für das instat. Lenkverhalten in:
Entwicklungsstand der objektiven Testverfahren

Kolloquiumreihe „Aktive Fahrsicherheit“

Verlag TÜV Rheinland GmbH, Köln 1978
- /6/ Bleck, U. Analyse der Lastwechselreaktionen mittels
Simu- lation und Messung
Heißing, B.
Meyer, G. VDI-Bericht Nr. 699, 1988
- /7/ Braun, H. Untersuchungen über Fahrbahnunebenheiten

Deutsche Kraftfahrforschung und
Verkehrstechnik, Heft 186, VDI-Verlag,

Düsseldorf

- /8/ Burckhardt, M. Der Einfluß der Reifenkennlinien auf
Signalgewinnung und Regelverhalten auf
Fahrzeuge mit ABS, Automobil-Industrie 3/87 S.
231
- /9/ Buschmann Handbuch der Kraftfahrzeugtechnik, Band I u. II,
Koessler Heyne Verlag München
- /10/ Deppermann, K-H. Fahrversuche und Berechnungen zum
Geradeauslauf von PKW

VDI-Fortschrittsberichte, Reihe 12, Nr. 133,
1989
- /11/ Donges, E. I. Aspekte der aktiven Sicherheit bei der
Führung von PKW, Automobil-Industrie 2/2

Aktive Hinterachskinematik - neue
II. Entwicklungsmöglichkeiten der
Fahrzeugquerdynamik, VDI-Bericht Nr. 778,
1989

Funktion und Sicherheitskonzept der aktiven
III. Hinterachskinematik von BMW

Vortrag auf der HDT-Tagung 30-930-056-9

Allrad-Lenkssysteme bei PKW 11/89
- /12/ Fiala, E. Kraftkorrigierte Lenkgeometrie unter
Berücksichtigung des Schräglaufwinkels, ATZ
61, 1959

- /13/ Förster, H.-J. I. Mercedes-Benz Servolenkungen
ATZ 80 (1978) 3
- II. Mercedes-Benz Servolenkungen
Teil 1 ATZ 74 (1972) 2
Teil 2 ATZ 74 (1972) 4
- /14/ Forkel, D. Ein Beitrag zur Auslegung von
Fahrzeuglenkungen, Deutsche
Kraftfahrtforschung und Verkehrs-technik, Heft
145, 1961
- /15/ Gerresheim, M. Kräfte und Bewegungen in der Aufstandsfläche
Hussmann, A. geradeausrollender Reifen, Teil 1
Automobil-Industrie 3/75
- /16/ Gnadler, R. Naßgriff und Aquaplaningverhalten von PKW-
Reifen, Verkehrsunfall und Fahrzeugtechnik
Teil 1 Heft 11/88
Teil 2 Heft 12/88
- /17/ Göhring, E. I. Beitrag zur Entwicklung eines
fahrmechanischen Konzepts für
Nutzfahrzeuge
Automobil-Industrie 4/80

II. Einfluß des Systems Reifen / Fahrbahn auf das Außengeräusch von Nutzfahrzeugen

VDI-Bericht, Nr. 778, 1989

- | | |
|---|--|
| /18/ Goes, F. | Theoretische und experimentelle Untersuchungen zur Beurteilung der Wirkung von Schwingungsdämpfern im Fahrzeug

Dissertation TH Braunschweig, 1963 |
| /19/ Gough, V.-E. | Seitenkraft und Seitenverschiebung in der Berührungsfläche zwischen Reifen und Fahrbahn

ATZ 19 (1961) |
| /20/ Hahn, W.-D. | Die Federungs- und Dämpfungseigenschaften von Luftreifen bei vertikaler Wechsellast

Dissertation TU Hannover, 1972 |
| /21/ Hennecker, D.
Jordan, B.
Ocher, U. | Elektronische Dämpfer-Control - eine vollautomatische adaptive Dämpferkraftverstellung für den BMW 635 CSi, ATZ 89 (1987) 9 |
| /22/ Heyer, G. | Trends in der Stoßdämpferentwicklung

Automobil-Industrie Nr. 6 / 88 |
| /23/ Hildebrandt, C. | Der neue VW Santana, ATZ 84 (1982) 2 |
| /24/ Hoffmann R. | Der neue BMW 7er |

- Lorenz, K. ATZ 89 (1987) 6
- Sagan, E.
-
- /25/ Klinkner, W. Adaptives Dämpfungssystem "ADS" zur fahrbahn- und fahrzustandsabhängigen Steuerung von Dämpfern einer Fahrzeugfederung
- VDI-Bericht Nr.778, 1989
-
- /26/ Krempel, G. Experimenteller Beitrag zur Untersuchung am Kraftfahrzeugreifen
- Dissertation TH Karlsruhe, 1965
-
- /27/ Laermann, F. J. Seitenführungsverhalten von Kraftfahrzeugen bei schnellen Radlaständerungen
- VDI-Fortschrittsberichte, Reihe 12, Nr. 73
-
- /28/ Lohr, F.-W. Opel Omega - Teil 1 ATZ 89 (1987) 1
- Teil 2 ATZ 89 (1987) 2
-
- /29/ Matschinsky, W. Die Radführung der Straßenfahrzeuge
- Analyse, Synthese, Elasto-Kinematik
- Verlag TÜV Rheinland GmbH, Köln 1987
-
- /30/ Mitschke, M. Dynamik der Kraftfahrzeuge, Springer-Verlag
- Berlin, Heidelberg, New York, 1975

- /31/ Olley, M. Road Manners of the Modern Car
Proc. Inst. Aut. Engers. 1946/47
- /32/ Rake, H. Umdruck zur Vorlesung Regelungstechnik der
RWTH Aachen, 1989
- /33/ Reimpell, J. Fahrwerktechnik: Reifen und Räder
Vogel-Buchverlag, Würzburg 1986
- /34/ Richter, B. Die Vierradlenkung des iRVW4
Vortrag auf der HDT-Tagung T-30-930-056-9
Allrad-Lenksysteme bei PKW 11/89
- /35/ Rönitz, R. Verfahren und Kriterien zur Bewertung des
Fahrverhaltens von PKW
Braess, H.-H. Teil 1 Automobil-Industrie 1/77
Zomotor, A. Teil 2 Automobil-Industrie 3/77
- /36/ Rompe, K. Variationsbereiche der Fahreigenschaften
heutiger PKW
Donges, E. Automobil-Industrie 2/83
- /37/ Rompe, K. Objektive Testverfahren für die
Fahreigenschaften von Kraftfahrzeugen
Heißing, B. Verlag TÜV Rheinland GmbH, Köln 1984

- /38/ Stall, E. Verfahren zur Vermessung und Simulation von
Straßenunebenheiten

Doktorvortrag, TH Aachen 1984
- /39/ Waldmann, D. Untersuchungen zum Lenkverhalten von
Kraftfahrzeugen. Deutsche Kraftfahrzeugforschung
und Straßenverkehrstechnik, Heft 218, 1971
- /40/ Wallentowitz, H. Hydraulik in Lenksystemen für 2 und 4 Räder

Vortrag auf der HDT-Tagung T-30-302-056-9

Hydraulik und Pneumatik im Kraftfahrzeug 3/89
- /41/ Weber, R. Beitrag zum Übertragungsverhalten zwischen
Schlupf und Reifenführungskräften

Automobil-Industrie 4/81
- /42/ Weber, R. Seitenkraft-Frequenzgänge von Luftreifen

Persch, H.-G. ATZ 77 (1975) 2
- /43/ Willumeit, H.-P. Seitenkraftverlust des schräglaufenden Reifens
unter dynamisch veränderlichen Radlasten und
konstantem Schräglaufwinkel

Automobil-Industrie 4/70
- /44/ Wolff, H. Untersuchung und Optimierung des
Federungsverhaltens von Rettungswagen unter
besonderer Berücksichtigung von
Reibungseinflüssen

Dissertation TH Aachen, 1975

- /45/ Zamov, J. Beitrag zur Identifikation unbekannter Parameter
für fahrdynamische Simulationsmodelle
VDI-Berichte Reihe 12, Nr. 217

- /46/ Zomotor, A. I. Fahrwerktechnik, Fahrverhalten
Vogel-Buchverlag 1987
- II. „Meßverfahren bei der Auslegung des
Fahrverhaltens“ aus: Entwicklungsstand der
objektiven Testverfahren für das
Fahrverhalten
Verlag TÜV Rheinland GmbH, Köln 1977